Laser Welding of Zinc Coated Steel

by

Rehan Akhter

July, 1990

A thesis submitted for the degree of Doctor of Philosophy of the University of London and for the Diploma of Imperial College

John Percy Group
Department of Materials
Imperial College of Science, Technology and Medicine
London SW7 2BP

and

Laser Centre
Department of Mechanical Engineering
University of Liverpool
Liverpool L69 3BX

To

My beloved parents

Abstract

This thesis is concerned with the lap welding of zinc coated mild steel sheet, a process of growing interest to the manufacturers of cars, washing machines and other components made from sheet steel and subject to corrosion.

Conventional clamping and welding of this material results in explosive ejection of the zinc vapour and an unsatisfactory weld. Several techniques are presented for the removal of the zinc from the interface or the control of the zinc vapours. Of these processes discussed in the thesis the use of a gap between the sheets to vent the zinc vapour is shown to produce satisfactory welds. The process is modelled and tested by experiment. The resulting welds made both by this gap technique and by welding uncoated material were tested for fatigue, impact resistance, mechanical strength, hardness and corrosion resistance to salt solutions.

The welds were made using a variety of lasers and the comparison in performance of these lasers is presented.

Techniques were studied for the modification of the weld composition both by alloying the weld ingot, coating the weld ingot or by recondensing the zinc vapour over the solidified weld. The corrosion properties of these welds is presented together with the corrosion of the standard welds. It was found that a corrosion resistant Zn-Fe alloy forms at the edges of these welds which sacrificially prolongs the life of the weld.

The thesis discusses these issues in the following sequence:

1. Background to laser welding and the current technology and application of zinc coated steel - chapter 1 & 2.
2. Description of the five lasers used in this work: - chapter 3

The Control Laser 2 kW FAF CO_2 laser,

The AVCO 15 kW transverse flow EB excited CO_2 laser,

The United Technologies 10 kW transverse flow CO_2 laser,

The MLI 8 kW transverse flow AC excited CO_2 laser,

The Ferranti 400 W slow flow CO_2 laser.

3. Description of the welding experiments and results - chapter 4 & 5.

   The Techniques used were :-

   Double pass welding, end edge welding, gap welding, modification of the weld composition, welding using dimples as method of setting the gap size.

4. Analysis of the gap welding process - chapter 6.

5. Analysis of the corrosion properties of the welds made by various techniques - chapter 7.

6. Conclusions and future work - chapter 8.

Acknowledgements

I would like to express my sincere appreciation and gratitude to my supervisor **Prof. W.M.Steen** for his consistent supervision, constructive criticism, ever ready help and assistance throughout my research. His guidance during the writing up of my thesis has enabled me to complete it successfully. I am also deeply grateful and indebted to **Prof. D.R.F.West** for his encouragement and support. My special thanks are due to **Dr. K.G.Watkins** for providing stimulating and congenial research environment and for his enthusiastic guidance, advice and friendship during my studies. I also wish to express my thanks to Dr. D. Brookfield, Dr. P. Morden, Mrs. Heather Garnett (Secretary), Mr. S. Pant, Mr. Jack Frith, Mr. R. Stracey (technicians), Dr. J. Gabzdyl, Dr. S. T. Shah, Dr. Lin Li, Dr. H. Y. Zhang, Mr. W. O'Neill, Mrs. Liu Zhu, Mrs. Yong Ling, Miss. Fiona Fellows, Miss. Sarah Sharky, Miss. Nicola McKeown, Miss. Karen Williams, Mr. Qi Ning, Mr. S. L. Chen, Mr. J. Y. Jeng, Mr. Geoff Shannon, Mr. S. Brocklebank, Mr. G. Abbas, Mr. Jafar, Mr. Thaer, Mr. M. J. Kadhim, Mr. Nigel Willmott, who helped make this research possible.

My thanks also go to EEC for funding this project through BRITE Project no. 1339, to RTM for providing necessary facilities to use their laser, to RENAULT Motors and CETIM for material supply.

I am deeply indebted to my parents, brothers, sisters and other members of my family for their patience, support and encouragement throughout my period of study in England. My special thanks are due to my friends Shaukat Hayat Khan, Shakil Khan and Muhammad Iqbal for their assistance in finalising this manuscript. My thanks are due to all my friends and colleagues in Liverpool and in Pakistan.

In the end I would like to extend my thanks to the Government of Pakistan, Ministry of Science and Technology, Pakistan for awarding me the scholarship without which this research would not have been possible.

Contents

	Abstract	
	Acknowledgments	
	Contents	i
	Figure Captions	ix

Chapter 1
Introduction

No.	Title	Page no.
1.1	Introduction	1
1.2	Application of lasers in welding	4
1.3	Laser welding	6
1.4	Outline of the problem of welding zinc coated steel	7
1.5	Materials	7
1.6	Research aims and objectives	8

Chapter 2
Literature Review

2.1	Introduction	9
2.1.1	Fundamentals of lasers	10
2.1.1.1	Fluorescence	10
2.1.1.2	Absorption	10
2.1.1.3	Stimulated emission	10
2.1.2	Properties of lasers	11
2.1.2.1	Coherence	11
2.1.2.2	Polarisation	11
2.1.3	Types of lasers	12

2.1.3.1	Solid state laser	12
2.1.3.2	Liquid or dye lasers	12
2.1.3.3	Gas lasers	13
2.1.3.3.1	Advantage in using gas as lasing medium	13
2.1.4	Types of carbon dioxide lasers	13
2.1.4.1	Lasing action in CO_2 lasers	14
2.1.5	Welding parameters	15
2.1.5.1	Laser parameters	17
2.1.5.1.1	Effect of laser power on penetration	17
2.1.5.1.2	Effect of beam mode on penetration	19
2.1.5.1.3	Wavelength	19
2.1.5.1.4	Effect of spot size on weld penetration	20
2.1.5.2	Characteristics of focussing optics	21
2.1.5.2.1	Focal length	21
2.1.5.2.2	Effect of focal position on penetration	21
2.1.5.3	Properties of workpiece	23
2.1.5.3.1	Reflectivity	23
2.1.5.3.2	Effect of welding speed on penetration	24
2.1.5.3.3	Thermal properties	26
2.1.5.3.4	Effect of gas shielding on penetration	27
2.1.5.3.5	Effect of gap between the sheets on penetration	29
2.1.6	Ripple formation during weld solidification	31
2.1.7	Weld bead humping and undercutting	34
2.1.8	Laser materials interaction and the influence of laser induced plasma on welding	35
2.1.8.1	Dynamic behaviour in laser welding	41
2.1.9	Conventional welding processes	44
2.1.9.1	Shielded metal arc welding	45
2.1.9.2	Gas metal arc welding	45
2.1.9.3	Submerged arc weld ng	46
2.1.9.4	Oxyacetylene welding	47

2.1.9.5	Resistance spot welding	48
2.1.9.6	Resistance seam welding	49
2.1.9.7	Projection welding	51
2.1.10	High energy density welding	52
2.1.10.1	Plasma arc welding	52
2.1.10.2	Electron beam welding	52
2.1.10.3	Laser beam welding	54
2.2	Materials	55
2.2.1	Galvanising	55
2.2.2	Application of zinc coating on steel	56
2.2.2.1	Hot dip galvanising	56
2.2.2.2	Electrogalvanising	57
2.2.2.3	Zinc spraying	58
2.2.2.4	Sherardising	58
2.2.2.5	Zinc rich primers	59
2.2.3	Additional properties of galvanised steel	59
2.2.3.1	Formability	60
2.2.3.2	Weldability	60
2.2.3.3	Paintability	60
2.2.3.4	Phosphating	61
2.2.3.5	Surface finish	61
2.2.4	Types of zinc coatings are available	61
2.2.4.1	One side galvanised steel	62
2.2.4.2	One and half side galvanised steel	62
2.2.4.3	Two side galvanised steel	63
2.2.4.4	Two side galvannealed steel	64
2.2.4.5	Iron-zinc alloy electroplated steel	64
2.2.4.6	Zinc-nickel coated steel	64
2.2.4.7	Galfan coating	65
2.2.4.8	Zn-Fe/Zn-Ni double layer electroplated steel sheet	65
2.2.4.9	Zn-Cr-CrO_X (Zincrox) electrogalvanised steel	66

2.2.5	Utilisation of zinc coated steel	66
2.2.5.1	Zinc coated steel in the automotive industry	67

Chapter 3

Design and Operation of the Equipment and Experimental Strategy

3.1	Introduction	72
3.2	Design and Working Principle of CO_2 Laser	72
3.2.1	Working principle of CLL laser	72
3.2.1.1	The effect of discharge current	75
3.2.1.2	The effect of tube pressure	76
3.2.1.3	The effect of gas composition	76
3.2.1.4	The effect of cavity optics	76
3.2.2	Working principle of AVCO laser	77
3.2.3	Working principle of UTRC laser	80
3.2.4	Working principles of MLI laser	82
3.2.5	Working principles of Ferranti laser (MF400)	83
3.3	Operation of the equipment	84
3.3.1	Focussing assembly and the estimation of focal point for CLL Laser	84
3.3.2	Beam alignment	87
3.3.3	Work tables	88
3.3.3.1	The X-Y hydraulic table	88
3.3.3.2	The CNC X-Y table and Z-Ax's moving optics	89
3.3.4	Powder feeding	90
3.3.5	Workpiece shielding	91
3.3.6	Overcoming the plasma prob em	92
3.4	Experimental strategy	92
3.4.1	Double pass welding	94
3.4.2	End edge welding	94
3.4.3	Gap welding	94

3.4.4	Welding with modification of the weld bead composition	94
3.4.4.1	Welding with metal powder injection	95
3.4.4.2	Welding using a side blown gas assist jet	95
3.4.4.3	Incorporation of metal powder just after welding	95
3.4.5	Lap welding using various laser beam modes	95
3.5	Evaluation and testing	97
3.5.1	Metallography	97
3.5.2	Optical microscopy	98
3.5.3	Scanning electron microscopy	98
3.5.4	Joining efficiency	98
3.5.5	Melting efficiency	99
3.5.6	Specific energy	100
3.5.7	Measurement of fusion zone area	100
3.5.8	Weld quality	100
3.5.9	Tensile testing	101
3.5.10	Microhardness measurement	101
3.5.11	Impact testing	102
3.5.12	Fatigue testing	102
3.5.13	Corrosion testing	102
3.5.13.1	Polarisation technique	102
3.5.13.2	Galvanic coupling technique	102
3.6	Design and manufacturing of press tool for setting gap size	103

Chapter 4

Processing Techniques - Results and Discussions

4.1	Introduction	106
4.2	Laser welding of zinc coated steel	106
4.2.1	Techniques used for welding zinc coated steel sheet	108
4.2.1.1	Double pass welding	108
4.2.1.2	End edge welding	112

4.2.1.3	Gap welding	115
4.2.1.3.1	Effect of gap size on welding performance of zinc coated steel	116
4.2.1.3.2	Effect of gap size on weld penetration and width	119
4.2.1.4	Welding with a side blown gas assist jet	123
4.2.1.4.1	Effect of assist gas jet velocity on weld penetration	124
4.2.1.5	Welding with modification of the weld bead composition	126
4.2.1.5.1	Welding with metal powder injection	127
4.2.1.5.2	Welding with redeposit on of volatilised zinc	133
4.2.1.5.3	Incorporation of metal powder just after welding	136
4.3	Weld quality assessment	142
4.4	Assessments of results on welds made by using dimples as a method of setting the gap size	146
4.4.1	Welding using fast axial flow CLL laser	146
4.4.1.1	Tests using plastic resin to assess gap size	146
4.4.1.2	Welds made using dimples as a method of setting the gap size	148
4.4.1.3	Welds produced with dimples between the sheets	148
4.4.1.4	Welds made by passing the beam over the dimples	149
4.4.1.5	Quality of the welds	149
4.4.2	Welding using laser at RTM laser centre	150
4.4.2.1	Welds made using dimples as a method of setting the gap size	150
4.4.2.2	Welds produced with dimples between the sheets	150
4.4.2.3	Welds made by passing the beam over the dimples	151

Chapter 5

Processing - Results and Discussions

5.1	Introduction	157
5.2	Welding using various lasers	157
5.2.1	Welding using fast axial flow CLL laser with doughnut beam mode	158
5.2.1.1	Effect of laser power on penetration	159

5.2.1.2	Effect of welding speed on penetration and width	160
5.2.1.3	Influence of laser beam polarisation in welding	164
5.2.2	Welding using SF/FAF oscillator/amplifier system with Gaussian beam mode	172
5.2.3	Welding using AVCO laser with multimode beam	175
5.2.4	Welding using MLI laser with ring type beam mode	178
5.2.5	Welding using UTRC laser with a top hat beam mode	179
5.3	Efficiencies	180
5.3.1	Melting efficiency	180
5.3.2	Joining efficiency	185
5.3.3	Effect of gap size on joining and melting efficiency	193
5.4	Mechanical tests	193
5.4.1	Tensile tests	194
5.4.2	Hardness measurement	197
5.4.3	Mechanical testing by collaborating partners	198
5.4.3.1	Impact testing	198
5.4.3.2	Fatigue test at Renault Motors	205
5.4.3.3	Fatigue test at CETIM	206

Chapter 6

The Gap Model for Welding Zinc Coated Steel

6.1	Introduction	212
6.2	The Gap Model	212
6.3	Application of the Model	220
6.4	How to use the model	239

Chapter 7

Corrosion Studies

7.1	Introduction	241
7.1.1	The mechanism of sacrificial protection	243

7.1.2	Corrosion resistance of welded joints	250
7.2	Experimental	251
7.2.1	Corrosion testing	251
7.2.1.1	Linear polarisation test	251
7.2.1.2	Galvanic coupling test	255
7.3	Results and discussion	257
7.3.1	Linear polarisation test	257
7.3.2	Galvanic coupling test	272
7.4	The corrosion morphology of laser welded zinc coated steel	280

Chapter 8
Conclusions and Future Work

8.1	Conclusions	285
8.1.1	Welding zinc coated steel	285
8.1.2	The formula for welding zinc coated steel	286
8.1.3	Effect of welding parameters	287
8.1.4	Modification of weld composition	290
8.1.5	Corrosion Tests	290
8.2	Suggestion for future work	291
	References	292
	List of publications	308
	Appendices	309

Figure Captions

Figure 2.1 (a) Three modes of vibration in CO_2 molecule.

(b) Energy-level diagram of CO_2.

Figure 2.2 Operational regimes for laser materials processing.

Figure 2.3 (a) Weld bead penetration as a function of laser power at various welding speeds.

(b) Minimum power for efficient welding.

Figure 2.4 Penetration depth of laser welds as a function of beam power for 316 stainless steel.

Figure 2.5 Transverse mode pattern in cylindrical symmetry.

Figure 2.6 The reflectivity of some metals (Fe, Al), a semiconductor (Si), and rock salt (NaCl) as a function of electromagnetic wavelength. The data corresponds to normal incidence and 20° C.

Figure 2.7 Narrowest weld is produced when penetration is maximum. Laser power 1.5 kW, Welding speed 50 in/min, focal length of the lens 2.5 in, all dimension are in inches,material 1018 steel.

Figure 2.8 Transverse profile as a function of focus position (Material 310, power 5 kW, speed 16 mm/s).

Figure 2.9 (a) The measured reflectivity at different laser beam intensities show a sharp decrease at the threshold intensity for plasma formation.

(b) The welding depth verses laser intensity demonstrate a sharp increase above a critical intensity. the threshold of welding depth corresponds to the threshold intensity for the formation of a laser induced plasma.

Figure 2.10 Welding depth versus welding speed at various laser intensities.

Figure 2.11 Laser welding 430 stainless steel, penetration versus speed at various powers.

Figure 2.12 Laser power required for welding A36 steel at different speeds.

Figure 2.13 Welding speed against power for Culham/Ferranti 5 kW CO_2 laser.

Figure 2.14 Measured relation between gas flow and welding depth.

Figure 2.15 Relation between welding velocity and penetration depth determined with various shielding gases.

Figure 2.16 Clamping and tolerances for (a) butt joint, and (b) lap joint; dimensions are in units of material thickness t.

Figure 2.17 Gap size, Z, versus shear stress, P_{sh}, tensile stress, P_s, diameter of the fusion zone, D, and depth of penetration of the bottom plate, Δ, for steel 47NKhR + Ni joint.

Figure 2.18 Strength of spot welded lap joints in 1Kh18N9T steel versus gap between the sheets. In every case the thickness of lower sheet was 0.5 mm and with different upper sheet thicknesses 1 - δ = 0.3 mm, 2 - δ = 0.2 mm, 3 - δ = 0.1 mm.

Figure 2.19 Surface roughness of a welding seam.

Figure 2.20 A cross section perpendicular to the laser beam path through the melt in the steady state condition.

Figure 2.21 Weld pool shapes in order of increasing travel speed.

Figure 2.22 Discontinuity regions in power versus travel speed for 0.01-in thick type 304 stainless steel.

Figure 2.23 Laser supported combustion (LSC) wave.

Figure 2.24 Plasma formation above steel surface.

Figure 2.25 Processing diagram for laser welding.

Figure 2.26 Streak photograph of the laser induced plasma during the welding process with a cw CO_2 laser. Strong plasma fluctuations are visible.

Figure 2.27 Radiation and sound emission measured during welding w th 100 Hz pulse frequency.

Figure 2.28 Schematic representation of the keyhole.

Figure 2.29 Dynamic model for penetration welding.

Figure 2.30 Shielded metal arc welding.

Figure 2.31 Gas metal arc welding.

Figure 2.32 Submerged arc weld'ng.

Figure 2.33 Oxyacetylene welding.
Figure 2.34 Resistance spot welding.
Figure 2.35 Resistance seam welding.
Figure 2.36 Projection welding process.
Figure 2.37 Plasma arc welding.
Figure 2.38 Electron beam welding.
Figure 2.39 Laser beam welding.
Figure 2.40 Hot dip galvanising process.
Figure 2.41 Electrogalvanising process.
Figure 2.42 Types of galvanised coatings [31]. Where OSGS; One Side Galvanised Steel, 2SGS; 2 Side Galvanised Steel, and 1-1/2 SGS; One and a Half Side Galvanised Steel.
Figure 2.43 Body structure of Peugeot 309 showing the zinc coated parts.
Figure 2.44 Typical automotive body panels fabricated from metallic coated steels.

Figure 3.1 Design and flow diagram of 2kW Control Laser Ltd.
Figure 3.2 The essential parts of AVCO HPL Industrial Laser.
Figure 3.3 AVCO laser channel schematic.
Figure 3.4 Schematic diagram of three module UTRC laser.
Figure 3.5 Beam transfer schematic.
Figure 3.6 Schematic diagram of MLI laser.
Figure 3.7 Slow axial flow CO_2 laser (Ferranti).
Figure 3.8 Schematic of laser layout.
Figure 3.9 Beam print obtained by passing the laser over an inclined perspex sheet to estimate the focal point position and the spot size of the beam.
Figure 3.10 CNC control working table at Liverpool University.
Figure 3.11 Design and features of powder feeding system.
Figure 3.12 The arrangement of gas shielding of the workpiece and plasma removal.

Figure 3.13 Beam prints obtained from various lasers.

Figure 3.14 Tensile test specimen.

Figure 3.15 Design of press tool and die (section view).

Figure 3.16 Clamping system for welding zinc coated steel in lap configuration.

Figure 4.1 Laser welding of zinc coated steel into two tightly clamped sheets in lap configuration shows explosive ejection of molten metal and zinc vapour.

Figure 4.2 A lap weld made by laser into two sheets of zinc coated steel tightly clamped, showing serious disruption of the weld.

Figure 4.3 Longitudinal cross section of a lap weld made by tightly clamping two zinc coated sheets together showing a lot of porosities in the weld.

Figure 4.4 Double pass welding.

Figure 4.5 The weld bead after second pass show the serious disruption of the weld due to zinc vapour ejection for the keyhole.

Figure 4.6 A weld bead showing three phenomenon (a) the plasma blocking of the laser beam, (b) weld bead pitting due to the ejection of zinc vapour from the keyhole, and (c) a sound weld bead.

Figure 4.7 Cross section of the weld (a) very little penetration due to plasma blocking of the beam, (b) undercut or pitting due to ejection of zinc vapour from the keyhole and (c) sound weld with full penetration of the beam to the bottom sheet.

Figure 4.8 End edge welding.

Figure 4.9 Three possible ways in which the beam can strike the end edge of the specimen.

Figure 4.10 Two kinds of welds normaly obtained using the end edge welding technique (a) weld with p'tting in the surface, and (b) sound and good quality weld.

Figure 4.11 The microsections of welds (a) zero gap between the sheets lead to a weld showing pits on the surface, and (b) the presence of a gap

between the two sheets gave a good quality weld.

Figure 4.12 Welding with a fixed gap formed by spacers between the two sheets.

Figure 4.13 Welding with a variable gap between the sheets.

Figure 4.14 The effect of gap between the overlapped sheets on welding performance of zinc coated steel.

Figure 4.15 Surface tension pulls the molten metal towards the edges if width of the weld is greater than the sheet thickness.

Figure 4.16 The weld bead during a single run at four different areas starting from zero gap to a larger gap of 0.4 mm.

Figure 4.17 The microsections of the weld at four point with increasing gap size. Laser power; 1 kW, welding speed; 15 mm/s; sheet thickness 0.7 mm, gap; (a) 0.0, (b) 0.09, (c) 0.15, (d) 0.28.

Figure 4.18 Penetration and width of the weld as a function of gap size. Laser power,1.00 kW, welding speed, 15 mm/s.

Figure 4.19 Laser welding with side blown gas assist gas.

Figure 4.20 Weld penetration as a function of side blown gas jet velocity. Laser power,2 kW, welding speed, 33 mm/s.

Figure 4.21 Dependence of penetration depth on gas flow rate.

Figure 4.22 Schematic diagram showing the incorporation of metal powder in the weld bead.

Figure 4.23 The weld microstructure with metal powder injection (a) normal weld, (b) nickel injected weld, (c) stainless steel injected weld and (d) tool steel injected weld.

Figure 4.24 The photograph showing the redeposition of volatilised zinc on the weld bead.

Figure 4.25 The EDAX analysis on weld bead at different flow rates of argon gas from the side jet. The peak height of zinc increases with increase in flow rate of gas from (a) to (e).

Figure 4.26 The part of a weld bead and the surrounding zinc coating in the form of lumps as a result of redeposition of volatilised zinc.

Figure 4.27 The EDAX analysis on the lumps around the weld shows that it mostly

consists of zinc w'th a small amount of iron also present.

Figure 4.28 The weld bead obtained as a result of tool steel powder incorporation just after welding.

Figure 4.29 The weld microstructure showing a coating of tool steel has been produced at the top surface during the incorporation of powder during the welding operation.

Figure 4.30 (a) Cross section of a weld with zinc powder incorporation just after welding, laser power; 1.8 kW, welding speed; 25 mm/s, flow rate of zinc powder; 17 g/min, gap; 0.14 mm.
(b) Cross section of a weld with zinc powder incorporation just after welding, laser power; 1.8 kW, welding speed; 25 mm/s, flow rate of zinc powder; 13 g/min, gap; 0.08 mm.

Figure 4.31 Zinc coating obtained as a result of zinc powder incorporation just after weld formation (a) at the weld surface, (b) at the heat affected zone.

Figure 4.32 Weld quality vs gap size for double pass welding using doughnut beam mode. Laser power; 2 kW.

Figure 4.33 Weld quality against gap size for nickel injection weld using doughnut beam mode. Laser power; 2 kW.

Figure 4.34 Weld quality vs gap size for Gaussian beam mode. Laser power 1 kW.

Figure 4.35 Weld quality against gap size for multi mode beam. Laser power 3 kW.

Figure 4.36 Weld quality against gap size for multimode beam. Laser power 5 kW.

Figure 4.37 Weld quality against gap s ze for multi mode beam. Laser power 8 kW.

Figure 4.38 Graph of pits per 100mm weld length vs gap using dimples as a method of setting the gap size.

Figure 4.39 Lap welding of zinc coated steel (a) with dimples to produce a gap between the sheets, (b) by passing the beam over the dimples.

Figure 4.40 Weld bead of specimen RM-9, laser power 1kW, welding speed 21

mm/s.

Figure 4.41 Weld bead of specimen RM-11, laser power 1kW, welding speed 21 mm/s.

Figure 4.42 Cross section of weld RM-9, laser power 1kW, welding speed 21 mm/s.

Figure 4.43 Cross section of weld RM-3, laser power 1kW, welding speed 25 mm/s.

Figure 4.44 Weld bead of specimen RM-3, laser power 1kW, welding speed 25 mm/s.

Figure 4.45 Weld bead of specimen RM-6, with laser beam passing over the dimples, laser power 1kW, welding speed 16.7 mm/s.

Figure 4.46 Weld bead of specimen RM-12, with laser beam passing over the dimples, laser power 1kW, welding speed 21 mm/s.

Figure 4.47 Welds cross section of specimen RM-6, laser power 1kW, welding speed 16.7 mm/s.

Figure 5.1 The beam profile of CLL laser.

Figure 5.2 Typical weld profile defining the depth and width of a weld.

Figure 5.3 Typical curve of laser power against penetration at constant welding speed of 56 mm/s. Sheet thickness 1.5 mm.

Figure 5.4 Typical hyperbolic curve for welding speed against weld penetration and width at laser power 1.60 kW. Bead on plate welding.

Figure 5.5 Weld penetration and width as a function of welding speed in double pass welding. Sheet thickness; 0.875 mm.

Figure 5.6 Weld penetration and width as a function of welding speed in side jet welding experiment. Sheet thickness; 0.7 mm.

Figure 5.7 Weld penetration and width as a function of welding speed for nickel injected weld.

Figure 5.8 Weld penetration and width as a function of welding speed for stainless steel injected weld.

Figure 5.9 Weld penetration and width as a function of welding speed for tool

steel injected weld.

Figure 5.10 Correlation between laser beam polarisation and the reflection at a metal surface as a function of the incident angle.

Figure 5.11 Cutting kerfs using p-polarised and s-polarised beam. Where V is cutting direction and P is plane of polarisation.

Figure 5.12 Influence of beam polarisation in welding with 5 kW laser power.

Figure 5.13 Penetration against the welding speed for p-polarised and for s-polarised beam under same welding conditions, laser power 1.77 kW.

Figure 5.14 Weld width against welding speed for p-polarised and s-polarised beam under same welding conditions. Laser power; 1.77 kW.

Figure 5.15 The weld microsections at various welding speeds using p -polarised beam.

Figure 5.16 The weld microsections at various welding speeds using s - polarised beam.

Figure 5.17 Experimental arrangement of SF/FAF oscillator amplifier, producing pure Gauss an beam.

Figure 5.18 The Gaussian beam profile.

Figure 5.19 Weld penetration and width as function of welding speed.

Figure 5.20 The beam profile of AVCO laser.

Figure 5.21 Weld penetration and width as a function of welding speed.

Figure 5.22 Weld penetration and width as a function of welding speed.

Figure 5.23 Weld penetration and width as a function of welding speed.

Figure 5.24 The beam profile of MLI laser.

Figure 5.25 Welding speed against penetration and width for MLI laser. Laser power;5.8 kW, sheet thickness 0.7 mm.

Figure 5.26 The beam profile of MLI laser.

Figure 5.27 Welding speed against penetration and width for UTRC laser. Laser power 2 kW.

Figure 5.28 Melting efficiency against welding speed. Laser power; 1.62 kW, sheet thickness 1.5 mm.

Figure 5.29 Welding speed against melting efficiency. Laser power; 2kW, sheet thickness 0.875 mm.

Figure 5.30 Welding speed against melting efficiency. Laser power; 2kW, sheet thickness 0.7 mm.

Figure 5.31 Welding speed against melting efficiency. Laser power; 1.77 kW, sheet thickness 0.7 mm.

Figure 5.32 Welding speed against melting efficiency. Laser.power; 2 kW, sheet thickness 0.7 mm.

Figure 5.33 Welding speed against melting efficiency. Laser power; 2 kW, sheet thickness 0.7 mm.

Figure 5.34 Welding speed against melting efficiency. Laser power; 1.54 kW, sheet thickness 0.7 mm.

Figure 5.35 Welding speed against melting efficiency. Laser power; 1 kW, sheet thickness; 0.7 mm.

Figure 5.36 Welding speed against melting efficiency. Laser power; 2 kW, sheet thickness 0.7 mm.

Figure 5.37 Welding speed against melting efficiency. Laser power 5.8 kW, sheet thickness 0.7 mm.

Figure 5.38 Welding speed against melting efficiency for AVCO high power laser. Sheet thickness; 0.7 mm.

Figure 5.39 Weld penetration against 1/V for bead on plate weld. Laser power 1.60 kW.

Figure 5.40 Plot of penetration T, against reciprocal of speed, 1/V, for double pass welding.

Figure 5.41 Penetration as function of 1/V, side jet welding technique. Laser power 2.00 kW.

Figure 5.42 Penetration against 1/V for p-polarised and s-polarised beam under same welding conditions, laser power, 1.77 kW.

Figure 5.43 Plot of penetration T, against reciprocal of speed, (1/V), for nickel injected weld.

Figure 5.44 Plot of penetration T, against reciprocal of speed, (1/V), for stainless steel injected weld.

Figure 5.45 Plot of penetration T, against reciprocal of speed, 1/V, for Gaussian beam mode.

Figure 5.46 Plot of penetration T, against reciprocal of speed, 1/V, for 3kW Multimode beam.

Figure 5.47 Plot of penetration T, against reciprocal of speed, 1/V, for 5 kW Multimode beam.

Figure 5.48 Plot of penetration T, against reciprocal of speed, 1/V, for 8 kW Multimode beam.

Figure 5.49 Penetration against 1/V. Laser power 5.8 kW.

Figure 5.50 Penetration against 1/V for UTRC laser.

Figure 5.51 Joining efficiency against melting efficiency for different techniques in welding zinc coated steel by using Control Laser Limited (CLL).

Figure 5.52 Joining efficiency against melting efficiency at higher power for AVCO laser.

Figure 5.53 Joining efficiency against melting efficiency for various lasers used.

Figure 5.54 Joining and melting efficiency as a function of gap size for a constant welding speed of 15 mm/s. Laser power, 1.00 kW.

Figure 5.55 Specimens after tensile test.

Figure 5.56 The hardness of fusion zone and heat affected zone as a function of welding speed.

Figure 5.57 Design of box sections. Where b = 50.5, c = 30 mm, and d = 15 mm.

Figure 5.58 The static collapse mode of the box section, (a) front view and (b) side view of the same specimen.

Figure 5.59 The dynamically crushed specimen arranged from left to right with increasing impact energy, (a) front view and (b) side view of the same specimen.

Figure 5.60 The collapse mode affects the energy absorption capability of the box section, (a) front view and (b) side view of the same specimen.

Figure 5.61 Absorbed energy against axial deflection.

Figure 5.62 Velocity against time.

Figure 5.63 S-N diagram corresponding to each welding conditions.

Figure 5.64 View of the fatigue machine at CETIM.

Figure 5.65 Welding configurations for fatigue tests.

Figure 5.66 Fatigue life for various weld configurations (σ_{max} = 100 M Pa).

Figure 6.1 The diagram representing the welding of zinc coated steel sheet with a small gap at the interface between the two sheets.

Figure 6.2 The model representing (a) the points of pressure variation and (b) the new boiling zinc position.

Figure 6.3 Photographs showing that the two sheets are pulled together due to the escape of the zinc vapour at the interface, and due to the condensation of the vapour.

Figure 6.4 Plot of gap, g, against $Vt_{zn}/(t_p)^{1/2}$ shows a straight line.

Figure 6.5 Plot of experimental and theoretical results for minimum gap size against $Vt_{zn}/(t_p)^{1/2}$.

Figure 6.6 Micrographs showing the effect of gap size on weld profile.

Figure 6.7 Data points plotted for g/t_p against $AVt_{zn}/(t_p)^{3/2}$.

Figure 6.8 Data points plotted for g/t_p against $AVt_{zn}/(t_p)^{3/2}$ for welds with different sheet thickness, and different zinc coating thickness.

Figure 6.9 The weld pool schematic during shrinkage.

Figure 6.10 Plot of g/tp against AVtzn/(tp)$^{3\ 2}$ for three kinds of welds (i) sound welds (ii) welds showing pitting and (iii) drop out welds.

Figure 7.1 Anodic and cathodic Tafel curves for corrosion of metal M showing the principle of cathodic protection.

Figure 7.2 Schematic mixed potential diagram for a zinc-steel couple in aerated salt water solution.

Figure 7.3 Mechanism of corrosion rate increase from i_{corr} to $i'_{corr} = i_{scr}$ on scribed specimen in deaerated solution.

Figure 7.4 Schematic diagram of corrosion cell for measuring polarisation.

Figure 7.5 Typical plot for polarisation at potential close to E_{corr}.

Figure 7.6 Schematic diagram for measuring the flow of current from zinc coating to the steel weld and to determine the Evans diagram.

Figure 7.7 Anodic polarisation curve for zinc coated steel sheet.

Figure 7.8 Cathodic polarisation curve for zinc coated steel sheet.

Figure 7.9 Typical data for polarisation of zinc coated steel sheet at potential close to E_{corr}.

Figure 7.10 Polarisation resistance vs time for unwelded (UNW) and normal welded (NRM) specimens.

Figure 7.11 Corrosion current vs time for unwelded (UNW) and normal welded (NRM)specimens.

Figure 7.12 Rest potential vs time for unwelded (UNW) and normal welded (NRM) specimens.

Figure 7.13 Corrosion current vs time for unwelded (UNW), normal welded (NRM) and nickel injected weld (NKL) specimens.

Figure 7.14 Rest potential vs time for unwelded (UNW), normal welded (NRM) and nickel injected weld (NKL) specimens.

Figure 7.15 Corrosion current vs time for unwelded (UNW), normal welded (NRM) and stainless steel injected weld (SST) specimens.

Figure 7.16 Rest potential vs time for unwelded (UNW), normal welded (NRM) and stainless steel injected weld (SST) specimens.

Figure 7.17 Corrosion current vs time for unwelded (UNW), normal welded (NRM) and tool steel injected weld (TST) specimens.

Figure 7.18 Rest potential vs time for unwelded (UNW), normal welded (NRM) and tool steel injected weld (TST) specimens.

Figure 7.19 Corrosion current vs time for unwelded (UNW), normal welded (NRM) and tool steel coated weld (TSTA) specimens.

Figure 7.20 Rest potential vs time for unwelded (UNW), normal welded (NRM) and tool steel coated weld (TSTA) specimens.

Figure 7.21 Corrosion current vs time for unwelded (UNW), normal welded (NRM) and zinc incorporated weld (ZIC).

Figure 7.22 Rest potential vs time for unwelded (UNW), normal welded (NRM) and zinc incorporated weld (ZIC).

Figure 7.23 Corrosion current against time of heat affected zone Fe-Zn alloy, compared with unwelded (UNW) and normal welded (NRM) specimen. Exposed heat affected zone 0.6 cm^2.

Figure 7.24 Rest potential against time of heat affected zone Fe-Zn alloy, compared to unwelded (UNW) and normal welded(NRM) specimen. Exposed heat affected zone 0.6 cm^2.

Figure 7.25 Corrosion current vs time for unwelded (UNW), normal welded (NRM) and zinc powder incorporated weld (ZPI).

Figure 7.26 Rest potential vs time for unwelded(UNW), normal welded (NRM) and zinc powder incorporated weld (ZPI).

Figure 7.27 Current variation with time for coupled zinc coating and normal steel weld (NRM).

Figure 7.28 Evans diagram for coupled zinc coating and normal steel weld (NRM) after24 hr exposure.

Figure 7.29 Evans diagram for coupled zinc coating and weld with injection of nickel powder (NKL) after 24 hr exposure.

Figure 7.30 Evans diagram for coupled zinc coating and weld with injection of stainless steel powder (SST) after 24 hr exposure.

Figure 7.31 Evans diagram for coupled zinc coating and weld with injection of tool steel powder (TST) after 24 hr exposure.

Figure 7.32 Evans diagram for coupled zinc coating and weld with tool steel powder incorporation (TSTA) after 24 hr exposure.

Figure 7.33 Evans diagram for coupled zinc coating and weld with zinc vapour incorporation (ZIC) after 24 hr exposure.

Figure 7.34 Evans diagram for coupled zinc coating and weld with zinc powder incorporation (ZPI) after 24 hr exposure.

Figure 7.35 Current variation with time for coupled zinc coating and different

modified composition welds.

Figure 7.36 Laser welded zinc coated steel specimen before corrosion.

Figure 7.37 Intermetallic zinc-iron alloy formed at HAZ at steel-zinc coating contact point.

Figure 7.38 Zinc coating on steel far from the weld, no evidence of intermetallic compound.

Figure 7.39 Laser welded zinc coated steel specimen after the corrosion of zinc coating revealed intermetallic Fe-Zn alloy (black layer).

Figure 7.40 The schematic diagram representing the formation of intermetallic as a result of welding of the zinc coated steel sheet.

Figure 7.41 SEM analysis on intermetallic (black) layer showing the presence of zinc-iron alloy.

Figure 7.42 The SEM analysis in Figure 7.34 on a patch showing that the intermetallic alloy started corroding.

Chapter 1

Introduction

1.1 Introduction

In 1975 the annual cost of iron loss in the world on account of corrosion was ≈ £ 20,000 m ; it is therefore not surprising that great efforts were made to reduce this. One of the more common methods adopted is the application of a zinc coating and ≈ 2 million tons of zinc were used annually for this purpose [1]. More recent figures [2] show that the Western world currently uses about 4.5 million tons of primary zinc each year for various applications, and 2.2 million tons of zinc are used worldwide each year for coatings.

Zinc coated steel is an important commercial material. It is relatively cheap and yet due to the cathodic protection afforded by zinc it is durable. Its uses are mainly in the automobile industry but they also extend to nearly all sheet metal industries such as those making domestic appliances, doors and ventilating systems.

Zinc coated steel is solidly established as the choice material for combating against corrosion in the automobile bodies. Manufacturers have for a long time used surface-finished sheet which, plus paint, has held rust at bay. However, the demand for rust proofing is now so strong that the undersides of cars are required to be made of surface-protected material as well. This means above all for private cars: steel sheet zinc coated on both sides.

The use of galvanised steel has increased from underbody members to the exterior panels. Today most cars contain some coated steel, the type of zinc coating will vary with location on the car. The main movement for the introduction of this

material into the standard ranges of cars has been since 1975 when consumer pressure in the States in particular demanded a longer cosmetic life than 18 months. Today our cars are expected to be corrosion protected cosmetically for 5 years and perforation protected for 10 years. This is possible thanks to coated steels.

Fortunately zinc coated steel in its many forms is doing an outstanding job of reducing both perforation and cosmetic corrosion. It offers a two-fold corrosion protection mechanism [3-5]. The zinc coating initially keeps the corrosive environment away from the steel surface, should the coating become perforated and moisture reach the exposed steel surface, the zinc coating becomes sacrificial and cathodically protects the exposed steel until the adjacent zinc is consumed in the electrolytic cell reaction. The protective property of zinc is not limited to its sacrificial action but also may provide mechanical blocking of corrosion sites, such as small cracks or gaps in the coating, by precipitation of the corrosion products of zinc.

Zinc coated steel is produced in a variety of ways, from the traditional hot dip galvanizing, through controlled thickness electrolytic single or double sided sheet, to multi layer deposits of Zn/Ni, Zn/Al (ZINCAL), Chrome/Chrome oxide (ZINCROX), electrolytic Zn/Mn and even ZnCoW. Methods of coating includes hot dip galvanising, spraying, electroplating, sherardizing, and painting with zinc rich paints; the advantage and disadvantages of these methods have been outlined by Porter [1].

However welding zinc coated steel poses many problems due to the marked differences in the physical and mechanical properties of the two metals. The difficulty of welding zinc coated steel by conventional means arises from the high surface resistance of the coating which causes overheating and splash in a conventional resistance seam welding process. Some improvements were obtained with preventive measures. For example, in seam welding of coated steels, the coating was being picked-up by the electrode which resulted in a variable resistance between the electrode and the component to be welded thereby giving rise to a variable heating effect and inconsistent weld quality. This problem was overcome by constantly

presenting an uncontaminated copper electrode to the workpiece. However, in doing so overheating of the copper electrode occured and the picking up of the zinc coating formed a series of complex brasses which led to cracking of the weld [6,7].

Other conventional techniques such as arc welding [8], shielded metal arc welding, gas metal arc welding, submerged arc welding or oxyacetylene welding [9] suffer from similar problems. Arc welding is particularly difficult due to the interference of the zinc vapours with the arc stability which also reduces the electrode life. However resistance spot welding is normally used in automatic welding of car bodies. Approximately 80% of welds in an automobile are resistance spot welds [4]. When welding zinc coated steel in lap configuration, the zinc at the interface between the two sheets melts and due to the electrode pressure the zinc is squeezed out of the weld area before the weld is formed. But this is a slow process and hence there is a need to develop a welding system which can more efficiently weld zinc coated steel.

An alternate technique which would allow high speed welding and crack free welds would obviously be beneficial. A possible alternate process which could be applied for welding of zinc coated steel is laser welding. This process is of great interest to the automobile industry. In this process, the heat necessary is not developed as a result of the basic electrical resistance of the material but is supplied directly from the energy of the laser beam.

Laser beams have now been used in a great variety of areas: for example they are used to measure, to cut many types of materials and also for welding. Many of the industries using zinc coated steel are also highly mechanised and value the possibilities of automatic or robotic processing as well as enhancing the production speed. These are two of the main advantages that laser offer over most competing processes. It is thus interesting to study the possibilities of welding this material with a laser.

1.2 Application of Lasers in Welding

The word "LASER" is an acronym for Light Amplification by Stimulated Emission of Radiation. The laser light travels in a single direction, forming a straight, nearly parallel beam of concentrated light which keeps its intensity, even over long distances. Some lasers generates visible light but others generate infrared or ultraviolet rays which are invisible.

Since lasers were invented twenty nine years ago, in 1960, the state of laser technology has advanced to the availability of multikilowatt lasers. The development of these lasers provide a reliable source of high average and peak powers. A laser beam is a source of optical frequency radiation which is monochromatic (i.e of one wave length), coherent (all waves in the cross section of the beam are in phase and have very little divergence).

Until the 1970's, the application of laser in welding had been mostly for precision work within the micro industry (i.e electronic components for printed circuits) [10]. Due to the increasing powers available the lasers application in the welding process has increased to a great extent.

More recently the automobile industry has invested in lasers for performing welding tasks, where once electron beam welding (EBW) would have been the natural choice. Now lasers (due to their minimum heat input) are taking over their role frequently, where low distortion welding is called for. Both laser welding and EBW are non-contact fusion processes in which a beam is finely focused to penetrate to a controlled depth. The main advantages of the laser over EBW is that the laser doesn't require a soft vacuum, also a laser can be used at more than one work station.

Lasers are now finding production line application in industrial environments. The laser is an industrial tool capable of producing intense heat in a material during laser-material interaction. The heat produced during the interaction can be used as

an energy source for material processing. Material processing applications for lasers are growing rapidly. They include welding, cutting, heat treatment, surface modification, cladding, alloying, surface marking, hole drilling etc.

The unfocussed raw output of the laser generally does not provide sufficient power density to raise the temperature of most materials above their melting or boiling points, but with a focussed beam rapid heating and melting can be achieved.

A general model depicting a laser processing application would include the following:

(i) the laser,

(ii) optics to direct and focus the raw beam onto the sample being worked,

(iii) the material itself.

The parameters of the laser beam are:

(i) total power and power stability,

(ii) power distribution or "mode",

(iii) wavelength,

(iv) beam diameter.

The main characteristics of the focussing optics are:

(i) focal length,

(i) tendency to spherical aberration, cleanliness,

(i ı) location of the focus.

The main properties of the workpiece and workstation are:

(i) surface reflectivity,

(i) traverse speed,

(ii') thermal diffusivity.

Many researchers have studied the effect of these parameters on materials processing (for details see chapter 2).

1.3 Laser Welding

In automotive industries, lasers are widely used in production for welding and cutting of sheet metals. The advantages offered by lasers are speed, quality, increased productivity and, therefore, reduced cost. Lasers provide a broader range of design possibilities and manufacturing methods, compared to tungsten inert gas (TIG), electron beam (EB), manual metal arc (MMA), or plasma methods.

In most welding processes the energy is deposited at the surface of the material and is brought into the interior by conduction, but in laser and electron beam welding the energy is deposited in a deep and narrow cavity which is created by the incident high intensity beam.

When a laser beam is focussed onto an opaque metal surface the radiant energy will be utilised in four principle ways:

(i) reflected,
(ii) absorbed and used in melting,
(iii) absorbed and used in vaporisation,
(iv) absorbed and used in conduction.

When a focussed beam of sufficient power is incident on a metal surface "keyholing" occurs [11...19]. The metal is initially highly reflective for 10.6 μm wavelength CO_2 laser radiation. But a small fraction of the energy is absorbed in the metal thus heating it. As the metal gets hotter the reflectivity decreases and the metal absorbs more of the radiation incident on it. As more energy is absorbed, the metal heats to the point where it melts and moves by surface tension forces. As the temperature increases, due to the interaction of the beam, vapourisation takes place.

This creates a hole in the material, called a keyhole. The keyhole acts as a black body and absorbs all the incoming laser radiation. The keyhole is filled with metal vapour. The pressure of the metal vapour keeps the hole open. As the substrate is moved relative to the laser beam the keyhole moves through the material and the molten metal flows from the front to the back of the keyhole where it resolidifies. The hole is completely surrounded by a layer of molten metal.

The power density required to produce keyholing in metal is in the range of 10^3 to 10^5 W/mm^2. At power densities below this range heating without extensive vaporisation occurs, not suitable for welding or cutting process which require keyholing. Above this range extensive vaporisation and particle-emission occurs which is undesirable.

1.4 Outline of the Problem of Welding Zinc Coated Steel

However, the laser welding of zinc coated steel has always presented a problem due to the low boiling point of zinc (906 °C) relative to the high melting point of steel (1530 °C). This mismatch is particularly important in lap welding where a zinc layer is present at the interface between the two sheets. Under these conditions the laser keyhole generates a very high vapour pressure in the zinc layer and there is an explosive ejection of zinc vapour from the keyhole which destroys weld continuity. Thus it is of great interest to develop a method of laser welding zinc coated steel to produce a satisfactory weld.

1.5 Materials

The materials used in this study were thin sheets of:

(i) uncoated mild steel of thickness 0.7 mm,

(ii) zinc coated steel of thickness 0.7 mm, with coating thickness 7.5 or

10 μm,

(iii) zinc coated steel of thickness 0.875 mm, with coating thickness 7 .5 μm,

(iv) zinc coated steel of thickness 0.55 mm, with coating thickness 10 μm.

The steel substrate was a BS 1449 extra deep drawing grade (CR2) with maximum composition limits (in weight percent) of C; 0.08, Mn; 0.45, S; 0.03, P; 0.025, Fe; balance [20]. The reason for choosing this material for investigation lies in the wide applications of the material for automotive industries.

1.6 Research Aims and Objectives

The present work on the welding of steel sheets is divided into the following sections:

1. A literature survey of the work done on laser welding by previous workers.
2. An experimental investigation to establish the optimum processing parameters involved in the welding of zinc coated steel sheets.
3. Survey of methods to solve the complex problem of welding zinc coated steel.
4. Comparison of the results obtained from different lasers.
5. A study of the quality of the weld bead obtained.
6. Construction of a model to simulate vapour exhaust from the weld bead - the gap model.
7. A study into the corrosion properties of the zinc coated sheet in the presence of exposed weld and to find a method to coat this exposed surface.

Chapter 2

Literature Review

2.1 Introduction

Since a number of scientific areas are involved in this study, the literature review is divided into two parts. The first part discusses the physics and types of lasers and the work done on laser welding by previous workers. The second part describes the galvanising process, types of zinc coating and the use of zinc coated steel in automobile industries.

In the past few years laser welding has become an acceptable and reliable processing tool for the manufacturing industry. It has found applications in areas where conventional processes are not able to perform work because of heat input, distortion, vacuum, location etc. Commercial laser welding systems are available with a few watts of pulsed 1.06 μm wavelength radiation from Nd-YAG laser to multi-kilowatts of continuous (cw) 10.6 μm wavelength radiation from a CO_2 laser. These systems are capable of melting nearly all types of metals and alloys.

Since the development of the high power CO_2 laser in the sixties, laser processing of materials has become a significantly important research field. Lasers provide an intense heat source which is very useful for welding, cutting, cladding, heat treatment etc. Each of these applications has now become a separate widespread research field. Hence in this part of the literature survey, no attempt is made to review the whole field of laser processing, but only the important aspects of CO_2 lasers, laser material interaction mechanisms, and an in-depth review of papers concerning laser welding will be covered.

2.1.1 Fundamentals of Lasers

The basic physics for producing laser light is the spontaneous emission and stimulated emission. There are three different ways in which radiation can interact with matter causing change in energy levels: (i) Fluorescence, (ii) Absorption and, (iii) Stimulated emission

2.1.1.1 Fluorescence

There are several ways in which an electron can be raised from a lower to higher energy level. Thus when this excited state is achieved, an electron may decay spontaneously to the lower energy level even in the absence of external electromagnetic field, emitting radiation energy.

2.1.1.2 Absorption

When light interacts with an electron lying in a lower energy level it raises the electron to a higher energy level. Thus the incident light is absorbed by the electron.

2.1.1.3 Stimulated Emission

Stimulated emission is a reverse process of absorption. An electron in the higher energy level is stimulated by incoming radiation of frequency ν, to release its energy and fall to a lower energy level. In other words stimulated emission results, when during an induced downward transition, a photon 'liberates' a new photon rather than being absorbed. The new photon has the same phase as the first photon. These photons can generate two more photons which have the same frequency and travel in the same direction. By this process a rapid accumulation of photons is obtained which are in phase with the incident photon. The CO_2 lasers have exited states based on molecular vibration (discussed later).

2.1.2 Properties of Lasers

The electromagnetic radiation from a laser has very special properties such as monochromaticity (i.e., it consists of only one wavelength), coherence and polarisation.

2.1.2.1 Coherence

The term "coherence" describes the different parts of an assembly of electromagnetic waves which are in phase with one another. There are two types of coherence named as spatial and temporal coherence, which are often used to refer to the output of lasers. Spatial coherence describes the phase relation in a plane perpendicular to the direction of propagation, while temporal coherence describes the phase relation in the direction of the beam.

2.1.2.2 Polarisation

The laser light travel in the form of transverse waves of electric and magnetic vectors which are perpendicular to the propagation vector (i.e., direction of travel of the wave). Polarisation refers to the orientation of the electric and magnetic vectors of the photons in a beam of radiation relative to the workpiece.

The simplest form of polarisation is the plane or linear polarisation for which the electric field orientation is constant with time, only the magnitude and sign of the field changing. If the electric field always points along the y-axis, the wave is said to be linearly polarised in the y-direction. Similarly if the light propagated in a given direction consists of independent wavetrains whose plane of vibration are randomly oriented about the direction of propagation then the laser light is called unpolarised. In circularly polarised beams the electric vector is rotating.

2.1.3 Types of Lasers

Lasers can be made from many different solids and liquids as well as from gases. The method of excitation for lasing varies too; it can be by electricity, light, chemical reaction or even another laser. The lasers can be classified as:

(1) Solid State Lasers
(2) Liquid or Dye Lasers and
(3) Gas Lasers

2.1.3.1 Solid State Laser

'Solid state' lasers are made from rods or slabs of solid, transparent material, such as synthetic ruby, emerald, Yttrium Aluminum Garnet (YAG) and Nd doped glass. They are excited into lasing by some energy input such as a brilliant flash of light or just focussed intense light. These lasers have to be made from clear crystals that will let in the light. The very first laser was a solid state ruby laser. The most common industrial solid state lasers are Neodymium-Yttrium Aluminum Garnet (Nd-YAG) and Neodymium glass (Nd-glass).

2.1.3.2 Liquid or Dye Lasers

Organic dye lasers have a different construction from gas or solid state lasers. They employ liquid solutions of certain dye materials. The dye materials are dissolved in organic solvents, commonly methyl alcohol. Thus the active medium for dye lasers is a liquid. Although dye lasers are not as common as either gas or solid state lasers, liquid lasers possess unique advantages [21] for certain applications. Solid state lasers have the possibility of damage to the active material due to thermal stress and gas lasers have a smaller concentration of active lasing atoms simply because the atoms are much further apart, making them larger for the same power, but liquid lasers have significantly higher concentrations of active atoms that can be varied

easily. The laser medium is cheap and relatively damage free and is not bulky nor as difficult to handle as a gaseous system. The important feature of dye lasers is that they produce beams of different tunable wavelength. This happens because in a liquid excited atoms provide a broad range of light. The laser has a prism to split this light into narrow wavelengths and so the beam can be tuned to different wavelengths, from near UV to near infrared. They are, unfortunately, very inefficient and currently only operate at low power.

2.1.3.3 Gas Lasers

Lasers in which gases are used as the lasing medium are referred to as gas lasers. Gas lasers can be operated continuously or on a pulsed basis; their output frequency range varies from ultraviolet to the infrared. Depending on the nature of the lasing medium, three types of gas lasers are distinguished: atomic, ionic and molecular. Although there are different methods of excitation, most lasers are usually excited into lasing by an electric discharge.

2.1.3.3.1 Advantage in Using Gas as Lasing Medium

There are many advantages [22] in using gas as an active medium. Although the volume of the material can be large as compared to a solid active medium, there is no possibility of damage to the material such as occurs in high power ruby and glass lasers. The material is homogeneous so that problems involving optical inhomogeneity that are common in solid lasers are avoided. Heat can be removed readily by transporting the heated gas out of the region of the interaction, in fact in suitable types of gas lasers, high power can also be achieved in this way.

2.1.4 Types of Carbon Dioxide Lasers

The carbon dioxide laser is by far most efficient gas laser and the most powerful continuously operating laser. The CO_2 laser works in the infrared at a

wavelength of 10.6 μm [23]. A few of the industrial applications of CO_2 lasers are welding, cutting, drilling and heat treatment.

There are three basic designs for CO_2 lasers, which are referred to as transverse flow (TF), slow axial flow (SF) and fast axial flow (FAF). For axial flow lasers the flow of gas, the discharge and the laser beam are co-axial while for transverse flow lasers, the discharge, laser beam and gas flow are orthogonal to each other. In all cases the gas is recirculated. Cooling is achieved by convection in TF and FAF, in contrast to slow axial flow in which the cooling is achieved through the cavity walls.

2.1.4.1 Lasing Action in CO_2 Lasers

The most important molecular laser uses CO_2 gas as its active medium. The CO_2 molecule is a linear molecule and undergoes three different types of vibrational oscillations as illustrated in Figure 2.1(a). These three vibrational configurations are called vibrational modes, and can be represented by V_1, V_2 and V_3. V_1 is a symmetrical stretching vibration (expansion and contraction), V_2 is a bending vibration and V_3 is an antisymmetrical stretching vibration. The gas mixture is composed of carbon dioxide, nitrogen and helium gases. Nitrogen molecules are excited from the ground state to the lowest vibrational state V_1 by collision with electrons in the gas discharge tube. The excited nitrogen molecules collide with carbon dioxide molecules and transfer their energy to CO_2 molecules because the excited N_2 energy level is nearly the same energy level as the upper laser level of the CO_2 molecules. This upper level vibrates in an antisymmetrical stretching mode, V_3, and the excited molecule then decays to one of the two lower energy levels, the V_2 bending mode or, the V_1 symmetrical stretching mode. Laser operation then proceeds at the wavelength of either 9.6 or 10.6 μm respectively [22] as shown is Figure 2.1(b).

The addition of nitrogen and helium (gas mixture is typically 5% CO_2, 18% N_2

and 50% He) considerably increases the overall power and efficiency of the laser. The role of nitrogen molecules is to improve coupling of the energy into the upper laser level through a collision process with the CO_2 molecule. The good thermal conductivity of the helium serves to increase the laser efficiency by speeding up the transition from the symmetrical stretch mode energy level (the receiving end of 10.6 μm laser transition) to the ground level, maintaining a large population inversion.

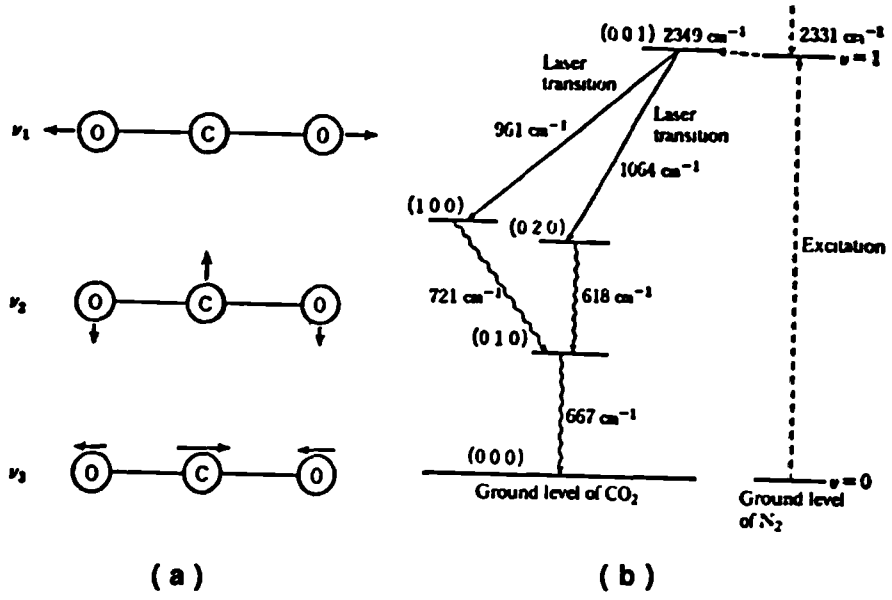


Figure 2.1 (a) Three modes of vibration in CO_2 molecule.
(b) Energy-level diagram of CO_2.

2.1.5 Welding Parameters

Until 1965, the laser had been used for the microwelding of electronic circuit boards, welding inside vacuum tubes and other similar low energy applications where conventional welding processes were not suitable. Since the development of high power cw CO_2 laser, the application of deep penetration welding has also occurred. The high power density energy beam can be used in many fields of materials processing. Figure 2.2 shows some of the operational regimes for laser materials

processing, plotted against power density (Watts/cm^2) and interaction time (seconds) [24]. Interaction time can be approximated to the beam diameter (D) divided by the traverse speed (V) i.e., D/V. The regimes are welding, cutting, drilling, cladding, etc.

When a metal is irradiated by a laser beam the processing depends upon many factors including the characteristics of the laser light, characteristics of focussing optics, the physical and chemical properties of the solid and nature of the ambient atmosphere. An important asset of laser welding is the high level of control which is available over the variables affecting the process. The weld can be tailored to meet the exact requirements of the job and the results can be readily duplicated. These parameters are described here.

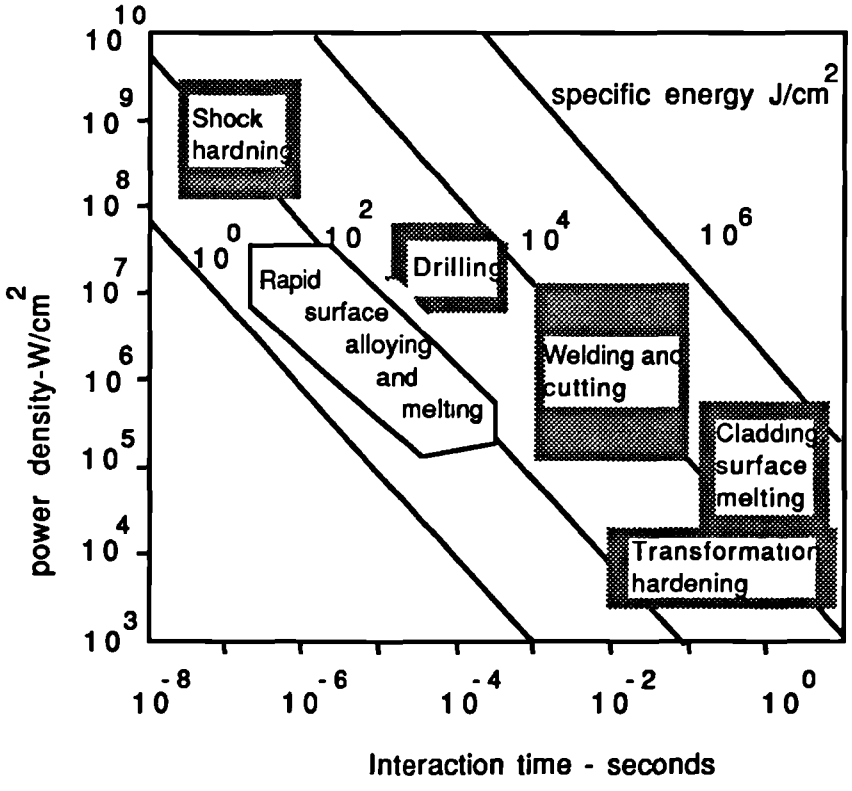


Figure 2.2 Operational regimes for laser materials processing [24].

2.1.5.1 Laser Parameters

2.1.5.1.1 Effect of Laser Power on Penetration

Laser power is the single most important factor affecting the welding process. It controls both the limit of penetration and the range of processing speeds. A Gaussian beam has a power intensity pattern with a peak in the centre and a decline in intensity to the edges. The power intensity distribution, I, as a function of, r, from the centre of a Gaussian beam is given by [17]

$$I(r) = I_o \exp\left[\frac{-2r^2}{r_o^2}\right] \qquad (2.1)$$

Where I_o is the intensity of the beam at the centre and r_o is the Gaussian beam radius, i.e., the radius at which the intensity has fallen to its central value by a factor of e^2, r is the radial position from the central Gaussian peak and I(r)is the laser beam intensity at radial point r.

The relationship between power and penetration has been studied by many workers. Baardsen *et al.* [25] and Lock *et al.* [26] showed a relationship between laser power and welding speed. They reported that penetration increases almost linearly with the increase in laser power (Figure 2.3 (a) & (b)). Willgoss *et al.* [27] showed a relationship between laser power and penetration using 7 kW laser power for stainless steel 316. They found a linear relationship in the power range of 2.5 to 7 kW, but below 2.5 kW beam power welding without keyhole formation occurred, and hence a decrease in penetration was observed, (Figure (2.4)).

For a Gaussian intensity distribution, the temperature in the beam centre at the surface of an infinite plane workpiece is given by [28]

$$T(0,0,0,t) = \frac{A}{2K\sqrt{\frac{\pi}{2}}} I\, r_f \tan^{-1}\sqrt{\frac{8\kappa t}{r_f}} \qquad (2.2)$$

Where A is absorptivity, K is heat conductivity, I is beam intensity, r_f is focus radius, κ is thermal diffusivity and t is interaction time.

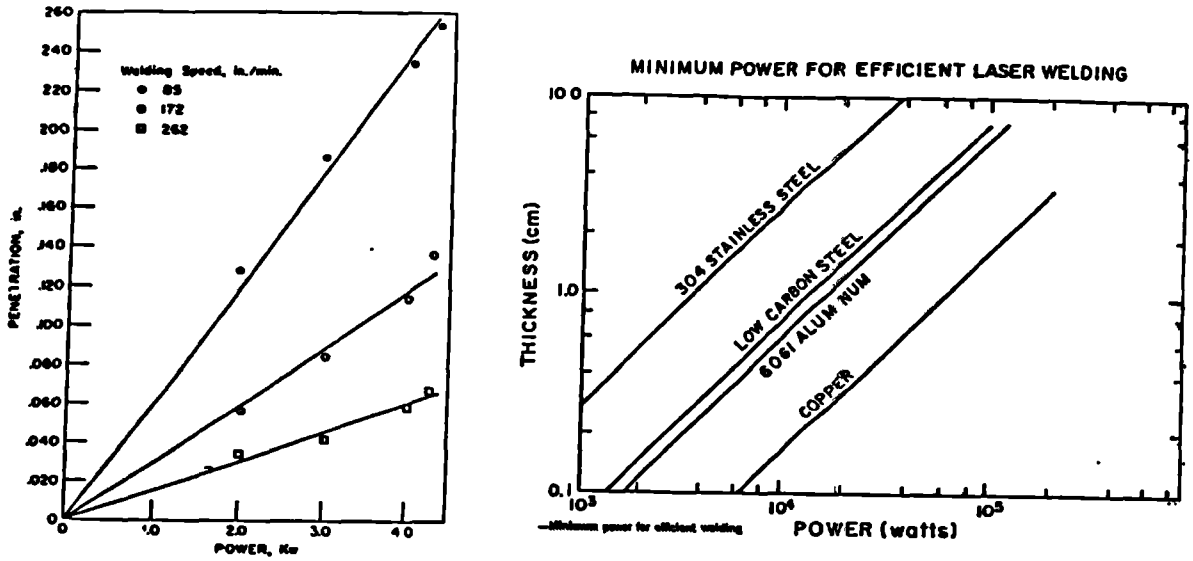


Figure 2.3 (a) Weld bead penetration as a function of laser power at various welding speeds [25], (b) Minimum power for efficient welding [26].

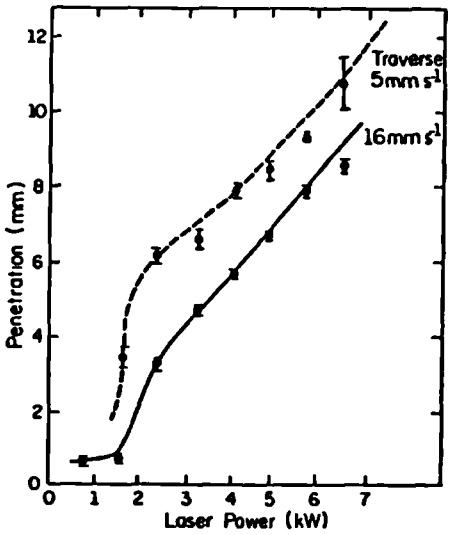


Figure 2.4 Penetration depth of laser welds as a function of beam power for 316 stainless steel [27].

2.1.5.1.2 Effect of Beam Mode on Penetration

The power distribution across the beam is referred to as the mode structure. The beam mode structure can be represented in either symmetrical of cylindrical symmetry by TEM_{mn}. Figure 2.5 shows some mode structures of the laser beam.

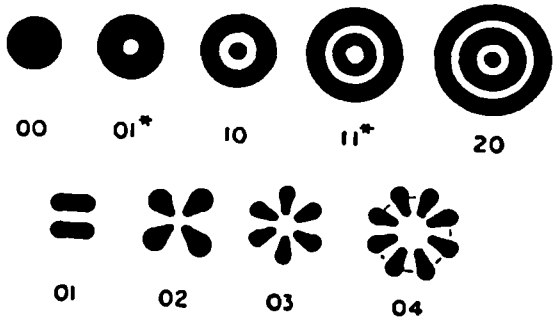


Figure 2.5 Transverse mode structures in cylindrical symmetry.

TEM_{00} is the lowest order mode, referred to as the "Gaussian" mode. The TEM_{10^*} mode is the so called "doughnut" mode. Factors that affect the mode structure include the geometry of the laser cavity and optics, the gain of cavity, inhomogenities in the laser medium, and the pumping power [29]. The affect of mode structure on laser processing is reported by Sharp and Steen [30], and Sharp *et al.* [31]. Sharp *et al.* showed that a higher order mode increases the width of the melted zone, but decreases the penetration. Sharp and Steen reported that the peak temperature distribution across the track is more uniform with the doughnut mode than with the Gaussian mode.

2.1.5.1.3 Wavelength

Figure 2.6 shows the reflectivity of various materials as a function of wavelength of the laser. The shorter wavelength gives less reflectivity and hence higher absorption of the laser beam, while the longer wavelengths are highly reflective to a range of materials and gives less absorption of the beam and hence the laser processing of the materials are badly affected (see also section on reflectivity).

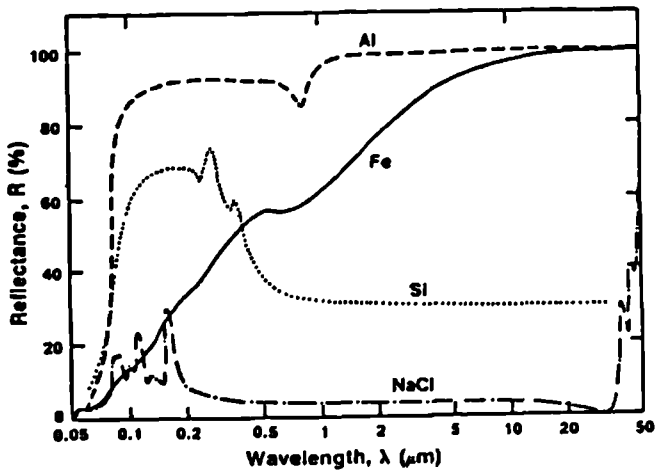


Figure 2.6 The reflectivity of some metals (Fe, Al), a semiconductor (Si), and rocksalt (NaCl) as a function of electromagnetic wavelength. The data corresponds to normal incidence and 20° C [32].

2.1.5.1.4 Effect of Spot Size on Weld Penetration

The spot size of a laser beam is one of the most important parameters in laser processing since it determines the power intensity of the beam. Ready [33] defined the unfocussed beam diameter as being the radius at which the power density has fallen to 1/e of the central value while Duley [17] defined it as the radius at which the intensity has fallen to $1/e^2$ of its central peak value. Ready [33] and Duley [17] have shown that for a Gaussian beam the minimum spot size D_f is given by

$$D_f = \frac{2\lambda f}{\pi D} \qquad (2.3)$$

or

$$D_f = \frac{2.4\lambda fm}{D} \qquad (2.4)$$

Where, m; mode factor, D_f; focussed beam diameter, f; focal length of the lens, λ; wavelength of the incident radiation, D; diameter of beam at lens. Thus the smaller the f/D ratio the smaller is the beam diameter. Therefore when a higher power

density is required, a low output of TEM_{00} mode may be more advantageous than a higher output power in higher order modes. For efficient welding a focussed beam with small f/D value i.e., (F-number) and a low order mode (i.e., small mode factor m) is desirable.

2.1.5.2 Characteristics of focussing optics

2.1.5.2.1 Focal Length

The focal length of the focussing optics also plays an important role. The longer focal length lens gives a longer depth of focus, but reduced penetration due to a bigger focal point. Work done by Ready [33], Seaman [34] and Engel [35] has shown that the use of a shorter focal length lens gives better penetration as it produces a smaller focal point and hence a higher power density on the surface of the metal. This advantage has to be weighed against the reduced accessibility of the process (i.e., the smaller distance between the lens and the workpiece), and a small depth of field. Hence a compromise must be made.

2.1.5.2.2 Effect of Focal Position on Penetration

The location of the focal point position is critical to maintaining adequate power density. Additionally, the positioning of the focal point with respect to the surface of the joint allows the user to control the width and penetration of the weld nugget. At the focal point, the power density is at its maximum. A knowledge of the effect of variation in focal position relative to the surface to be welded is therefore important. The effect of focus on penetration depth and on the shape of fusion zone has been studied by several workers [27,34-40]. The optimum position of focus was found by these workers to be just inside of the material. Engel [35] found the optimum position of focus (the position which gives the maximum penetration) for several metals (for example 1018 steel) to be in the range of 1.27 to 2.54 mm below the surface (Figure 2.7). Wilgoss *et al.* [27] studied the effect on weld profile, by

moving the focal point 2.5 mm distance each time towards the workpiece. When the beam was focussed well above the level of workpiece surface a large "nail head" (width broadening) with a consequent loss of penetration was observed. Too deep focus inside the workpiece gave a V-shaped weld. Wilgoss *et al.* [27] reported that an almost straight sided weld was formed with the focus 1 mm below the surface of the workpiece (Figure 2.8). Alexander J. [36] used a 5.65 kW laser and a welding speed of 40 mm/s. She found that the maximum penetration is obtained with the focus of the beam 2 mm below the surface of the workpiece. Banas [38] and Eboo [40] found that the most effective penetration was achieved with focus at the surface. Seaman [34] suggested that the optimum position depends upon laser power.

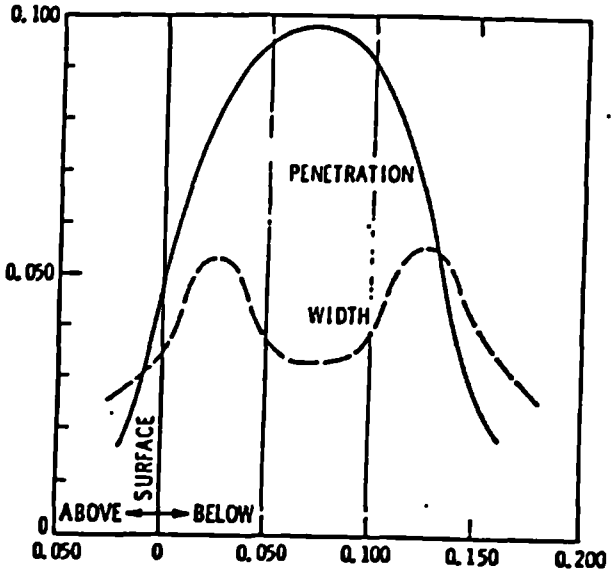


Figure 2.7 Narrowest weld is produced when penetration is maximum. Laser power 1.5 kW, welding speed 50 in/min, focal length of the lens 2.5 in, all dimension are in inches, material 1018 steel [35].

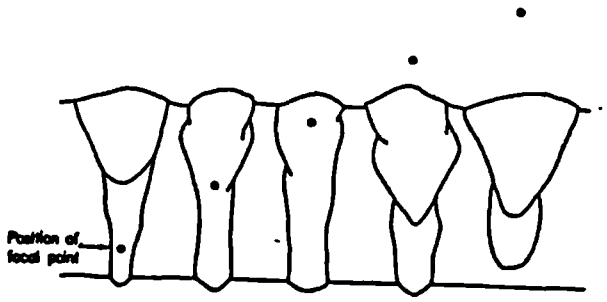


Figure 2.8 Transverse profile as a function of focus position (Material 310, power 5 kW, speed 16 mm/s) [27].

2.1.5.3 Properties of Workpiece

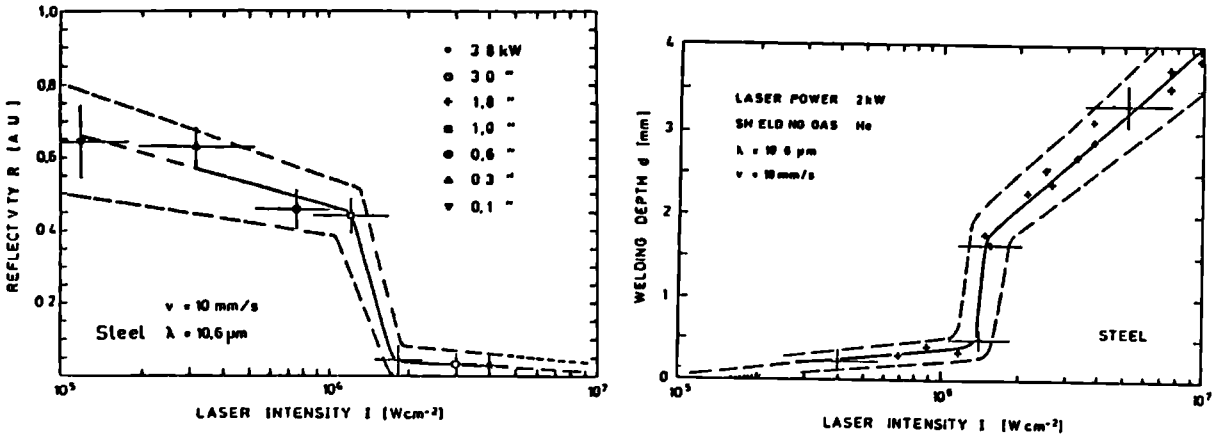
2.1.5.3.1 Reflectivity

For an opaque solid, the fraction of the incident radiation absorbed is $\varepsilon = 1-R_o$ where ε is the emissivity and R_o is the reflectivity at normal incidence. The reflectivity R_o varies with the angle of incidence of the light on the surface, the wavelength of laser radiation, its polarisation, and the temperature of the material. Figure 2.6 shows the normal incidence, room temperature reflectivity of several types of materials as a function of wavelength [32]. It is evident that for laser processing of Si and NaCl a wavelength between 1 & 10 μm is suitable and for Fe and Al the shorter wavelength are suitable. But at the wavelength of CO_2 laser (10 μm) both metals are highly reflective. As the material becomes hotter, the reflectivity, and hence, the coupling coefficient (laser intensity absorbed/incident laser intensity) changes, depending upon the material's intrinsic optical properties at the wavelength of the laser.

As the laser light falls on a surface it heats up the surface and hence increases the absorptivity of the laser beam to the workpiece [32] until the laser intensity approaches a critical value I_c, the absorption instantaneously rises to higher values approaching unity and hence the laser processing efficiency increases considerably.

Herziger [41-43] showed that the reflectivity R, of a steel surface decreases with increasing intensity (Figure 2.9 (a)). Above the critical value of the intensity I_c, R decreases sharply to a smaller value, which is often below the limit of measurement. Simultaneously with the decrease of reflectivity R a strongly enhanced coupling of the laser energy into the workpiece is observed. Welding depth against laser intensity (Figure 2.9 (b)) shows that the welding depth increases at the same value of intensity at which the reflectivity decreases. In addition to laser intensity, the welding depth also depends upon processing and laser parameters such as welding speed and laser power [44]. Figure 2.10 shows the welding depth as a function of

welding speed. At a certain threshold speed the welding depth decreases sharply. This threshold cut- off point also depends upon the beam intensity.



(a) (b)

Figure 2.9 (a) The measured reflectivity at different laser beam intensities show a sharp decrease at the threshold intensity for plasma formation. (b) The welding depth verses laser intensity demonstrate a sharp increase above a critical intensity. The threshold of welding depth corresponds to the threshold intensity for the formation of a laser induced plasma [42].

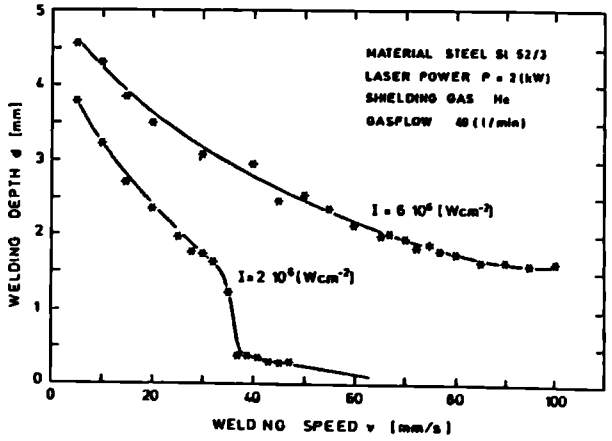


Figure 2.10 Welding depth versus welding speed at various laser intensities [42].

2.1.5.3.2 Effect of Welding Speed on Penetration

The second primary control over weld penetration is provided by welding speed. The welding speed, like power, determines under given conditions of welding the depth

of penetration that can be achieved in the material. The relationship between traverse speed and penetration has been reported by many workers [35,36,45,46]. The results of penetration verses welding speed [47] are shown in Figure 2.11. It can be seen that increasing the welding speed decreases the penetration. Merchant [16] reported that insufficient penetration results if the welding speed is too fast and if the speed is too low, the molten material simply falls out of the keyhole before it resolidifies. At very low speeds there is an increased interaction between laser beam and plasma which lessens the penetration [26]. Metzbower [48] reported the scalability of high power laser welding for A36 steel, and is illustrated in Figure 2.12. This shows that the power required to weld various thickness of steel is a function of welding speed.

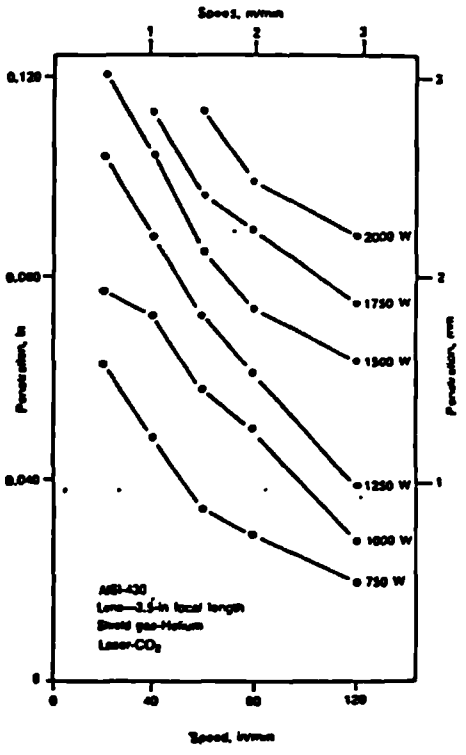


Figure 2.11 Laser welding 430 stainless steel, penetration versus speed at various powers [47].

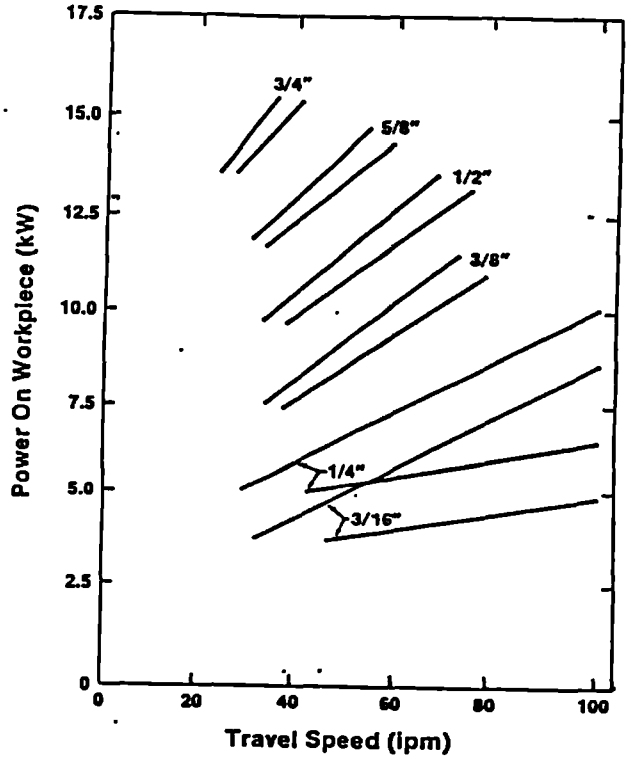


Figure 2.12 Laser power required for welding A36 steel at different speeds [48].

Mazumder and Steen [49] showed for a particular power there is a range of

welding speed beyond which full penetration can not be achieved. The lower speeds give excessive melting and loss of material while higher speed gives improper penetration. Their results for range of welding speeds against power for 6Al-4V-Ti is shown in Figure 2.13. The range of welding speed (i.e., range between maximum and minimum weld speed) for successful welding decreases with increasing thickness, as reported previously by Adams [50].

Herziger [42] reported that at a certain threshold speed the welding depth decreases sharply, which also depends on the laser beam intensity Figure 2.10. This sharp decrease may be due to the poorer keyhole stability at threshold speeds.

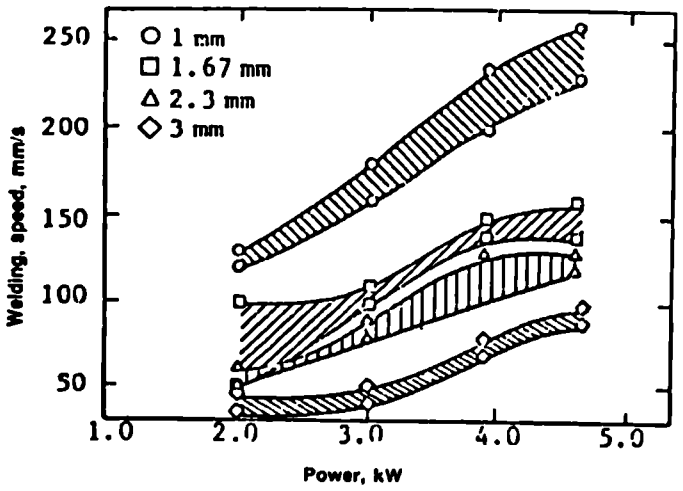


Figure 2.13 Welding speed against power for Culham/Ferranti 5 kW CO_2 laser [49].

2.1.5.3.3 Thermal Properties

During laser/material interaction light is absorbed in the material generating heat, which causes one or more phase changes to occur. This can consume much of the available energy. The specific heat C, density ρ, and latent heat L, determine the fraction of the energy consumed. The thermal conductivity κ, and thermal diffusivity $\alpha = \kappa/\rho C$, determine how rapidly the heat is conducted away from the irradiated region and the consequent temperature distribution.

Some materials posses a combination of thermal and optical parameters rendering them difficult to work. For example, the high thermal conductivity of copper and aluminum removes heat very rapidly from the region of interaction. Further, the high reflectivity of these metals in the solid state gives inefficient coupling of the incident light into the material. Thus high power densities are needed to obtain requisite temperature rises.

2.1.5.3.4 Effect of Gas Shielding on Penetration

During a welding operation it is necessary to blanket the weld by a shielding gas to prevent the weld from oxidising. Helium and argon are both inert gases commonly used in laser welding. Due to the ionisation of the shielding gas, plasma can be produced during laser welding. At high speeds this enhances the coupling and at low speeds the plasma thickness interferes with the beam.

Seaman [51], Bousseau & Signamarcheix [52] and Herziger [53] investigated the effect of different shielding gases on penetration. They found that Helium gas gives better penetration than any other gas. This was due to the higher ionisation potential (24.6 eV) and consequently reduced absorption of radiation. On the other hand argon increases the plasma which develops above the melting zone and also increases the absorption of energy, hence reduced penetration is obtained at low speeds. Seaman reported that both the composition and flow rate of shielding gas influence the depth of penetration. The addition of 10% argon to helium is beneficial as it gives increased welding speeds while maintaining satisfactory blanketing.

Herziger [53] reported that the flow rate of the shielding gas influences the depth of penetration and an increased plasma absorption above the workpiece occurs at a critical shielding gas flow rate when using argon (Figure 2.14). Thus if the shielding gas parameters are not properly matched to the processing parameters, a laser induced shielding gas plasma is generated. Herziger showed a relationship between welding velocity and penetration depth with various shielding gases as shown

in Figure 2.15. A shielding gas influence is visible at low processing velocities by using 2kW power. This influence increases with increasing laser beam power and intensity.

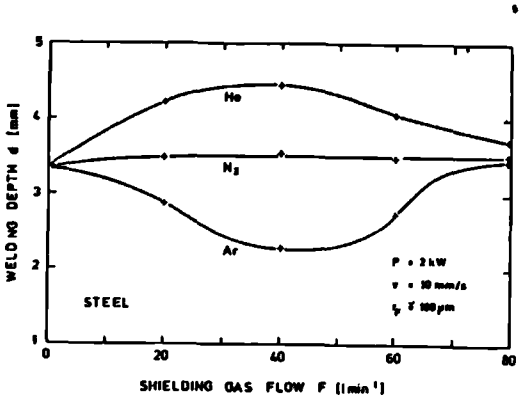


Figure 2.14 Measured relation between gas flow and welding depth [53].

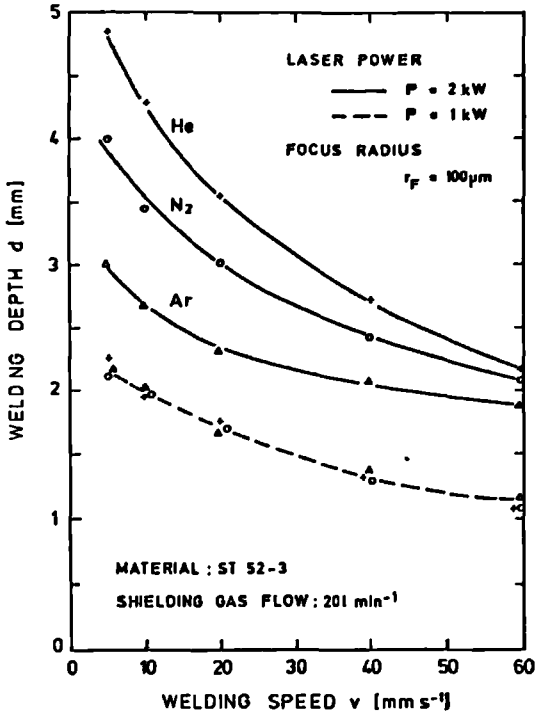


Figure 2.15 Relation between welding velocity and penetration depth determined with various shielding gases [42].

A second function of the shielding gas is focussing lens protection. The lens is close to the keyhole from which vapour and molten metal is ejected with considerable force. In laser powers up to 2 kW a gas stream coaxial to the laser beam can stop this material from hitting the lens while protecting the weld. In multi-kilowatt lasers the ejection is more vigorous and separate shielding is requ'red for the lens and the weld. Arata *et al.* [54] used a side blown gas assist jet to blow the plasma away. They found that increase of gas flow rate removed the plasma from the beam-metal interaction point very effectively. The penetration depth increased with gas flow rate up to a certain limit and gradually decreased with gas flow. Too high a gas flow rate did not increase the penetration further but removed the molten metal, thus affecting the weld shape and the beam hole.

2.1.5.3.5 Effect of Gap Between the Sheets on Penetration

Engel [35,55] reported that, for lap joints, the air gaps between the pieces to be welded severely limit the penetration and/or rate of the welding. Thus a compressive clamping, as in Figure 2.16, should be used to maintain separation less than 25% of the material thickness. When materials of different thickness are welded, the thinner material should be welded to the thicker [35,55,56]. Shewell [57] reported that for pulsed laser spot welding of lap joints the maximum gap for ferrous and nickel alloys is 0.15 times the material thickness, and it is less for higher conductive materials.

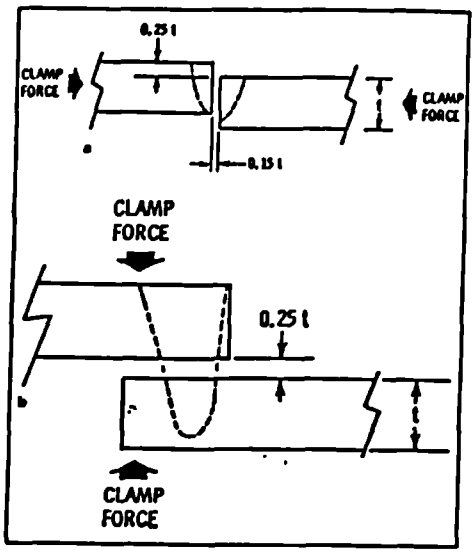


Figure 2.16 Clamping and tolerances for (a) butt joint, and (b) lap joint, dimensions are in units of material thickness t [55].

Baranov *et al.* [58] studied the influence of gap size on the formation and strength of a spot lap joint in laser welding. They found that the joint strength decreased with increasing gap, as a result of reduction of the area of the fusion zone and of the depth of penetration of the bottom plate.

Baranov *et al.* [58] showed that on increasing the gap size there is a reduction in the breaking load, P, the diameter of the fusion zone, D, and the depth of

penetration of the bottom plate, Δ, (Figure 2.17). Velichko *et al.* [59] reported that the dependence of the tensile strength of a spot weld on the gap width becomes less as the depth-to-width ratio of the weld decreases (Figure 2.18), which is due to the decrease in the fusion zone dimension as the gap increases. Baranov et al reported that, by making the upper plate thinner the strength of the welded spots decreases, as the gap increases. They found that, the shape of the weld pool also changes at different gap sizes [58].

For butt joints it is not necessary to level the edges of materials to be laser welded, and sheared edges edges are acceptable if they are square and straight. Engel [35] found that, the fit-up tolerance should be less than 15% of the material thickness as shown in Figure 2.16. To avoid laser beam wandering, misalignment and out-of-flatness of the parts, should be less than 25% of material thickness. Mazumder [49] reported that, the transverse alignment should be kept within half of the focussed beam diameter. Compressive clamping of the material is recommended, buckling is not a problem unless the material to be welded is thinner than 0.25 mm [35].

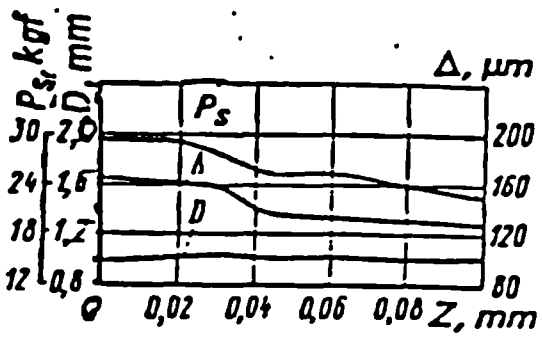


Figure 2.17 Gap size, Z, versus shear stress, P_{sh}, tensile stress, P_s, diameter of the fusion zone, D, and depth of penetration of the bottom plate, Δ, for steel 47NKhR + Ni joint [58].

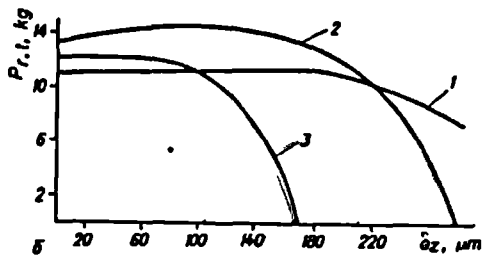


Figure 2.18 Strength of spot welded lap joints in 1Kh18N9T steel versus gap between the sheets. In every case the thickness of lower sheet was 0.5 mm, and with different upper sheet thickness
1 - δ = 0.3 mm, 2 - δ = 0.2 mm,
3 - δ = 0.1 mm [59].

2.1.6 Ripple Formation During Weld Solidification

In laser welding, alloying or surface melting a flat surface is never achieved. Instead, due to considerable fluid flow in the small melt pool during the laser processing, a significant roughning called rippling [60] results (see Figure 2.19). Hawkes *et al.* [61] reported three kinds of ripples depending upon the processing parameters: (i) a fine ripple pattern with a wavelength of around 5 ~15 μm observed at all processing speeds, (ii) a coarse ripple pattern with wavelength ~100 μm, also at all speeds, (iii) Central humping with under cutting at the sides of the track, observed only at certain critical speeds. Hawkes [61] reported that the fine (5~15μm) ripple formed are independent of fluid flow since they were present in almost all samples produced in wide range of processing conditions and on various alloys with different properties. Ishizaki [62] suggested that the fine ripple pattern which defines the solidification front may be caused by periodic oscillation of the liquid contact angle at the solidification front.

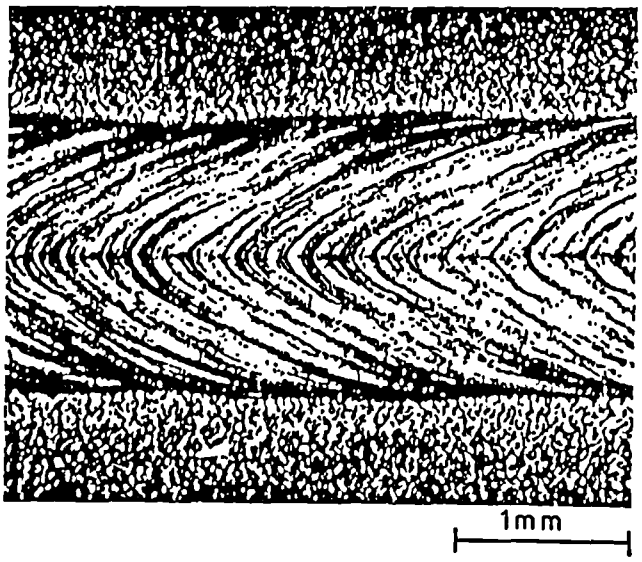


Figure 2.19 Surface roughness of a welding seam [66].

Many reasons put forward by researchers [36,60-65] about the formation of coarser ripples and humping were related to fluid flow. Anthony and Cline [60] showed that surface tension gradients generated by temperature gradients provide the

driving force for fluid flow (i.e., Marangoni force). When a Gaussian beam irradiates the metal surface, due to Gaussian intensity distribution, a temperature gradient extends radially away from the centre of the beam. Under the beam, the temperature of the liquid is at its highest and the surface tension of the liquid is at its lowest value. As the temperature of the liquid decreases away from the centre, the surface tension of the liquid usually increases. The high surface tension at the edges pulls the liquid away from the centre and results in a depression at the centre and an elevation at the edge of the molten pool. A pressure head is developed due to the height difference and this induces a counter flow of liquid back towards the region of the lower liquid level beneath the beam, as shown in Figure 2.20, for the steady state condition. In the unsteady state condition, (i.e., scan speed not equal to zero), as the solidification rate of liquid metal is high, the liquid solidifies before it flows back to the centre and hence results in a roughened surface as shown in Figure 2.19. According to Anthony and Cline [60], if the laser beam speed exceeds a critical value, the liquid does not have sufficient time to form ripples, and hence rippling from surface tension gradients can be avoided. However, experimental evidence shows that such a critical speed does not exist.

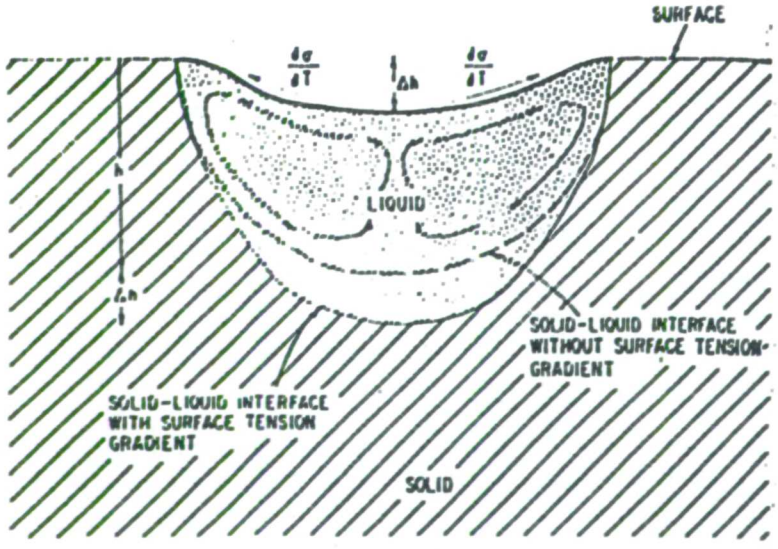


Figure 2.20 A cross section perpendicular to the laser beam path through the melt in the steady state condition [60].

Intermittent flow of the molten trail is thought to be caused by variety of mechanism. Copley *et al.* [63] suggested that the intermittent flow is due to the periodic melting caused by variation in power coupling. The variation in power coupling is due to the formation of a bow wave ahead of the beam that changes the beam liquid incident angle. Moore *et al.* [64] considered that the variation of vapour pressure or sometimes plasma expansion above the molten pool depresses the liquid surface and also causes intermittent flow of fluid. As the beam moves ahead, the liquid at the leading edges of the pool flows back around the sides of the depression and merges again behind it and solidifies to give the characteristic rippling pattern.

Alexander [36] reported that intermittent melting leading to ripple formation is a result of periodic beam power fluctuation caused by the fluctuation of the power supply unit of the laser system. Beyer *et al.* [66] using a cw-CO_2 laser found that the ripples are formed due to the fluctuation of plasma, caused by the variation of metal vapour density i. e., the expansion of plasma above the keyhole (see section 2.1.8).

Kotecki *et al.* [65] investigated the formation of ripples on the surfaces of GTA spot and seam weld in thin metal sheet using high speed motion pictures. They found that ripples were observed to form solely due to oscillation of the weld pool during solidification. Using a high speed camera they observed that the weld pool surface shows virtually no oscillation while the arc is on. An arc plasma exerts sufficient physical pressure on the weld pool surface to displace liquid metal from the position it would occupy if the pressure were absent. When the arc is shut off, the plasma pressure on the top of the pool is suddenly removed and surface tension pulles the pool back towards its equilibrium position. This sets the pool into oscillation. Since solidification occurs while the pool is oscillating, the changes in surface displacement due to oscillations become frozen into the solidified metal and appear as ripples.

2.1.7 Weld Bead Humping and Undercutting

With the use of lasers in automotive industries it is expected to increase the production line by increasing the welding speed of a weld. Unfortunately increasing the welding speed leads to undercutting and humping of the weld bead. Albright *et al.* [67] found that five types of weld bead exist at higher traverse speed (i) smooth weld, (ii) weld bead with cutting and regular and irregular hole formation, (iii) undercutting, (iv) ropy bead and (v) humping.

The relationship between weld pool shape and size and characteristic weld face surface is summerised in Figure 2.21 . Cutting and hole formation were associated with long, full penetration weld pools. Ropy bead, undercut and humping occur when an elongated projection, or pool "tail" develops in the back of the weld pool. Albright found that the five characteristic weld types occupied distinct regions on a plot of laser beam power verses traverse speed as shown in Figure 2.22. Ropy bead, undercut and humping occurred in that order with increasing travel speeds beyond the smooth weld region.

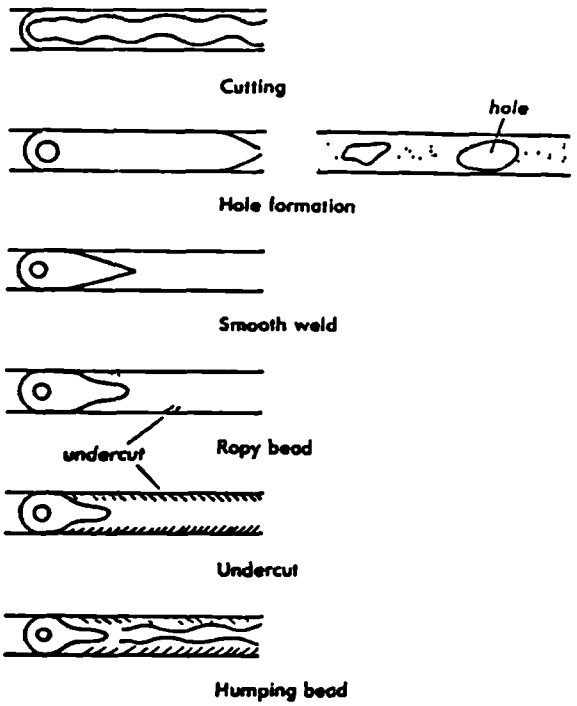


Figure 2.21 Weld pool shapes in order of increasing travel speed [67].

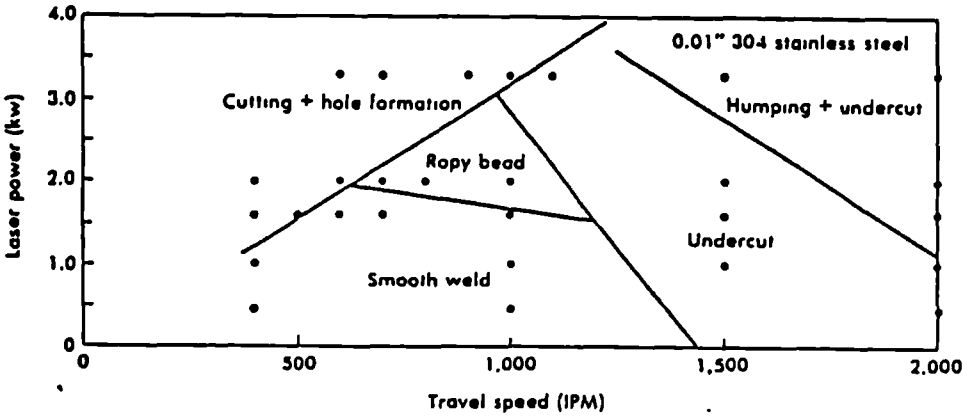


Figure 2.22 Discontinuity regions in power versus travel speed for 0.01-in thick type 304 stainless steel [67].

Bradstreet [68] found that humping is always associated with undercutting. Undercutting occurs as a result of surface tension forces, when the weld metal solidified too rapidly, before the groove is completely filled. While humping is a regular series of swellings in the weld face. He proposed that humping is caused by differences in pressure within the molten weld pool. Wealleans and Adams [69] investigated the effect of welding variables on weld bead characteristics. They concluded that both the surface tension and the solidification rate of the weld metal had significant effects on the development of undercut.

2.1.8 Laser Materials Interaction and the Influence of Laser Induced Plasma on Welding

Unfortunately many of the materials that are of interest for laser processing are highly reflective in the visible and infrared part of the electromagnetic spectrum making a poor processing efficiency. But to increase the absorption of an incident laser, a layer of high absorptivity can be deposited on the target surface [70].

When a laser beam strikes the metal surface part of it is absorbed and the rest is reflected. A photon of laser light is absorbed by a free electron or lattice phonon.

The energy of the photon is transferred to the electron, raising its speed or energy level. This collides with the lattice nuclei and phonons causing them to vibrate, which we detect as heat. The heat is then conducted into the material. When the surface reaches the melting temperature, a liquid interface propagates into the material. With continued irradiation, the surface begins to vaporise and a "keyhole" is generated. If the laser intensity is high, absorption in the vapour leads to a high temperature plasma, which may seriously interfere with the beam.

In general, the definition of a plasma is a gas of free positive and negative charges, a condition probably reached before the absorption of the laser radiation. However this point is not critical because the life time of free charges in an atmosphere of gas is very short. Thus the free charges must be generated at a rate sufficient to produce a free charge density which will absorb the laser radiation. When this occurs the plasma is said to be initiated which simply refers to its observability on a microscopic scale.

As the plasma begins to absorb laser radiation, the temperature of the plasma increases. A pressure wave is generated which moves along the laser beam axis. As the plasma continues to absorb energy and with increase in temperature it begins to move into the surrounding region via radiation along the beam axis with a velocity of 10^5 cm/s [41]. These conditions describe a Laser Supported Absorption (LSA) wave [71-72]. Dixon and Lewis [72] using a 400 Watts pulsed Nd-YAG (1.06 μm wavelength) found that at low power the plasma requires a longer initiation time and with the increase in power the plasma initiation time decreases. Also with the help of high speed photography they found that multiple plasmas exist during one laser welding pulse of 7.8 m sec pulse and at 325 Watts of power.

The plasma additionally absorbs the laser radiation and re-radiates the energy at shorter wavelengths with the shorter wavelength radiation absorbed by the surface, thus increasing the coupling of energy into the surface. This laser-induced,

surface initiated vapour-breakdown plasma is generally referred to as a Laser Supported Absorption (LSA) wave. The extreme cases of the LSA wave can be defined according to penetration depth $T = 1/\alpha$ (α is absorption coefficient) of the laser radiation into the induced plasma [73]. In the limit ($T \rightarrow \infty$) the induced plasma is essentially transparent to the incident radiation corresponding to a weakly ionized vapour state. In the limit ($T \rightarrow 0$) the incident radiation is fully absorbed within a thin layer of induced plasma, thereby, completely shielding the workpiece from further energy coupling. The absorption of all incident radiation in this thin plasma layer, with subsequent explosive propagation away from the surface is referred to as a Laser Supported Detonation (LSD) wave. In an intermediate region between both the extreme cases occurs what is referred to as a Laser Supported Combustion (LSC) wave with enhanced coupling of the beam energy into the surface (Figure 2.23).

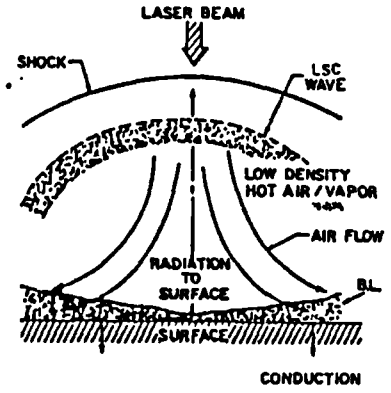


Figure 2.23 Laser supported combustion (LSC) wave [71].

For low intensities an opaque plasma is observed which is confined to the surface region towards the laser. The plasma improves the energy coupling [42] into the workpiece by heat conduction, optical radiation, and beam lensing changing altogether the beam distribution and the beam power in the interaction zone. With increasing intensity the degree of ionization is also increasing and the attenuation of the incident laser radiation by the laser induced plasma is growing [44].

For high intensities the plasma plume starts to decouple from the surface (Figure 2.24) because of the attenuation so that little laser energy is delivered to the

workpiece surface. After complete decoupling, the optically dense plasma plume completely shields the workpiece surface i.e., the vaporisation and consequently, the processing is interrupted [74]. Since the substrate no longer supplies incandescent particles, and the plume begins to dissipate, yielding an optical thin plasma, its attenuation effect is diminished. In addition the plume has propagated back towards the laser to a position where the intensity is lower. The transparency of the plasma plume becomes higher and plasma ignition starts again.

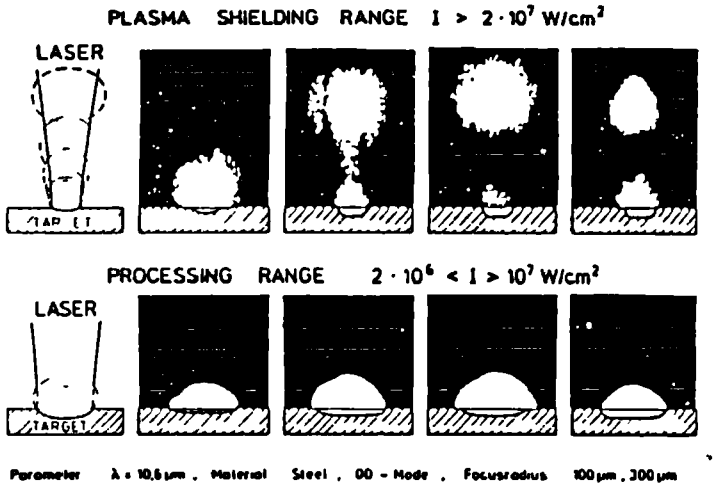


Figure 2.24 Framing images of the plasma formation above a steel surface at different intensities of a pulsed CO_2 laser (interframe time 50ns). At laser intensities above 2 x 10^7 W/cm^2 the plasma detaches from the target [74].

The laser induced plasma changes dramatically the processing conditions. In the limit of weak absorption the plasma plume changes the original beam geometry. In the limit of strong absorption the plasma substantially absorbs the incoming radiation. In either case, the processing is no longer controlled by the laser parameters, but rather by the generated plasma plume influencing the processing results and - by optical feedback - intensity and mode structure of the laser itself. The working process may become totally irregular. In particular the welding of zinc coated steel is prone to plasma blocking problems due to the ready generation of plasma.

Figure 2.25 shows a processing diagram for laser welding [42]. The dotted

line, which is in agreement with experimental observations, is the calculated critical intensity for a laser induced plasma near the processing surface. The straight line for plasma shielding has been taken from investigations of high-speed photography. The shaded region shows the optimum laser parameters for high efficiency machining.

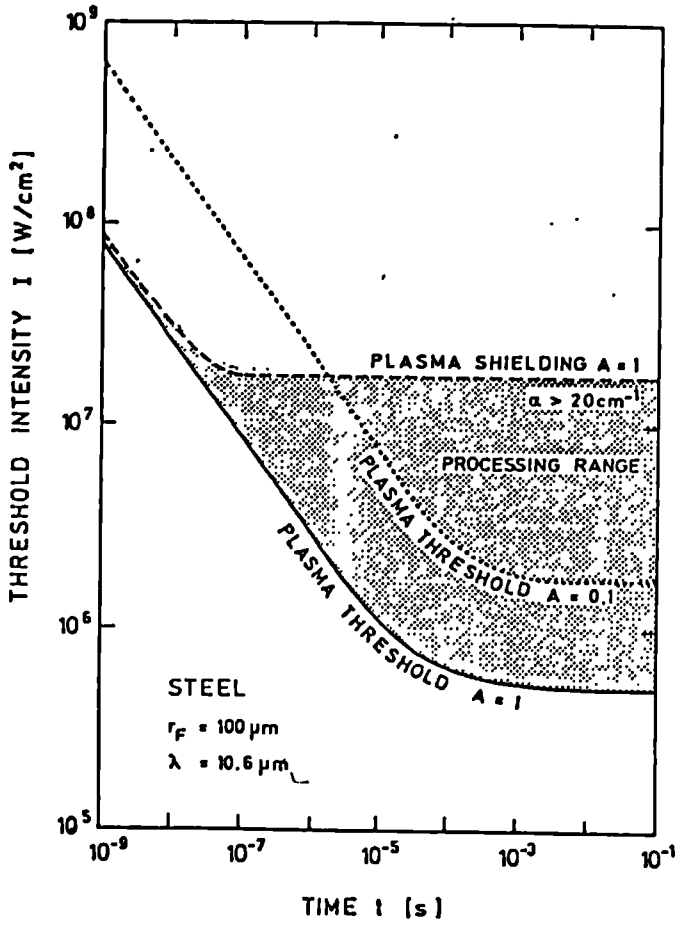


Figure 2.25 Processing diagram showing the calculated threshold intensities for plasma formation and plasma shielding [42].

In laser welding, the penetration depth can be increased considerably if the laser induced plasma is adequately controlled by aerodynamic or other measures [75].

The interaction of high power laser radiation with metals and other solids is capable of providing industry with a variety of novel and useful processing tools. However the overall efficiency of this new technology is limited in many instances, by difficulty of obtaining effective coupling between incident laser radiation and the

workpiece. High reflectivity, plasma shielding and gas absorption all conspire to reduce the overall coupling of laser radiation to solids and particularly to metals. At room temperature most elemental metals and alloys absorb less than 10% of incident radiation of wavelength 10.6 μm, the wavelength of CO_2 laser, so that some 90% of incident laser power is wasted unless steps are taken to artificially reduce sample reflectivity. During sample processing the ejection of material from the laser interaction region may create a plasma that can also absorb incident laser radiation.

During the welding process the laser induced plasma is formed at beam intensities above 10^6 W/cm^2. The plasma consists of metal vapour. The value of metal vapour density is an important factor in plasma formation and plasma absorption. The metal vapour density $n_M(t)$ can be calculated by a model developed by Krokhin [76] and Afanav'ev [77]. The model was slightly modified to take into account power losses by thermal conduction [78]. The vapour density, $n_M(t)$ is given by

$$n_M(t) = \text{Const.}\left[AI - \frac{\sqrt{2\pi}\, T_v K / r_f}{\tan^{-1}\frac{\sqrt{8\kappa t}}{r_f}} \right] \qquad (2.5)$$

Where A; absorptivity, I; laser intensity, T_v; the temperature of vaporisation, K; thermal conductivity, r_f; focus radius of the beam, κ; thermal diffusivity, t; interaction time. Typical values for n_M are between 10^{18} (cm^{-3}) and 10^{19} (cm^{-3}). During laser processing the material is evaporated from the surface of the material producing free electrons, these free electrons form the plasma. Electrons inside the interaction volume are accelerated in the laser radiation field by inverse Bremsstrahlung until the kinetic energy is as high to ionize the ambient gas or metallic vapour increasing the number of electrons by avalanche ionization [79]. Thus the vapour density is essential for the formation of laser induced plasma, which is determined by the power density distribution and the power losses by heat conduction.

Beyer *et al.* [66,78], using a cw CO_2 laser for welding of metal found that the visible plasma was not constant. By looking at the plasma with a high temporal resolution, a strong fluctuation was visible (Figure 2.26). During this fluctuation the plasma disappeared completely for a time of 0.2 ms. There exist two reasons for the fluctuations of the plasma, one was the laser power fluctuation and the other was the variation of metal vapour density. But using a laser with small fluctuations only the second reason was of interest. Thus the fluctuation in the plasma was found to be due to the variation of the metal vapour density. This happens if more or less molten material moves into the cross-section area of the laser beam inside the vapour capillary (keyhole).

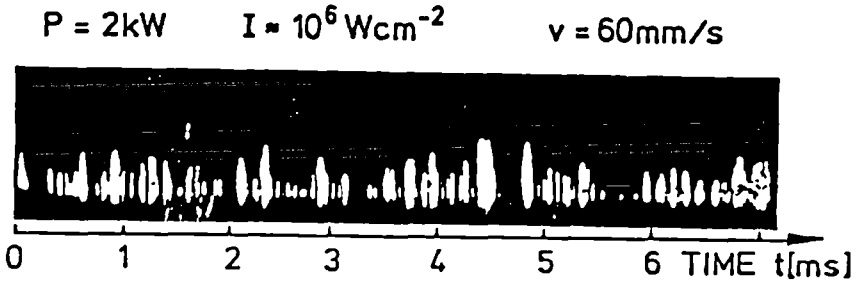


Figure 2.26 Streak photograph of the laser induced plasma during the welding process with a cw CO_2 laser. Strong plasma fluctuations are visible [66].

Using an Ar-laser beam reflected from the melt pool just after the keyhole, Beyer *et al.* [66] measured the frequency of oscillation of the molten metal. They found it to be in the range of some hundred cycles per second. They related it to the surface rippling of the weld seam which is also some hundred cycles per second.

2.1.8.1 Dynamic Behaviour in Laser Welding

Gatzweiler *et al.* [80] presented a model of dynamic behaviour in laser beam welding. They found that the plasma fluctuations (Figure 2.26) and the sound emission (Figure 2.27) reflect the pressure variations in the keyhole.

The plasma expands only for overcritical outflow because in this case the pressure p_e (Figure 2.28) is higher than the pressure p_0 in the environment. As the ratio of p_i to p_e for overcritical outflow is constant, a higher internal pressure results in a higher overpressure at the exit as well as a higher mass flow rate out of the keyhole. The consequence is a broader expansion of the plasma, a higher change of pressure and an increased height of the plasma. The outflow plasma reaches the maximum of its width at a certain distance above the workpiece. Due to the short influence of this high pressure it does not destroy the keyhole.

In the Figure 2.29(a), the recoil pressure is lower than the capillary pressure and the convective heat transport is reduced. The temperature and the thickness of the melt at the front increases. With increasing temperature, the evaporation rate increases exponentially. If the pressure is superior to the capillary pressure, after a certain time delay, the melt moves from front to rear. The metal vapour density is superior to the critical value and a plasma develops (Figure 2.29(b)). The increasing pressure results in an increase of the mass flow rate out of the keyhole as well as of the rate of condensation of atoms and recombination of ions and the volume of the keyhole. These three factors and the convective heat transport, which reduces the evaporation rate, also reduces the density of the atoms and ions and thus the pressure.

The decrease of pressure results in a drop of the mass flow rate, the rate of condensation and recombination and after a certain time also of the volume of the keyhole. Moreover depending upon the pressure of the processing gas, it penetrates into the keyhole (Figure 2.29(c)).

In the case of full penetration welding, if the average pressure in the keyhole is low, the keyhole opens at the bottom side . This opening is reduced or closed if the internal pressure increases because the pressure forces melt to the bottom side.

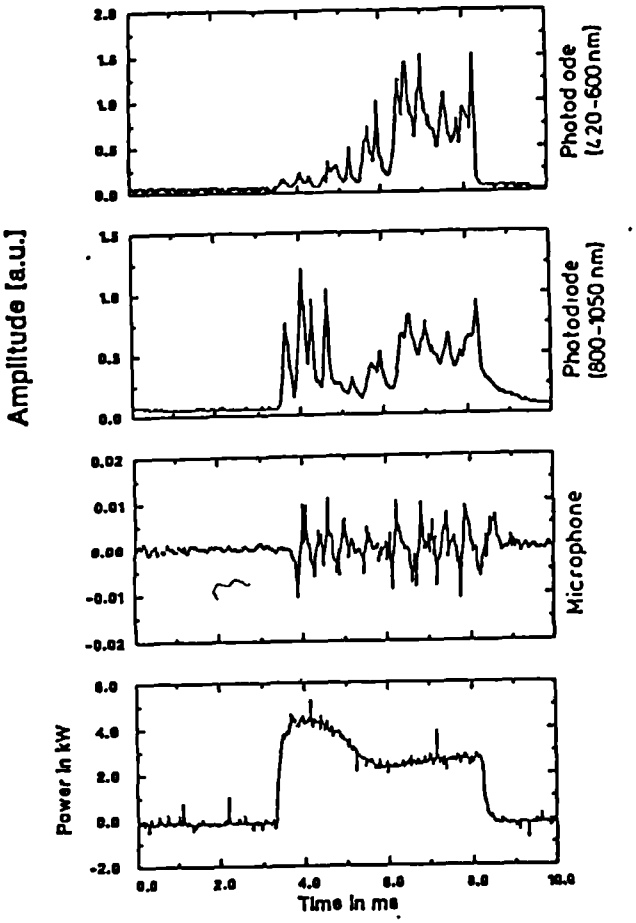


Figure 2.27 Radiation and sound emission measured during welding with 100 Hz pulse frequency. At the begining of the laser pulse, several metal vapour fluctuations as well as the plasma fluctuations detected, go hand in hand with the pressure variations [80].

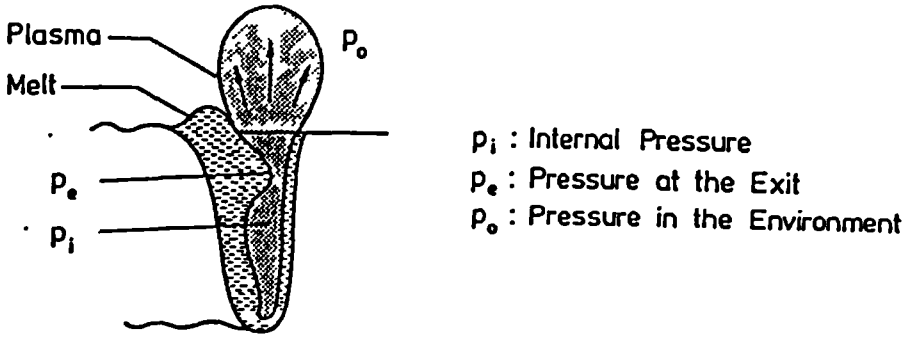


Figure 2.28 Schematic representation of the keyhole [80].

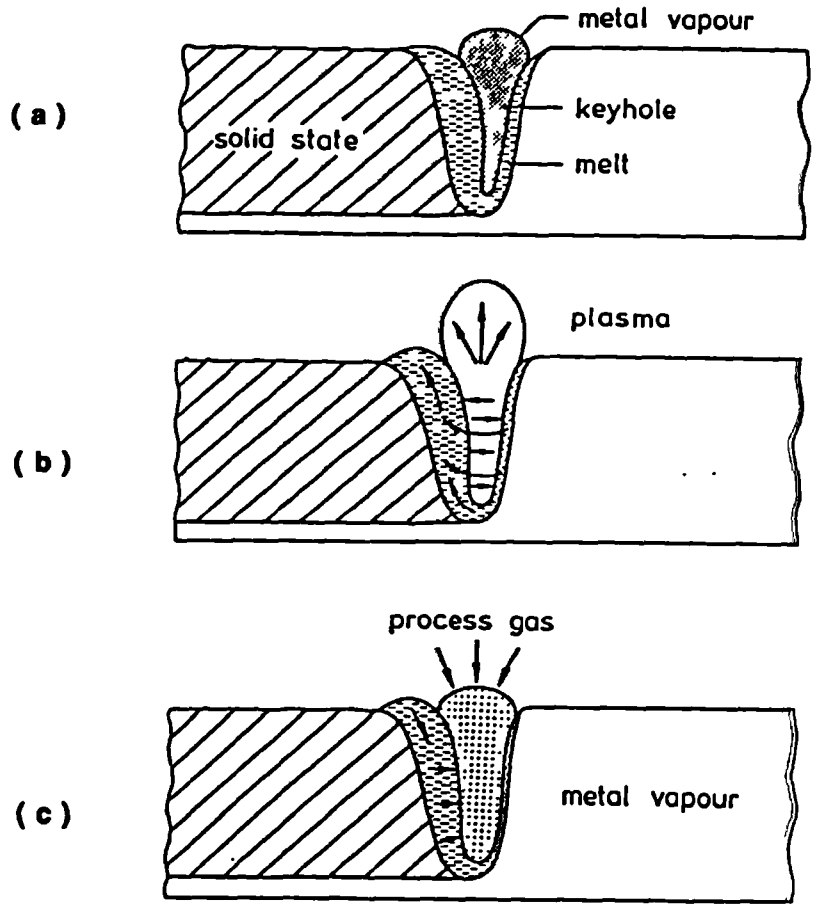


Figure 2.29 Dynamic model for penetration welding [80].

2.1.9 Conventional Processes for Welding Zinc Coated Steel

While imparting excellent corrosion properties to steel, zinc coatings can adversely affect the weldability of steel. When galvanised steel sheets are brought into the welding process, special adjustments have to be made to the resistance and gas shielding conditions to get we ding results on a par qualitatively with those obtained from non-galvanised materials. Moreover the protective gas nozzle has to be cleaned after a certain number of welds to ensure that the flow of gas from the nozzle will remain uniform and the weld will be properly covered with protective gas. Some of the processes used at present are briefly described here.

2.1.9.1 Shielded Metal Arc Welding

Shielded Metal Arc Welding (SMAW) is an arc welding process in which joining of the metals is produced by heat from an electric arc that is maintained between the tip of a covered electrode and the surface of the base metal be ng welded [81]. A sketch of the shielded metal arc welding process is shown in Figure 2.30. Shielded metal arc welding of galvanised steel is accomplished with similar procedures and amperages to those for uncoated steels, however, certain manipulation of the electrode is useful in vapourising the zinc coating ahead of the weld pool. During welding, repeated, intermittent movement of the welding arc ahead of the weld pool will melt and vaporise the zinc coating. This procedure reduces porosity by decreasing zinc vapour entrapment, and also lowers the probability of zinc penetration cracking.

Nielbock [82], using 0.8 mm electrogalvanised and hot dipped galvanised sheet, found that the zinc evaporated from the overlapped joints escapes through the molten puddle resulting in the deterioration of the weld and affecting the arc welding process. He found that the zinc if trapped in the melt causes porosity formation. Nielbock reported that welds free of porosity can be made at the expanse of reduct'on in the welding speed. The slower welding speeds accompanied by an increase in the energy of expansion promotes the evaporation of the zinc layer in the immediate neighbourhood of the electric arc ahead of the melt, so that less of the vapour has to escape through the melt. He found that the welding speed has to be reduced with the increase in zinc thickness for optimum welding.

2.1.9.2 Gas Metal Arc Welding

Gas Metal Arc Welding (GMAW) is an electric arc welding process that produces joining of metals by heating them with an arc established between a continuous filler metal (consumable) electrode and the workpiece [83]. A sketch of the process is shown in Figure 2.31. Shielding of the arc and the molten metal is

usually obtained by argon or helium gas. Owing to the use of inert gas the GMAW process is also called Metal Inert Gas (MIG) welding Gas metal arc welding of galvanised steel is conducted with similar procedures to those for uncoated steel, however, the travel speed must be decreased to allow for vaporisation of zinc ahead of the weld pool, and larger root openings must be used to allow zinc vapour to escape. Gregory [8] found that a large amount of spatter is evolved when MIG welding galvanised steel.

Welding with silicon deoxidised filler increases the probability of zinc penetration cracking while low silicon wire has low cracking susceptibility. Using CO_2 shielding and short circuit transfer, spatter is increased when welding galvanised steel as compared to bare steel. Spatter adherence can be reduced by spraying the gun and workpiece with an antispatter compound prior to welding.

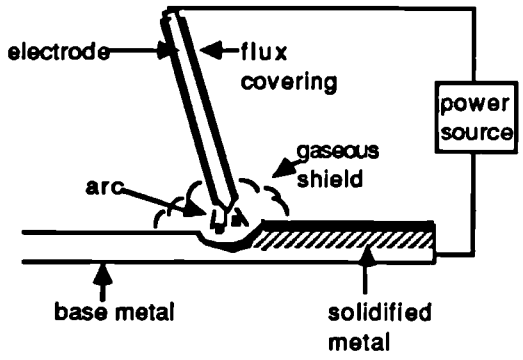


Figure 2.30 Shielded metal arc welding.

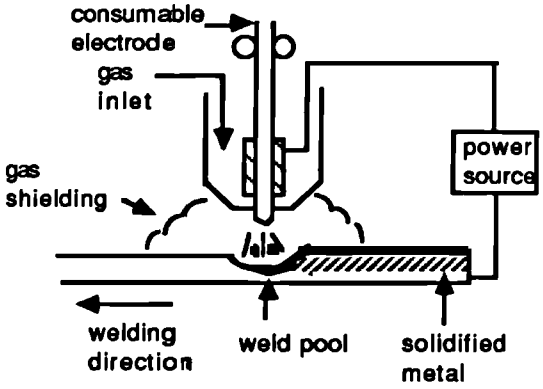


Figure 2.31 Gas metal arc welding.

2.1.9.3 Submerged Arc Welding

Submerged Arc Welding (SAW) is an arc welding process in which joining of metals is produced by heating them with an arc between a bare consumable electrode and the workpiece, the arc being shielded by a blanket of granular, fusible material placed over the welding area. This process differs from other arc welding processes in that the welding area, including the arc, is covered by the granular, fusible material. Figure 2.32 is a sketch of the SAW process.

As for the previous two processes, submerged arc welding of galvanised steel utilises similar procedures compared with similar welding of uncoated steel. A typical joint configuration, if the joint faces are galvanised, is a 70° V-groove with a 0.66 mm (0.026 in) wide root face to allow for escape of zinc vapour. Similarly, when welding a square groove joint with galvanised faces, a root opening of 1.5 mm to 3.3 mm (0.06 in. to 0.13 in.) will a low zinc vapour to escape an unbacked joint. However, the quality of the weld will remain dependent of current, travel speed and zinc coating thickness. Typical problems include an irregular weld bead face and slag removal is usually more difficult when compared with welding bare steel. Suggested root openings for fillet welds are similar to those previously mentioned for square groove welds.

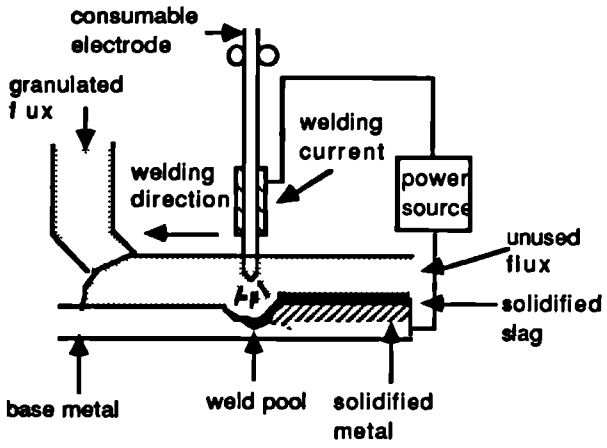


Figure 2.32 Submerged arc welding.

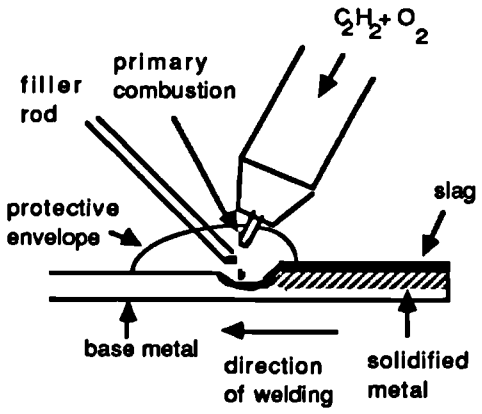


Figure 2.33 Oxyacetylene welding.

2.1.9.4 Oxyacetylene Welding

This process employs the use of a fuel gas combined with oxygen as a heating medium. The oxyacetylene welding process, owing to its high flame temperature is the most commonly used gas welding process. Figure 2.33 is a sketch of the oxyacetylene welding process. The use of flux may or may not be required, depending on the degree of the protection of the weld needed during welding. The low heat input inherent with this process produces a relatively large heated zone, therefore, zinc vapourisation is also quite widespread. This results in exposure of the underlying

steel after which welding can proceed in the same manner as for bare, low carbon steel.

2.1.9.5 Resistance Spot Welding

Figure 2.34 shows the sketch of the resistance spot welding process. In most automotive industries the method of resistance spot welding has been widely used. Resistance spot welding is idea ly suited for joining sheet materials and is well adapted to mass production industries. In addition, operating costs for this process are relatively low. The American Welding Society defines Resistance Spot Welding as; "A resistance spot welding process wherein coalescence at the faying surface is produced in one spot by the heat obtained from the resistance to the flow of electric current". Ideally the point of highest resistance, that is the point where the most heat is generated, is at the faying surface [4].

In resistance welding, much work has been performed on the effect of material parameters [84-87], process parameters [88-95], electrode life, configuration and composition [96-97]. Production of a satisfactory weld will depend upon the amount of current and local electrical resistance [88-90]. More welding current is needed when spot welding galvanised steel than would be required for the equivalent thickness of uncoated steel [86]. This is a general feature of all coated steels and has been attributed to the physical properties of the coating interfaces.

For uncoated sheet joined in lap configuration the copper electrode to steel has a low resistance while at the steel to steel faying surfaces the contact resistance is high which produces ohmic heating at the desired location. In the case of galvanised steel the low melting point of zinc results in the early melting either at the electrode/sheet interface or at the sheet/sheet faying surface. The pressure applied by the electrodes causes displacement and spreading of the molten zinc resulting in increased contact areas and shunting of the welding current. Alloying of the electrode tip due to repeated contact with the molten zinc causes rapid deterioration and changes the electrical

properties and effective area of the contact surface. Higher electrode temperature due to the necessary increase in current (shunting) clearly increases the rate of electrode damage.

The higher melting point and electrical resistance and lower activity of the intermetallic compounds in zinc-iron alloy coatings are more favourable to electrode life [85,98]. In fact the welding behaviour of sheet coated on both sides with the zinc-iron alloy approaches that of cold rolled steel. Experience has shown that for welding zinc coated steels, the welding current (for constant time) has to be increased by 20 to 30 % and the electrode force by 20%. Electrode life may be decreased by 50% or more based on a conservative estimate of 10,000 welds on bare steel [91,99]. Spot welding calls for special precautions because of the reduction in electrode life.

2.1.9.6 Resistance Seam Welding

In resistance welding, contact resistance is considered to be an important factor. It is quite possible that during the welding operation, the electrode/steel resistance may be changed due to a progressive chemical reaction between the surface film and the electrode material. Seam welding of coated steel presents problems of the coating being picked up by the electrode. This pick-up results in a variable resistance between the electrode and the component to be welded thereby giving rise to a variable heating effect and inconsistent weld quality. The problem of electrode pick-up is overcome by constantly presenting an uncontaminated electrode to the workpiece. In case of laser welding no such problems are encountered.

It is generally considered that the resistance seam welding of coated steel is a critical process requiring very closely defined operating limits. A sketch of the seam welding process is shown in Figure 2.35. As with resistance spot welding, the major problems encountered are the avoidance of electrode pick-up and difficulties in determining optimum welding conditions. In forming a seam weld, the electrodes are

subjected to a more severe mechanical and thermal treatment than during spot welding. It is also more difficult to effectively water cool seam welding electrodes. Consequently, conventional seam welding practice is not recommended for the welding of most coated steels, particularly if zinc coated, because of the problems of excessive contamination of the electrode wheels, thus resulting in the need for excessive wheel maintenance. However certain modifications to the basic system were made to enable satisfactory resistance seam welding [6,7]. In resistance seam welding, a spring loaded scraper device is located ahead of the rollers to remove any heavy build-up of coating on the roller electrode. In some cases the electrode/sheet resistance is maintained constant by feeding a copper wire between the electrode wheels and the sheet surface. By this method any coating pick-up is continuously removed on copper wire and the weld is effectively made by "clean" electrodes at all times. Figure 2.35 shows the seam welding using wire roller electrodes.

Resistance welding requires access to both sides of the workpiece, while lasers can weld from a single side. The electrodes mark both pieces, causing cosmetic problems. Electrode maintenance is required because they oxidise and pick up metal from the workpiece. Lasers can lap weld sheet metal without contact.

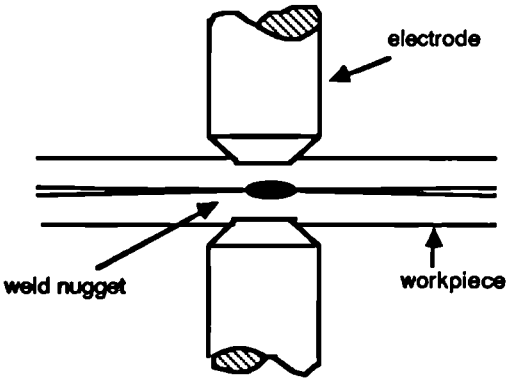
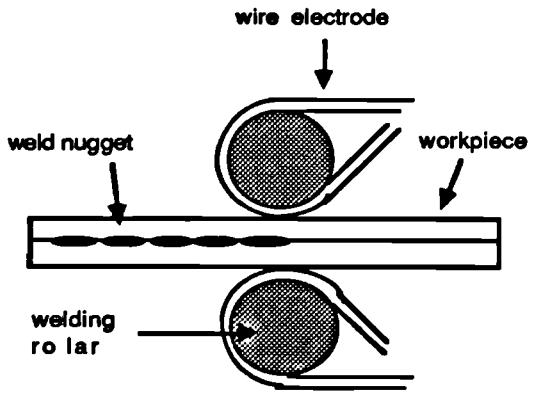


Figure 2.34 Resistance spot welding.



F'gure 2.35 Resistance seam welding.

2.1.9.7 Projection Welding

In this process, current concentration is achieved by shaping the workpiece so that when two halves are brought together in the welding machine current flows through limited points of contact. A projection is raised in one sheet (as shown in figure 2.36) of a lap joint through which the current flows to cause local heating and collapse of the projection. Both the projection and the metal on the other side of the joint with which it makes contact are fused so that a localised weld is formed.

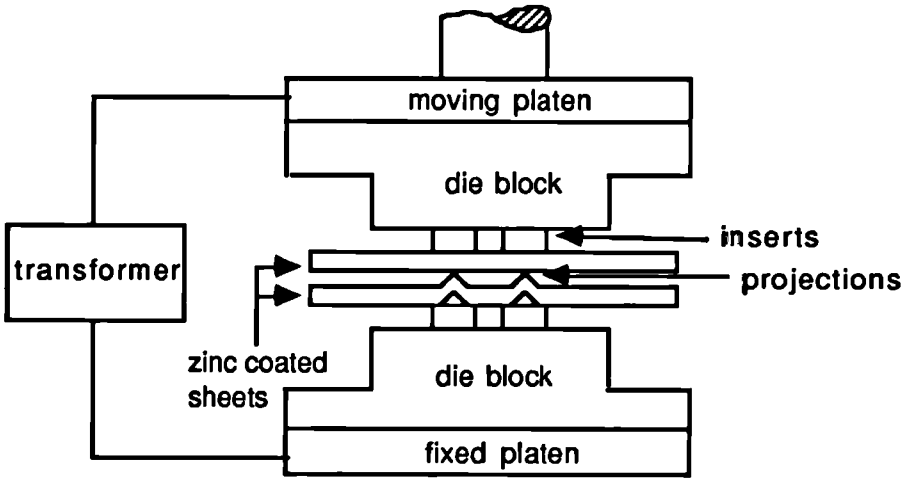


Figure 2.36 Projection welding process.

Thorne *et al.* [100] utilised a high current short duration energy pulse which concentrates the heat generated at the weld interface and did not allow the heat to be dissipated before the projection collapsed and the weld nugget was grown. Total heat input to the weld was minimised due to the lack of losses because of the short time of welding. Fast follow-up of the welding electrode is essential due to the rapid collapse of the projection. If the follow up speed is insufficient, the actual weld force will decrease to the point where severe expulsion occurs and the weld quality is lost.

Jessop and Roswell [101] studied the projection welding of mild steel and zinc coated steel (both hot dipped and electrogalvanised). They found that with mild steel, heating occurred in the sidewalls causing the projection to collapse. Heat also

generated at the interface and thus the total heat generation resulted in melting the whole of the projection and surrounding metal giving a fusion weld. With the hot dipped and electrogalvanised steel, heat was likewise generated at the interface and at the projection sidewalls, but when the projection collapsed no melting of the steel occurred. They found that the molten zinc which formed around the periphery of the weld shunted the current and thereby limited the heat generated. To avoid this the weld must be made before the sheets get close enough for the zinc to shunt the current. At high heat conditions severe expulsion of zinc and steel occurred which resulted in a cavity at the centre of the weld and the high current density in the sidewalls causes them to shear.

2.1.10 High Energy Density Welding

These processes employ power densities which are significantly higher than conventional welding processes. These include plasma arc welding, electron beam welding and laser welding.

2.1.10.1 Plasma Arc Welding

Plasma Arc Welding is an arc welding process in which fusion is produced by heating with a constricted arc between an electrode and the workpiece. Figure 2.37 shows a sketch of the plasma arc welding process. It is similar to the gas tungsten arc welding in that a tungsten electrode is also used. However owing to the converging action of the orifice gas nozzle, the arc in the PAW process is more constricted than GTAW process, and consequently welds produced are narrower and deeper. No data has been available for welding zinc coated steel with this process.

2.1.10.2 Electron Beam Welding

This is a high energy density process that accelerates a beam of electrons onto a workpiece (Figure 2.38). Tremendous heat is generated in a small volume,

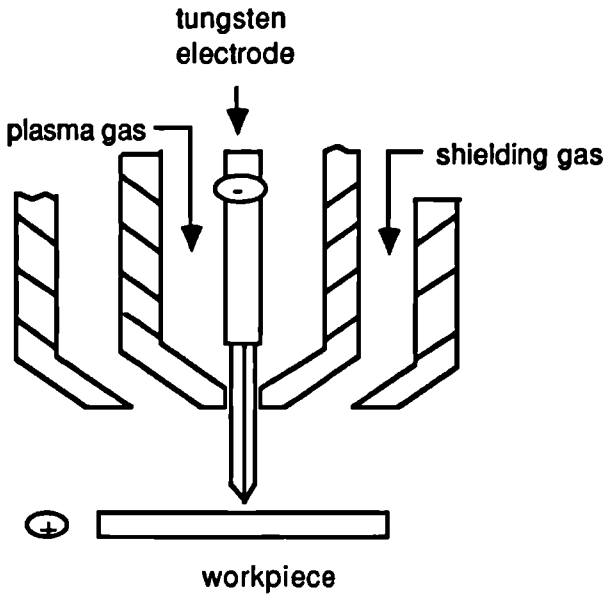


Figure 2.37 Keyhole welding with Plasma arc process.

generating a keyhole and producing deep penetration welds. The primary disadvantage of electron beam welding is that high vacuum is required to prevent beam scattering. Production parts must shuttle through air locks, which slow cycle times and are a major maintenance problem. Non-vacuum electron beam welds may be performed, but are not as well focused due to scattering.

Secondary problems include magnetic deflection and X-ray emission. Since electrons are charged, they are deflected by magnetic fields, requiring electron beam welded parts to be demagnetised. Emission of X-rays, strongest at the highest voltages, requires radiation shielding for personnel protection. Lasers can perform an equivalent weld, within their range, without vacuum chambers, demagnetisation, or X-ray shields. Electron beam welding of zinc coated steel is virtually impossible due to the additional problem of maintaining the vacuum. To-date no data has been available for welding zinc coated steel using an electron beam.

2.1.10.3 Laser Beam Welding

A simple diagram of the laser welding process is shown in Figure 2.39. The galvanised sheets must have a certain width for producing part of the car in certain single press operations. Since this material is produced in Europe only in a certain limited width, CO_2 lasers are used to produce the necessary size of the sheet by welding two parts together. Lasers have been used by many researchers [102-106] to weld zinc coated steel in butt configuration for the above mentioned purpose without any difficulty. But the problem arises in the welding of galvanised steel in lap configurations (see section 1.4). Many authors [107-113] working on the welding of the galvanised steel in lap configuration, found that a gap between the sheets is necessary for welding with laser. Heyden *et al.* [113] using a pulsed laser predicted that no gap is needed for welding zinc coated steel if the pulse frequency is matched with the volume of the evaporated zinc.

Decker *et al.* [114] studied the influence of surface layers on the metallugical properties of laser beam welds. Using zinc coated sheets, noneof the coating elements was found in the welding material.

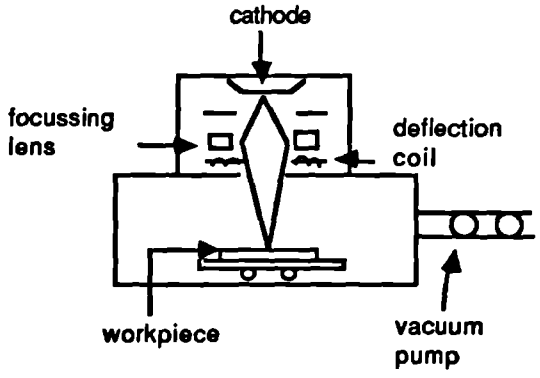


Figure 2.38 Electron beam welding.

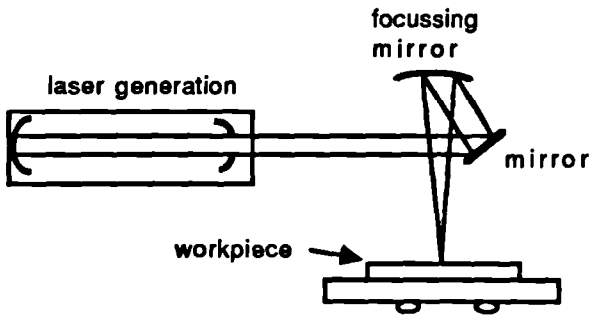


Figure 2.39 Laser beam welding.

2.2 Materials

Sheet steel is the main material used for the construction of the body of a motor vehicle. Steel is relatively cheap, has good mechanical properties, and can be economically formed to make parts with complicated shapes. The parts can then be welded to form a complete car assembly. Over the past few years the car industries has increased the use of zinc coated steel due to consumer pressure requiring car bodies to be durable, economical and corrosion resistant.

Car manufacturers are aiming to guarantee cars for 5 years against cosmetic corrosion (on the outer surface of the car body) and for 10 years against perforation corrosion (propagating from the inner surface of car body) [115]. This challenge is particularly difficult to meet in regions where salt damage may occur as a result of snow-melting agents that are sprinkled on roads to ensure safe traffic in the winter. To meet this challenge the automotive industry has dramatically increased the usage of zinc coated steels.

It is estimated [5] that approximately 40% of the world production of zinc is consumed in hot-dip galvanising of iron and steel, and this adequately demonstrates the worldwide use of zinc as a protective coating. The success of zinc can be largely attributed to ease of application, low cost and high corrosion resistance.

2.2.1 Galvanising

The application of a zinc coating on steel is termed 'galvanising'. Galvanising is one of the oldest, simplest and generally the cheapest method used for the protection of steel against corrosion. The term "galvanising" is derived from Luigi Galvani who was Professor of Physiology at the University of Bologna, Italy during the second part of Eighteenth century [116]. It was Galvani who discovered the first chemical process for generating electricity. Galvani found that by dipping two dissimilar metals into an electrolyte and connecting them electrically, a current flowed between them. Zinc

behaves in this manner when coupled to steel and provides sacrificial protection to steel (see section 7.1.1).

2.2.2 Application of Zinc Coating on Steel

Zinc coatings can be applied by a range of techniques that afford varying degrees of protection and serve different technical requirements. The actual structure and composition of zinc coatings depends upon the method of deposition. There are five common methods for the application of zinc to steel:

(i) Hot dip galvanising, (ii) Electrogalvanising (Electroplating),
(iii) Metal spraying, (iv) Sherardising and (v) Zinc rich primers.

The methods of application of zinc have been investigated by many researchers and are described briefly here:

2.2.2.1 Hot Dip Galvanising

The coating on galvanised material is applied by immersion in molten zinc. Figure 2.40 describes the process diagrammatically. Details of the method have been described elsewhere [1,5,117-122]. The steel strip is passed through a molten zinc bath at about 450-480 °C. A reaction [119] takes place between solid iron (or steel) and molten zinc which forms an alloy of (Zn/Fe) at the contact line. A small amount of aluminium (0.1-0.3 %) is added to the molten zinc bath to depress the formation of zinc-iron alloy on the steel surface.

When the strip is galvanised it is drawn continuously through the bath and on emerging is passed through rolls or an air jet to remove excess zinc. The actual thickness of the coating depends upon the time of residence of the steel strip in the molten bath. The thickness is controlled by means of air knives before the zinc solidifies.

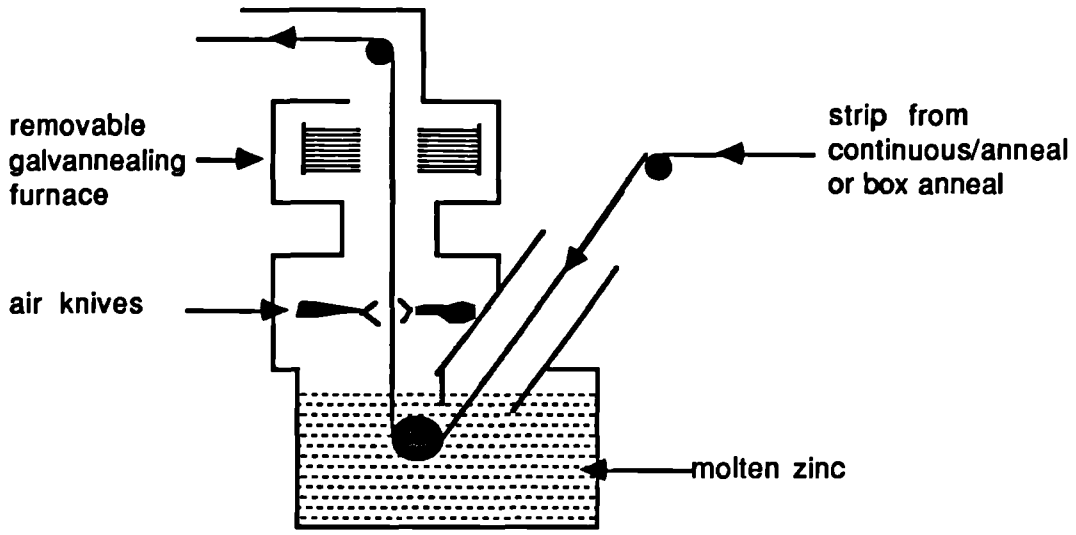


Figure 2.40 Hot dip galvanising process.

2.2.2.2 Electrogalvanising

Electrogalvanising is one of the important methods for producing coated strips. Many researchers [115,122-125] have described the process, hence, complete detail is not necessary here.

The metallic strip is passed through a solution of flowing zinc salt ($ZnSO_4$ or $ZnCl_2$) i.e., through a plating cell. The steel strip is made the cathode of the cell (Figure 2.41), so that metallic zinc is deposited at the exposed surface of the strip. The cell is lined with zinc anodes. The zinc anode dissolves replacing the metal lost at the cathode. The overall process is metal (zinc) transfer from anode to cathode via the solution. The main cathodic process is usually the reduction of dissolved ions to metal in the form of an adherent and coherent coating.

This process occurs at rather low temperature (50-75 °C) so that no alloying effect with the substrate and no heat treatment of the steel will occur. The deposited thickness is easily controlled by the number of coulombs passed per square meter, and binary alloys (or even ternary alloys) may be obtained by making use of suitable bath compositions and electrolysis conditions.

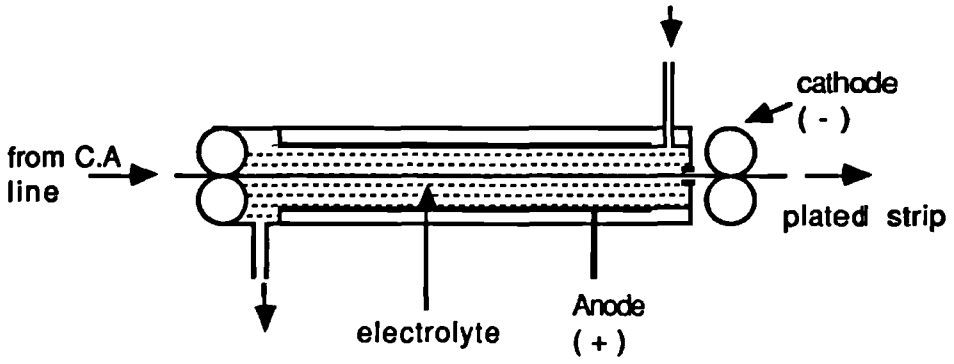


Figure 2.41 Electrogalvanising process.

2.2.2.3 Zinc Spraying [1, 5]

In this process, zinc powder is mixed with a stream of combustible gas or air. The stream is fed into a central nozzle, surrounded by an annular orifice. The orifice is fed with a fuel-gas and oxygen mixture which would give a blow-pipe flame on ignition. The passage of the powder through the flame results in the melting of most of the particles. Compressed air or other gas is fed through a second annular orifice surrounding the gas ports, with the result that the molten powder particles are projected forward as in the molten metal process.

Besides zinc powder, a wire can also be used. The wire is fed axially into a blow-pipe flame where it melts and a jet of compressed air atomises and sprays it.

2.2.2.4 Sherardising [1, 5]

In this process an iron or steel article is packed in a powder containing zinc dust and a dilutent such as silica or sand. The powder and the articles are then placed in a steel drum which is slowly rotated while the temperature is raised to between 350 and 400° C, i.e., below the melting point of zinc. The temperature is maintained for 3 10 hr depending upon the size of the components and the coating thickness required. Usually, rapid cooling is obtained by removing the drum from the furnace

and spraying it under a water jet while rotating slowly.

2.2.2.5 Zinc Rich Primers [2, 115, 126]

A typical zinc rich primer is produced by mixing very fine metallic zinc powder into a resin system to develop a complex film. Zinc rich primers, such as Dacrometal and Zincrometal are also available. In the Dacromet process, the metallic coating is obtained from lamellar zinc in suspension in an aqueous chromic solution containing organic compounds. After curing at a rather high temperature (300° C), most of the organic species are removed and the protective layer contains mainly zinc and chromium oxide, thus providing a weldable primer layer. The Dacromet system on steel is called Dacrometal.

At present a continuous strip coating can be obtained by a method based on two layers: the first is the Dacromet layer about 2 μm thick baked at only 150 °C, while the second layer is of Zincromet, a zinc-rich resin designed to allow resistance welding and to protect the Dacromet layer during forming, the whole system being baked at 260 °C.

2.2.3 Additional Properties of Galvanised Steel

The corrosion performance of the coating is only one of a number of factors which must be considered before a particular coated steel is chosen for a specific application within the car body. A coating must also have the adhesion and flexibility to withstand deformation when formed into sub-assembled parts by roll forming or stamping operations. Since the end user must further assemble these coated parts, the coating system must be weldable. The coating must also be compatible with conventional topcoat or exterior finish coatings.

2.2.3.1 Formability

Galvanised steels in general exhibit somewhat different base metal and surface characteristics in comparison to cold rolled mild steel that they have replaced. Surface effects play an important role in its forming behaviour. The electro-galvanising variables have a considerable effect on the surface topography and large differences may exist between products. The surface roughness difference between coatings may result in significant variations in press performance for materials of similar base metal properties. Increased tooling/steel friction may result from coarser deposits unless an adequate lubrication practice is followed at the stamping plant. Successful use of galvanised steels for formed automotive panels requires good tooling maintenance, adequate lubrication and particular attention to the stamping operation. Major gains in formability of the galvanised products can be obtained by the reduction in the carbon content of the base steel [127].

2.2.3.2 Weldability

The automotive industry widely employs welding in the joining and assembly of components. The weldability of the steels and the safety of the welded joints are important considerations affecting the development of automotive steels. Production of a satisfactory weld by spot welding will depend upon the amount of current and local electrical resistance. For welding zinc coated steels, the welding current (for constant time) has to be increased by 20 to 30 % and the electrode force by 20%. Electrode life may be decreased by 50%. The weldabil ty of galvanised steel using different methods is already discussed in section (2.1.9).

2.2.3.3 Paintability

For the protection of exterior surface of automotive body panels two side coated steel is required. For the exterior surface, the paint adhesion is as important as corrosion resistance. The alloy side of the one and a half side galvanised steel (1-1/2

SGS) product (Figure 2.42) has proven to be desirable for exterior panels because of its smooth surface, superior paint adherence and corrosion resistance (both cosmetic and perforation). The porosity of the alloy surface provides a high efficient mechanical keying of the paint system primer.

2.2.3.4 Phosphating

Sheet steels, whether coated or uncoated, are normally given a phosphate treatment by automobile manufacturers as a pretreatment to the subsequent primer painting, for corrosion resistance and adherence of paint coating. Compatibility of this treatment to the precoated sheet has to be borne in mind while selecting a particular precoated sheet. Zinc phosphate coating on bare cold rolled surface essentially consists of hopeite $\{Zn_3(PO_4)_2.4H_2O\}$, and phosphophyllite $\{Zn_2Fe(PO_4)_2.4H_2O$ crystals [128,129]. With respect to zinc coated sheets, no formation of phosphophyllite takes place, because phosphophyllite is produced on Fe-Zn alloy when the Fe content in the alloy coating is more than 28% [129]. These crystals gives a better paint adhesiveness to the sheet steel. Phosphating reduces the corrosion rate by increasing the polymer/substrate adhesion and slowing down crack growth at the interface.

2.2.3.5 Surface Finish

The surface characteristics of galvanised sheet are of primary importance and have an impact on most of the fabrication processes used in automotive production. The free zinc side should be smooth which implies a temper rolled minimised spangle surface (for hot dipped material) free of coating defects. A smooth surface is necessary for uniform friction against the punch during the stamping.

2.2.4 Types of Zinc Coatings Available

There are many types of zinc coatings available. Different areas of a vehicle

require different zinc coatings and coating thicknesses to meet appearance and performance criteria [130]. The various combinations of surfaces available are summarised in Figure 2.42.

2.2.4.1 One Side Galvanised Steel

In this case, free zinc is applied to one side of the steel sheet either by hot dip or electrolytic process. The uncoated side is mainly used for outer body panels as it provides a good surface for paint appearance, while the free zinc inside the car protects against perforation corrosion. The electrolytically coated one side galvanised products provide good characteristics for acceptable appearance after stamping.

Since the thickness of the electrodeposited layer can be readily controlled during deposition (and is usually maintained at approximately 10 μm in these applications) the electrogalvanised material has advantages over the thicker coatings produced by hot dipping. Since there are no embrittling intermetallics and the coating is thinner, formability is good compared with hot dipped (galvanised) material. Surface finish is intrinsically superior because of the absence of spangle and the suitability of the electrogalvanised material for a phosphatising prepainting treatment. However, the duration of the sacrificially protective effect of the thin coating is a limiting factor in the applicability of the material.

2.2.4.2 One and Half Side Galvanised Steel

In this type of material, one side of the sheet is coated with free zinc, and a thin layer of zinc-iron alloy is formed on the other side. This product is mainly produced by the hot dip process [99, 131]. The coating, when passed through the furnace, is heated on one side only to convert that side into iron-zinc alloy. This product is used for exposed body panels. The zinc-iron alloy provides cosmetic protection on the outer side exposed panels and the free zinc side provides perforation protection. Belleau and Kelley [127] found that one and half side (differentially coated)

galvanised steel is a suitable corrosion resistant substitute for the traditional cold rolled steel in automobile bodies and is very useful for exposed application. One drawback of the product to date has been its susceptibility to surface defects, being a hot dipped product, which has limited its use on critical surface panels, such as the hood and deck lid outer panels.

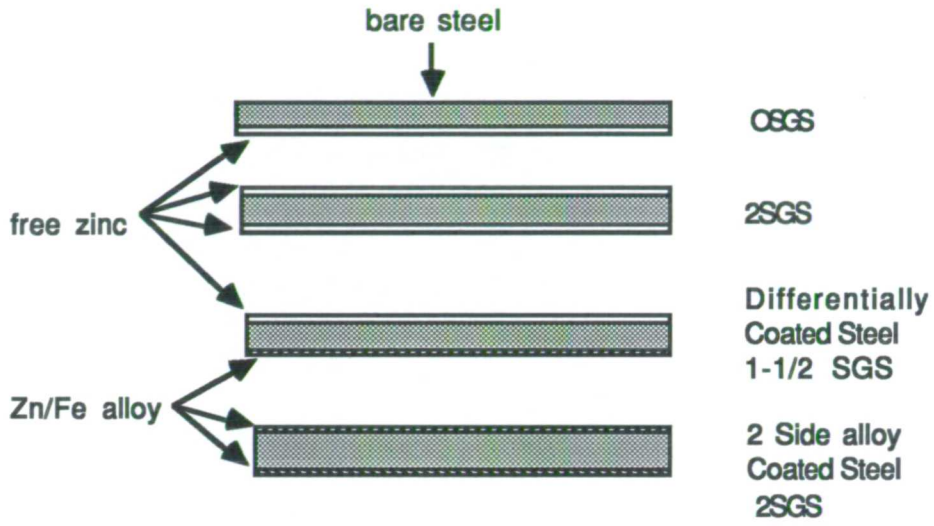


Figure 2.42 Types of galvanised coatings [31]. Where OSGS = One Side Galvanised Steel, 2SGS = 2 Side Galvanised Steel, 1-1/2 SGS = one and a half Side Galvanised Steel.

2.2.4.3 Two Side Galvanised Steel

This material employs free zinc on both sides of the steel sheet with equal or differential coating thicknesses. It is used mainly for unexposed applications where corrosion protection is required from both sides. A few automobile manufacturers have recently incorporated two side galvanised for exposed applications. This material is primarily produced by the hot dip process, but is also available as electrolytically coated. Out of all galvanised sheet steel, this product is the most widely available.

2.2.4.4 Two Side Galvannealed Steel

This material has a zinc-iron coating on both sides of the sheet with equal or differential coating thicknesses. The product is mainly produced by the hot dip process where free zinc is alloyed in a galvannealing furnace above the zinc bath. The most common usage in the automotive industry is for unexposed panels. This material has better resistance welding and paintability characteristics than two side galvanised steel.

2.2.4.5 Iron-Zinc Alloy Electroplated Steel

Two side zinc-iron alloy coated products have been available from steel makers for some years, but their application to automotive components is recent. The iron-zinc alloy is electronegative to iron. Due to the nature of the process electrogalvanised steel exhibits higher coating uniformity and therefore higher surface quality than hot dip products [132]. These steels are being considered for exposed as well as unexposed applications.

Fe-Zn alloy was originally developed for the purpose of preventing inside-out perforation type corrosion, and for the purpose of obtaining better formability than galvannealed steel. For the exterior surface, paint adhesion is considered to be as important as corrosion resistance. Fe-Zn alloy showed a good paintability. Fe-Zn alloy showed better weldability than galvanised steel, because iron-zinc alloy is harder and has a higher melting point than pure zinc. Moreover, as iron-zinc alloy has a poor reactivity with the copper electrode, the electrode life is prolonged [132].

2.2.4.6 Zinc-Nickel Coated Steel

This product is produced exclusively by the electrolytic process which employs a zinc-nickel alloy on one or both sides of the sheet. Because this coating is less reactive than free zinc, or zinc-iron coating, typical coating thicknesses are lower.

Presently, the majority of zinc-nickel steel is produced in Japan [133]. This product exhibits good weldability, better coating adhesion and paintability [134]. This alloy is electronegative to iron and shows good corrosion resistance.

2.2.4.7 Galfan Coating

This coating consists of zinc-5% aluminum plus a small addition of mischmetal (a naturally occurring mixture of rare earth elements) < 0.1%. The corrosion resistance of Galfan is more than twice that of conventional galvanised steel under similar conditions and similar coating thicknesses [135]. This coating also have good ductility under cold forming conditions and behaves comparably to conventional galvanised steel with respect to spot weldability and paintability. Several paint systems now used for conventional galvanising are equally satisfactory for Galfan [135].

The adherence of the coating is superior to conventional galvanised coatings. However, in the galvanising process, new fluxes are required since the conventional galvanising fluxes break down in the presence of 5% aluminum content of Galfan.

2.2.4.8 Zn-Fe/Zn-Ni Double Layer Electroplated Steel Sheet

In order to obtain good formability and good weldability, coated steel sheet with a thin and high corrosion resistant plated layer are required for automobiles. Zn-Ni is considered to be the most preferable from the view point of commercial production and corrosion resistance. Paint adhesion to Zn-Ni electroplated steel sheet, however, is inferior to that of cold-rolled and galvanised steel sheets. In order to improve this characteristic, a double-layer alloy electroplated steel sheet was developed [136]. The steel sheet was composed of an upper Zn-Fe (80-90% Fe) alloy layer which had good paint adhesion and a lower Zn-Ni (10-15% Ni) alloy layer which has good corrosion resistance. This coated steel sheet was revealed to be suitable for the automotive use.

2.2.4.9 Zn-Cr-CrO_X (Zincrox) Electrogalvanised Steel

This new Multilayer Electro Galvanised (MEG) product (Zincrox), consists of a continuously superimposed electrolytic layers of Zn-Cr-CrO_X. The coating is still 99% Zn, but the thin layers of Cr-CrO_X have solved critical problems: formability, conventional weldability, welding fumes, electrode wear, paint adhesion, and resistance to the most severe corrosion tests with a reduced zinc thickness [137].

The MEG product, Zn-Cr-CrO_X, was given the trade name ZINCROX®. The better conventional welding of ZINCROX can be explained by the Cr-CrO_X layers which prevent contact between the copper of the electrode and the zinc of the coating, thus eliminating the possibility of brass formation and consequently electrode wear.

Catanzano [137] found that the corrosion resistance of the ZINCROX was 8-10 times higher than the galvanised product. This was due to the electrolytic Cr-CrO_X layer which deactivates the zinc and protects it from corrosion. This is the major point in the thinking behind ZINCROX: the zinc is necessary but must be protected in order to delay its main activation as far as possible. If coating damage occurs, the zinc will have to be sacrificed, but not before.

The chrome oxide layer provides good paint bonding. The MEG product has high base steel formability (cold process), high coating formability (electrodeposition), excellent weldability (Cu-Zn contact neutrialised by Cr-CrO_X coating).

2.2.5 Utilisation of Zinc Coated Steel

Zinc coatings are successfully used in a very wide field to protect iron and steel goods from corrosion attack. The building trade is one of the largest users of zinc coated steel. The frameworks of large modern buildings can be either galvanised or zinc sprayed before erection, or sprayed on site. Where a framework is accessible, zinc-rich paints provide an excellent way of renovating old buildings. Apart from the

structural aspect, galvanised sheeting is used for roofing, ventilation ducts and gutters, as well as for water tanks and cisterns, and galvanised pipe is used for public and domestic services.

Zinc coated structures are used in pylons carrying electrical transmission lines, in masts for radio, television and radar aerials, and for supports for overhead wires on electrified railways. An interesting new use of galvanised steel is for reinforcement of concrete. This reduces the risk of spalling and staining or can enable the depth of cover to be reduced leading to slimmer structure of lower cost.

More recently British Steel has increased the production of galvanised steel to fulfill the requirement of galvanised steel for automotive and building industries [138].

2.2.5.1 Zinc Coated Steel in the Automotive Industry

The use of zinc coated sheeting for automobile bodies is developing rapidly and has become a sales argument. Pierre [139] has reviewed the use of zinc coated steel by all the European and American vehicle manufacturers as well as the types of zinc coating used. Electrogalvanised (zinc coated) steel has become a material of choice in the fabrication of automobile bodies that will meet the guarantee lifetime of 5 years resistance to cosmetic corrosion and 10 years resistance to perforation that have been adopted by the industry [115].

Figure 2.43 give exploded views of the body work of the Peugeot 309, illustrating the extensive use of zinc coated steel in car manufacturing industries. The individual manufacturers have particular preferences for using certain types of coated steel in specific components. Figure 2.44 gives a range of different coated steel products used to construct a car body [130]. Table 2.1 lists typical automotive applications for the various coated steels ava'lable. It is apparent that for a given application individual automobile manufacturers use different material. Two side hot

dip galvanised is the major material utilised by U.S automobile manufacturers for protection of unexposed components. Its high availability and proven corrosion protection make it an attractive product, but difficulties in spot welding this material with existing equipment have limited its application at many automobile manufacturers.

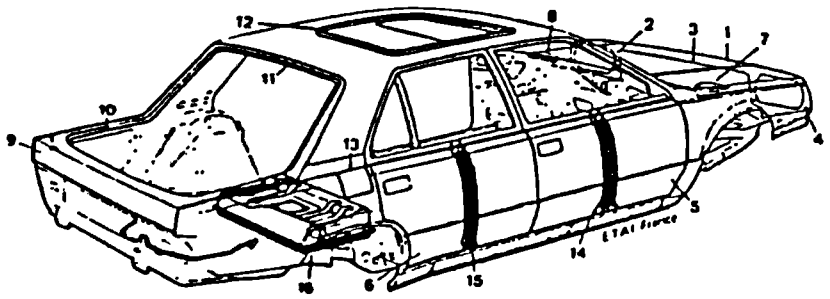


Figure 2.43 Body structure of Peugeot 309 showing the zinc coated parts [139].

4. Front mudguard (*Zincrometal*)

Sheet Electrogalvanised on One Side

1. External panel
2. Sheet carrying headlamps
3. Upper radiator stay
5. Panel, frame and hinges for front door
6. Panel, frame and hinges for rear door
7. Front bumper
8. Front bumper
9. External panel of boot lid
10. Lower channel of boot lid
11. Upper boot-lid stay
12. Supporting frame for opening roof
13. Patrol cap

Sheet Electrogalvanised on both sides

14. Stiffner for front door panel
15. Stiffner for rear door panel
16. Fuel tank

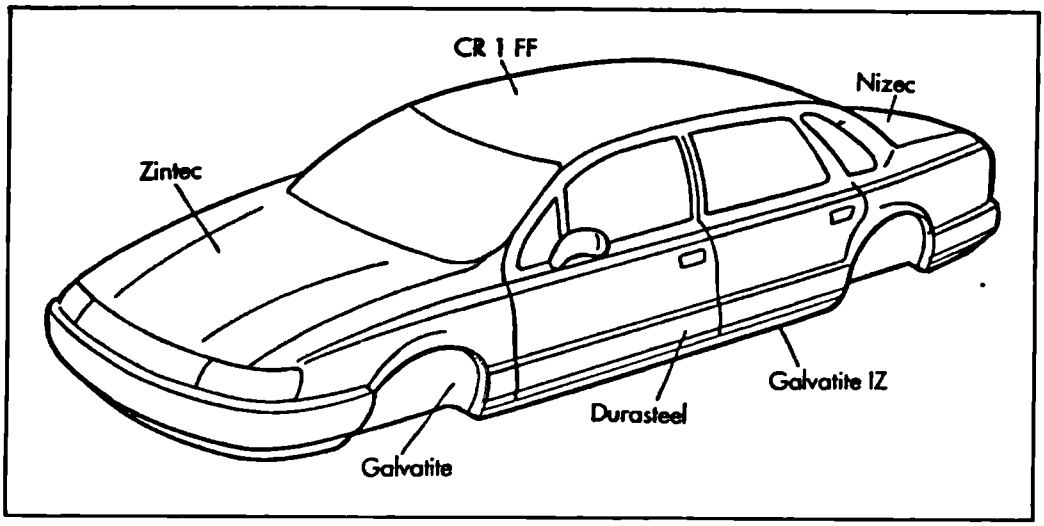


Figure 2.44 Typical automotive body panels fabricated from metallic coated steels [130].

No.	Trade name	Coating Type	Application
1.	CR 1 FF	Colled rolled steel	Hood,
2.	Galvatite	Hot dipped	Wheel arches,
3.	Galvatite IZ	Hot dipped and reheated to give Fe-Zn alloy (8% Fe) at zinc-iron interface.	Floor pan,
4.	Zinctec	Electroplated zinc	Door inners and outers,
5.	Nizec (11-15% Ni)	Electroplated	Boot and door inners,
6.	Durasteel	1 μm organic resin on Nizec	Door inners.

TABLE 2.1 Current Automotive Uses of Zinc Coated Sheet Steel

2 Side Coated		1 Side Coated			1-1/2 Side
Free Zinc	**Zinc-Iron**	**Free Zinc**	**Zinc-Iron**	**Zinc-Nickel**	**Zinc/Zinc-Iron**
Exposed:	**Unexposed:**	**Exposed:**	**Exposed:**	**Exposed:**	**Exposed:**
Doors, Liftgate, Tailgate (Differentially coated)	Floorpan Components, Rail, Hood, & Deck Inner Panels, Front Engine Crossmember	Hood, Deck, Fenders, Doors Roof, Quarters, Liftgate	Hood, Deck Fenders, Doors Roof, Quarters, Liftgate	Fenders, Doors, Quarters	Fenders, Doors Liftgate **Unexposed:** Door Inners, Liftgate Inners
Unexposed: Floorpan, Rails Hood & Deck Inner Panels, Engine Crossmember, Rear Suspension Crossmember, Suspension Control Arms, Radiator Yoke.					

Electrolytic zinc coated sheet steel is now widely used for automotive applications due to its superior surface quality and formability. In 1984 the worldwide availability was 11.4 million metric tons of hot dipped and 3.8 million metric tons of electrolytically coated steel. But there has been a strong trend towards electro-zinc type coatings and this is mirrored by the installed capacity from 1982 to 1987 which has increased twofold [140]. Table 2.2 lists the changeover in steel makers electro-galvanised capacity.

Table 2.2 Changeover in Steel Makers Electrogalvanised Capacity (/1000 t)

	1982	1983	1985	1986/87
Nippon Steel Corp	1060	1420	1660	1660
Nippon Kokan	268	422	422	588
Kawasaki Steel Corp.	370	370	430	790
Sumitomo Metals	180	540	540	540
Kobe Steel Ltd.	216	216	216	570
Nisshin Steel Corp.	0	0	0	120
Total	2094	2968	3268	4274

Chapter 3

Design and Operation of the Equipment and Experimental Strategy

3.1 Introduction

This chapter discusses the design and working principles of the CO_2 lasers. The experimental strategy for welding zinc coated steel is briefly described and the methods of evaluation of the weld properties are illustrated. The lasers used in this project were:

(i) 2 kW CLL laser at Imperial College London, and Liverpool University, U.K.
(ii) 15 kW AVCO laser at RTM, Vico Canavese, Turin, Italy.
(iii) 9 kW UTRC laser at Senter for Industriforskning, Oslo, Norway.
(iv) 8 kW MLI laser at Quantum Laser Corporation, Edison N. J. USA.
(v) 400 W FERRANTI laser MF400 at Imperial College, London, U.K.

3.2 Design and Working Principle of CO_2 Lasers

The basic working principle of all the lasers used are described here.

3.2.1 Working Principle of CLL Laser

CLL laser is a 2kW continuous wave CO_2 laser which works in infrared at a wavelength of 10.6 μm. This is particularly suitable for welding, cutting, drilling and heat treatment. The laser is designed on fast axial flow system and the basic features are shown in Figure 3.1. This figure shows the flow diagram of the laser and general layout of the system. A gas mixture of helium, carbon dioxide and nitrogen is used as a lasing medium. A roots blower circulates the mixture of gases through the

system at 75 m^3/min. The gas in the laser tube is at a relatively high pressure of 30-35 Torr (mm of Hg) in order to increase the number of molecules in the light path.

Water cooled heat exchangers were used to cool the circulating gases. A rotary vacuum pump is used to evacuate the system initially and subsequently to remove fraction of the gas mixture which will be passed through a catalytic regeneration oven to remove plasma generated mixtures of CO, NO, N_2O etc. The discharge tubes were supported on a rigid 4 meter long laser bench. The total cavity was 8 m long, folded once to give the laser length of 4 m. The gas mixture flows into the optical cavity at a high speed of 500 m/s. Inside the optical cavity a plasma was generated by a D.C. electrical discharge of 30 kV and 150 mA/tube. The cavity produces an output beam of diameter 20-25 mm which was transmitted through a partially transmitting zinc-selenide (Zn-Se) window. The actual size of the beam is dependent on the cavity optics and alignment. The output beam is then directed to the laser head by means of water cooled mirrors. The mirrors were made of copper and were coated with gold to give 100% reflectivity. A 45° mirror directed the beam into the lens assembly where the beam was focussed, by a potassium chloride lens of the desired focal length, onto the workpiece.

The gas mixture is continuously consumed by the laser and since helium represents a large proportion (>70%) of the constituents gas mixture, a recirculator has been incorporated as standard to minimise the cost of helium. The mixture of gases is recirculated after cooling by water cooled heat exchangers. There is also a purge cycle to replenish the gases.

The laser uses an output window made of water cooled partially transmitting zinc selenide which has 35% reflectivity to 10.6 μm radiations. The laser light emitted from the output window was then directed to the focussing head and work station via a 45° mirror. The light path was through a shutter box into which a 45° mirror can be introduced by means of an air operated shutter valve. From this

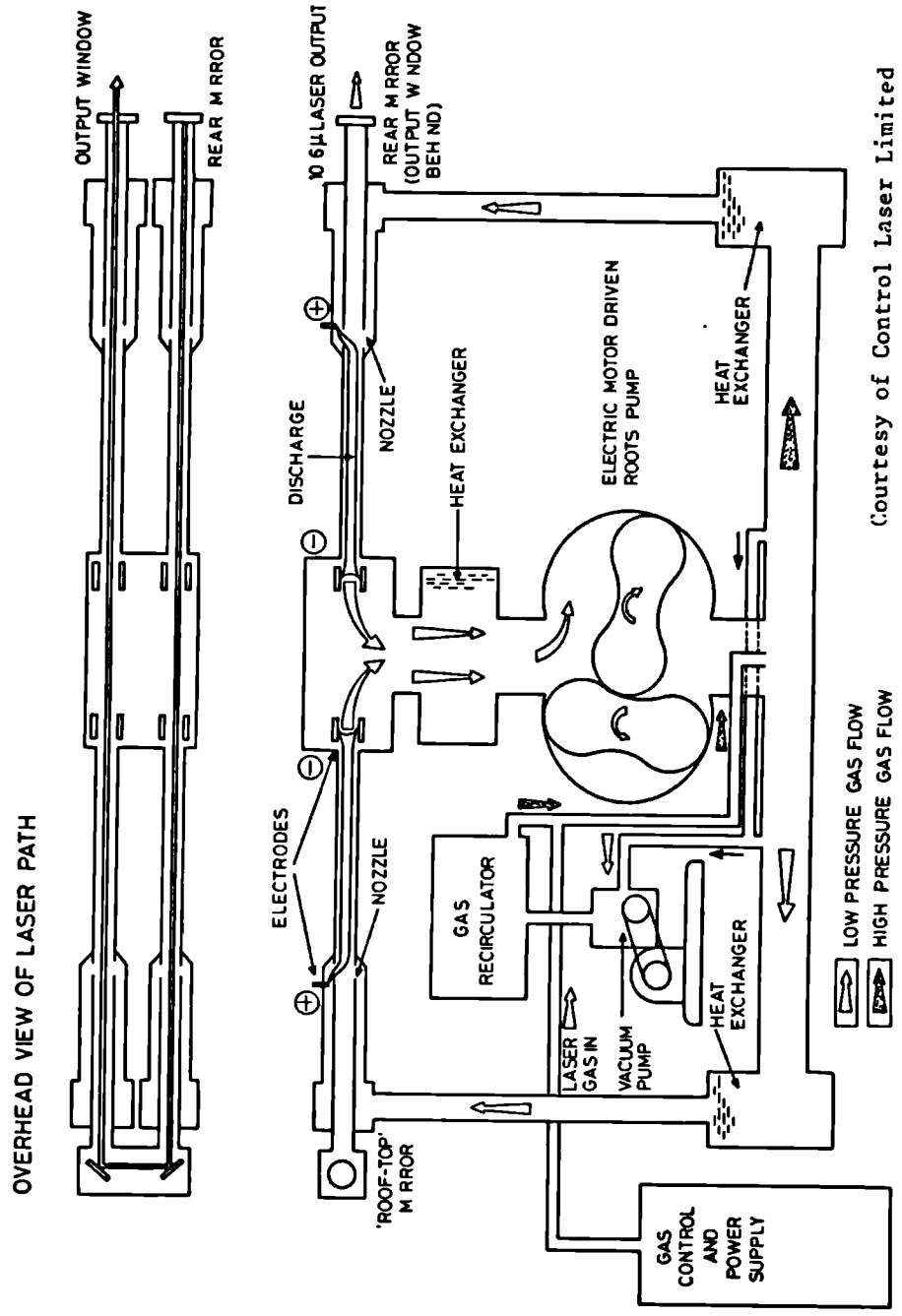


Figure 3.1 Design and flow diagram of 2kW Control Laser Ltd.

mirror the light was deflected into the cone of a water cooled calorimeter which acted as an output power measuring device. The laser beam is dumped into calorimeter when not in use. The calorimeter acted as a blackbody and absorbed all the incoming radiations. Thermocouple measure the incoming and out going water temperature flowing around the calorimeter which determined the power of the beam. The power of the beam was then displayed on a digital voltmeter. When the beam was used, the calorimeter mirror was retracted and the beam was directed to the workpiece by means of mirrors and focussing lens. The power of the laser can be increased by increasing the current through the discharge tube upto 150 mA/tube. Detailed description about the construction and operation of the laser can be found in the operating manual for BOC Model 901 [141].

The output power can be affected by a number of factors that includes the discharge tube pressure, the gas composition, the tube current and cavity optics. These are briefly describe here:

3.2.1.1 The Effect of Discharge Current

The discharge current determines the rate at which CO_2 molecules in the laser tube are pumped by direct electron excitation and via collision with excited N_2 molecules. The maximum output power thus increases with increasing current in the discharge. However a point is reached on increasing the current at which the heating effect at the tube axis becomes substantial so that the gain decreases. The output power will then saturate at a particular point as the discharge current is increased and may actually decrease as the current is further increased. The output beam of CLL laser is normally stable at a current of 150 mA and the power is unaffected by minor fluctuation in the electrical supply. A lower power could be achieved by reducing the discharge current.

3.2.1.2 The Effect of Tube Pressure

The discharge current for maximum power output from a particular tube depends on the gas pressure. The reduction in the gas pressure reduces the laser power. Under normal conditions the laser is operated at 40-45 torr pressure, but this can be reduced to 20-25 torr by altering all three gas regulators such that the gas mixture remains the same. Alterations in the gas mixture can be made according to the BOC manual.

3.2.1.3 The Effect of Gas Composition

Reducing the pressure of one of the constituent gases (He, N_2, CO_2) will alter the gas composition. A gas composition less than the optimum gas mixture will reduce the output laser power. Carbon dioxide gas is the most important constituent of the lasing gas mixtures, because of its vibrational and rotational transitions that cause the lasing action [33]. But the gas composition, set at around the optimum value, is not a sensitive variable on the laser performance. However small quantities of hydrocarbon vapour, SF_6 vapour and thus molecules capable of absorbing radiation in the cavity do have a devastating effect in performance.

3.2.1.4 The Effect of Cavity Optics

Clean optics also play an important part in maintaining the output beam power. Unclean mirrors contain dirt particles. Any particle or scratch on the mirror surface can lead to a serious fall of power due to scattering caused by particles and scratches. Every effort should be taken to keep the laser optics clean. Extra care should be taken with ZnSe output window since any dirt on the surface would cause local absorption of laser power and subsequent cracking of the window. Slight misalignment in the cavity optics greatly reduces the output laser beam power.

3.2.2 Working Principle of AVCO Laser

The AVCO HPL industrial laser is a continuous wave CO_2 laser with a wavelength of 10.6 μm. The device converts electrical energy into optical energy in an electron beam stabilized discharge and has a rated output power of 15 kW. Figure 3.2 shows the essential parts of the laser. The laser itself consists of a steel chamber approximately 2 m cube. Inside the main chamber is a closed cycle wind tunnel which circulates the lasing gas mixture. The lasing action occurs inside the unstable resonator optical cavity. The lasing medium is a gaseous mixture of He, N_2, CO_2 and CO in the ratios of 6:4:1:1. A high electron beam ionizes the gas raising its electrical conductivity enough to allow current to flow between the sustainer electrodes and therefore, through the medium on the optical cavity. Electrons constituting the sustainer current excited the gas molecules which emitted the photons of laser light. The flow path of gas mixture goes through the channel to a water cooled heat exchanger, followed by a chilled ethylene glycol/water mixture heat exchanger, then to the blowers and finally back to the channel.

The gas pressure in the wind tunnel, nominally 0.1 atm (76 torr) is maintained by an industrial process control device. The wind tunnel turns the flow of gas into a converging section that directs the flow into the channel. The channel - also called unstable resonator optical cavity - is where the actual lasing process takes place and is shown in Figure 3.3. Mounted on the inside and outside walls of the channel are the cathode and anode respectively. The laser gas flows downward between the electrodes while the current flows across the 10 cm space from the cathode to the anode. The gas flow, the current flow and the laser cavity optical axis are all mutually perpendicular as shown in Figure 3.3. A 400 Hz motor-generator is used to operate the blowers that circulate the lasing gas mixture in the main chamber.

Since some degradation of the gases occurs during the lasing process a small portion of the circulating flow is replenished automatically on a continuous basis during laser operation. At the channel ends are the mirror that defined the optical

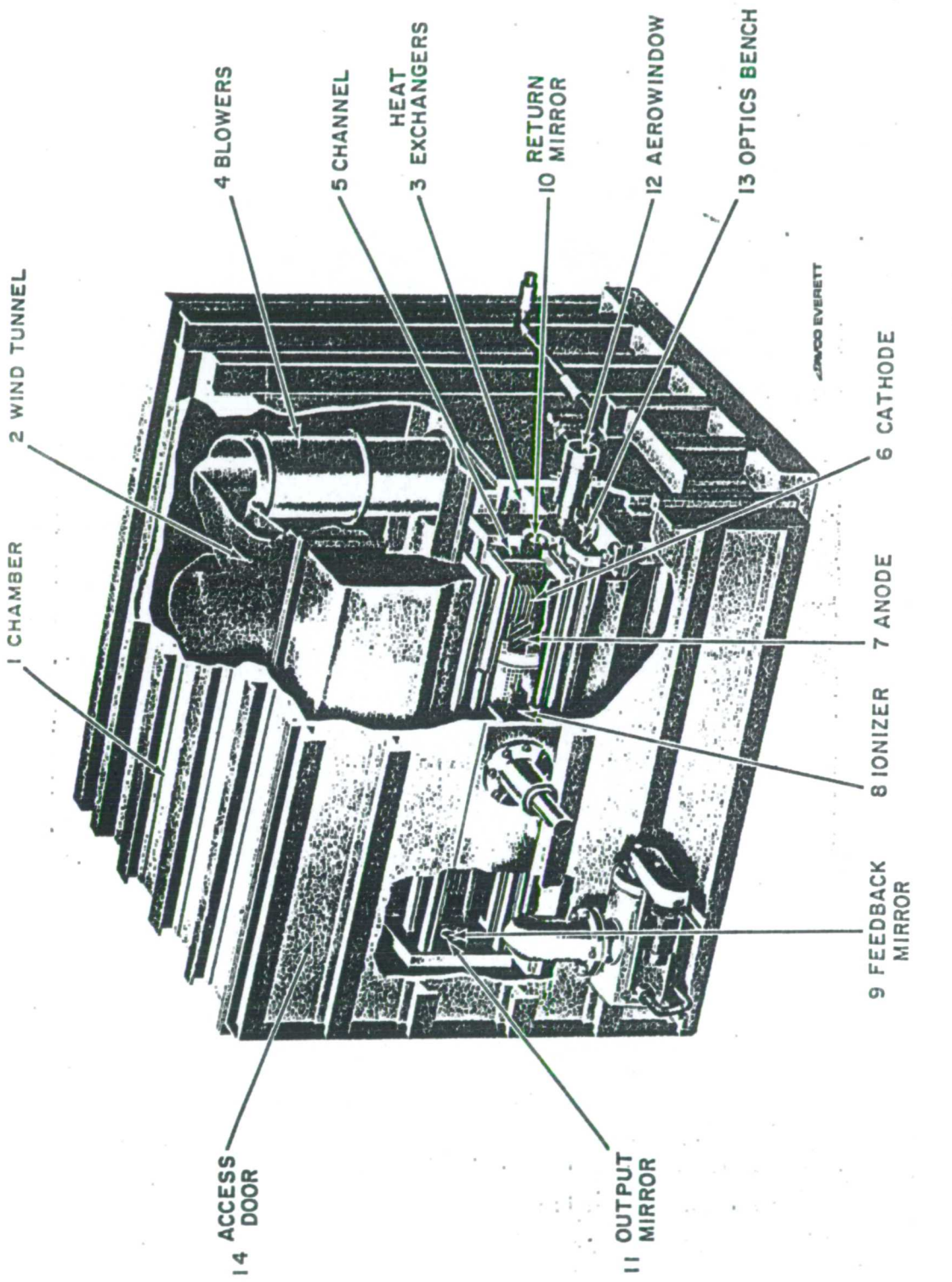


Figure 3.2 The essential parts of AVCO HPL industrial laser.

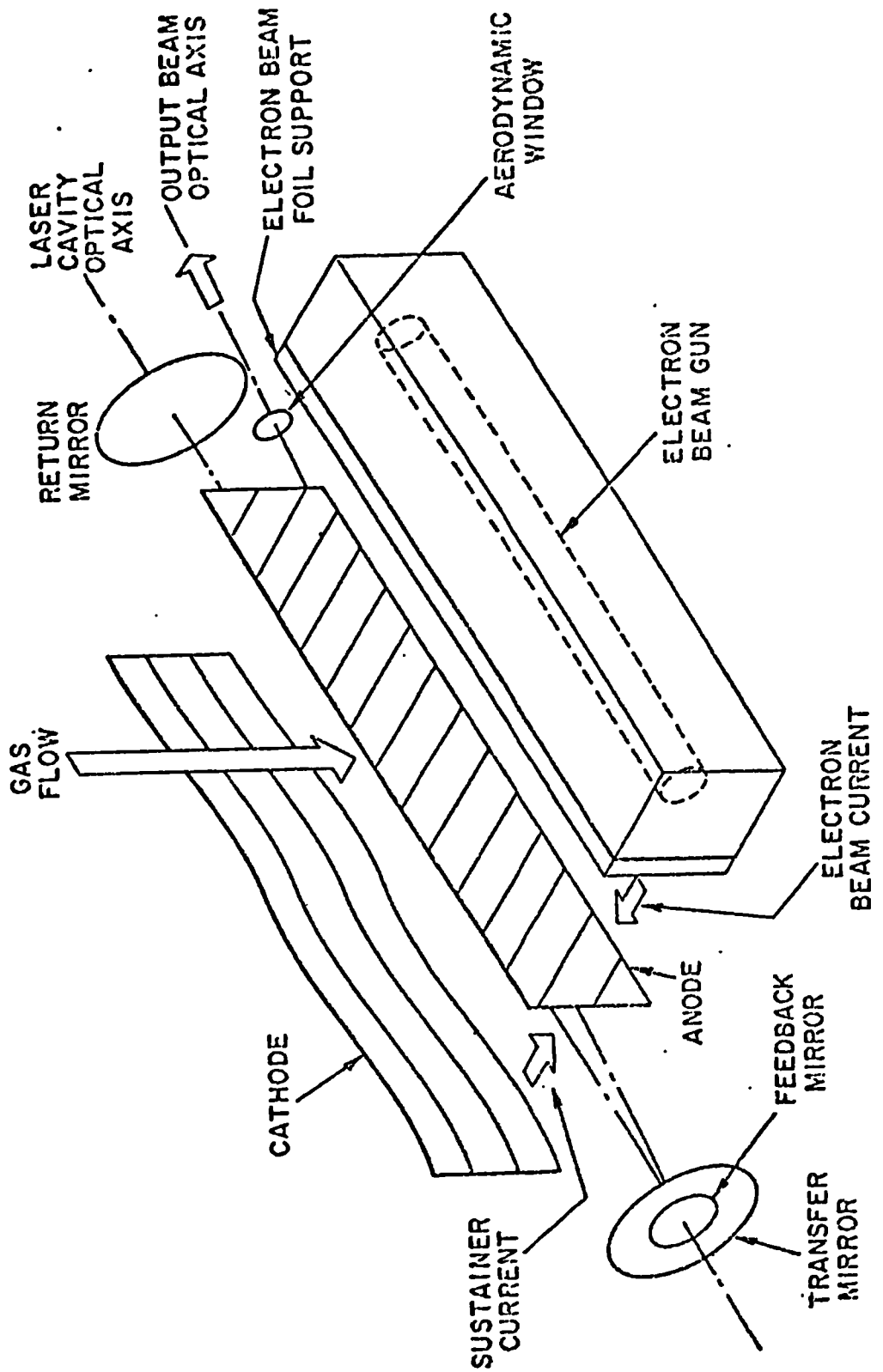


Figure 3.3 AVCO laser channel schematic.

cavity of the system. Detailed description about the construction and operation of the laser can be found in the operating manual [142].

3.2.3 Working Principle of UTRC (United Technology Research Centre) Laser

UTRC laser consists of three modules joined in series to build a 10 kW laser. Each module provides a laser power capability of 3 kW, and equipped with its own gas circulation and discharge sections. The modules are integrated into a single system with a common optical section and control. This is a standard transverse flow DC excited laser.

A sketch of a three module system is depicted in Figure 3.4. The beam transfer cabinet located at the output end of laser houses accessories to monitor and control the beam and a periscope to direct the beam to a work station, as shown in Figure 3.5. The other cabinets contain the power supply, discharge ballast and control system.

All the mirrors used are gold plated and water cooled. Output beam is transmitted out of the optical cavity by focussing the beam through an aerodynamic window as shown in Figure 3.5. The laser had an unstable resonating cavity. A He-Ne laser is mounted on the optical platform inside the CO_2 laser which is used to align both the cavity and any external optics used in directing and focusing the beam on the workpiece. The He-Ne beam is injected into the optical cavity, where it replicates the CO_2 cavity mode. This visible beam emerges from the optical cavity at the same size as the CO_2 beam and is automatically boresighted with it. By visualising the shape and uniformity of the He-Ne beam, the optical cavity can be tuned to a lasing condition before the power is applied to the system. The external alignment uses another He-Ne laser situated in the beam transferring cabinet.

To observe the beam intensity distribution during tuning, a low power image of

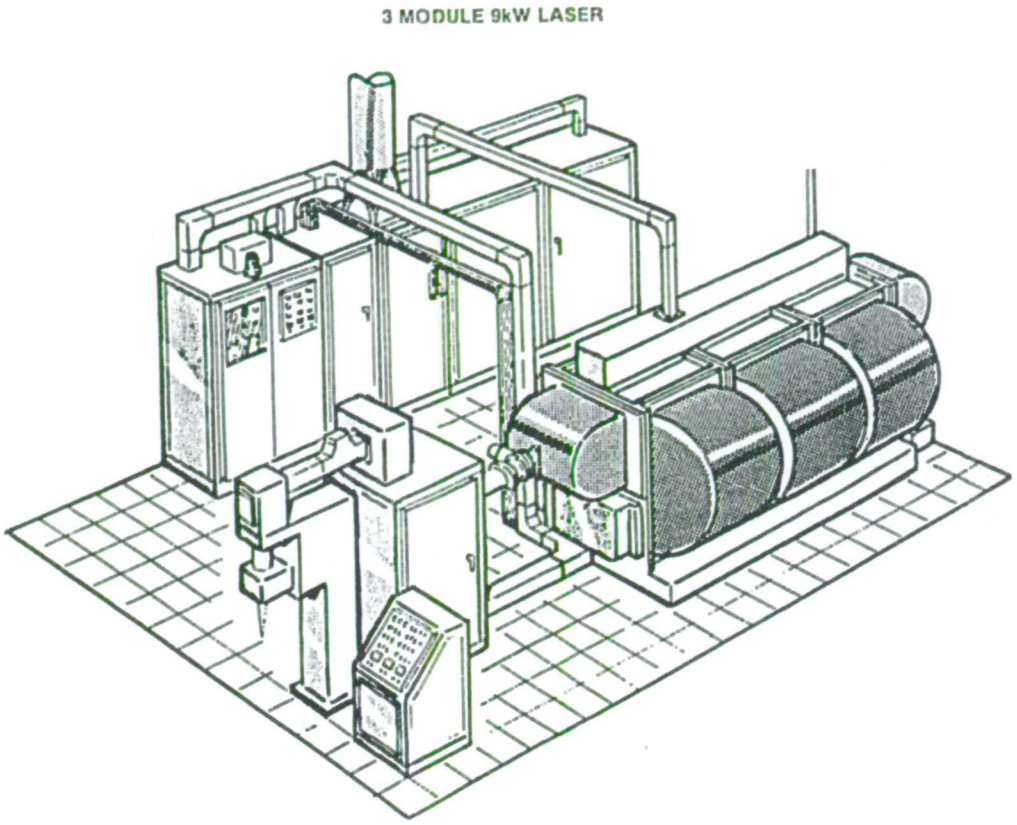


Figure 3.4 Schematic diagram of three module UTRC laser.

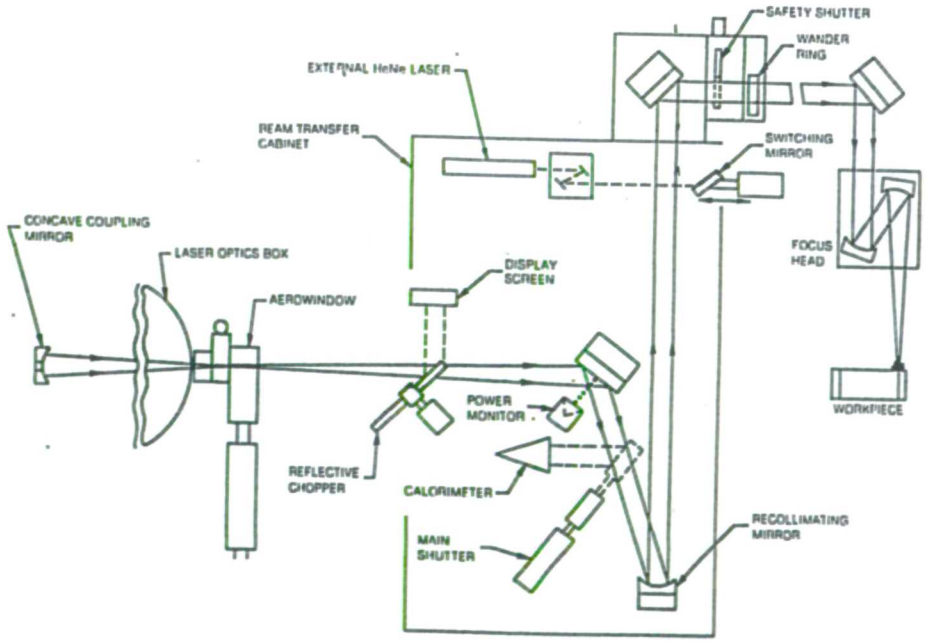


Figure 3.5 Beam transfer schematic.

the entire beam is directed to a fluorescent screen. The image of the beam is displayed on a TV screen. Details of the UTRC laser system is given in reference [143].

3.2.4 Working Principles of MLI Laser

The MLI laser is a transverse flow laser with a ring cavity shown in Figure 3.6. One of the major problems with transverse flow lasers is that the gases heat up as they flow through the plasma discharge causing an uneven amplification and hence a strong tendency to multimode oscillations which are more difficult to focus. The MLI laser overcomes this to some extent by having a ring beam which causes the heating effect to switch from side to side as shown in the Figure 3.6. The cooled gas mixture enters through the centre of the ring cavity where it is spread to all four side walls passing through the beam path. As the gases pass through the discharge they heat up

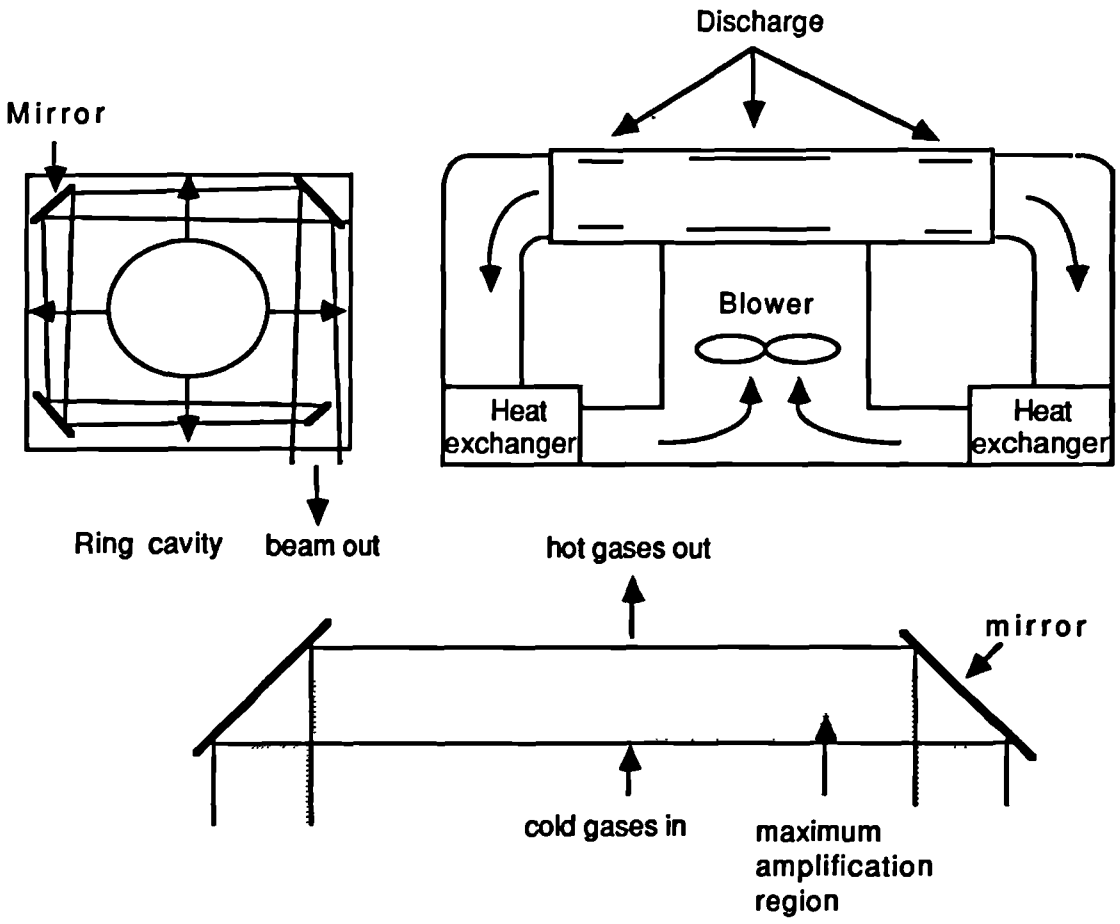


Figure 3.6 Schematic diagram of MLI laser.

causing a reduction in amplification. The gases are then recycled through heat exchangers prior to entering the discharge again.

The laser has an unstable cavity having an expanding beam. The output is taken around the perimeter of a final sclapper mirror. The ring beam from the unstable cavity is more uniform than with standard transverse flow lasers. The MLI laser is AC pumped at 10kHz.

3.2.5 Working Principle of Ferranti Laser (MF400)

The MF400 is a slow axial flow CO_2 laser with 12 m of water cooled discharge tubing mounted on a cylindrical optical bench. The optical cavity is folded to produce a compact device as shown in Figure 3.7. Each folded leg has two separate central anodes each feeding one discharge tube. Each anode is fed through a separate ballast resistor from a single H.T. source. The H.T. current is stabilised using saturable reactors in the primary circuit of the H.T transformer. A lasing gas mixture (He; 72%, N_2; 19%, CO_2; 9%) is fed into the tubes at an input pressure of 30-50 psi The gases are drawn through the discharge tubes by a vacuum pump. The exhaust gas from the pump is processed in a recirculation oven and fed back to the laser. Small

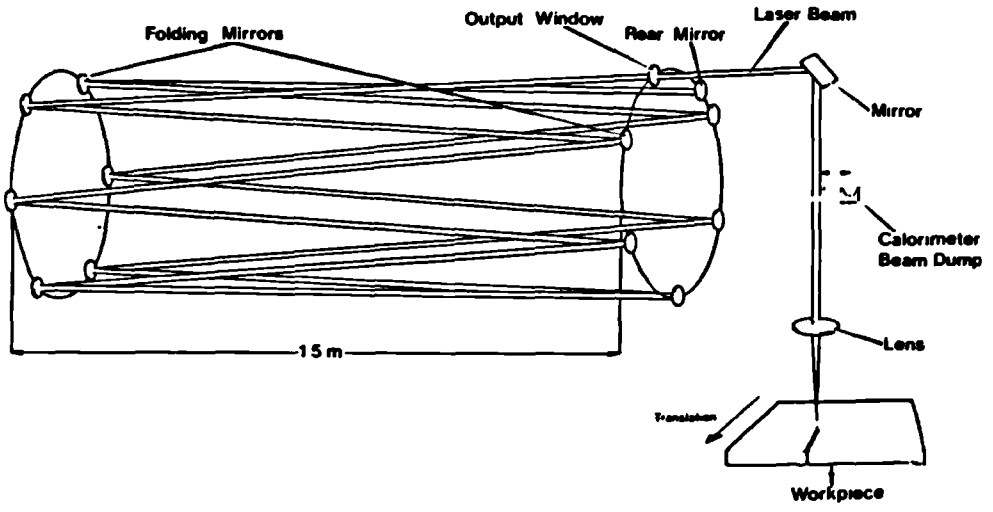


Figure 3.7 Slow axial flow CO_2 laser (Ferranti).

losses of the gas mixture are compensated for by feeding in pulses of fresh gas mixture at automatically timed intervals.

The out put beam is deflected by a mirror in the output channel which deflects it into a water cooled calorimeter. The rise in temperature of the calorimeter cooling water is used to measure the power of the beam. The deflecting mirror is moved out of the path of the output beam when a solenoid is activated allowing the laser beam to emerge from the laser head.

The MF400 laser operates at a high voltage (15 kV) and produces a maximum of 400 W beam of radiation at a wavelength of 10.6 μm. The discharge is DC excited. The mode structure is of a very low order (TEM_{00}) due to the low Fresnel number ($r^2/L\lambda$, r; tube radius, L; tube length and λ; wavelength) of the long thin optical resonator. This makes these lasers particularly easy to focus. Unfortunately the slow flow principle has insufficient cooling to allow high gains as in the convectively cooled lasers (transverse flow and fast axial flow), so most slow flow lasers are less than 1 kW. Complete details of the Ferranti MF400 laser system is given in operating manual [144].

3.3 Operation of the Equipment

This section describe the necessary arrangements needed for an experiment. This includes the estimation of focal point, beam alignment and operation of the equipment.

3.3.1 Focussing Assembly and the Estimation of Focal Point for CLL Laser

The optical arrangement for CLL laser is shown in Figure 3.8. The beam, after passing through the ZnSe window, is directed by a number of water cooled, beam guidance mirrors to a focussing assembly called a laser head. The laser head was designed in such a way as to allow the shielding gas to flow coaxially with the laser

beam to serve the functions of shrouding the workpiece and protect the lens from spatter. A plano-convex lens is normally used for focussing the beam. The lens is made from ZnSe or KCl. ZnSe is stronger and has a less tendency to absorb moisture from the air and so can last much longer provided it is not damaged by process spatter. However, as KCl is much cheaper than ZnSe it is usually used in the laboratory. At the lower end of the lens holder assembly a nozzle of required diameter is positioned coaxially with the beam.

The position of the focus was estimated by passing a perspex sheet slightly inclined to the beam axis across the laser beam under the focussing laser head. The focus can be observed from the longitudinal beam print on the perspex sheet as illustrated in Figure 3.9. A sheet metal was then placed at the estimated focal point and laser was fired with argon shrouding to observe a blue flash at the focal point.

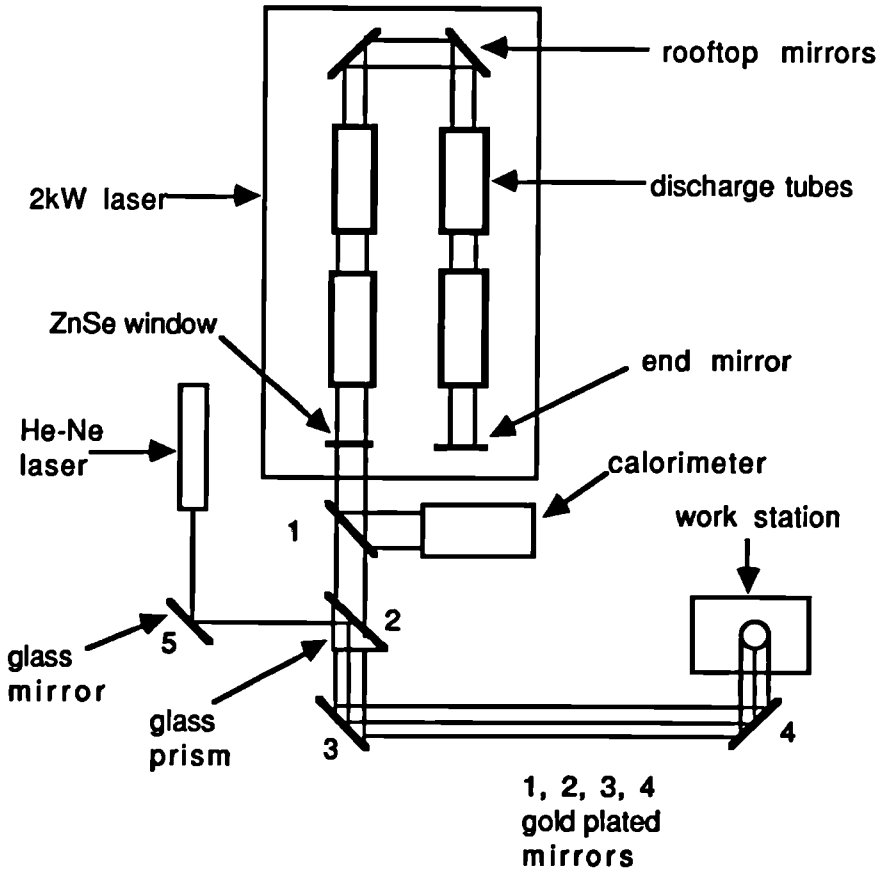


Figure 3.8 Schematic of laser layout.

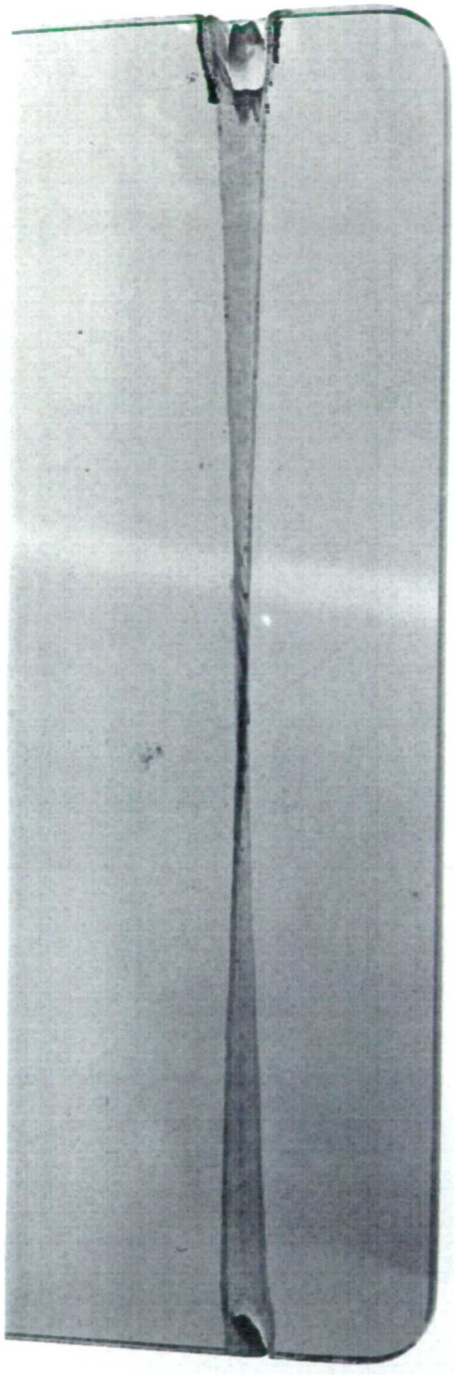


Figure 3.9 Beam print obtained by passing the laser over an inclined perspex sheet to estimate the focal point position and the spot size of the beam.

The depth of focus was determined by measuring the distance within which the blue flash was observed. The exact focal position was then taken as the mid position of the blue flash range.

3.3.2 Beam Alignment

Infrared CO_2 laser radiation at 10.6 μm wave engtth is invisible, hence prior to processing one needs to know where the beam will strike on the workpiece surface. Mis-alignment of the beam can cause many problems, e. g., if the beam is not aligned with the nozzle it will be truncated and consequently there will be a loss of incident beam power and the nozzle may gets very hot or even damaged. Mis-alignment with the laser head and lens assembly may cause the burning of the O-ring seal around the lens. This would lead to the cracking of the lens due to the smoke causing surface absorption on the lens. Hence a system is needed to align the laser beam with the lens, nozzle and the workpiece. A small He/Ne laser was fitted to the main laser head in such a way that its beam (0.6238 μm) was collinear with the infrared beam. This is illustrated in Figure 3.8. The movable arm which inserted the prism for the He/Ne beam into the main beam path was interlocked to the main beam shutter to prevent firing if it was in place. The procedure adopted to align the laser beam with lens, nozzle and the workpiece is described here:

1. *Alignment of He/Ne beam with CO_2 beam.*

   (a) (i) Place fire brick at a position near to the CO_2 laser,
   (ii) fire CO_2 laser to make a mark on the brick,
   (iii) align He/Ne beam using mirror '5' in Figure 3.8 with the CO_2 spot.

   (b) (i) Place fire brick just prior to laser head,
   (ii) make mark with CO_2 beam,
   (iii) align He/Ne laser us ng mirror '5' in Figure 3.8.

(c) Check alignment at first position as in (a). If this in no longer aligned then the He/Ne laser mount will need adjusting. This is not usually the case.

2. *Alignment of He/Ne beam with 45° mirror, lens nozzle and workpiece.*

Using upstream mirror adjust He/Ne beam to be central on each successive element until the beam falls centrally on the lens. If the beam is not central with the nozzle then the tilt of the laser head should be adjusted.

3. *Check alignment.*

(i) Remove nozzle and make a perspex burn print using CO_2 beam,

(ii) Replace nozzle and make another burn print.

If the alignment is correct then the prints should be identical.

3.3.3 Work Tables

3.3.3.1 The X-Y Hydraulic Table

An X-Y hydraulic table was used for moving the sample underneath the laser beam. The X-axis movement was controlled by hydraulic piston while Y-axis was manipulated manually. The table top consists of two aluminum plates separated by a channel. The sample was positioned over the channel and held in place by clamps. The table can be raised or lowered by using four threaded legs, which also allowed the table top to be levelled. The speed of the table was adjusted by a needle valve controlling the flow of hydraulic fluid. The speed was calculated by a timer which gave the number of seconds for 100mm movement of the table in X-direction. This

table was available at Imperial College, London. The high power lasers used at all other locations were equipped with automatic and computer controlled workstations similar to that at Liverpool University.

3.3.3.2 The CNC X-Y Table and Z-Axis Moving Optics

A CNC laser work station supplied by Control Laser Ltd. (CLL) was upgraded at Liverpool University [145]. The station consisted of a CNC X-Y table and Z-axis moving optics. The X-Y table moved the workpiece under the beam while Z-axis moving optics controlled the laser beam focus and spot size on workpiece by altering the lens/workpiece distance. The X-Y table made of aluminum, had two permanent magnetic DC motors/tachos coupled to the stainless table lead screw through a pulley/belt mechanism. The X-Y table rested on an adjustable drill stand.

The Z-axis moving optics was also supplied by CLL, which consisted of a 45° adjustable mirror, lens holder and nozzle assembly. The lens assembly can be moved up and down through a rack and pinion mechanical system. A permanent magnetic DC motor/tacho was directly coupled to the pinion. All the axis were controlled by CNC controller. Figure 3.10 showed the CNC working station used at Liverpool University.

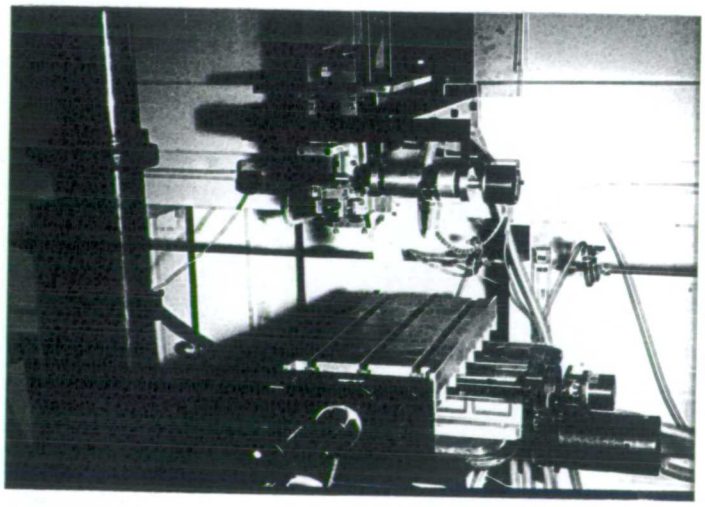


Figure 3.10 CNC control working table at Liverpool University.

3.3.4 Powder Feeding

A screw type of powder feeder (developed at Imperial College, London) was used for injecting a metal powder into the weld pool through a side jet during certain laser welding experiments. Figure 3.11 describes the design features of the powder feeding system.

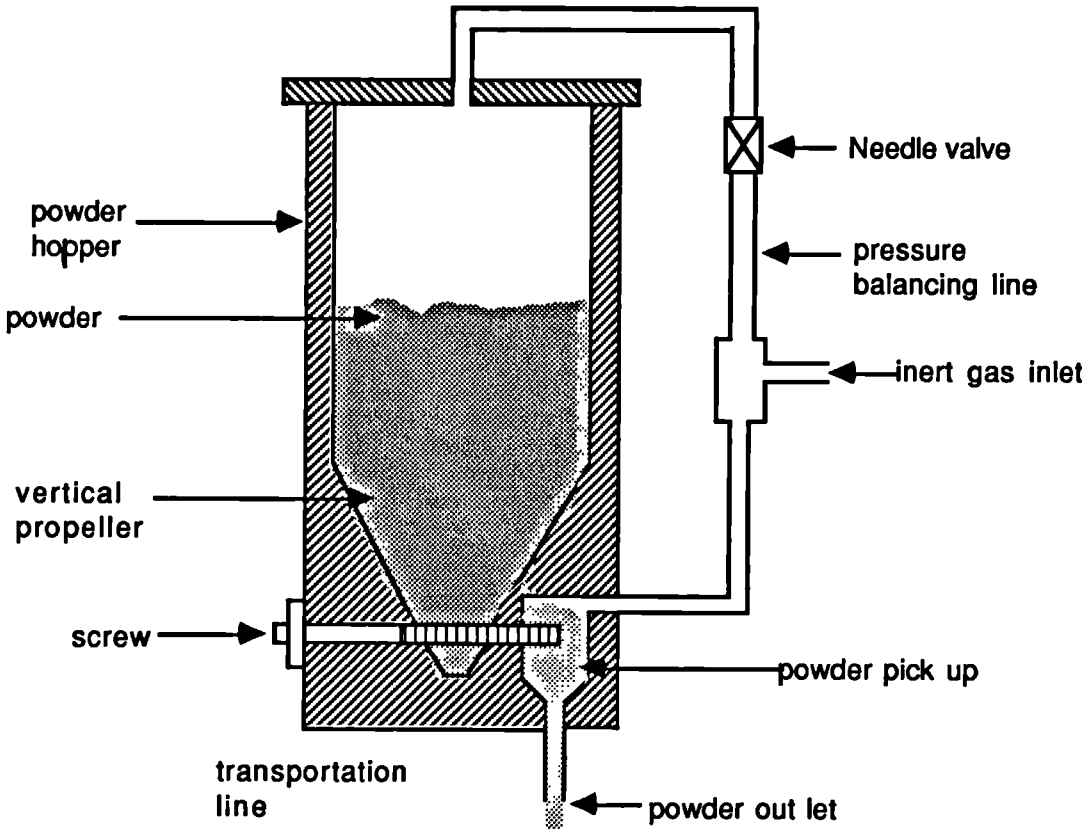


Figure 3.11 Design and features of powder feeding system.

The powder feeder consists of a hopper containing metal powder. A standard twist drill type of screw - used to feed the powder - was situated at the bottom of the hopper. The screw was rotated by means of a variable speed motor. The quantity of powder fed into the weld pool was controlled by the speed of the motor and by the flow rate of argon gas used to entrain the powder. The argon gas carried the powder particles to the impingement point of the focussed laser beam through a 3 mm diameter copper tube.

Weerasinghe [146] showed that the gas flow rate and speed of rotation of the feeder had a significant effect on feed rate, feed uniformity, and particle velocity. For the feeder to work successfully the powder must flow so that its angle of recline is less then vertical. In this study an average particle size of 70 μm (100 mesh) was used .

3.3.5 Workpiece Shielding

The oxygen-weld metal reaction can occur as a result of incomplete weld metal protection from atmospheric air. Oxygen contamination can deteriorate the mechanical properties of the weld metal. Seferian [147] showed that the strength, toughness and ductility of mild steel welds all decrease with increasing oxygen content. Hence an effective shielding of the workpiece is necessary to obtain uncontaminated and oxide- free weld surface. The arrangement for gas shielding of the workpiece is shown in Figure 3.12.

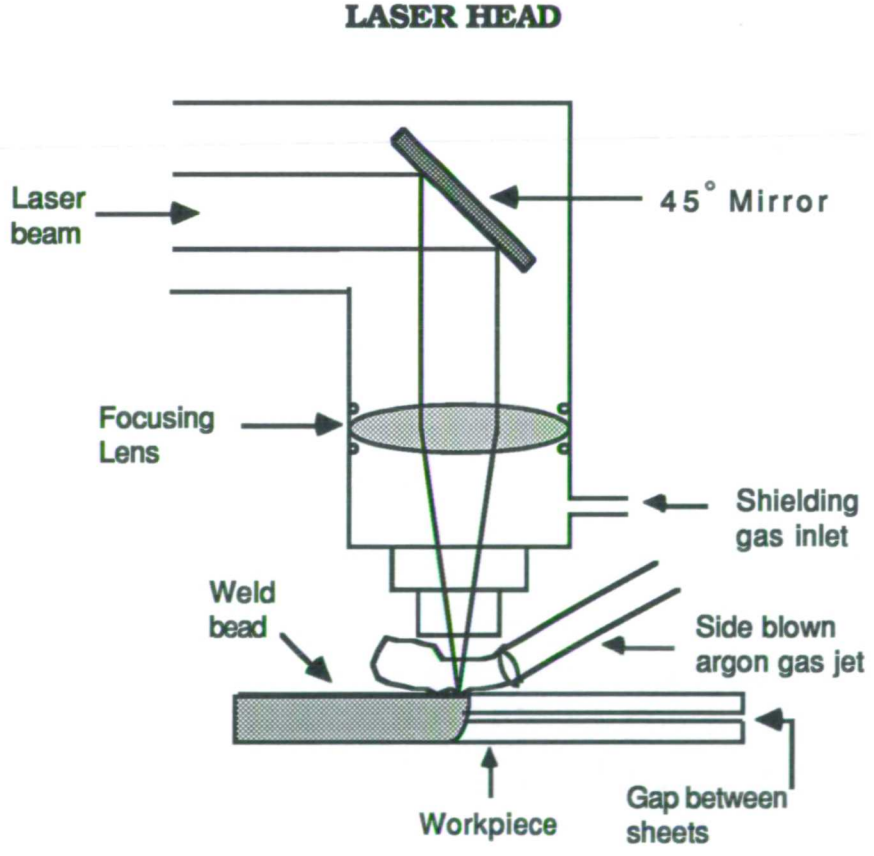


Figure 3.12 The arrangement of gas shielding of the workpiece and plasma removal.

An inert gas is used for this purpose. The gas enters the laser head through a small pipe and exits coaxially through the nozzle towards the workpiece. The gas had two-fold purpose, firstly, the gas jet from the coaxial nozzle kept the lens cool and protected it from metal vapour or particles ejected from the laser generated melt pool and, secondly, it gave inert shielding of the workpiece surface in the interaction zone.

3.3.6 Overcoming the Plasma Problem

When the laser beam is absorbed on the metal surface it vaporises some of the metal. These metal vapour will be ionised if sufficiently hot, forming a plasma. The plasma is absorbing to the laser beam which can react with free electrons (inverse Bremsrahlung). This heats the vapour further and blocks the beam from the workpiece both by scattering and direct absorption, thus reducing the coupling coefficient (energy absorbed/energy incident). A side blown gas assist jet was used to displace the plasma plume above the metal surface to increase the coupling coefficient. The experimental arrangement of gas shielding and the plasma removal above the workpiece is schematically shown in figure 3.12. The side jet also gave an effective shielding of the hot reactive metal.

3.4 Experimental Strategy

Laser beam weldments of zinc coated steel were fabricated in lap configuration using a continuous wave CO_2 laser. These lap welds were produced on 0.55, 0.7, and 0.875 mm thick sheets. The laser beam had a wavelength of 10.6 μm (infrared) and a diameter of 23 mm at the laser output window, with a doughnut beam configuration as measured from an acrylic print. The beam was focused to a spot of approximately 0.2 mm diameter using a KCl lens of 125 mm focal length.

The experiments were performed with the intention of knowing (a) whether sound weld in zinc coated steel can be achieved using lasers, (b) the effect of different welding parameters in laser welding, (c) quality of the weld obtained, (d) possibility

of modifying the weld composition to make it more corrosion resistant.

These objectives were achieved by making a series of welds with a laser using various welding parameters. Most of the welds were made in lap configuration while a few bead on plate welds were also made. The variable studied in the process were: thickness of the sheet, thickness of the zinc coating, laser power, welding speed, side jet gas flow rate, etc. The general procedure adopted was:

(i) check the beam mode structure by making a beam print on a perspex sheet,

(ii) align the He/Ne laser with the main CO_2 laser, with the nozzle and with the workpiece,

(iii) degrease the each specimen before welding,

(iv) mount the specimen on an X-Y table which can be moved under the stationary laser beam,

(v) provide argon gas coaxially with the laser beam to protect the weld from oxidation,

(vi) focus the laser beam on the workpiece,

(vii) move the table under the beam and fire on to the workpiece,

(viii) the welds were examined in detail by, metallography, SEM study, tensile testing, fatigue testing, impact testing and corrosion studies.

The problem of welding zinc coated steel in lap configuration has already been described in chapter 1. However it does serve to illustrate the problem to be solved. It is necessary in welding this sort of material that either the zinc is removed from the weld area (double pass technique), or it is condensed (metal injection technique and side jet welding) or it is vented (end edge and gap welding). These ways of welding are discussed in detail in chapter 4 and are briefly described here.

3.4.1. Double Pass Welding

In this technique the focussed laser beam was first passed at a high speed of 125 mm/s and then with a slower speed to create the weld. The aim was to provide sufficient preheat to the zinc coating at the interface between the two sheets such that the zinc would move away from the weld area due to the surface tension forces during the first non penetrating pass.

3.4.2 End Edge Welding

This arrangement was assumed to obtain a weld by passing the laser beam at the edge of upper sheet with a minimum penetration to the bottom sheet so as to allow an advantage in welding speed. It was also assumed that this arrangement would allow sufficient vent area to the zinc vapour that can be exhausted without damaging the weld.

3.4.3 Gap Welding

The welding of zinc coated sheet required a small gap between the sheets to help vent the zinc vapour. Hence in this technique a fixed gap was formed using spacers for a single weld. In an other experiment a variable gap was formed to estimate an optimum gap size that could give sound weld from a single weld pass.

3.4.4 Welding With Modification of the Weld Bead Composition

In the welding of zinc coated steel, with a laser beam, the zinc layer in the welded area volatilises and escapes leaving an exposed steel surface. Hence to protect this exposed area from corroding the weld composition was modified using three technique, (a) injection of metal powder into the melt pool during welding, (b) by using a side blown gas assist jet, and (c) incorporation of zinc powder just after welding.

3.4.4.1 Welding With Metal Powder Injection

The workpiece was moved under the stationary laser beam by the computer controlled table and the powder - using argon gas carrier - was incorporated into the melt pool. Nickel, tool steel, or stainless steel powders were fed into the weld pool in separate experiments. Hence in this way the weld composition was modified to obtained a weld that would give protection to the weld from corrosion.

3.4.4.2 Welding Using a Side Blown Gas Assist Jet

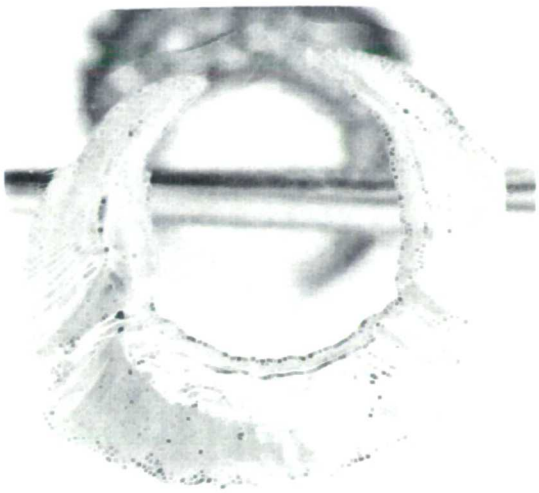
This technique had two aims: (i) to establish whether improved beam coupling could be obtained by reducing the plasma thickness in the beam path, (ii) to incorporate into the weld bead zinc that had been volatilised as a result of the welding operation. Thus argon gas was entrained through the side jet at a certain flow rate and directed at the weld bead during welding.

3.4.4.3 Incorporation of Metal Powder Just After Welding

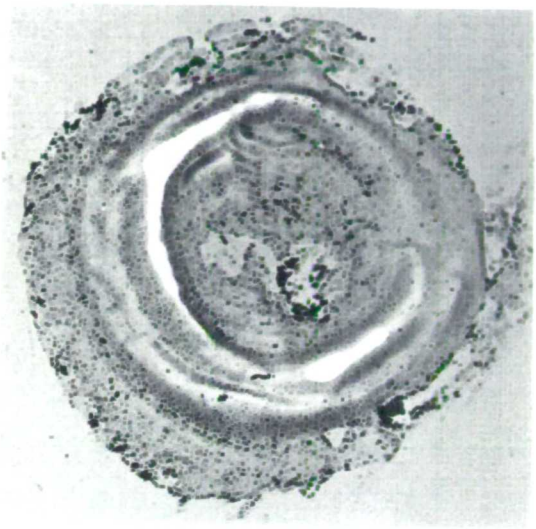
In this technique an experiment was carried out in which metal powder was incorporated just after weld formation. The experimental arrangement employed a side jet carrying metal powder. The powder was deposited at the trailing edge of the hot weld where it was melted and formed a coating on the weld.

3.4.5 Lap Welding Using Various Laser Beam Modes

A number of lasers were used to weld mild steel and zinc coated steel in lap configurations. All the lasers had different beam mode structure depending upon the optical cavity. The beam mode obtained from lasers were Gaussian, Doughnut, multimode and ring type as shown the Figure 3.13. The beam prints were obtained by



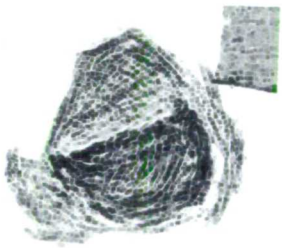
(a) **AVCO Laser**



(b) **MLI Laser**





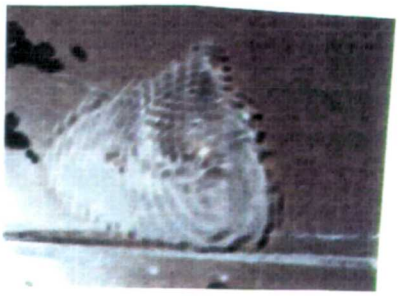


Input beam 400W Output beam 300W Amplified beam 1100W

(c) **Oscillator Amplifier system**



(d) **CLL Laser**



(e) **UTRC Laser**

Figure 3.13 Beam prints obtained from various lasers.

firing the laser on a perspex sheet for a very short time. Penetration and beam coupling studies were performed with these beams in lap welds at various welding speeds. The welds were produced by passing the workpiece under the stationary focussed laser beam.

3.5 Evaluation and Testing

3.5.1 Metallography

The welds were sectioned for metallography. The specimens were mounted in cold setting resin and left for 24 hours to harden. A specimen mounting press machine was also used to mount the sample in conductive Bakelite for SEM study. The specimens were polished in the usual way, first ground on an emery paper starting at Grade 120 going upto 1200 in stages, and then polished on 14, 6, and 1 μm diamond polishing wheels.

The polished specimens were etched in a solution of 2% nital in order to examine the fusion zone, heat affected zone and base metal. However to reveal presence of Fe-Zn alloy after welding the cross section was etched with amyl nital (one drop of HNO_3 in 10ml of amyl alcohol). The zinc coating was difficult to view optically because of the small thickness of only 7.5 μm. Metallography of the cross section, using plastic setting resin, did not reveal many details, mainly because of beveling at the edge of the cross-sectioned sample. Edge beveling occurred during the grinding and polishing process as well as the etching process in which sharp corners or edges were usually rounded off. To avoid this problem some specimen were mounted using special edge retaining powders (Bakelite) that keep the edges of the specimen flat. Hence the beveling can be avoided in this way and a detailed study can be made in the thin zinc coating.

3.5.2 Optical Microscopy

The Reichert projection microscope was used to observe the detail in the parent metal, heat effected zone and the fused zone. The cross-section, longitudinal section and surface topography of laser tracks were studied. Photographs of the fusion zone, heat affected zone and the base metal were taken. The weld dimensions i.e., weld width and penetration were measured using a Projection microscope.

3.5.3 Scanning Electron Microscopy

Scanning Electron Microscope (SEM) was used to supplement the optical microscope to provide higher magnification and surface conditions. The scanning electron microscope employs a beam of electrons directed at the specimen. An electron gun, usually of the tungsten filament thermionic emission type, produces electrons and accelerates them to an energy between about 2 k eV and 40 k eV. Two or three condenser lenses then focus the electron beam until it hits the specimen with a diameter of 2-10 nm. Thus the fine beam of electron is made to scan across the specimen surface. SEM has several advantage over the optical microscope in that, in SEM the depth of focus in the image is very large and the resolution is typically between 20-50 nm, while optical microscope does not give a large depth of focus. SEM can be used for the chemical analysis of the specimen using X-ray fluorescence, back scattered electron, while optical does not.

Scanning Electron Microscope JEOL-CF JSM-35 was used for the EDAX analysis of the specimen. In particular, it was used to investigate how much zinc was held in the fusion zone.

3.5.4 Joining Efficiency

The joining efficiency is a crude form of coupling efficiency which shows, how much of the available laser energy is effectively utilised for welding and how much is,

for various reasons, dispersed. The aim in welding is to join two surfaces. Thus an optimum weld would have no width only depth. Thus the joining efficiency, area joined/J is a better measure of quality than the melting efficiency. The joining efficiency can be defined as

$$\eta_j = \frac{VT}{P} \qquad m^2/kJ$$

= Area joined/unit of energy delivered.

where, V; welding speed, m/s, T; penetration, m, P; available laser power, Watts.

The joining efficiency was calculated for each experiment. A constant joining efficiency can be used to predict the weld fusion depth.

3.5.5 Melting Efficiency

Melting efficiency is defined as the ratio of the energy required to melt the material in the weld to the total energy delivered to the workpiece. Hence

$$\eta = \frac{\rho VA(C_p T_m + L_m)100}{P}$$

= percentage of delivered energy used to melt the substrate.

Where

P = laser power delivered to the workpiece	Watts
η = melting efficiency	%
ρ = density of the material	kg/m^3
C_p = specific heat capacity	kJ/kg-°C
T_m = Temperature of melting	°K
L_m = latent heat of melting	kJ/kg
A = cross section area of the fusion zone	m^2

After measuring the fusion zone area these variable parameters were then used to calculate the melting efficiency for all the welds. This parameter gave a more detailed view of how the incident power was used.

3.5.6 Specific Energy

This is the term often used in correlating welding data, it is proportional to the energy deposited/unit area of the surface.

$$\text{Specific energy} = \frac{P}{DV} \qquad J/m^2$$

$$\text{Specific energy} = \frac{P}{DV} = \frac{\rho T(C_p T_m + L_m).100}{\eta} \qquad J/m^2$$

When P and D are also constant then

$$1/V \propto T$$

Where, D; Beam diameter on the surface, m.

3.5.7 Measurement of Fusion Zone Area

A square millimeter grating was xeroxed onto a transparency and the transparency was then placed over the weld profile. The number of squares within the fusion zone were counted. This was then divided by an appropriate factor in order to get the actual area of the fusion zone.

3.5.8 Weld Quality

The quality was evaluated by counting the number of pits or holes in a 100

mm length of weld. This gave an average value of pits/cm as a comparator between these techniques. Pitting was the main deleterious effect of the zinc on the weld.

3.5.9 Tensile Testing

Some specimen were made to enable the production of tensile tests specimens. Mechanical tests were performed to compare the tensile strength of the weld with that of the parent material. Specimen size for tensile tests on laser welded sample is shown in Figure 3.14. The weld was present at the centre of the specimen. The sample prepared, as specified in Figure 3.14, was placed in the grips of the testing machine. An axial load was applied on the sample through mechanical lever system until the specimen is broken. Yield strength, percentage elongation and percentage reduction in area was also calculated.

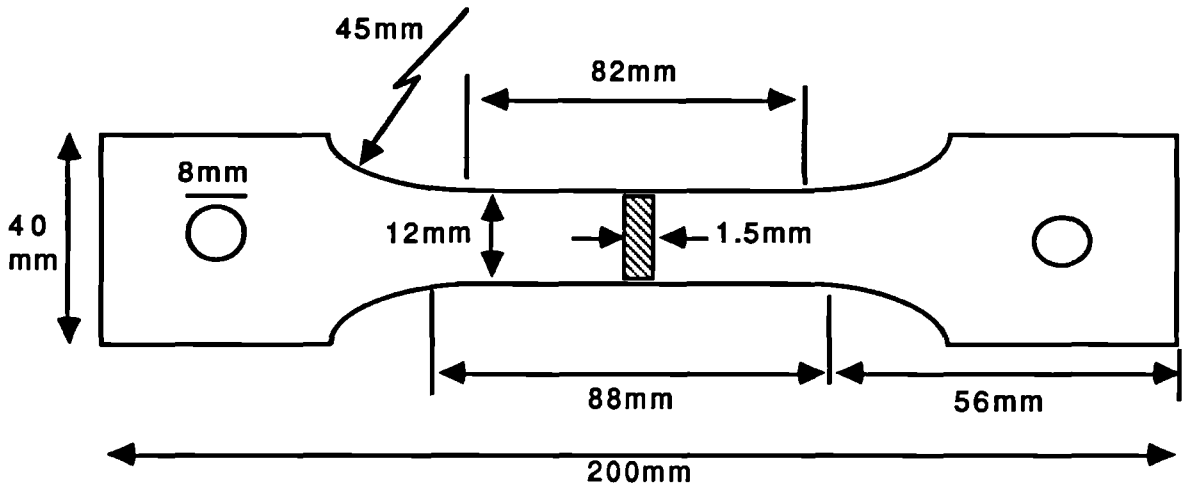


Figure 3.14 Tensile test specimen.

3.5.10 Microhardness Measurement

Leitz microhardness tester was used to investigate the hardness of the fusion zone, heat affected zone and the base material. In general the hardness values were taken at three points and the average of the three was taken.

3.5.11 Impact Testing

The test was carried out on thin-walled box section steel structural members supplied by RTM Research Centre, Turin, Italy. The box sections were subjected to static and dynamic axial crushing and its effects were examined.

3.5.12 Fatigue Testing

A few welded samples of uncoated steel were sent to CETIM and RENAULT for fatigue testing. The results are described.

3.5.13 Corrosion Testing

Welds fabricated were used for corrosion testing. Two techniques were used to determine the corrosion rate of the zinc coating in the presence of the weld, (a) polarisation technique and (b) Galvanic coupling technique.

3.5.13.1 Polarisation Technique

Some unwelded specimens were also prepared in order to compare the corrosion rates of welded and unwelded samples. The procedure followed was to allow the specimen to freely corrode in the test solution whilst monitoring the corrosion rate established at intervals during a 50 h period by means of the linear polarisation technique.

3.5.13.2 Galvanic Coupling Technique

To investigate the galvanic current established between the weld and the surrounding zinc and to construct an Evans diagram [148] for the system.

The specimens were galvanically coupled in 1N NaCl solution of pH 4 at 30°C.

Variation in the galvanic current with respect to time was monitored by means of a zero resistance ammeter when the value of resistance set on the resistance box was zero. This test was periodically interrupted to allow the determination of the Evans diagram.

A series of tests were performed on each type of weld i.e., normal weld (NRM), nickel injected weld (NKL), stainless steel injected weld (SST), tool steel injected weld (TST), tool steel incorporated just after welding operation (TSTA), zinc vapour incorporated weld (ZIC) and weld made by zinc powder incorporation.

3.6 Design and Manufacturing of Press Tool for Setting Gap Size

During the welding of zinc coated steel it was realised that using shims as a method of setting the gap had limitations, these were:-

(i) gaps could only be set in steps of 0.05 mm,
(ii) the use of shims effectively reduced the venting area to a thin band ahead and behind the weld pool,
(iii) variations in gap size were large.

An alternative method was required. It was decided to put small dimples in the surface of one sheet to keep the sheets apart. Thus a method of inducing the dimples in the surface of the sheet had to be found. The method had to be simple and easy to use and be reasonably accurate. The method chosen was to press a small hard ball into the surface of the sheet, deforming it into a die and the force required to do this was implemented using a fly press.

Figure 3.15 shows the design of the tool used. A ball bearing was used to deform the surface of the steel sheet into a lower die, consisting of a small chamfered hole. The size of the dimples was controlled using the fly press stop. Initially, control of dimple size was attempted using the face of the punch but this caused too much damage

to the sheet surface. The spacing and configuration of the dimples were investigated to ensure that the gap stayed within the set limits. This also has the advantage of not restricting the venting area and that the method could lend itself to use in the mass production industries.

In addition to the use of dimples a clamping arrangement was implemented. This used a ridged base block and straight clamping bars as shown in Figure 3.16. The samples were clamped on a variable speed X-Y table so that they could be moved under the stationary laser beam. The samples were positioned correctly using a helium-neon laser which was aligned with the main CO_2 laser.

RTM research centre, Italy, showed an interest in this method of setting the gap size. A few samples were produced and sent to RTM for trials on their high power laser. The results obtained are also presented.

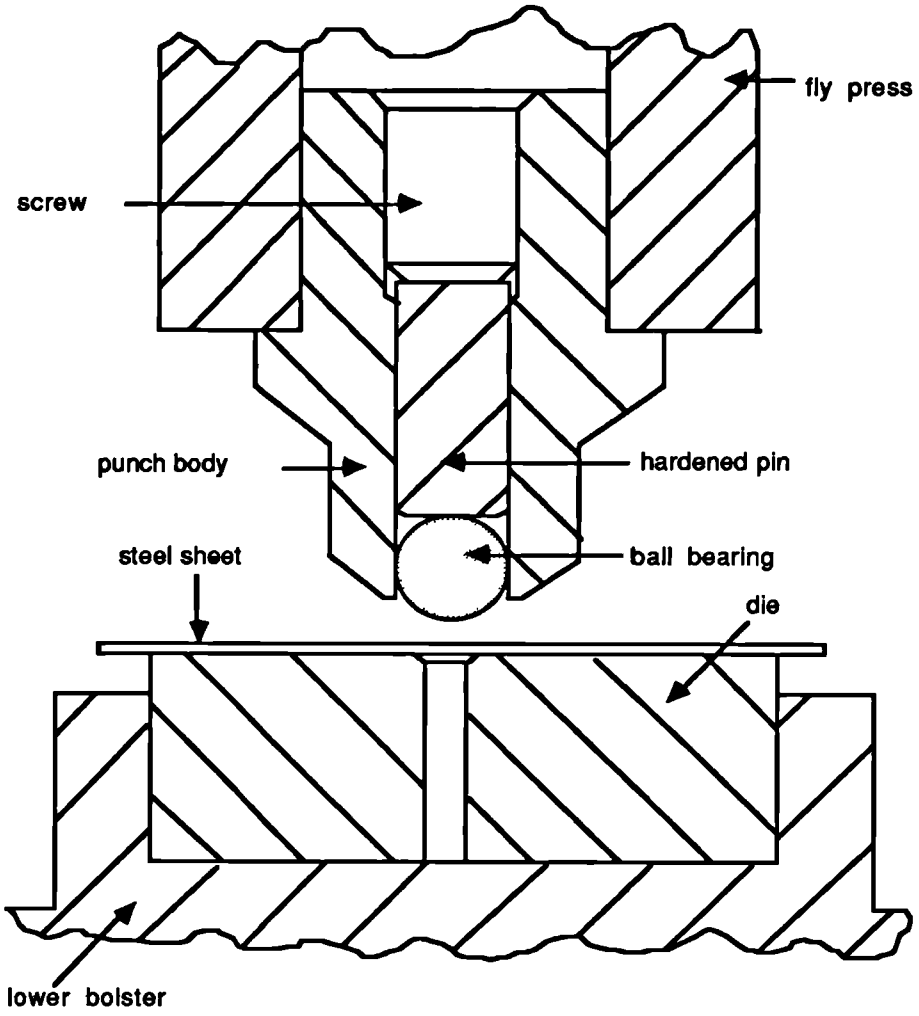


Figure 3.15 Design of press tool and die (section view).

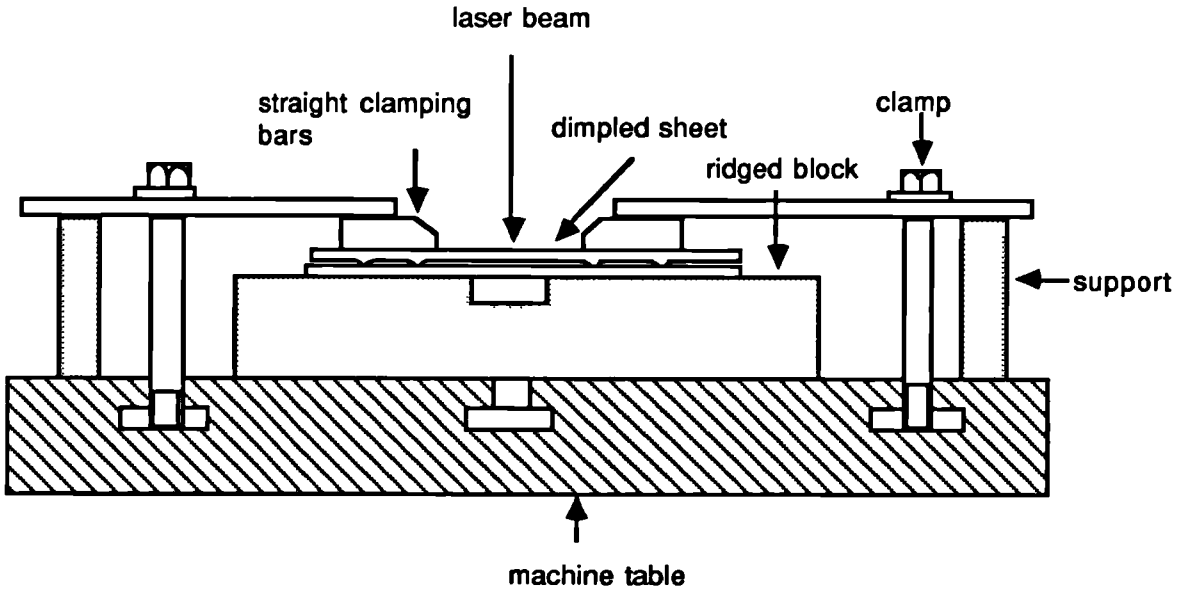


Figure 3.16 Clamping system for welding zinc coated steel in lap configuration.

Chapter 4

Processing Techniques - Results and Discussion

4.1 Introduction

Laser welding of zinc coated steel in butt configuration has not shown any problem so far. However, the problem arises when welding zinc coated steel with a laser in lap configuration. This can lead to the explosive ejection of zinc vapour from the 'keyhole' formed by the laser beam when the material is penetrated. This zinc vapour arises from the volatilisation of the zinc coating that is present between the overlapping sheets and is a consequence of the low boiling point of zinc (906° C) compared with the high melting point of steel (1530° C). The explosive ejection of zinc vapors from the keyhole can destroy the weld bead and severe undercut can result.

This chapter deals with the possible ways in which zinc coated sheet steel can be welded in lap configuration. Also the problems during the welding of this material are identified. This has been shown that a small gap between the sheets helps to exhaust the zinc vapour (generated at the interface between the two sheets) through the gap thus giving a good quality sound weld. The laser welding parameters, such as speed, power, flow rate of argon gas and gap between the sheets was varied in order to find out the effect of these parameters on the penetration, width, melting and joining efficiency and the weldability of zinc coated sheet.

4.2 Laser Welding of Zinc Coated Steel

Figure 4.1 illustrates the welding of zinc coated steel by laser into two tightly clamped sheets in lap configuration. Figure 4.2 shows a resulting weld bead. The

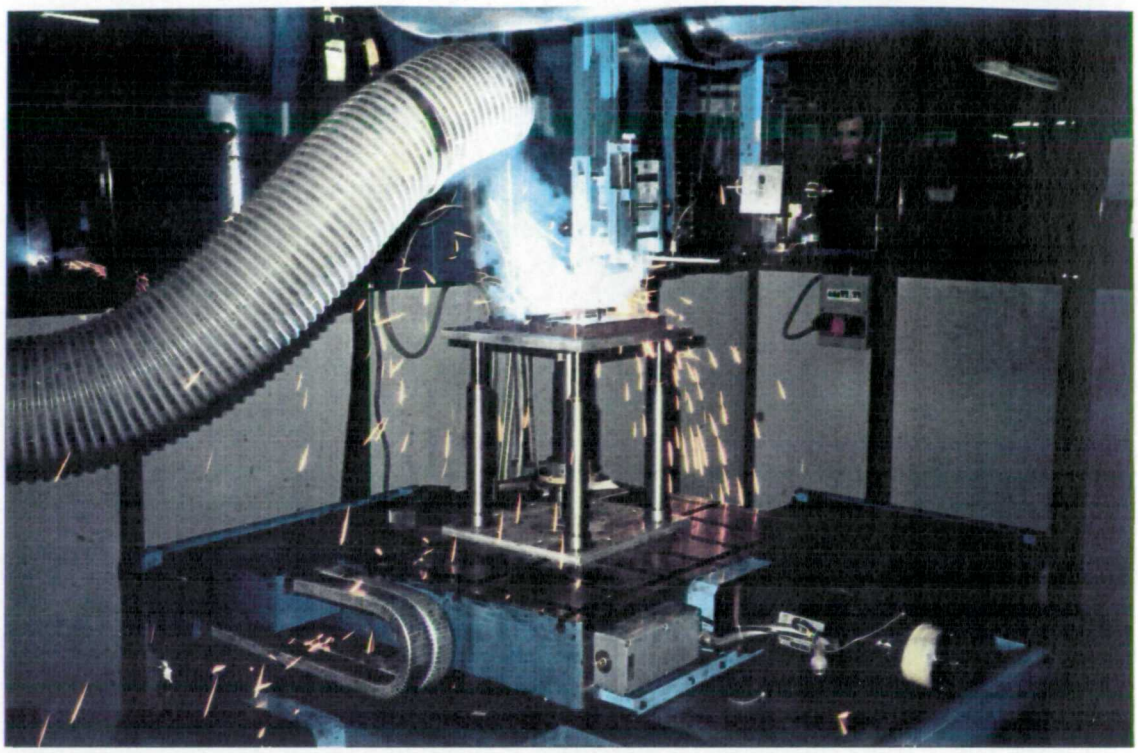


Figure 4.1 Laser welding of zinc coated steel into two tightly clamped sheets in lap configuration shows explosive ejection of molten metal and zinc vapour.



Figure 4.2 A lap weld made by laser into two sheets of zinc coated steel tightly clamped, showing serious disruption of the weld.

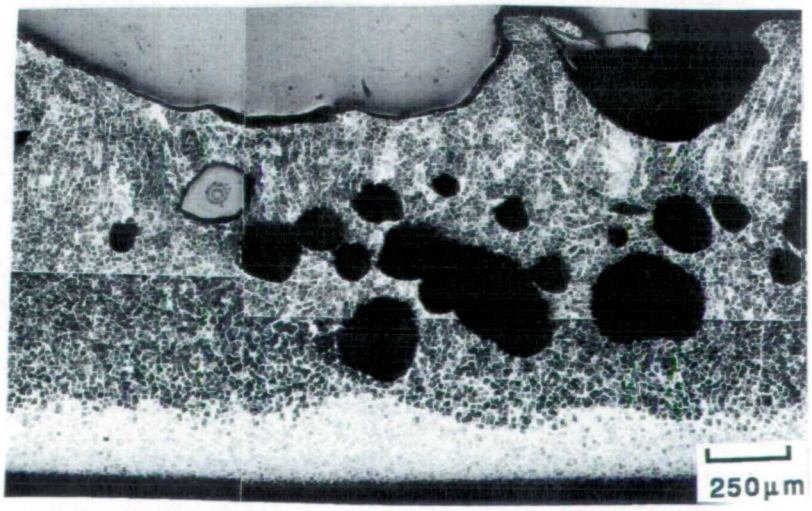


Figure 4.3 Longitudinal cross section of a lap weld made by tightly clamping two zinc coated sheets together showing a lot of porosities in the weld.

serious disruption of the weld by the escaping zinc vapour is obvious and makes this welding technique unacceptable. The longitudinal cross section (Figure 4.3) of one such weld showed a lot of porosities in the weld. However it does serve to illustrate the problem to be solved. It is necessary in welding this sort of material that either the zinc is removed from the weld area (double pass technique), or it is condensed (metal powder injection technique and side jet welding) or it is vented (end edge and gap welding). These ways of welding are discussed here.

4.2.1 Techniques Used for Welding Zinc Coated Steel Sheet

A 2kW CLL laser was used for the welding of zinc coated steel. The method adopted were:

(i) Double pass welding, (ii) End edge welding, (iii) Gap welding, (iv) Welding using side jets, (v) Welding with metal powder injection.

4.2.1.1 Double Pass Welding

Figure 4.4 shows the lap welding configuration used for double pass welding. By this technique it was hoped that the zinc would move away from the weld area due to surface tension forces during the first non penetrating pass. Thus, the focussed laser beam was first passed at a high speed and then passed again with a slower speed to create the weld. Argon gas from the nozzle coaxial with the laser beam was used for shrouding the workpiece.

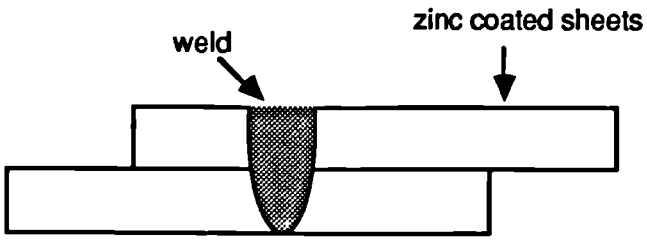


Figure 4.4 Double pass welding.

In this experimental arrangement a rigid clamping system was used to ensure that no gap is present between the two sheets. First a series of bead on plate welds were made on a 0.7 mm thick zinc coated steel sheet with varying the welding speed at a constant laser power. The aim was to find a speed at which there was only a slight melting of the zinc coating at the bottom of the sheet. Three speed were selected for first pass from the above runs. They were 60, 65 and 70 mm/s for a laser power of 1.54 kW. These speeds were expected to give a better understanding about the removal of zinc due to surface tension forces at the interface between the two sheets. The laser was then passed for the second run at a speed of 25 mm/s to create the weld.

One of the resulting weld beads after second pass in this technique is shown in Figure 4.5, the other two weld bead were similar to the one shown here. It can be seen that the weld bead has lot of pits on the surface. Further the visual observation showed that a lot of pits and deterioration of the weld bead had already occurred during the first pass showing that the zinc at the interface have been vapourised and exploded out of the keyhole. This has made the technique unacceptable for welding zinc coated steel. It must be remembered that it is difficult to obtain such a speed for first pass that the penetration of the beam is just near to the zinc coating at the interface, where it only melts the zinc coating without vapourising it. A higher welding speed for first pass could lead to non-melting of the zinc coating at the interface, thus giving no advantage of this technique. A lower welding speed will vaporise the zinc coating at the interface between the two sheets, this on first pass will give a weld with serious deterioration on the surface. Thus it can be concluded that the first pass will need a very high accuracy to achieve such a condition that the temperature of the zinc coating at the interface does not exceed the boiling point of zinc. This might help to move the molten zinc away from the welding area due to surface tension forces, which will make the welding of zinc coated steel by this technique possible.

In an other experiment a loose clamping of the specimen to the working table was mainta ned. Two small G- clamps were used at the two ends of the specimen to grip it to the working table. Hence the two ends of the specimen had almost no gap,

but it was revealed that for this type of clamping system an upside bend in the upper sheet, and hence a small gap, is left between the two sheet, which was not expected to be constant through out the length of the weld.

A series of welds were made on a 0.875 mm thick zinc coated steel by varying the welding speed. Careful studies of the weld bead revealed three kinds of weld bead morphologies, (i) little melting at the top surface (ii) pitting, and (iii) sound weld bead. Figure 4.6 shows a weld bead which had all three kind of morphologies in one run. It is evident from the figure that a part of the weld (marked as 'a') showed hardly any true welding. It seems that only the top zinc coating has been melted with a very little penetration to the substrate. Thus it is most likely that the zinc plasma generated at the beam metal interaction point is shielding the laser beam from transmitting to the workpiece. The weld also showed pitting 'b' and sound weld bead 'c'.

Cross section of the welds were made at these three point (a, b, c, in Figure 4.6) for each type of weld surface. Figure 4.7 (a), (b) and (c) shows the cross sections of these welds. It is evident from the Figures 4.7 (a) that a very little penetration was found in case of weld with zinc plasma blocking the beam. In case of weld with pitting the cross section (Figure 4.7 (b)) showed a zero gap between the two overlapped sheets. This lead to the zinc vapour ejection from the keyhole thus deteriorating the weld bead. It was found that the penetration of the laser beam had also been affected due to the zinc vapour exploding out of the weld pool. In the case of pitting in the weld bead and beam blocking by zinc plasma the penetration is seriously reduced as is apparent in Figure 4.7 (a) & (b). On the other hand in the case of sound weld bead the cross section (Figure 4.7 (c))showed a small gap between the sheets. This provided an alternate route for the zinc vapour to exhaust and hence a sound weld has been resulted. The sound weld bead has shown a full penetration to the bottom sheet.

The lack of a gap between the sheets led to the explosive ejection of zinc vapour which in turn led to the laser beam blocking due to zinc plasma. This seriously

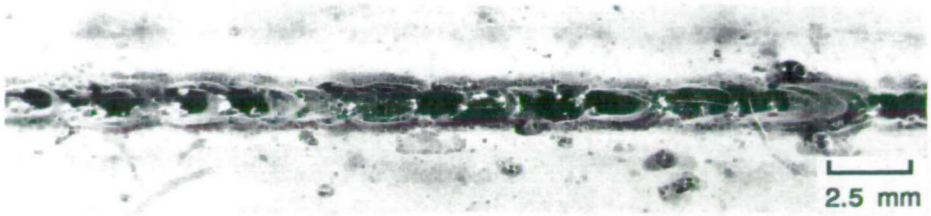


Figure 4.5 The weld bead after second pass show the serious disruption of the weld due to zinc vapour ejection for the keyhole.

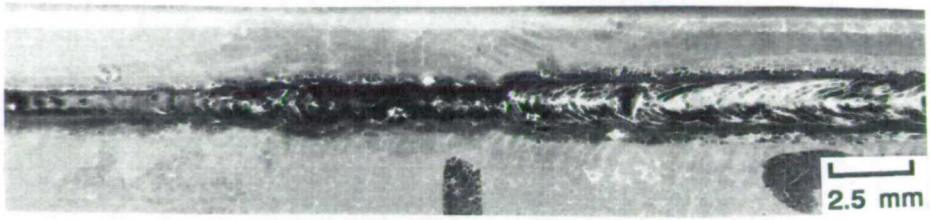


Figure 4.6 A weld bead showing three phenomenon **(a)** the plasma blocking of the laser beam, **(b)** weld bead pitting due to the ejection of zinc vapour from the keyhole, and **(c)** a sound weld bead.

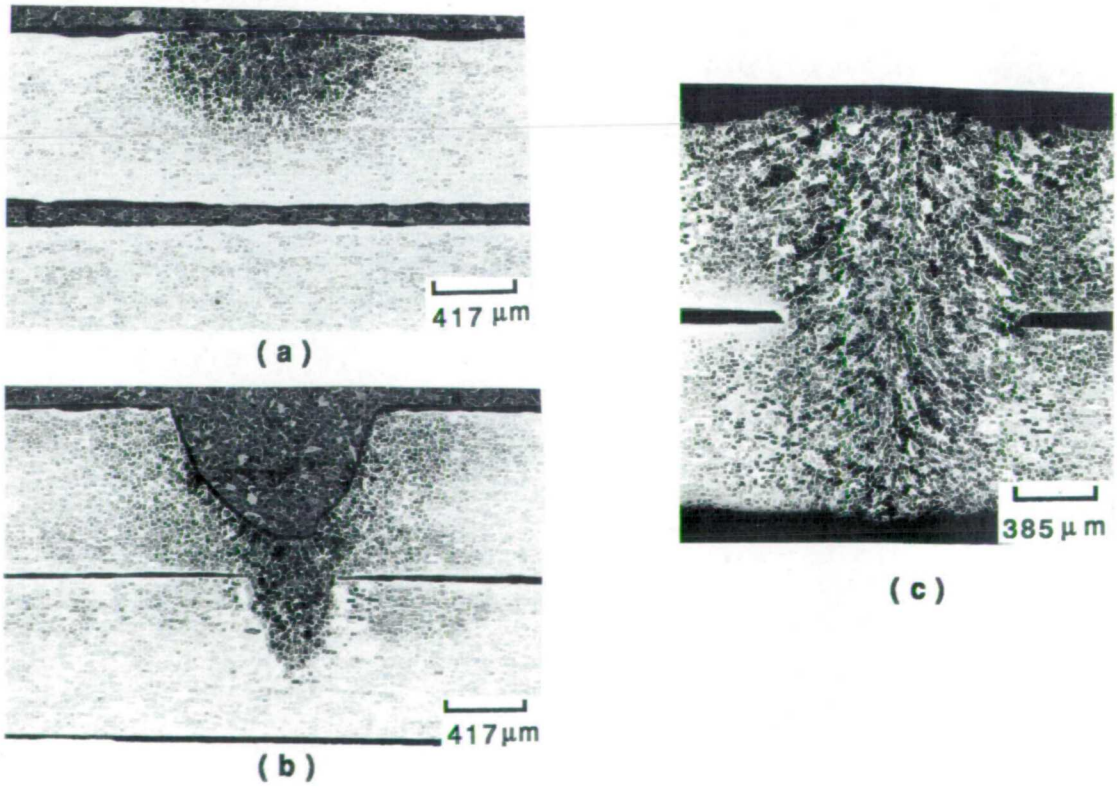


Figure 4.7 Cross section of the weld **(a)** very little penetration due to plasma blocking of the beam, **(b)** undercut or pitting due to ejection of zinc vapour from the keyhole and **(c)** sound weld with full penetration of the beam to the bottom sheet.

reduces the weld penetration. Hence it was difficult to know the real penetration when there is pitting or plasma blocking problem, thus for beam penetration measurement the microsections were to be obtained from that region of weld where it showed no pitting and a reasonably good weld bead surface.

There was no evidence of the removal of zinc from the interface due to surface tension forces. Thus the sound welds obtained in this technique were due to the presence of a small gap at the interface rather then due the removal of molten zinc. Hence this technique of double pass welding is not suitable for the welding of zinc coated steel. But the presence of a small gap is recommended for the sound welding of this material.

4.2.1.2 End Edge Welding

The end edge welding configuration is shown in Figure 4.8. It was felt that this arrangement would allow the seam to be sealed with minimum penetration giving advantages in speed and subsequent surface treatment such as painting. It was also felt that if the ends were properly presented then sufficient vent area would exist to allow the zinc to be exhausted without damaging the weld. Shrouding of the weld area was achieved by a coaxial argon jet. The shroud gas flow rate was approximately 4 litres/min.

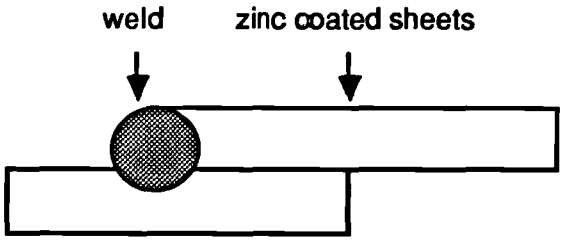


Figure 4.8 End edge welding.

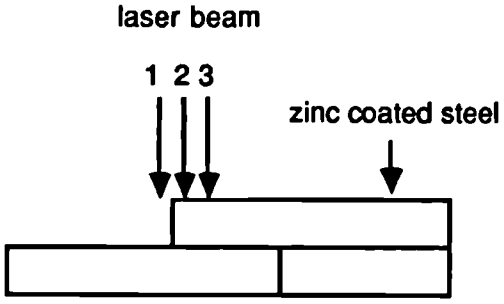


Figure 4.9 Three possible ways in which the beam can strike the edge of the specimen.

In this type of welding the beam alignment with the workpiece is also an important factor which affects the weld penetration. As shown is Figure 4.9 three possibilities may exist (i) the beam may strike the bottom sheet with very slight melting of the top sheet, (ii) half of the beam may strike the upper sheet and the remaining half goes down to the bottom sheet with melting of both sheets, (iii) all the beam may fall on the upper sheet and penetrated down to the bottom sheet as a lap weld. In all cases the beam penetration would be expected to be different.

In the first case i.e., when beam strikes on to bottom sheet then there will be only a slight melting of the upper sheet. Although the two sheets can be joined together but the width of the weld at the joining of the two sheets would be very small and will not be expected to give a reasonable tensile strength of the weld.

In the second case, when half the beam spot strikes the upper sheet and remaining half of the beam spot strikes the bottom sheet, more of the material from the upper sheet melts and moves down to the bottom sheet and hence there would be much wider width of the weld at the joining giving a good sound weld. The tensile testing of such a weld (discussed later) showed that the fracture occurred in the base metal away from the weld.

In the third case, when the whole beam spot strikes the upper sheet, then the welding is no more an end edge but a lap weld. Hence the ideal condition of welding

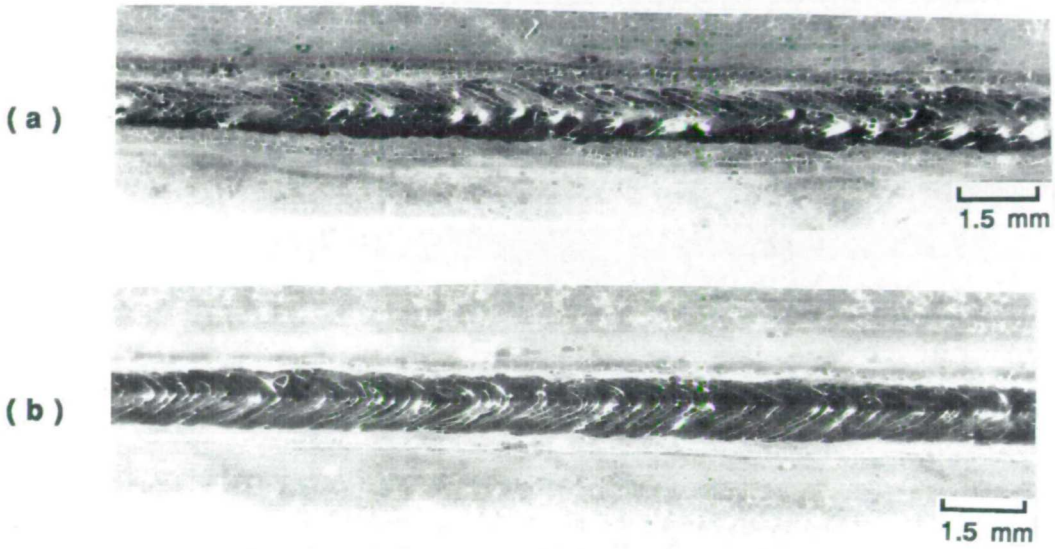


Figure 4.10 Two kinds of welds normally obtained using the end edge welding technique **(a)** weld with pitting in the surface, and **(b)** sound good quality weld.

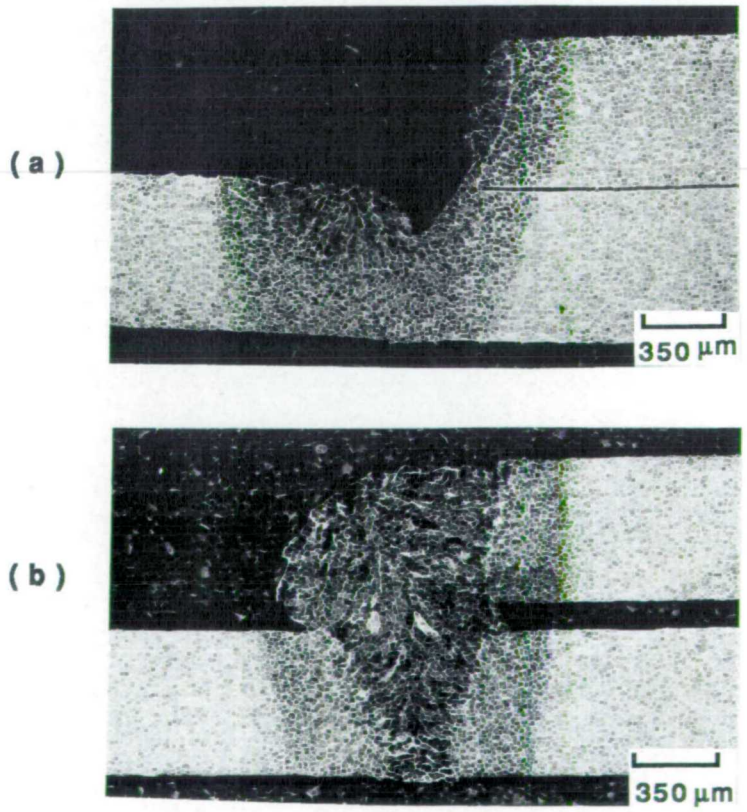


Figure 4.11 The microsections of welds **(a)** zero gap between the sheets lead to a weld showing pits on the surface, and **(b)** the presence of a gap between the two sheets gave a good quality weld.

two sheets in end edge configuration is to allow the beam fall on the end edge such that half of the beam strikes the upper sheet and the remaining half of the beam strikes the bottom sheet. Under such conditions both the sheets are melted and joined to give an ideal width of the weld at the joining.

The weld bead obtained by this technique showed a similar type of welding behaviour as discussed in double pass welding. Two types of weld bead were normally seen (a) weld bead with pitting and (b) sound weld without pitting (Figure 4.10 (a) & (b)). The microsection of two such welds are shown in Figure 4.11 (a) & (b). It can be seen that the tightly clamped sheets which had no gap between the sheets showed pits on the weld surface. The sheets which had a small gap between them were welded without any deterioration of the weld. Thus the use of this technique for welding of zinc coated steel require a certain gap for zinc vapour to be vented. Hence a sound and good quality weld can be obtained if a small gap is maintained between the two sheets.

4.2.1.3 Gap Welding

The previous two techniques initiated the idea for welding zinc coated steel with a gap. Also the RTM Laser Centre, Italy, recognizes the need to vent the zinc vapour from the weld area [197]. This it does by arranging a gap between the pieces to be welded. In some experiments a fixed gap was formed using spacers as shown in Figure 4.12. In other experiments a variable gap was formed as shown in Figure 4.13. The aim was to produce a weld with variable gap under highly similar welding conditions for each gap size. The only way to achieve high accuracy was to vary the gap between the two overlapped sheets and to weld in just one laser pass. Thus the gap was varied starting from zero at one end to 0.3 or 0.4 mm at the other end. A shim of 0.4 mm was inserted between the sheets at one end. The laser was passed through the overlapped sheets to create a weld. Hence by welding this way an estimate of the optimum gap size could be obtained from a single weld pass.

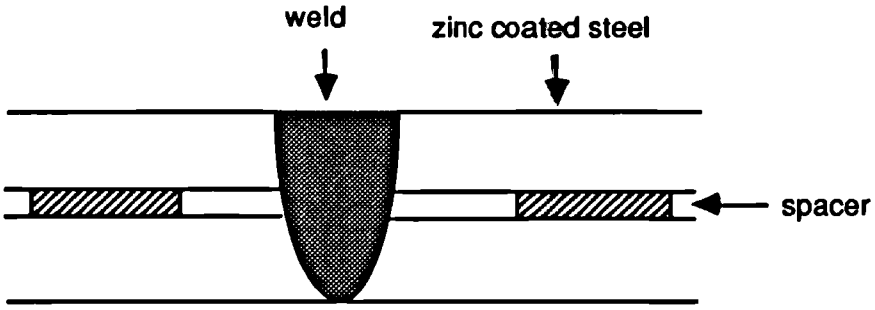


Figure 4.12 Welding with a fixed gap formed by spacers between the two sheets.

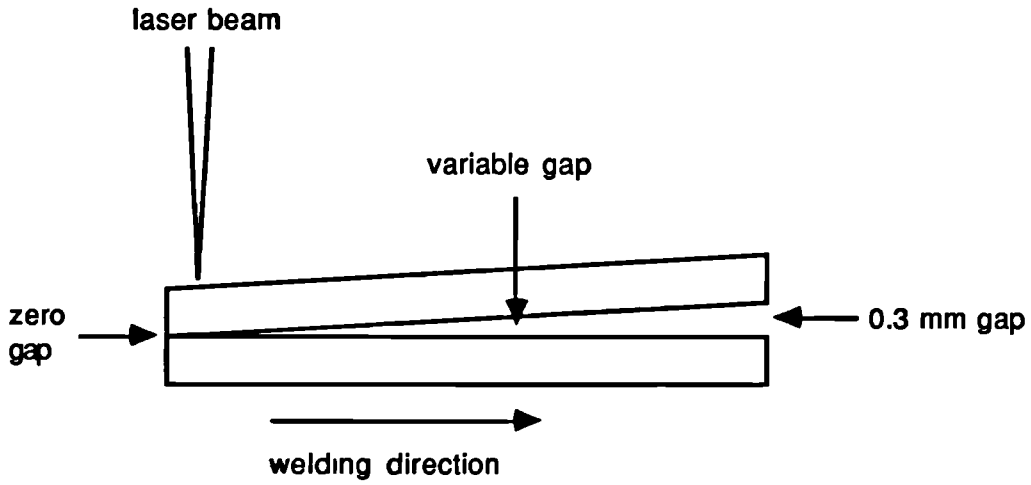


Figure 4.13 Welding with a variable gap between the sheets.

4.2.1.3.1 Effect of Gap Size on Welding Performance of Zinc Coated Steel

In this study a thin sheet of 0.55 mm was used with a zinc coating thickness of 10 μm on one side only. Welding was performed with both the zinc coating thickness placed at the interface giving a 20 μm thickness of zinc at the joining point. A fixed gap was given for each welding run using spacers according to Figure 4.12.

Figure 4.14 (a) to (f) shows the effect of gap between the overlapped sheets on welding performance of zinc coated steel. It is apparent from the Figure 4.14 (a)

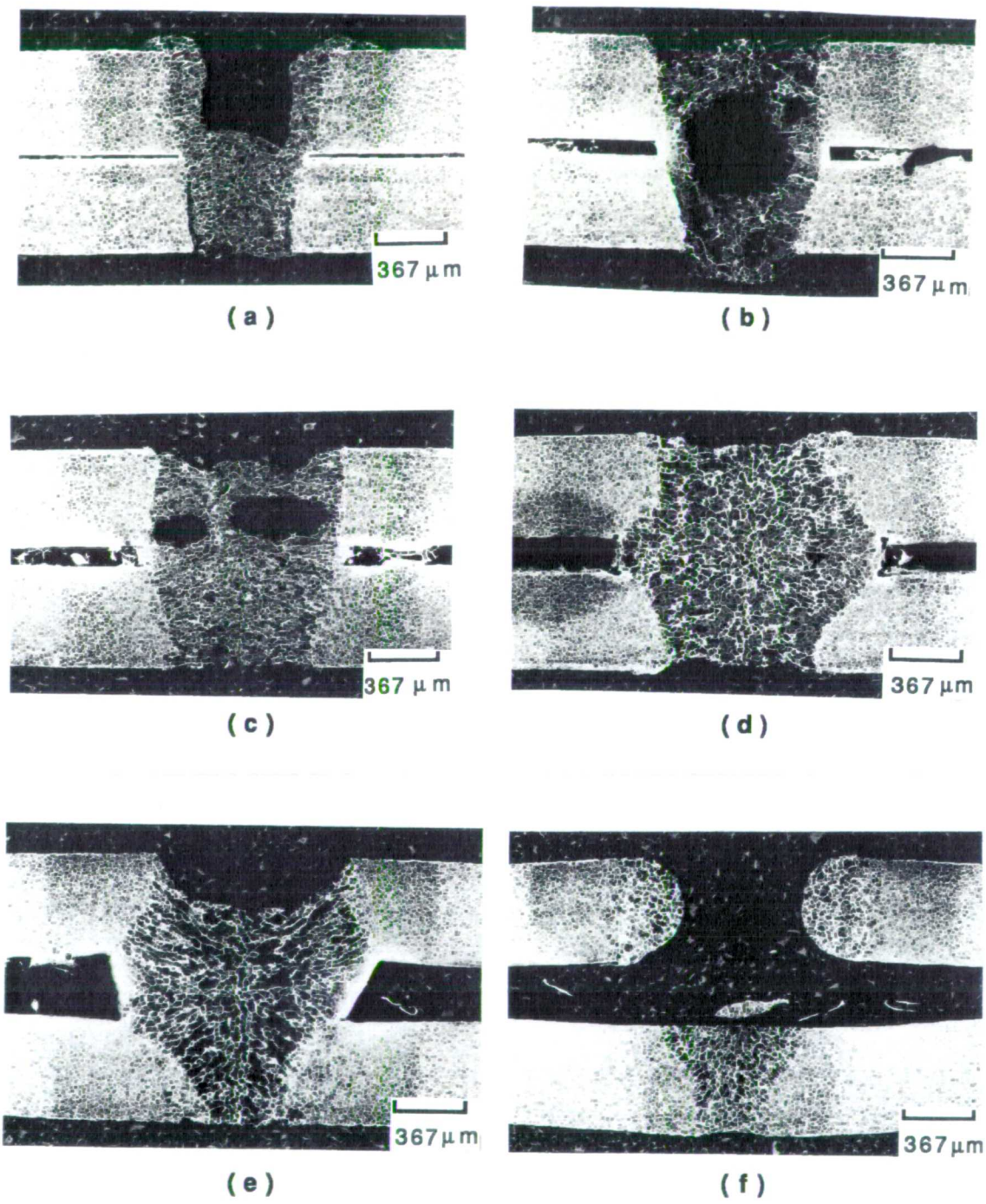


Figure 4.14 (a) to (f) shows the effect of gap between the overlapped sheets on welding performance of zinc coated steel. Laser power; 1.54 kW, sheet thickness; 0.55 mm, welding speed; 20 mm/s, gap size; **(a)** 0.0, **(b)** 0.07, **(c)** 0.11, **(d)** 0.18, **(e)** 0.33, **(f)** 0.36 mm.

that a zero gap between the sheets led to the deterioration of the weld bead and lot of molten metal was blown out of the keyhole by evaporating zinc vapour. Similarly a smaller gap lead to porosities in the weld bead (Figure 4.14 (b) & (c)). While a gap of 0.18 mm between the sheets gave a good sound weld (Figure 4.14 (d). A larger gap of 0.33 mm gave a weld which showed a concave depression in the weld surface as can be clearly seen in Figure 4.14 (e). Further larger gap of 0.36 mm gave a weld which appeared like a cut (Figure 4.14 (f)). This could have been the result of a poor thermal contact with the second sheet, allowed the pool to be effectively held only by the top sheet of 0.55 mm thickness. According to Quigley [149] if the weld width is larger than the depth then there is a risk of surface tension pulling the melt to the sides, as shown in Figure 4.15, resulting in an undercut.

Thus an optimum gap size can lead to a good sound weld free of pit or concave depression in the weld bead. Here the gap of 0.18 mm was found to be suitable for welding this material. According to the gap model presented in chapter 6, the optimum gap size for sound quality, calculated for this run is 0.14 mm. Thus a gap less than 0.14 mm lead to pitting and porosities, while a gap greater than 0.14 gave sound welds up to a limit arising from drop out.

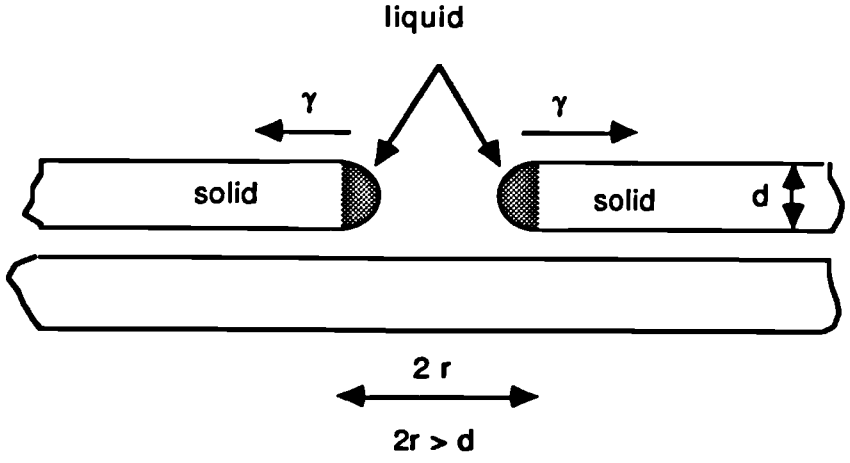


Figure 4.15 Surface tension pulls the molten metal towards the edges if width of the weld is greater than the sheet thickness.

In the second experiment a 0.7 mm thick sheet with a zinc coating of 7.5 μm was used. A variable gap between the two sheets was given as shown in Figure 4.13. Figure 4.16 (a) to (d) shows weld bead during a single run at four different points starting from zero gap to a larger gap of 0.4 mm. It is apparent from Figure 4.16 (a) that a zero gap between the sheets led to the deterioration of the weld bead. As the gap size increases the weld begins to show a better surface. At an optimum gap size (Figure 4.16 (b) a good quality weld bead is seen. A larger gap gave a weld which showed a concave depression in the weld bead (Figure 4.16 (c) and its cross section is given in chapter 6 (Figure 6.6 (c)). Further larger gap gave a weld bead which showed that the molten metal pushed down to the bottom sheet filling the gap between the sheets, but an undercut, as shown in Figure 4.16 (d) is left in the top sheet which can seriously affect the strength of the weld.

The cross section of all these weld bead (Figure 4.16) are shown in (Figure 6.6). It is clear that a gap of 0.1 mm gave a good quality weld in this type of experiment. In the presence of a gap, the joint formation takes place as a result of flow of the molten metal of the top sheet through the gap to make contact with the bottom sheet. There is a partial flow of the metal of the top sheet into the gap, and with sufficient large gap depression or concavity is formed in the top sheet. Hence to obtain a good sound weld, free of pit or holes, an optimum gap size is necessary.

4.2.1.3.2 Effect of Gap Size on Weld Penetration and Width

In laser spot welding of a lap joint the presence of a gap decreases the weld penetration. Also the joint strength decreases with increasing gap, as a result of reduction of the area of fusion and of the depth of penetration of the bottom sheet [58]. But since a gap is necessary for welding zinc coated steel sheet, it is interesting to investigate the influence of gap size on the weld penetration for zinc coated steel. For this work an arrangement already described in Figure 4.13 was used. This experiment is different from the one described above in the sense that a full penetration to the bottom sheet was not aimed. The aim was to study the effect of gap

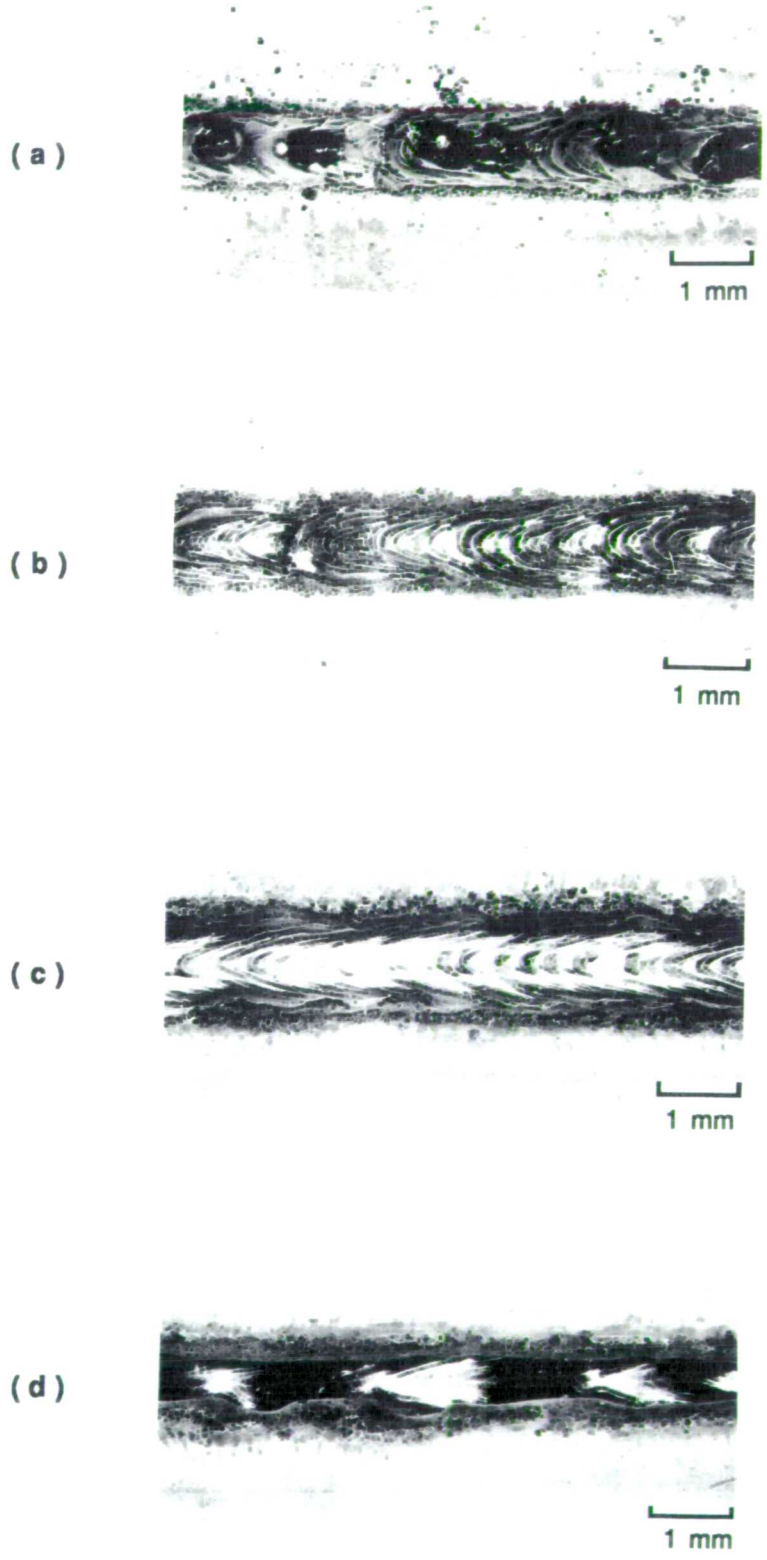


Figure 4.16 (a) to (d) The weld bead during a single run at four different points starting from zero gap to a larger gap of 0.4 mm. Laser power; 1.54 kW, welding speed; 20 mm/s, sheet thickness; 0.7 mm.

size on the penetration of the beam. Hence a lower laser power of 1 kW was used in this study.

After passing the laser in a single pass a weld was obtained which had a variable gap along the length of the weld. Cross sections were made at four different points to obtain the weld micrograph at different gap size. The weld penetration, width and the gap size was then measured.

Figure 4.17 (a) to (d) shows the microsection of the weld at four point with increasing gap size. Figure 4.17 (a) shows a zero gap between the overlapped sheets and a full penetration to the bottom sheet is resulted, but is also evident that the zinc vapour has exhausted through the keyhole thus blowing out the molten metal leaving unacceptable pits on the weld bead. In figure 4.17 (b) & (c), it can be seen that the presence of a gap has reduced the weld penetration and a non-through weld resulted, suggesting a lower welding speed is needed for a full penetration weld. It is interesting to note that the presence of a small gap between the sheet helped to exhaust the zinc vapour through the gap and thus a sound weld free of pits or porosity is obtained. Further too high a gap (Figure 4.17 (d) reduces the width of the weld at the interface between the two sheets, which could not be acceptable for the strength of the weld.

From the examination of the cross sections of welds, it can be seen that the depth of penetration and the weld width at the interface between the two sheets decreases as the gap size is increased (Figure 4.17), and also the shape of the weld is different at different gap sizes.

The penetration and width of the weld were plotted as a function of gap size in Figure 4.18. It is apparent from the curve that the weld penetration decreases as the gap is increased. Also the width of weld increases with the increase in gap size. The presence of gap leads to the extensive heating of the top sheet and is apparent from the Figure 4.17 (a) to (d) that the heat affected zone (HAZ) also have a larger width for a

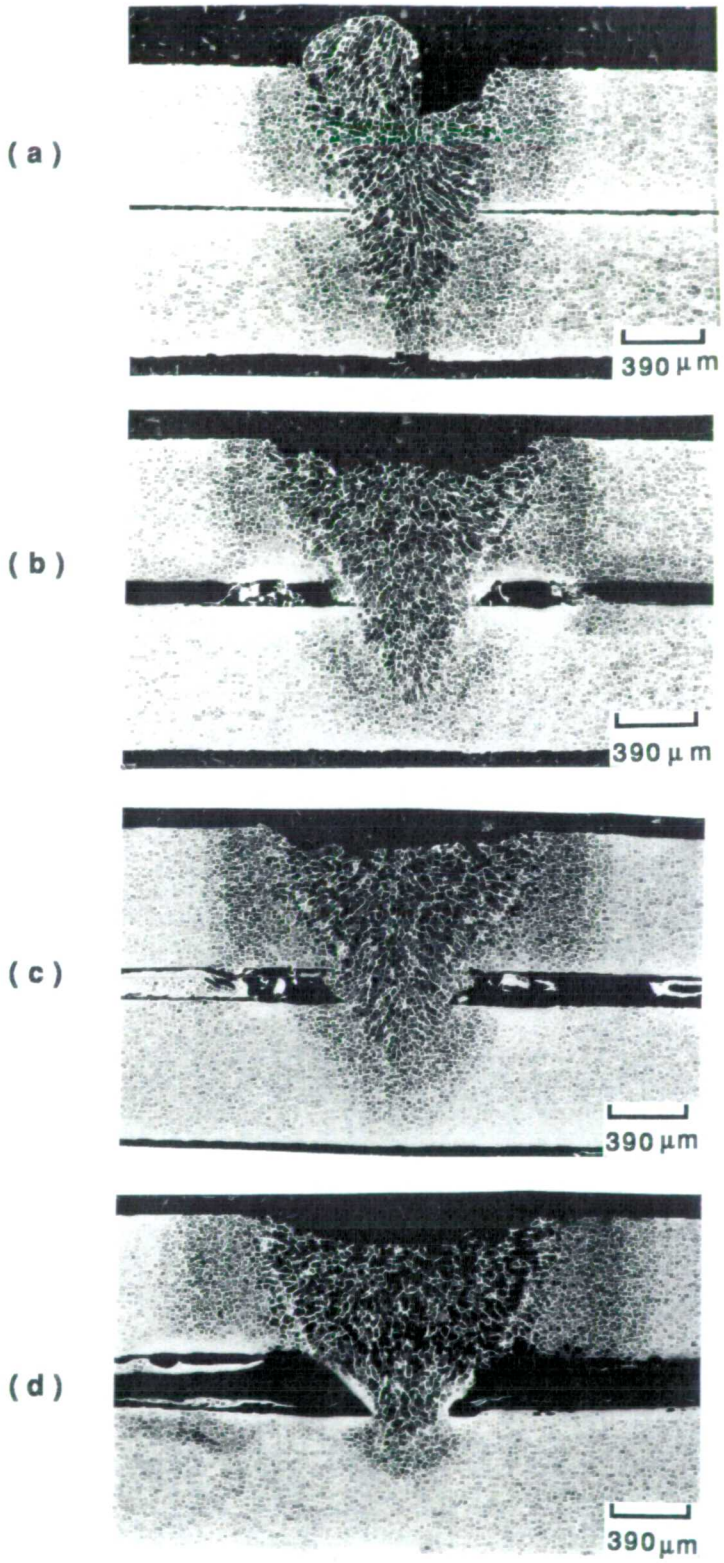


Figure 4.17 The microsections of the weld at four point with increasing gap size. Laser power; 1 kW, welding speed; 15 mm/s; sheet thickness 0.7 mm, gap; **(a)** 0.0, **(b)** 0.09, **(c)** 0.15, **(d)** 0.28 mm.

large gap size.

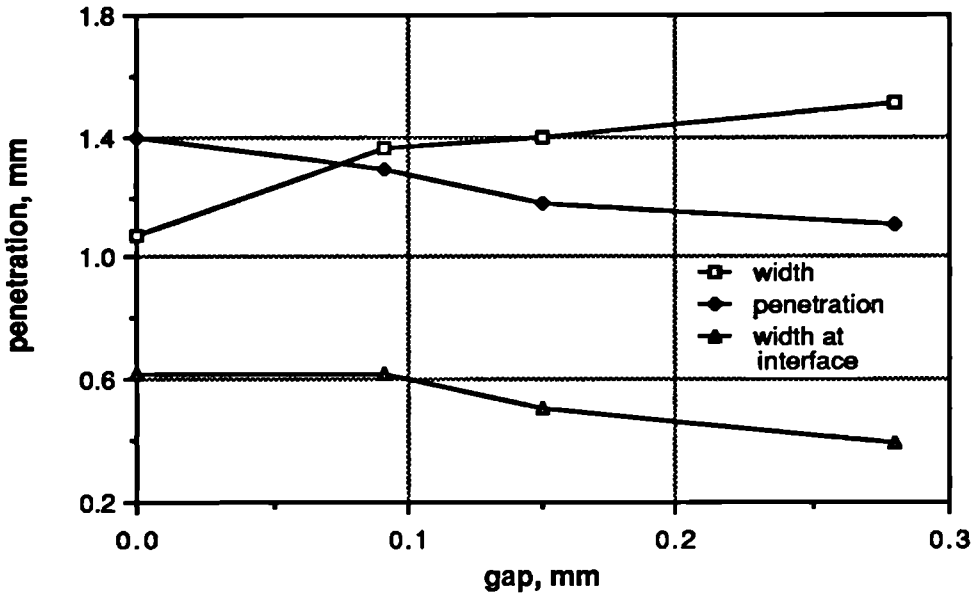


Figure 4.18 Penetration and width of the weld as a function of gap size. Laser power; 1.00 kW, welding speed; 15 mm/s, sheet thickness 0.7 mm; zinc coating 7.5 μm.

4.2.1.4 Welding With a Side Blown Gas Assist Jet

This technique was primarily aimed to establish whether improved beam coupling could be obtained by reducing the plasma thickness in the beam path. Secondly the objective was to incorporate into the weld bead zinc that had been volatilised as a result of the welding operation (this is discussed in section 4.2.1.5.2). Welds were produced using the arrangement shown schematically in Figure 4.19 . Argon gas was entrained through the side jet at a certain flow rate and directed at the beam metal interaction point during welding.

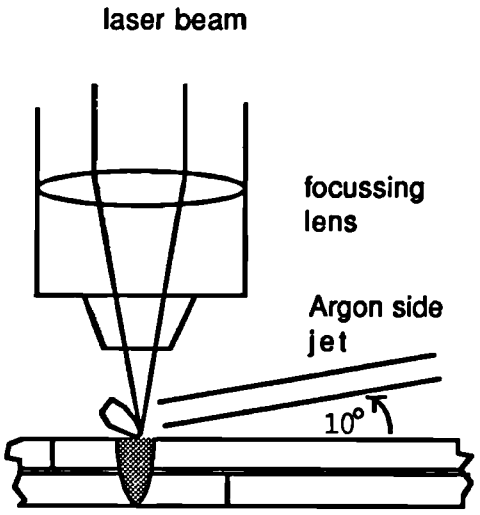


Figure 4.19 Laser welding with side blown gas assist gas.

4.2.1.4.1 Effect of Assist Gas Jet Velocity on Weld Penetration

Laser beam is a useful tool for material processing, especially for welding of materials. However, laser beam produces plasma during welding due to its high energy density. This plasma prevents the laser beam from passing to the materials. In this work an attempt has been made to suppress this laser generated plasma by using an argon assist gas. For th's purpose an argon jet made of copper tube was fixed near to the nozzle at an angle of 10° to the working table. The distance of the argon jet from the beam impingement point was 10.0 mm and it was 3.0 mm above the workpiece. The point of impact of the argon gas from side jet was away from the beam impingement, i.e., the gas was d rected almost parallel to the workpiece and slightly off set from the sheets to be welded.

A series of welds were made with this set up. Figure 4.20 illustrates the results obtained using this technique. The figure shows a dependence of penetration on gas jet velocity at a laser power of 2 kW and a welding speed of 33 mm/s. At zero velocity of argon gas , the penetration is rather shallow compared to that with a certain gas jet velocity. However the penetration increases as the side blown gas jet is introduced. The penetration reaches to about 1.6 times, at a gas jet velocity of

222 m/s, compared to that with zero gas velocity. Further higher gas jet velocity showed a decrease in penetration.

During laser welding a significant amount of metal is vaporised at the interaction point and the vapour is then ionised by the incoming laser beam, forming a thick dense cloud called "plasma". This plasma scatters the incoming laser beam and only allows enough of the laser beam to penetrate to the workpiece to maintain the vaporisation. Hence less penetration is achieved in the workpiece. When the plasma is blown away by the side jet assist gas, then a thin plasma formed above the workpiece does not interfere with the beam and allows most of the beam to be utilised for deeper keyhole formation. A further increase in the gas jet velocity does not increase penetration any more, instead there is a small decrease in penetration. The reason for this phenomenon might be related to the plasma removal. Alexander [36] found that a small amount of plasma at higher welding speeds is helpful in coupling the beam to the workpiece. Thus in this experiment, higher gas jet velocity may lead to the removal of most plasma above the workpiece that might otherwise be helpful in beam coupling to the workpiece.

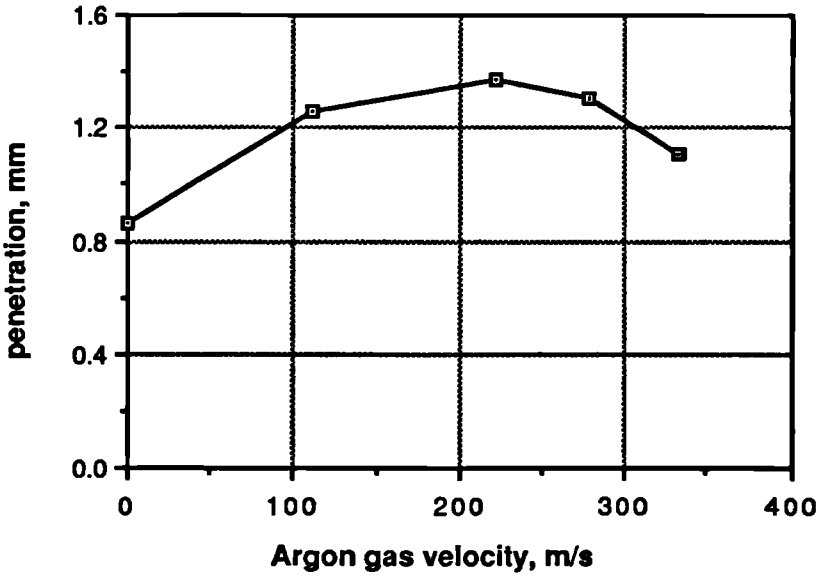


Figure 4.20 Weld penetration as a function of side blown gas jet velocity. Laser power, 2 kW, welding speed, 33 mm/s.

The work is in agreement with Arata *et al.* [54], where, they (using a laser power of 5 kW and a welding speed of 10 mm/s on SM41 steel) found that the penetration obtained with no side jet assists gas, for deep penetration welding, was 4 mm, but with side jet assist gas at a certain flow rate, a penetration of 6 mm was achieved. At low argon gas flow rate, more plasma is produced and even less penetration is obtained as compared to penetration without gas assist. The amount of plasma decreases with increasing gas flow rate and hence a deeper penetration is achieved. They found that using a gas flow rate of over 12 l/min, a 1.5 times deeper penetration is obtained than with no assist gas flow (Figure 4.21). Lock *et al.* [26] reported that, a far deeper penetration is obtained with side jet assist gas than without side jet.

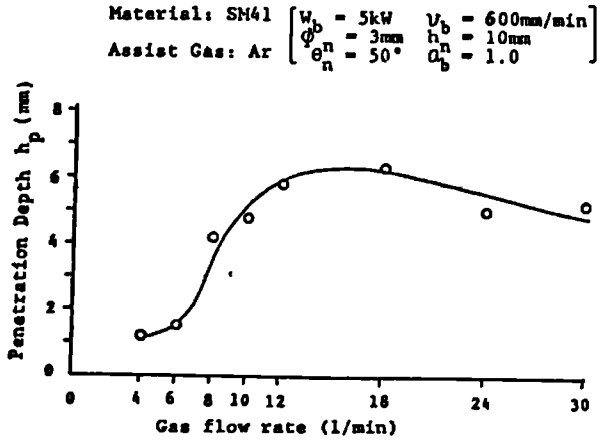


Figure 4.21 Dependence of penetration depth on gas flow rate [54].

4.2.1.5 Welding With Modification of the Weld Bead Composition

During the welding of zinc coated steel, with a laser beam, the zinc layer in the welded area volatilises and escapes leaving an exposed steel surface. Thus there is a need to protect this exposed area from corroding. The aim of these experiments was to obtain a fusion zone which should resist the corrosion of the material even though the zinc had been removed from the weld area.

High power lasers can be used to modify the composition of the weld with the injection of metal powder into the keyhole. Such modifications can improve the corrosion resistance of the weld, if a suitable material is selected. The processing conditions used were selected in order to facilitate the welding of zinc coated steel in lap configuration, together with alloying of the metal powder during welding.

A CO_2 laser (Control Laser Ltd.) was used to fabricate lap welds in the zinc coated steel. The laser beam had a wavelength of 10.6 μm (infrared) and a diameter of 23 mm with a doughnut beam configuration as measured from an acrylic print. The beam was focused to a spot of approximately 0.2 mm diameter using a KCl lens of 125 mm focal length. For each experimental weld the specimen was mounted on a 3-axis computer controlled table which moved under the stationary laser beam. A stream of argon gas was used to provide an inert gas shield over the hot reactive weld and to reduce plasma formation.

The normal welds were produced by simply passing the workpiece under the stationary focussed laser beam. A small gap was maintained between the two overlapped sheets to help vent the zinc vapour at the interface. The welding speed was varied until a fully penetrating weld was obtained.

Three techniques were developed to modify the composition of this exposed weld bead: **(a)** injection of metal powder into the melt pool during welding, **(b)** redeposition of volatilised zinc by use of a side blown gas assist jet, and **(c)** incorporation of metal powder just after weld formation.

4.2.1.5.1 Welding With Metal Powder Injection

The experimental arrangement is shown schematically in Figure 4.22. Welds were produced in the zinc coated steel by moving the workpiece under the stationary laser beam using a computer controlled table. In this technique a powder feeder

(described in Chapter 3) was used to feed metal powder at the beam impingement point through a small copper pipe which carried the powder particles in an argon gas carrier. Nickel, tool steel, or stainless steel powders were fed into the weld pool in separate experiments. The composition of the various powders used is listed in Table (4.1). The feed rate of the powders was low (approximately 0.2 to 0.3 g/s) since at higher rates excessive powder shielded the workpiece from the beam and produced inefficient welding. In addition higher feed rate lead to the pulsing of the outlet powder.

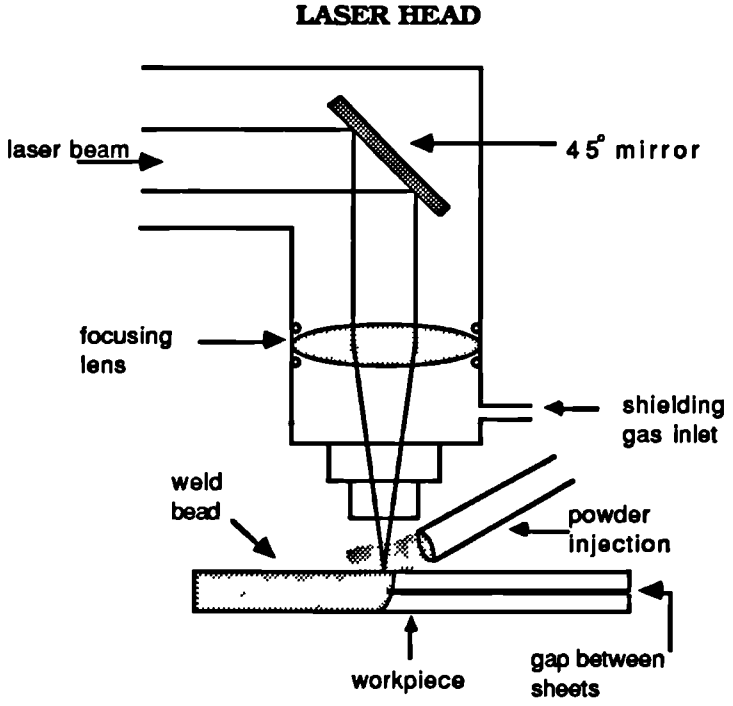


Figure 4.22 Schematic diagram showing the incorporation of metal powder in the weld bead.

Using this technique of metal powder injection similar problems also existed as explained earlier i. e., the pit formation. For those welds in which the gap was not specifically controlled showed two phenomena on the same weld length (i) pitting on the weld bead and (ii) sound weld bead. In the case of nickel and stainless steel injected welds, in which the gap was not specifically controlled, showed this problem. The weld bead surface was similar to that described in Figure 4.6. Hence from the

previous experience it can be concluded that pits formation occurred due to zero gap between the sheets and a sound weld is a result of the presence of small gap. Although the two welds i. e., nickel injected and stainless steel injected (Figure 4.23 (b) & (c)) did not show any gap between the two sheets it is unlikely that all the zinc vapours exploding out of the keyhole were condensed due to the injection of metal powder, since visual observations confirmed the presence of pits on the weld bead. For the case of tool steel injected welds a small gap of approximately 0.15 mm was maintained between the two sheets, hence all the welds obtained in this case did not show any pit formation on the weld bead.

Using the technique of metal powder injection the cross sections of the welds obtained for normal weld, nickel injected weld, stainless steel injected weld and tool steel injected weld are shown in Figure 4.23 (a) to (d). It can be seen that each type of weld has different microstructure due to the alloying of weld metal with various elements. In the case of weld with nickel injection, it was found that the nickel was not mixed thoroughly with the molten metal. EDAX analysis showed that the white phase (Figure 4.23 (b)) had a much higher amount of nickel (approximately 33%), as compared to homogeneous parts of the weld metal which had a small amount of nickel (2.1 %). A small fraction of zinc was also present in the weld metal. This is due possibly to the zinc condensation on the powder particle which were passing through the zinc plasma. The EDAX analysis on weld metal without any metal powder injection did not show any presence of zinc in the weld metal. EDAX analysis on two such specimen are shown in Table 4.2.

Table 4.1 Composition of Metal Powders for Injection During Welding

No.	Metal powder	Composition wt /
1	Nickel	99.9
2	Tool steel	C = 1.0, Cr = 40, B = 4, Fe = Bal.
3	Stainless steel	C≤ 0.03, Cr = 17, Ni = 11, Mo = 2.2, Fe = Bal.

Table 4.2 Weld Metal Composition of Normal and Nickel Injected Welds

Sr. no.	Element	Normal weld wt %	Nickel injected weld wt %
1	Fe	99.22	97.26
2	Zn	0.00	0.056
3	Ni	0.10	2.12
4	Si	0.44	0.41
5	Cr	0.027	0.00
6	Mn	0.21	0.16

A 'nail head' (enlarged width of the weld at top) is seen in case of nickel injected welds at slower speed while the welds without any metal powder injection do not show any nail head. At slower speeds more powder is incorporated into the melt pool and this probably causes the nail head to be formed i.e., the enlargement of the weld at the surface. At intermediate speeds a better coupling (discussed in next chapter) was obtained between the beam and the workpiece, possibly due to the presence of a small amount of powder cloud at the beam metal interaction point. At higher speeds these nail heads are not present. Visual observations revealed that only the powder particles were melted and also a slight melting of the workpiece occurred. Due to the presence of excess material (metal powder) most of the beam was prevented from going into the material to form a keyhole. Melting efficiency at these higher speeds showed far less value than the usual value (see next chapter Figure 5.32 & 5.33).

In the case of stainless steel injected weld similar results to those for nickel injected welds were obtained. For slow welding speeds an enlarged weld width (nail head) as can be seen in Figure 4.23 (c) was similar to that obtained in the case of nickel injected weld. Again at intermediate welding speeds a better beam coupling (discussed later) was obtained using an optimum feed rate of stainless steel powder. At higher welding speeds melting of powder together with a small melting of the substrate occurred due to the metal powder shielding the workpiece from laser beam.

In the case of tool steel injected welds, it was found that tool steel powder was mixed with the weld metal. The cross section of the weld is shown in Figure 4.23 (d). The tool steel powder composed of Cr; 40%, B; 4%, C; 1% and Balance Fe. According to the work done on welded and casted specimen on this material by Dr. H. Berns at Bochum University [150] there is a primary solidification of Cr-Borides of $(Cr,Fe)_3 B_2$ - type, which are embedded in a $(Cr,Fe)_3C$/Martensite eutectic. There is also a possibility of solidification of a eutectic hard phase of $(Cr,Fe)_{23}$ $(B,C)_6$-type. Hence after solidification a network of cracks may be expected.

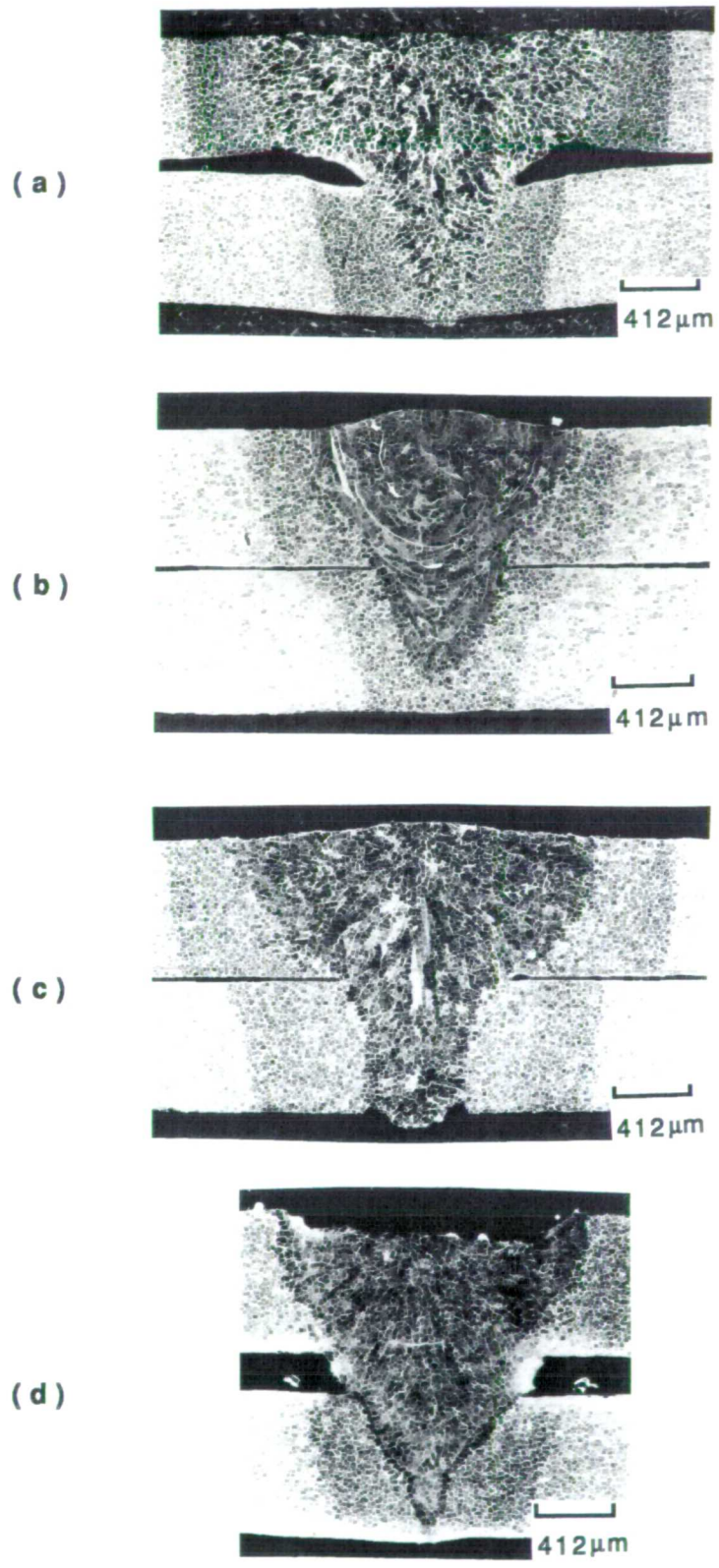


Figure 4.23 The weld microstructure with metal powder injection **(a)** normal weld, **(b)** nickel injected weld, **(c)** stainless steel injected weld and **(d)** tool steel injected weld.

It has been seen that not all the weld in the case of tool steel injected weld had a net work of cracks. A few cracks were found at a slow welding speed when more of the tool steel powder has been incorporated. At relatively higher welding speed cracks were not seen. In order to avoid the problem of cracking in the weld, the powder was incorporated just after weld formation and is discussed in the later section.

The corrosion behaviour of all these metal powder injected welds is discussed in Chapter 7. These specimen were subjected to tensile testing to determine the strength of the weld. The result (see chapter 5) showed that the fracture occurred far from the weld.

4.2.1.5.2 Welding With Redeposition of Volatilised Zinc

The main objective in this technique was to incorporate into the weld bead, zinc that had been volatilised as a result of the welding operation. By using this technique it was hoped that the redeposited zinc will form a thin layer onto the bare weld and would be considered to provide improvements in the protection of the weld bead against corrosion.

Welds were produced using the similar arrangement to that shown schematically in Figure 4.22, except that no metal powder was incorporated. Argon gas was entra'ned through the side jet at a certain flow rate and was directed at the weld bead during welding operation. Many welds were fabricated with the side jet in different positions. The most expedient was that in which the side jet was positioned in front of the beam at the leading edge of the weld. This pushed the zinc plasma, which was formed during the interaction of the laser beam and the zinc coated steel, back onto the trailing edge of the weld. In this way a small amount of zinc was condensed onto the weld bead behind the laser beam.

Figure 4.24 shows a weld bead using this technique. The zinc vapours that had

been deposited on the weld surface were found to be comprised of small pimples and was considered to be in the form of a very thin layer with bare weld revealed between the pimples.

A series of welds were performed using this technique to achieve a condition under which a maximum amount of zinc, that had been volatilised during welding operation, is redeposited on the weld bead. The laser power and welding speed were taken as constant parameters. The flow rate of the argon gas from the side jet was varied from zero to 40 litres/min in steps of 10 litres/min. It was found that without any argon gas from the side jet a very small amount of zinc vapour is deposited. At a certain higher flow rate of the gas a higher amount of zinc is redeposited on the weld bead. Too high a flow rate pushed down and/or blown away the the molten metal and hence left a concave surface in the weld bead, which can seriously affect the strength of the weld. Hence an optimum flow rate of the assists gas is of importance to redeposit the volatilised zinc.

The EDAX analysis were obtained at a certain area on the weld bead at same magnification for each weld type at different flow rate of side jet assist gas. The analysis on weld bead with no gas flow from the side jet showed the presence of a small amount of zinc (Figure 4.25 (a)). With the introduction of side jet gas the amount of zinc on the weld bead gradually increases with the increase in gas flow rate as is evident by the increase in peak height of the zinc element in Figure 4.25 (a) to (e). As is apparent from the analysis, a side jet gas flow rate of 30-40 litres/min is optimum flow rate at which a maximum amount of zinc can be redeposited on the weld bead.

Figure 4.26 illustrates a part of the weld bead and surrounding zinc coating by using the welding technique of redeposition of volatilised zinc. It should be remembered that all the zinc that had been volatilised cannot be redeposited. Besides the redeposition of zinc on the weld bead, a substantial amount of zinc is lost to the environment during the welding process and a small amount of zinc is redeposited on

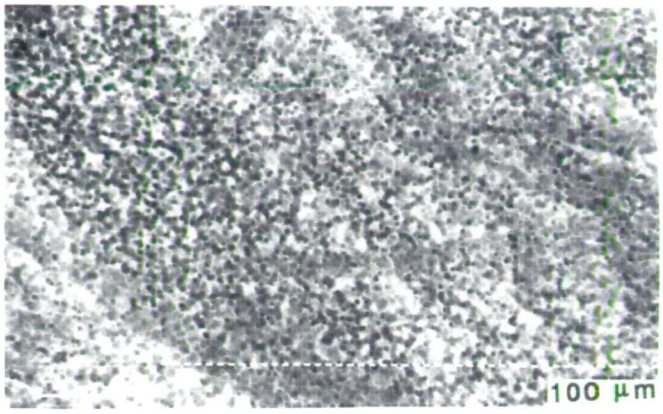


Figure 4.24 The micrograph showing the redeposition of volatilised zinc on the weld bead.

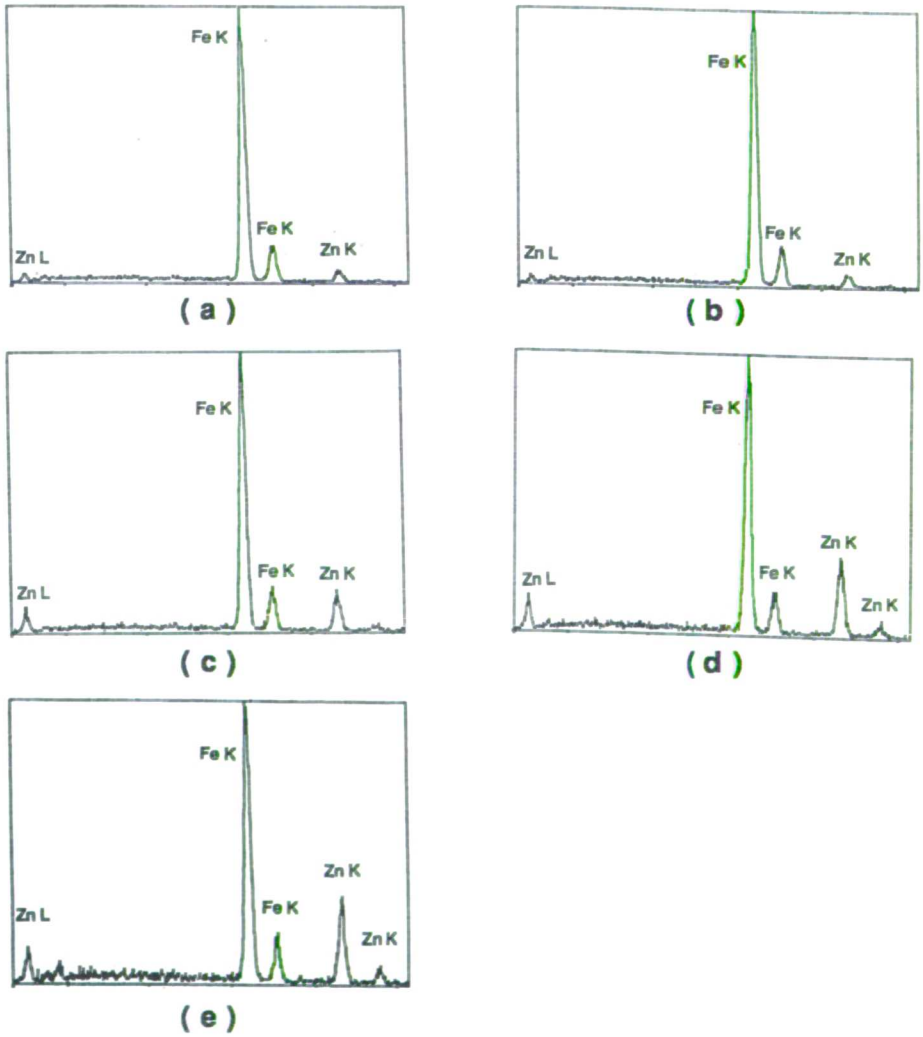


Figure 4.25 The EDAX analysis on weld bead at different flow rates of argon gas from the side jet. The peak height of zinc increases with increase in flow rate of gas from (a) to (e).

either sides of the weld bead due to the design of the side jet pointing at the larger area than the width of the weld. This hot zinc vapours melts the base metal zinc coating just next to the weld and is found in the form of lumps of iron-zinc alloy. The EDAX analysis showed that these lumps mostly consists of zinc with a small amount of iron as is apparent in Figure 4.27. The small amount of iron might have come from the plasma which contain some iron vapours together with zinc but is more likely to have come from diffusion from substrate. The corrosion resistance of such a weld in which the zinc vapours were redeposited on the weld bead was found to be better than the normal weld and is discussed in detail in Chapter 7.

4.2.1.5.3 Incorporation of Metal Powder Just After Welding

It has been described earlier that the injection of tool steel powder into the weld pool leads to the formation of cracks in the weld metal. The presence of a eutectic hard phase $(Cr, Fe)_{23}$, $(B, C)_6$-type produces a net work of crack during solidification of the material. The corrosion rate on such a modified weld was found to be lower than that of normal welded specimen (see chapter 7), hence this material is advantageous in terms of the corrosion resistance. Hence to avoid the presence of cracks in the weld metal, it was decided to blow the tool steel powder just after the welding operation, instead of blowing directly into the keyhole. The objective was to utilise the high temperature of the weld to melt the powder particles at the weld bead and consequently to coat the welded surface with a new corrosion resistant layer.

Since the tool steel had a higher melting temperature close to the melting temperature of mild steel, it was decided to blow the powder very near to the beam, but just after the beam. So that the weld metal is still hot enough to melt the tool steel powder. Thus there is always a possibility that a small amount of powder particles can slip into the keyhole.

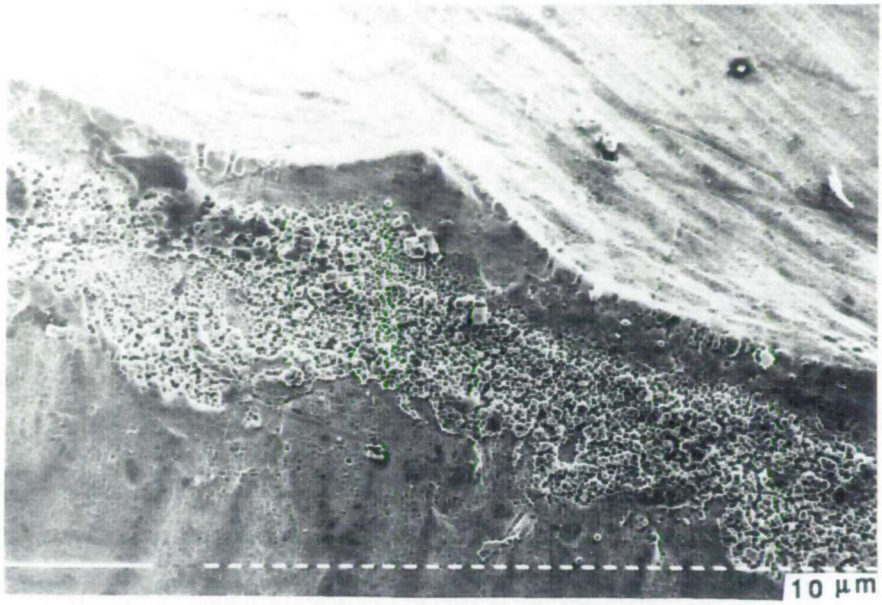


Figure 4.26 The part of a weld bead and the surrounding zinc coating in the form of lumps as a result of redeposition of volatilised zinc.

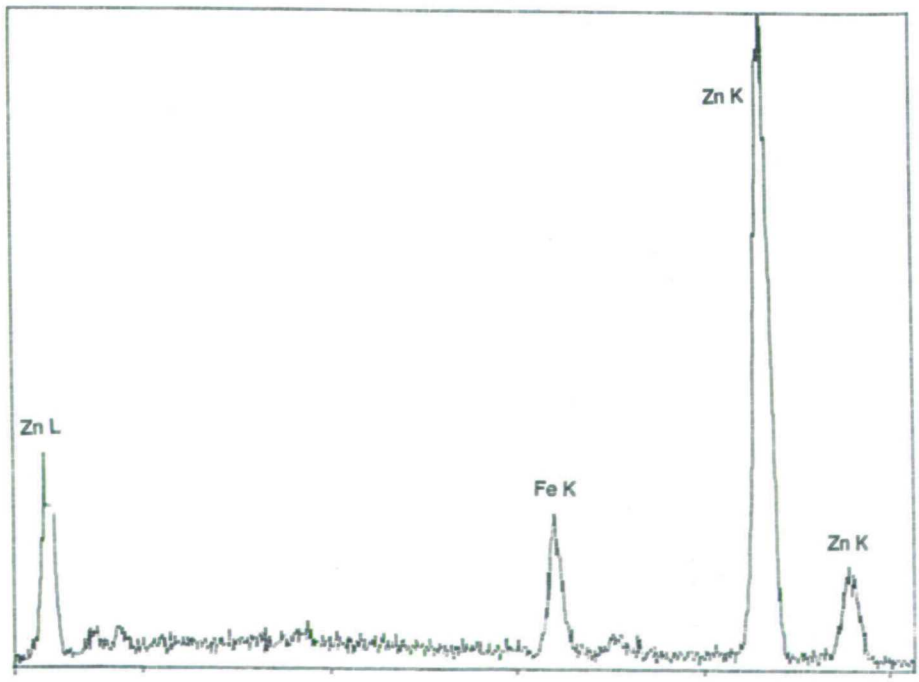


Figure 4.27 The EDAX analysis on the lumps around the weld bead shows that it mostly consists of zinc with a small amount of iron also present.

The weld bead obtained for such an operation produces a positive result. The weld bead obtained using this approach is shown in Figure 4.28. The cross section of the same weld is presented in Figure 4.29. It is evident from the figure that the reasonably good and smooth weld bead can be made using this technique. The cross section of the weld clearly showed that the metal powder had been melted by the hot reactive weld and then solidified to give a good coating on the weld bead. The coating thickness varied between 50 to 75 μm. The corrosion test on zinc coated steel in the presence of such a weld bead showed a lower corrosion rate than a normal welded specimen (see chapter 7).

It is evident that the weld microstructure is very different from that of normal welded specimen. The study into the microstructure of such weld was not attempted. Future work on to the microstructure of the modified composition weld is suggested.

In another experiment, instead of tool steel powder, zinc powder was incorporated just after weld formation. The experimental arrangement was similar to that described earlier (Figure 4.22) except that the side jet carrying zinc powder was adjusted in such a way as to allow the zinc powder to be deposited at the trailing edge of the weld hot spot where the weld was still hot enough to melt the zinc powder (m.p. 419.5° C). The position of the side jet was also important because of the low boiling point of zinc. The side jet was positioned across the weld as to avoid the powder going directly into the beam. The low boiling zinc powder, if staying in the beam path, will produce lot of zinc plasma and shielding of the workpiece can occur.

Figure 4.30 (a) & (b) shows the cross section of two welds in which zinc powder was incorporated just after weld formation. The two weld were produced in almost under same conditions except that in case (a) the flow rate of zinc powder was slightly higher than in the case of weld (b).

Figure 4.30 (a) shows the cross section of a weld in which a higher gap between the sheets led to a concave depression on the weld bead. The position of the small pipe

feeding the zinc metal powder was at a small angle to the workpiece. Due to the depression on the weld bead the powder particles fell at one edge of the weld, simultaneously a higher flow rate of the powder led to the accumulation of the particles at one edge of the weld and a small portion at the other edge is left bare. It has been seen that the powder particles were not fully melted in this case up to the top surface.

Figure 4.30 (b) shows the cross section of a weld made under similar conditions described above, except that the flow rate of zinc powder was slightly lower than the one mentioned above. Also a smaller gap was maintained between the sheet. The smaller gap between the sheets led to a smooth weld surface at the top with no depression in the weld bead. Hence a smooth zinc coating was achieved at the weld bead using this technique.

The cross section of the weld (Figure 4.30 (b)) revealed that coating thus obtained is very uniform showing that all the zinc powder that had fallen on to the hot weld bead, has been melted even at the heat affected zone (HAZ) of the weld. The enlarged view of the zinc powder incorporated coating thus obtained is shown in Figure 4.31 (a) & (b). Some cracks were found on the coating at the centre of the weld bead (Figure 4.31 (a)), where the temperature of the weld was much higher than the HAZ temperature. From the corrosion point of view these cracks in the coating do not have any significant detrimental effect. Because the zinc coating provides the sacrificial protection to the steel even if a crack or porosity exists in the coating. The sacrificial action of zinc coating is discussed later in Chapter 7, but the weld obtained using this technique provide more zinc to the weld bead and has shown a better protection against corrosion than the normal welded specimen.

On the other hand the coating obtained at the HAZ was very uniform without any cracks as is apparent in Figure 4.31 (b). Hence the temperature of the weld is also an important factor to be considered. Thus the distance at the point where the zinc powder falls onto the weld bead to the point where beam metal interaction takes place



Figure 4.28 The weld bead obtained as a result of tool steel powder incorporation just after welding.

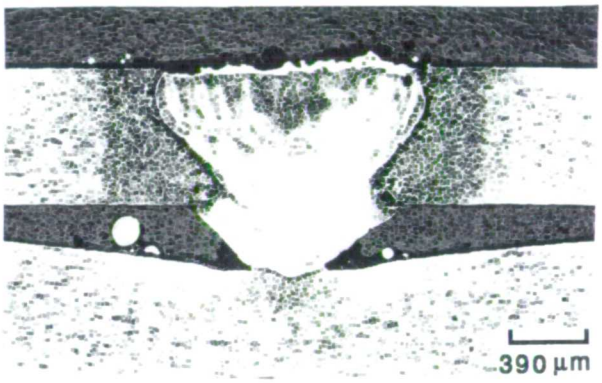


Figure 4.29 The weld microstructure showing a coating of tool steel has been produced at the top surface during the incorporation of powder during the welding operation.

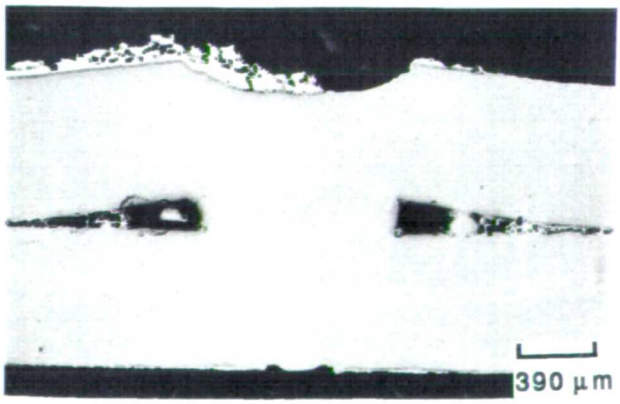


Figure 4.30 (a) Cross section of a weld with zinc powder incorporation just after welding, laser power; 1.8 kW, welding speed; 25 mm/s, flow rate of zinc powder; 0.28 g/s, gap; 0.14 mm.

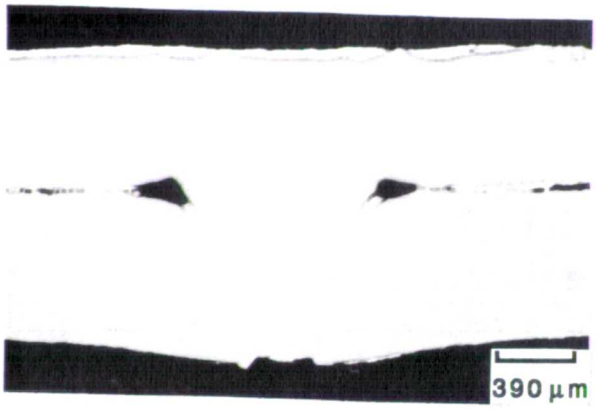
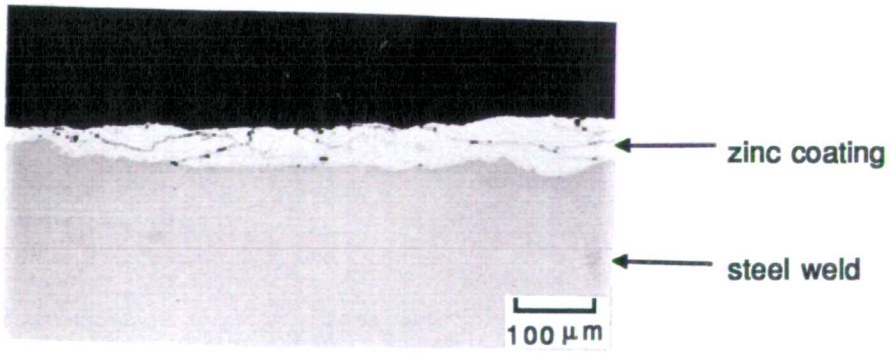
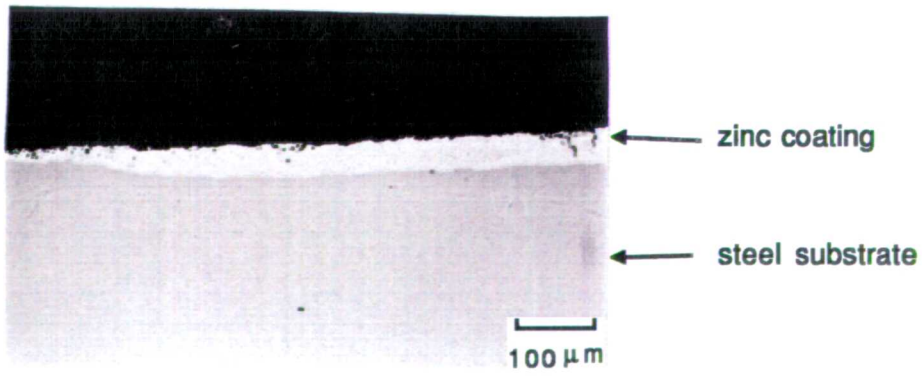


Figure 4.30 (b) Cross section of a weld with zinc powder incorporation just after welding, laser power; 1.8 kW, welding speed; 25 mm/s, flow rate of zinc powder; 0.23 g/s, gap; 0.08 mm.



(a)



(b)

Figure 4.31 Zinc coating obtained as a result of zinc powder incorporation just after weld formation **(a)** at the weld surface, **(b)** at the heat affected zone.

is also an important parameter. A point very near to the keyhole will result in a higher temperature and the zinc particle will experience a higher temperature. At a further distance away from the keyhole the temperature will be less and all the zinc powder falling onto the weld bead may not be melted.

Thus by using this technique a zinc coating was formed on the weld bead and also at the HAZ thus providing more zinc for the corrosion protection to the steel substrate and the weld.

4.3 Weld Quality Assessment

All the welds produced were assessed visually and with the help of a low power magnifying glass. Pitting was the main deleterious effect of the zinc on the weld. The weld quality was evaluated by counting the number of pits or holes in a 100 mm length of the weld. This gave an average value of pits/cm as a comparator between these techniques. The zinc vapour at the interface require a certain gap to be vented out. If the gap is not present the vapours are exhausted through the keyhole taking molten metal with it and thus leaving pits and holes on the weld bead. If a small gap is present then the vapours are exhausted through the gap, without disturbing the keyhole and hence, a sound weld free of pits and holes can be obtained.

The use of Talyserf machine to measure the surface roughness was not possible because the roughness of the sample exceeded the measuring range of the instrument available(i.e. the sensitivity was too good for the welded sample where there were many pits and holes in the weld bead. Hence a visual examination together with number of pits counted gave a good assessment of the weld bead quality. Transverse and longitudinal (for a few welds) microsections also gave a good assessment of the weld quality.

The weld quality measured as pits/cm varied with each technique and along the length of individual welds. In all cases of good quality pit free welding the weld section showed that a gap between the plates had been present. The pitting was clearly due to

the presence of the zinc at the interface since some of the side jet experiments performed with no zinc at the centre but only on the outer faces showed no pitting even with the sheets tightly clamped.

In the experiment of double pass welding, using CLL laser, where the gap was not specifically controlled the sheets were distorted during welding, thus giving a variation in the gap width and obscuring any other effects on controlling pit formation. Figure 4.32 shows a graph of gap size against the number of pits/100 mm weld length. This figure suggests that there is an optimum gap width at which good quality welds can be obtained.

A more detailed study of the effect of the gap was made. The results are shown in Fig 4.32 to 4.37. These figures suggest that there is an optimum gap width at which a sound and good quality weld is obtained.

For the case of nickel injected weld, a 10 μm zinc layer was present at the interface. It was found that for a gap of 0.14 mm between the two sheets, a good quality weld without pits or holes was obtained (Figure 4.33). As the gap between the sheets reduces the number of pits increases, showing the weld bead quality is affected due to the zinc vapours exhausting through the keyhole. For stainless steel welds pitting was found in only one weld from a series of welds. Similarly tool steel injected welds had a large gap and none of the welds showed any pit formation. Thus the data are not available for these welds.

Various other lasers were used for welding this material in lap configurations, their performance and results are discussed in chapter 5. It has been found that the poor quality i.e., pits formation has been a result of zero gap or less gap then the required, irrespective of the type of laser used. Thus the weld quality obtained using various lasers is discussed here.

For the case of Gaussian beam mode the quality is plotted against the gap in

Figure 4.34. It is evident that a gap of 0.1 mm between the sheets for 10 μm zinc layer at the interface, gave a good quality weld showing almost no deterioration of the weld. But as the gap size is reduced the weld quality is badly affected showing a lot of pits or holes on the surface of the weld. Hence reducing the gap size, a poor quality weld is obtained.

For AVCO laser welds at higher powers (3-8 kW), and 15 μm zinc layer at the interface, except a few welds most of the welds showed a poor quality (Figure 4.35 to 4.37), but a gap of 0.2 mm seems to be reasonable, since it gave a smaller number of pits.

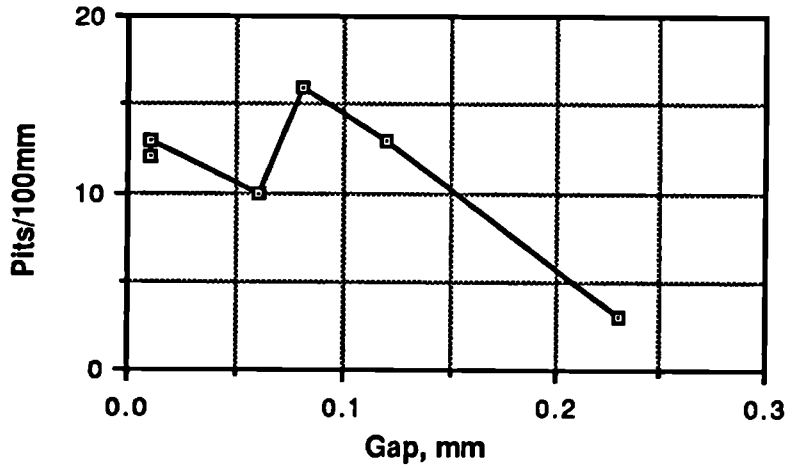


Figure 4.32 Weld quality vs gap size for double pass welding.

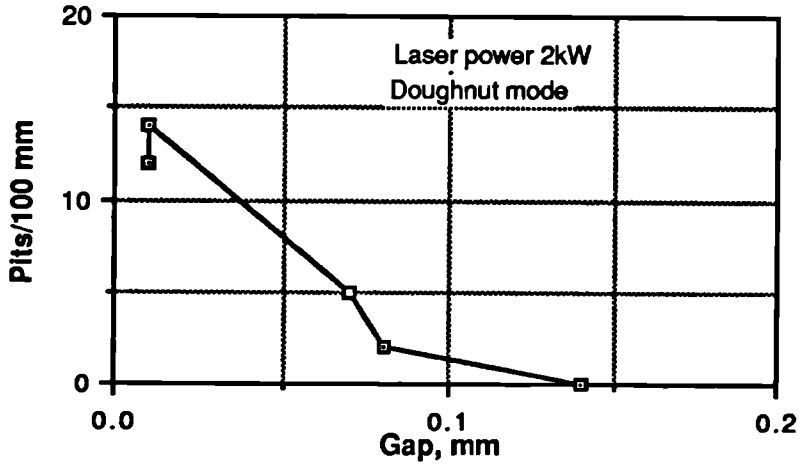


Figure 4.33 Weld quality against gap size for nickel injection weld.

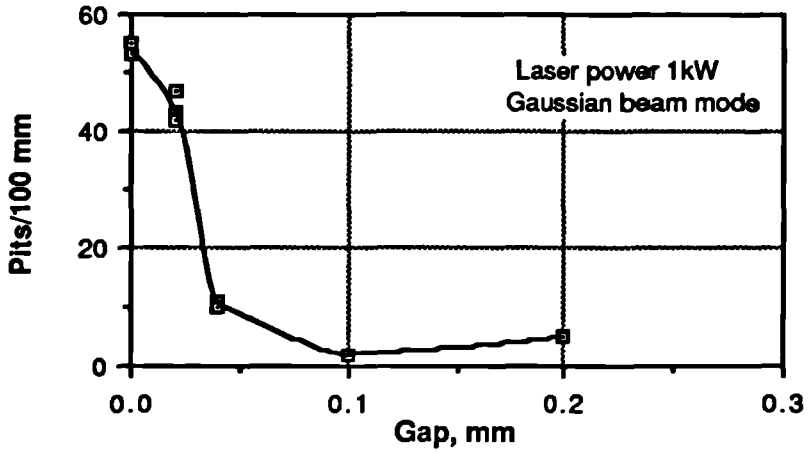


Figure 4.34 Weld quality vs gap size.

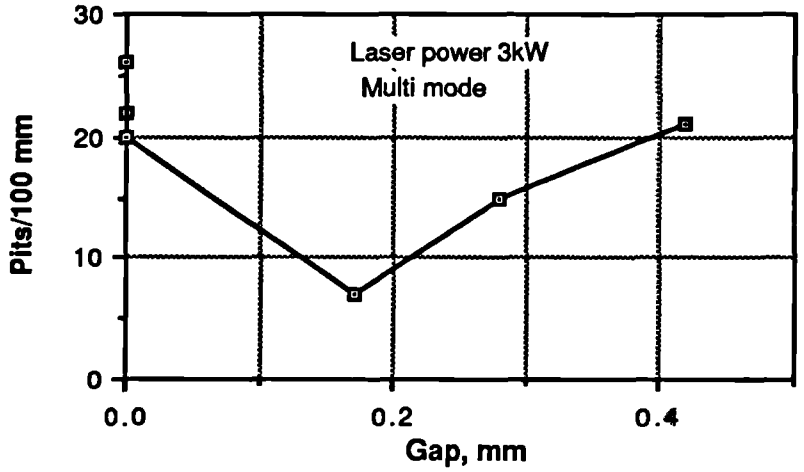


Figure 4.35 Weld quality against gap size for multi mode beam.

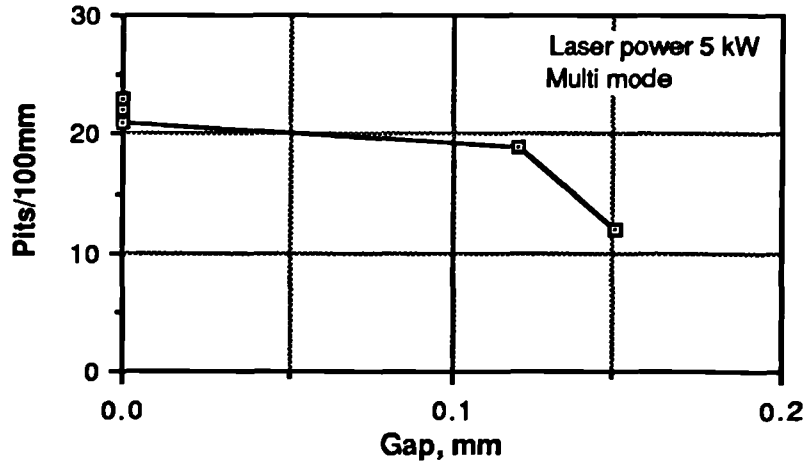


Figure 4.36 Weld quality against gap size for multimode beam.

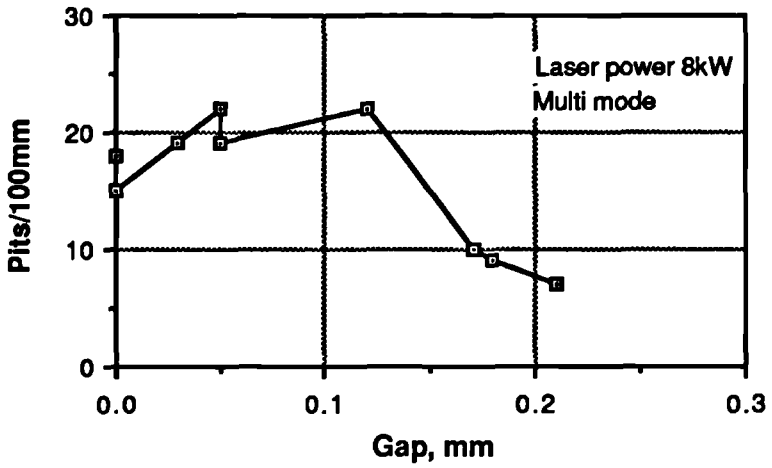


Figure 4.37 Weld quality against gap size for multi mode beam.

4.4 Assessments of Results on Welds Made by Using Dimples as a Method of Setting the Gap Size

4.4.1 Welding Using Fast Axial Flow CLL Laser

In the following experiments a CLL 2 kW CO_2 laser (10.6 μm wave length) was used to perform lap welds in sheets of steel clamped together on an X-Y table. A small gap was maintained between the two overlapping sheets by making dimples on one of the sheet as described in chapter 3.

As shown in Table 4.3 the main experimental parameters - laser power, focal length, welding traverse speed, sheet thickness, zinc coating thickness and gas flow rate - were each maintained at a constant value and the gap size was varied in order to assess the effect on weld quality.

4.4.1.1 Tests Using Plastic Resin To Assess Gap Size

In a preliminary experiment sheets which were prepared with dimples in the surface to set the gap size were tested by clamping two sheets together as described in Chapter 3 (Figure 3.16). Prior to clamping a small amount of plastic resin was

placed between the sheets to bond them together. Once the two sheets were clamped on the rigid block they were left overnight to cure. When they were unclamped the plastic resin sheets were measured to obtain the gap size. This gave an indication of the effectiveness of the dimples as a method of setting the gap size.

A comparison of the nominal gap with that determined by infiltration of plastic resin when dimples are used to separate sheets prior to welding is shown in Table 4.4. These results using the new indentor showed an improvement in accuracy and consistency of gap size compared with the use of shims. Errors in gap size have been about 11% maximum using the new indentor. This technique was found to be useful in performing further experiments and it is considered that it could be implemented later in a manufacturing environment.

Table 4.3 Weld Parameters During Laser Welding at Different Gap Sizes.

Sr. no.	laser power (kW)	welding speed (mm/s)	sheet thickness (mm)	zinc coating thickness (μm)	no. of pits/ 100mm	nominal gap (mm)	measured gap (mm)	% error in gap size
1	1.94	15	0.7	7.5	9	0.15	0.14	7
2	1.94	15	0.7	7.5	20	0.125	0.09	28
3	1.50	15	0.7	7.5	8	0.10	0.08	20
4	1.50	15	0.7	7.5	6	0.087	0.07	19
5	1.50	15	0.7	7.5	5	0.07	0.05	28
6	1.50	15	0.7	7.5	18	0.05	0.03	32
7	1.50	15	0.7	7.5	27	0.037	0.01	67

Table 4.4 Comparison of Nominal and Measured Gap Size in Sheets Prior to Welding

Sr. no.	sheet thickness (mm)	zinc coating thickness (μm)	configuration	nominal gap (mm)	measured gap (mm)	% error in gap size
1	0.7	7.5	lap	0.10	0.11	11
2	0.7	7.5	lap	0.05	0.0505	1

4.4.1.2 Welds Made Using Dimples as a Method of Setting the Gap Size

Samples were prepared using the indentor as described above. Thus two sheets were clamped on the rigid block as shown in Figure 3.16. Then the laser beam was passed over the surface of the sheets at a known feed rate. Some additional samples were made with larger sheet sizes (150 x 200 mm) to enable tensile test specimens to be made and tested. Also some welds were produced with the weld run passing through the location of the dimples. From these experiments an indication of the usefulness of the dimples as a method of setting the gap size was obtained together with a count of the number of pits per 100 mm weld length.

4.4.1.3 Welds Produced With Dimples Between the Sheets

Results and operating parameters for welds implemented on samples produced using the indentor are given in Table 4.3. This includes a listing of counted number of pits per 100 mm weld length, gap size and percentage error in gap size. A plot of pits per 100mm weld length vs gap size is shown in Figure 4.38.

From these results it can be seen that an improvement in visible defects is obtained when a gap is present between the sheets. It can also be seen that there seems

to be an optimum gap size at approximately 0.07-0.10 mm. Thus it is shown that the presence of a gap between the sheets enables a sound weld to be produced.

4.4.1.4 Welds Made by Passing the Beam Over the Dimples

Several welds were performed with the rum passing over the position of the dimples on the sheet. It was noted that only a marg nal deterioration of weld continuity was incurred. This could be due to the small size of dimples. As the weld passed over them there still a large venting area available. Thus it is feasible to continuously run the weld over the dimples, thus making setting the gap simpler.

4.4.1.5 Quality of the Welds

It can be seen in the graph of pits per 100 mm weld length vs gap (Figure 4.38), that there is an increase in the number of pits at larger gap sizes. This was due to the fact that the laser beam incident power was 1.94 kW. This is useful to illustrate the effects mentioned previously, that at larger powers the traverse speed is of great importance since if it is too slow material is evaporated and/or ejected from the weld pool. Also, as the temperature at the keyhole is increased more zinc vapour is created which may also disrupt weld continuity.

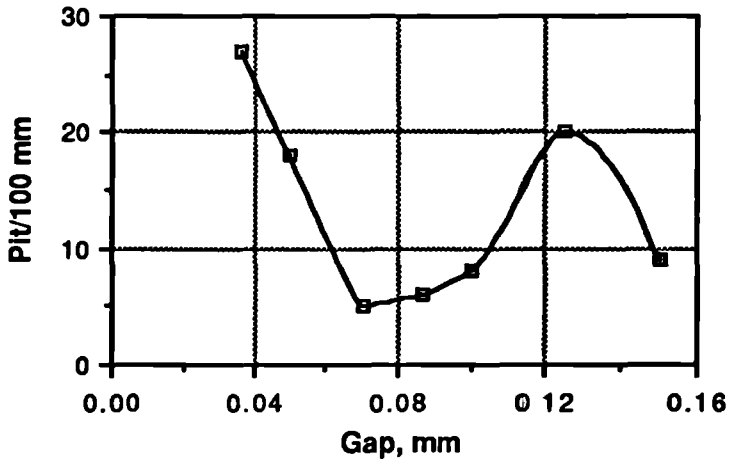


Figure 4.38. Graph of pits per 100mm weld length vs gap using dimples as a method of setting the gap size.

4.4.2 Welding Using Laser at RTM Centre

RTM research centre, Italy, showed an interest in this method of setting the gap size. A few samples were produced and sent to RTM for trials on their laser. The welds were produced by passing the laser beam alongside the dimples. Some welds were produced by passing the beam over the dimples. The results of the welds made in this way are discussed here.

4.4.2.1 Welds Made Using Dimples as a Method of Setting the Gap Size

Laser beam weldments of zinc coated steel were fabricated in lap configuration using a continuous wave CO_2 laser at RTM research centre. These lap welds were produced on 0.7 mm thick sheets with a zinc coating thickness of 7.5 or 10.0 μm. The welding parameters are listed in Table 4.5. The dimples were made on one side of the sheet as a method of setting a gap between the sheets. Figure 4.39 (a) & (b) describe the way in which the welding was performed. A majority of welds were produced as shown in Figure 4.39 (a), in which the laser was passed alongside the dimples and with variation of the distance of dimples from the beam metal interaction point. Two welds (RM-6 & RM-12) were produced by passing the laser beam over the dimples as shown in Figure 4.39 (b). From these experiments an indication of the usefulness of the dimples as a method of setting the gap size was obtained together with a count of the number of pits per 100 mm weld length.

4.4.2.2 Welds Produced With Dimples Between the Sheets

Results and operating parameters for welds implemented on samples produced using the indentor to make the dimples are given in Table 4.5. This includes a listing of counted number of pits per 100 mm weld length, of both under bead and under cut.

The variation of the distance of the dimples from the weld bead had a very slight

effect on the weld bead quality. The number of pits/100mm increased slightly as the distance is reduced. In all the cases the dimples had been able to form a small gap. Figures 4.40 & 4.41 show the weld bead of the specimens RM-9 and RM-11. Figure 4.4 shows that the dimples are at a farther distance from the weld than for the weld bead in Figure 4.40, yet there is only a slight difference between the weld quality (Table 4.5). When the dimples are very near to the weld, as in Figure 4.40, weld has not deteriorated at that point.

The cross section of the weld RM-9 is shown in Figure 4.42, which shows that the presence of the dimples near the weld reduces the gap on that side of the weld. Figure 4.43 shows that a smooth weld (RM-3) can be obtained with a gap of 0.1 mm between the sheets. The corresponding weld bead is shown in Figure 4.44.

4.4.2.3 Welds Made by Passing the Beam Over the Dimples

Two welds were produced with the beam passing over the position of the dimples on the sheet. Figure 4.45 & 4.46 shows the weld bead of such run for specimen RM-6 & RM-12 respectively. Figure 4.47 shows the cross section of weld RM-6. It can be noted that only a marginal deterioration of weld continuity was incurred.

Table 4.5. Laser Welding Parameters For Sheets With Dimples

Focal length of the lens = 5 in. or 127 mm

Shrouding gas coaxial with laser = Helium

Shrouding gas at interface between the two sheets = Argon

Thickness of zinc coating = 7.5 μm

Sr. no.	laser power (kW)	welding speed (mm/s)	gap (mm)	dimple distance from the weld (mm)	weld quality pits/100mm under bead	under cut
RM 1	1.00	25.0	0.1	3.5	2	1
RM 2	1.00	16.7	0.2	2.5	7	8
RM 3	1.00	25.0	0.2	2.5	3	2
RM 4	1.00	25.0	0.1	3.0	2	2
RM 5	1.00	25.0	0.1	2.0	6	3
RM 6	1.00	16.7	0.1	0.0	6	7
RM 7	1.00	16.7	0.1	3.0	2	2
RM 8*	1.00	16.7	0.1	3.0	4	3
RM9	1.00	21.0	0.1	1.5	4	4
RM 10	1.00	16.7	0.1	- -	2	2
RM 11	1.00	25.0	0.1	3.5	2	1
RM 12	1.00	21.0	0.1	0.0	6	4
RM 13	1.00	25	0.1	2.5-4.5	4	3

*Focus 1 mm below the surface.

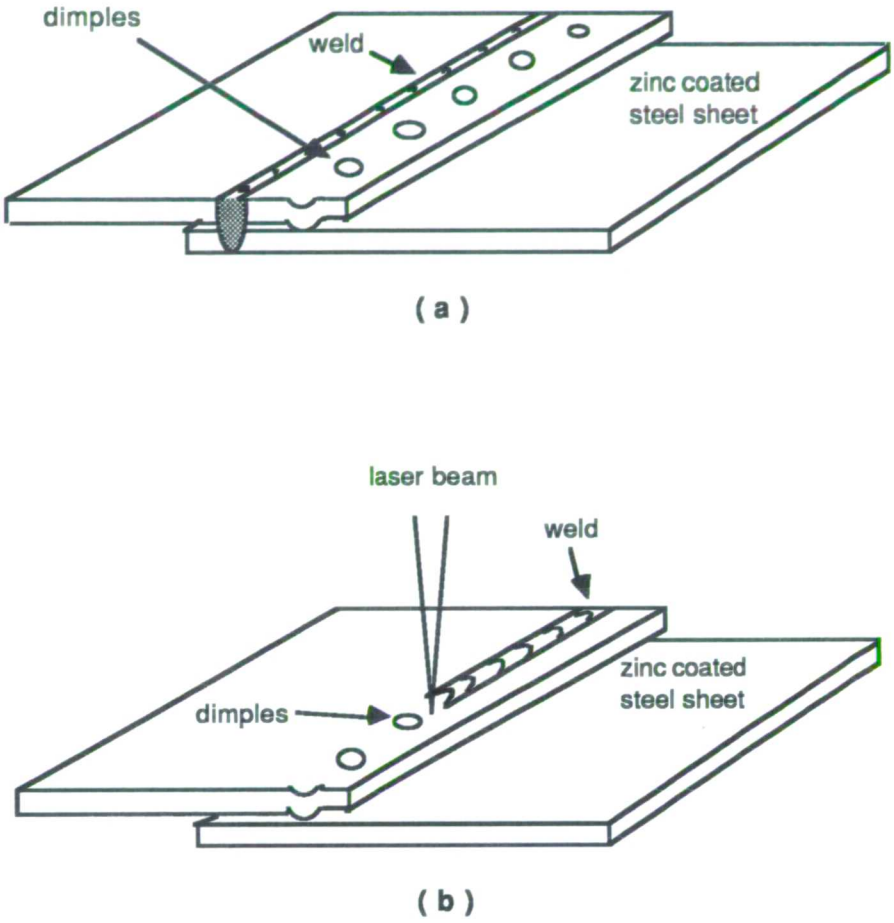


Figure 4.39 Lap welding of zinc coated steel **(a)** with dimples to produce a gap between the sheets, **(b)** by passing the beam over the dimples.

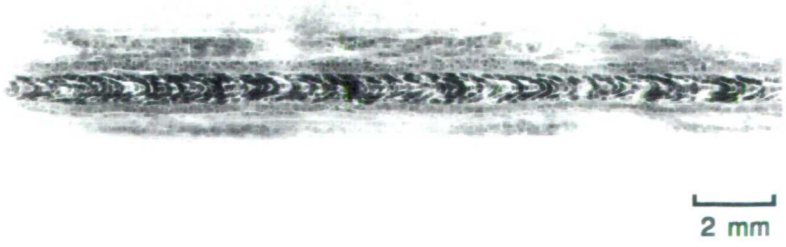


Figure 4.40 Weld bead of specimen RM-9, laser power 1kW, welding speed 21 mm/s.

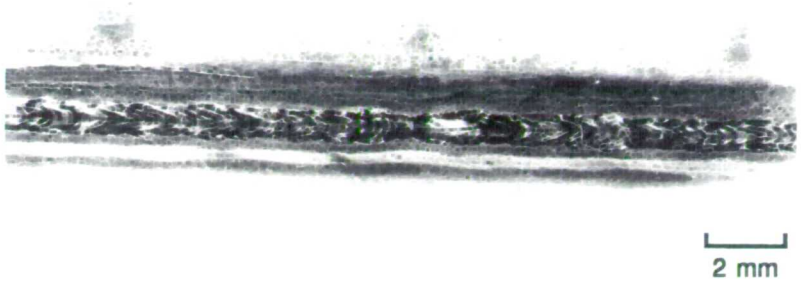


Figure 4.41 Weld bead of specimen RM-11, laser power 1kW, welding speed 21 mm/s.

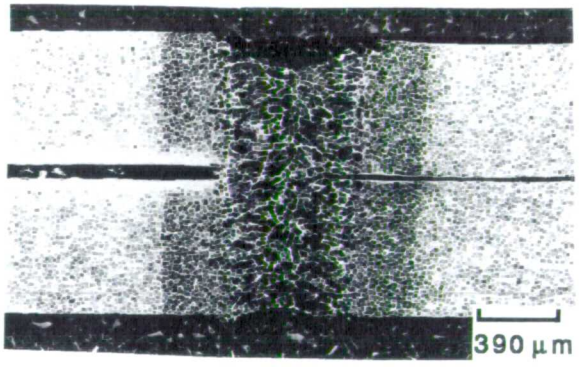


Figure 4.42 Cross section of weld RM-9, laser power 1kW, welding speed 21 mm/s.

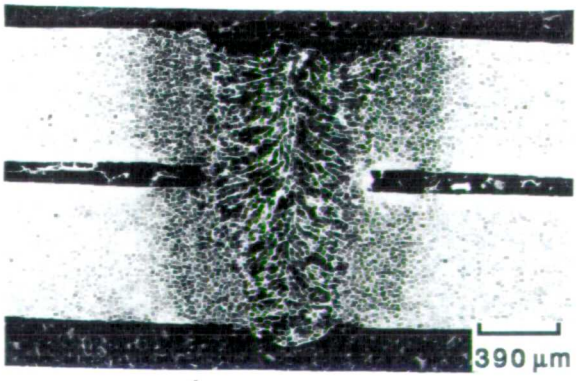
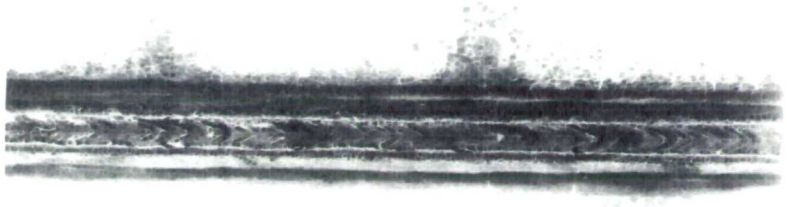
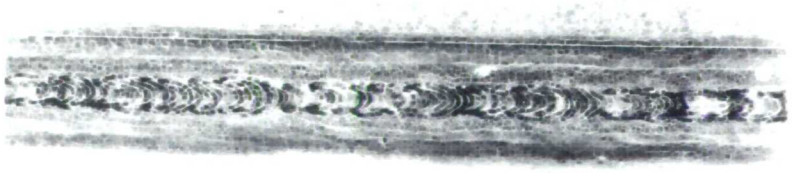


Figure 4.43 Cross section of weld RM-3, laser power 1kW, welding speed 25 mm/s.



2.7 mm

Figure 4.44 Weld bead of specimen RM-3, laser power 1kW, welding speed 25 mm/s.



2.7 mm

Figure 4.45 Weld bead of specimen RM-6, with laser beam passing over the dimples, laser power 1kW, welding speed 16.7 mm/s.



2.7 mm

Figure 4.46 Weld bead of specimen RM-12, with laser beam passing over the dimples, laser power 1kW, welding speed 21 mm/s.

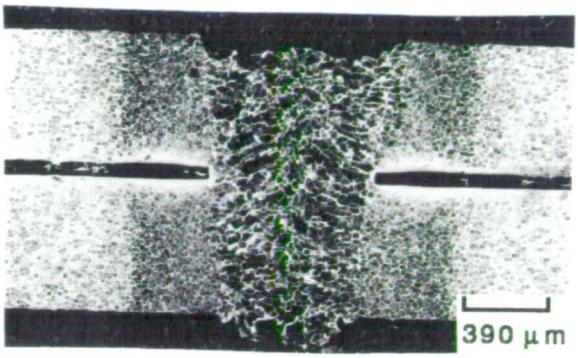


Figure 4.47 Welds cross section of specimen RM-6, laser power 1kW, welding speed 16.7 mm/s.

Chapter 5

Processing- Results and Discussion

5.1 Introduction

There are many types of lasers available commercially. These lasers provide a variety of different beam modes which depends on the design of the laser cavity. Thus it is interesting to study the performance of these lasers in the welding of uncoated and zinc coated steel sheets. The performance standard of these lasers can be compared through the deepest penetration obtainable in a given material. The experimental conditions and welding parameters differ for most systems, but a well founded comparison can be made giving a proper representation of welding proficiencies of each laser.

A number of experiments has been undertaken to present the data obtained from different lasers, with the aim of comparing the results and identifying which laser could be best suited for welding process. This chapter therefore describes the evaluation of the welding capabilities of each of the lasers used and a comparative assessment of their performance. It is shown that for welding purposes a Gaussian beam is most suitable laser mode that can give the best deepest penetration. Results of tensile tests performed on the welded specimen are also presented together with the results of fatigue and impact tests on the welded specimens performed by the collaborating partners.

5.2 Welding Using Various Lasers

This section describes the results of zinc coated steel welding by using various lasers.

5.2.1 Welding Using Fast Axial Flow CLL Laser With Doughnut Beam Mode

The major part of the welding study on zinc coated steel involved lap welds. Some bead on plate welds were performed to get an idea of welding speed range for a given power. Laser beam weldments of zinc coated steel were fabricated in lap configuration using a continuous wave CO_2 laser. These lap welds were produced on 0.55, 0.7, and 0.875 mm thick sheets.

The laser beam had a wavelength of 10.6 μm (infrared) and a diameter of 23 mm at the laser output window, with a doughnut beam configuration as measured from an acrylic print. The beam was focused to a spot of approximately 0.2 mm diameter using a KCl lens of 125 mm focal length. For each experimental weld the specimen was mounted on an automatic tables as described in section 3.3.3. The specimen was moved under the beam at a known feed rate to create a weld. The beam mode is sketched in Figure 5.1.



Figure 5.1 The beam profile of CLL laser.

The effect of laser welding variables, i.e., power and welding speed were investigated on a (bead on plate) 1.5 mm thick zinc coated sheet. These samples were produced to give an indication of the welding response of the material under various welding conditions. These welds were simple to produce and were considered to give a good indication of the likely response under actual welding conditions. Experiments were carried out to find a correlation between laser parameters and the corresponding results of penetration of the weld zone. The range of laser parameters

studied were, beam power 1-2 kW, and the welding speed. The cross section of the weld zone profile was clearly defined in all the samples by the melted region. Depth and width of the melted zone were defined in a way as indicated in Figure 5.2, which shows a typical weld profile produced by a laser.

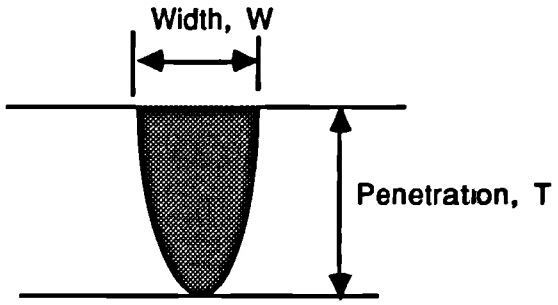


Figure 5.2 Typical weld profile defining the depth and width of a weld.

5.2.1.1 Effect of Laser Power on Penetration

The laser power required for welding depends on the material, its thickness and the welding speed. A series of bead on plate welds were produced in zinc coated steel for different laser powers. The effect of power as a function of speed is shown in Figure 5.3.

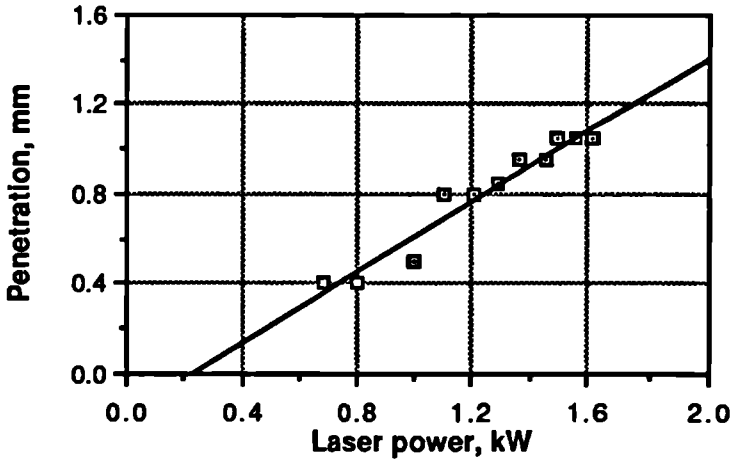


Figure 5.3 Laser power against penetration at constant welding speed of 56 mm/s. Sheet thickness 1.5 mm.

This figure shows the power variation from 700 W to 1620 W. Under the conditions considered here, as indicated in Figure 5.3, the penetration depth generally increases with power at constant speed. It can be seen that a linear relationship is observed with a constant joining efficiency (VT P) of 44.5 mm^2/kJ. From the graph of laser power (P) versus penetration (T), it can be seen that the penetration just starts at a laser power of 250 W for a welding speed of 56 mm/s.

5.2.1.2 Effect of Welding Speed on Penetration and Width

Welding speed is a function of laser output power, the material and its thickness. It has been found from a range of laser power and welding speed used that there is a maximum speed for a given laser power and workpiece thickness above which incomplete penetration results. Also there is a minimum speed below which the fusion zone is very large and the molten metal drops out of the keyhole and the weld bead shows irregular holes.

The variation of speed on penetration and width of a bead on plate weld is shown in Figure 5.4, for a constant laser power. The figure shows a typical hyperbolic curve for speed against both penetration and width. Generally the penetration decreases hyperbolically as the speed is increased. The penetration against welding speed for lap welds using different techniques are plotted in Figures 5.5 to 5.9 using CLL laser. The welding parameters for bead on plate welds and for welds using different techniques (described in chapter 4) are listed in appendix 1 to 6, together with the results obtained. It can be seen that the penetration decreases with the increase in welding speed.

It has already been described in the previous chapter that the presence of a gap reduces the weld penetration, the amount of variation depends upon the gap size. In the case of lap welding a small variation in gap width (0.0-0.2 mm) lead to variations in penetration and width of the weld. Thus the graph of penetration and width against welding speed may show variations in the hyperbolic curve as is shown

in Figures 5.5 to 5.9. In the case of double pass welding curve (Figure 5.5) an odd point is due to a higher gap between the sheets led to the non-penetration of the beam to the bottom sheet, and hence less penetration was obtained at that point. The penetration could be expected to be higher, had there been a smaller gap between the sheets so that the two sheets could be joined. In case of side jet experiments the velocity of the assist gas jet was fixed at 278 m/s, i.e., at a speed of argon gas at which a maximum penetration was achieved (see Chapter 4). The laser power was kept constant and the welding speed was varied to create the welds. The graph of penetration against welding speed is given in Figure 5.6. In both the cases of double pass and side jet experiments the penetration decreases almost hyperbolically with increase in welding speed. Also the width of the welds was decreased with an increase in welding speed. In most cases the width of the welds were found to be larger than the penetration,typical aspect ratio being 0.6 - 0.8.

For the case of metal powder injected welds the penetration and width of the welds decreases more sharply. In these types of experiments it is found that at constant laser power the feed rate of the powder together with the welding speed is also an important parameter. For same welding speed too high flow rate of metal powder interferes with the beam and leads to inefficient welding. The melted powder accumulated on the weld bead with a very little penetration to the substrate. A controlled feed rate of powder gave efficient weld with just enough of the metal powder going in to the melt pool. Too low a flow rate may not have enough metal for modification of weld composition. Similarly for a controlled feed rate of metal powder the welding speed is also important. Too slow a welding speed incorporated more powder and the increased amount of metal powder interfered with the laser beam producing inefficient welding. A controlled welding speed allowed an optimum thickness of metal powder at the beam metal interaction point that gives a good penetration by trapping the radiations between the particles. A higher welding speed does not allow enough time for the laser beam to penetrate to the substrate, the presence of metal powder at the interaction point also restrict the beam to just melting of the powder with only a slight melting of the substrate. Hence for the case

of nickel and stainless steel injected welds the penetrat'on decreases more sharply at higher welding speeds (Figure 5.7 & 5.8). For the case of tool steel injected powder the data for the whole sheet thickness (0 to 1.4) is not available only a very small range of penetration (1.2 to1. 5 mm) is available.

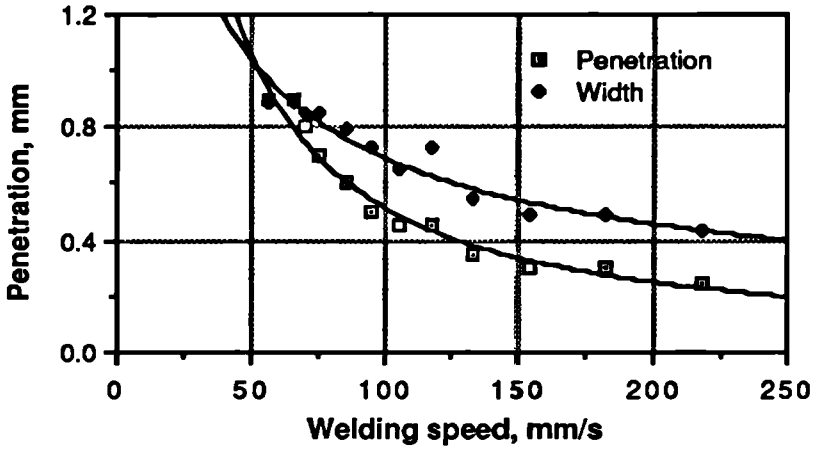


Figure 5.4 Typical hyperbolic curve for welding speed against weld penetration and width at laser power 1.60 kW. Bead on plate welding.

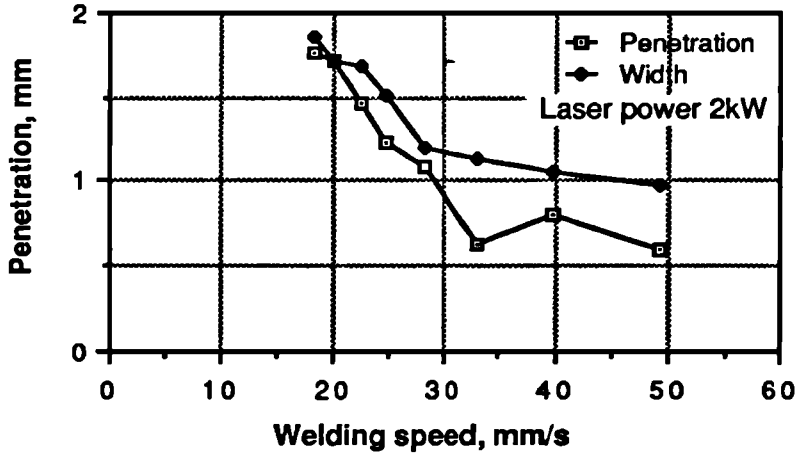


Figure 5.5 Weld penetration and width as a function of welding speed in double pass welding. Sheet thickness; 0.875 mm.

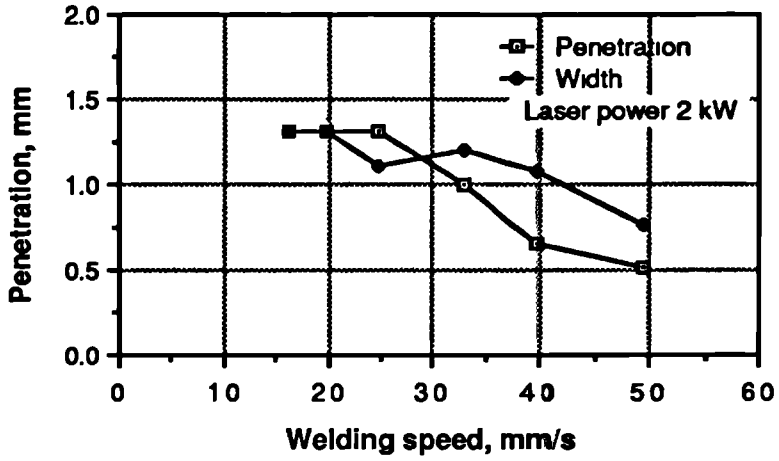


Figure 5.6 Weld penetration and width as a function of welding speed in side jet welding experiment. Sheet thickness; 0.7 mm.

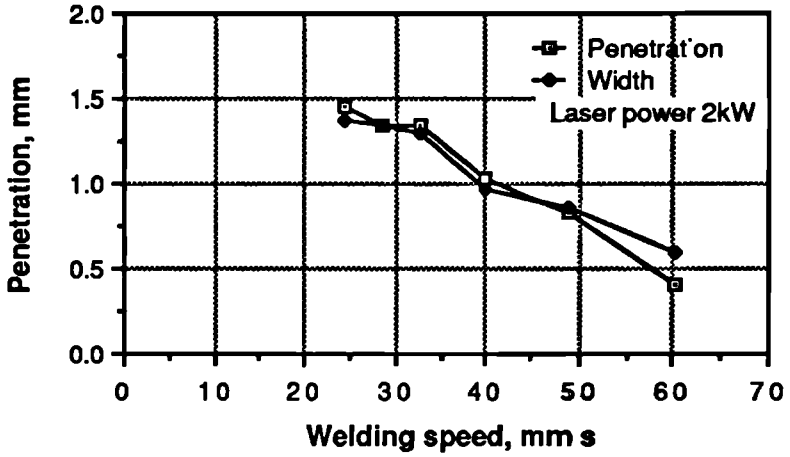


Figure 5.7 Weld penetration and width as a function of welding speed for nickel injected weld.

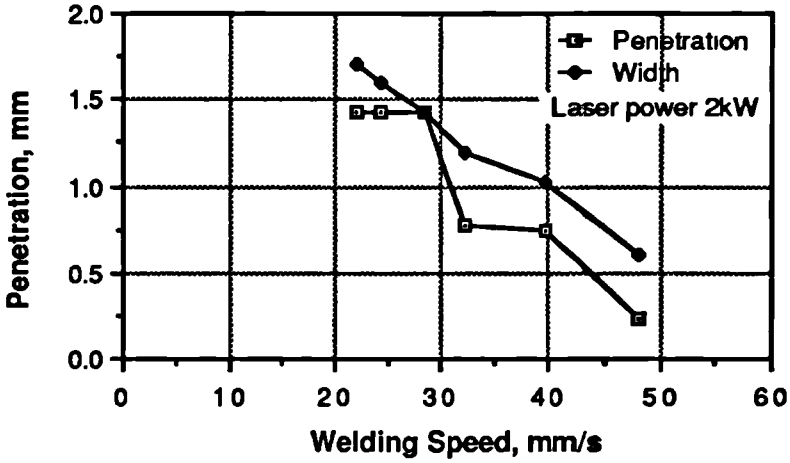


Figure 5.8 Weld penetration and width as a function of welding speed for stainless steel injected weld.

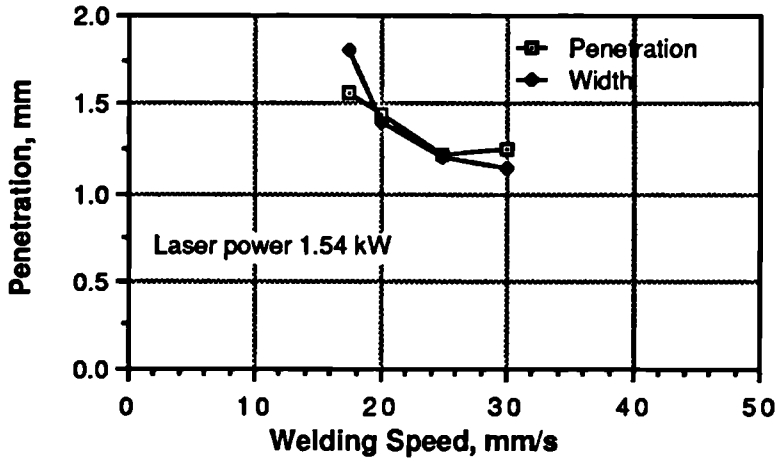


Figure 5.9 Weld penetration and width as a function of welding speed for tool steel injected weld.

5.2.1.3 Influence of Laser Beam Polarisation in Welding

The polarisation of the laser beam has a significant influence on laser materials processing, especially for cutting of metallic materials. Olsen [151,152] first discovered the effect of laser light polarisation on cutting processes. He found that the absorption of laser beam on smooth surfaces can be described by the Fresnel formula [153]. The reflectivity of a material surface irradiated by a laser beam can be calculated as:

$$R_p = \frac{\tan^2(\varphi_2 - \varphi_1)}{\tan^2(\varphi_2 + \varphi_1)} \qquad (5.1)$$

$$R_s = \frac{\sin^2(\varphi_2 - \varphi_1)}{\sin^2(\varphi_2 + \varphi_1)} \qquad (5.2)$$

Where R_p is the reflectivity for light polarised in a plane parallel to the plane of incidence, and R_s is the reflectivity for light polarised in a plane perpendicular to

the plane of incidence. The angles φ_1 and φ_2 are the angle of incidence and the angle of transmission. The Snell theorem [153] relates the transmission angle, φ_2, to the angle of incidence and the index of refraction, n, of the material, as:

$$n = \frac{\sin \varphi_2}{\sin \varphi_1} \qquad (5.3)$$

The index of refraction of a material depends upon the electric properties of the material, which are dependent on the wavelength of the light. The Fresnel formula gives a dependence of the absorptivity on the polarisation and on the angle of incidence as shown in Figure 5.10 for a steel surface, irradiated by a CO_2 laser [151]. The curves show, that laser material processing is influenced by the polarisation of the laser light. This influence is most significant for processing materials with a high reflectivity for normal incident radiation, i.e., metallic materials.

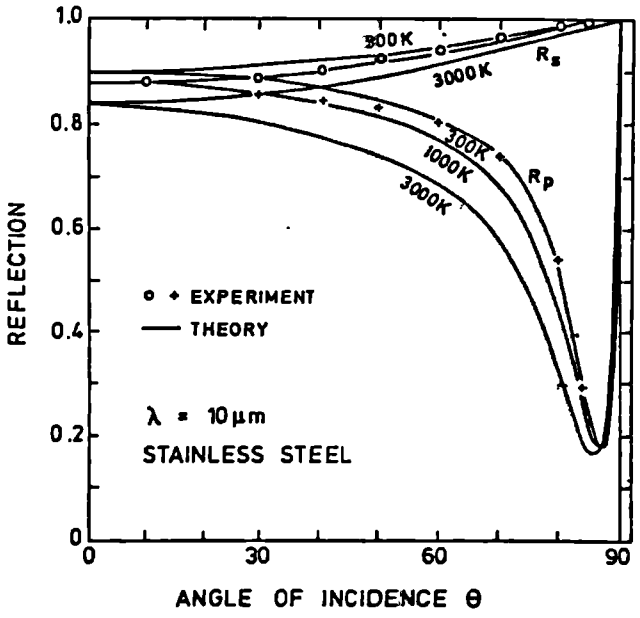


Figure 5.10 Correlation between laser beam polarisation and the reflection at a metal surface as a function of the incident angle [151].

At p-polarisation (i.e E-vector parallel to the plane of incidence) a marked maximum in the absorption can be observed at the so called Brewster angle. On s-

polarisation (i.e., E-vector perpendicular to the plane of incidence), however, only very poor absorption is obtained [154].

When cutting with a linear polarised laser is performed in a material with a high reflectivity, the absorption of energy in the cutting kerf depends upon the angle, φ, between the plane of polarisation of electric vector, E, and the cutting direction, V, as shown in Figure 5.11.

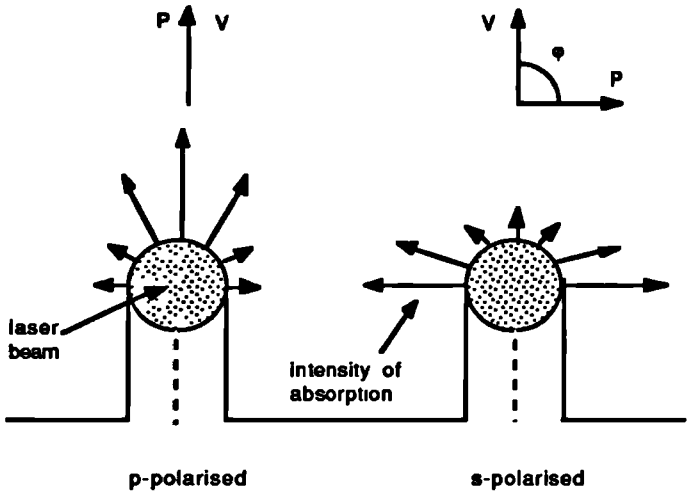


Figure 5.11 Cutting kerfs using p-polarised and s-polarised beam. Where V is cutting direction and P is plane of polarisation [152].

When the angle, φ, is 0°, the front of the cutting kerf will absorb more energy than the sides. When the angle, φ, is 90°, the front of the cutting kerf will absorb less energy than the sides. This means that when cutting in the same direction as the plane of polarisation, the cutting speed can be higher than when cutting in a direction perpendicular on the plane of polarisation. Olsen [151] found that experiments with an almost linear polarised CO_2 laser showed maximum cutting rates for $\varphi = 0°$ which were about 50% higher than maximum cutting rates for $\varphi = 90°$.

Similar conditions of laser beam absorption as shown in Figure 5.11 can be expected during laser welding. Welding with polarised beam has been reported by Beyer *et al.* [155] and Behler *et al.* [156]. Figure 5.12 shows the influence of

beam polarisation in welding with 5kW beam power. Above a speed of 3 m/min, the welding depths changes between 3.9 mm and 2.8 mm as a function of beam polarisation. The difference in penetration for p- and s-polarised beam persists at higher welding speeds. Beyer *et al.* [155] found that above 3 m/min the welding depth is 1.4 times higher in case of p-polarised beam than in the case of s-polarised beam. However, no explanation of the better absorption of p-polarised beam as compared to s-polarised beam has been reported.

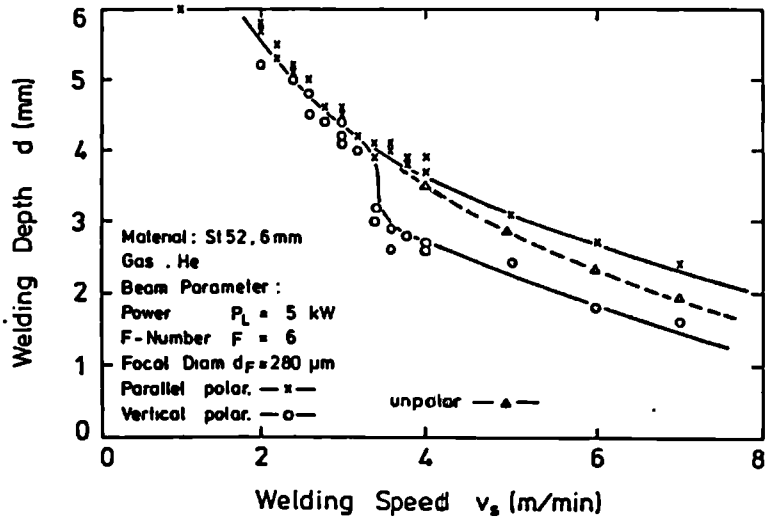


Figure 5.12 Influence of beam polarisation in welding with 5kW laser power [155].

The effect of polarisation on the penetrability of CO_2 laser radiation was carried out on a 0.7 mm thick zinc coated steel sheet with a zinc coating thickness of 7.5 µm. The welding parameters are listed in Appendix 7 for p-polarised beam and in Appendix 8 for s-polarised beam. Experimental investigations were made on penetration in the sheet steel by a plane polarised CO_2 laser radiation. Two sets of experiment were performed. The zinc coated steel sheet was welded under conditions when the angle φ between the plane of polarisation and the welding direction was equal to 0° (i.e., p-polarised) and 90° (i.e., s-polarised). The penetration and width of the weld made were than measured.

Figure 5.13 demonstrate the influence of beam polarisation on the weld

penetration under the same welding conditions. The weld penetration is plotted against the welding speed. It is evident that the penetration decreases hyperbolically with increasing speeds. Also a better penetration is achieved in case of p-polarised beam than with s-polarised beam. It is worth noticing that the weld penetration is about 1.5 time greater in case of p-polarised beam as compared to s-polarised beam. This is in agreement with the work performed by Beyer *et al.* [155] as just noted, and Garashchuk and Kirsey [157]. Garashchuk and Kirsey [157] found that the penetration was 1.4 to 1.7 times greater in case of p-polarised beam than with s-polarised beam. They also reported that a better quality weld is obtained in case of s-polarised beam.

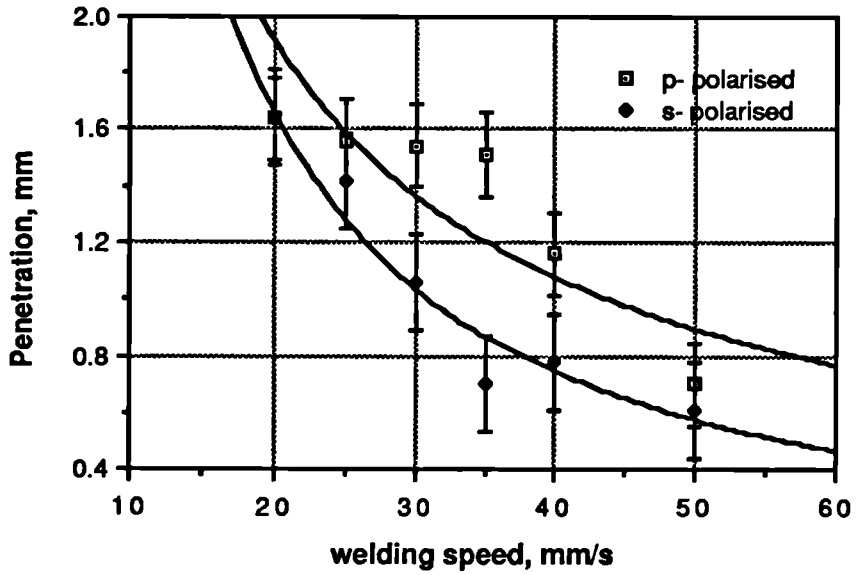


Figure 5.13 Penetration against the welding speed for p-polarised and for s-polarised beam under same welding conditions, laser power 1.77 kW.

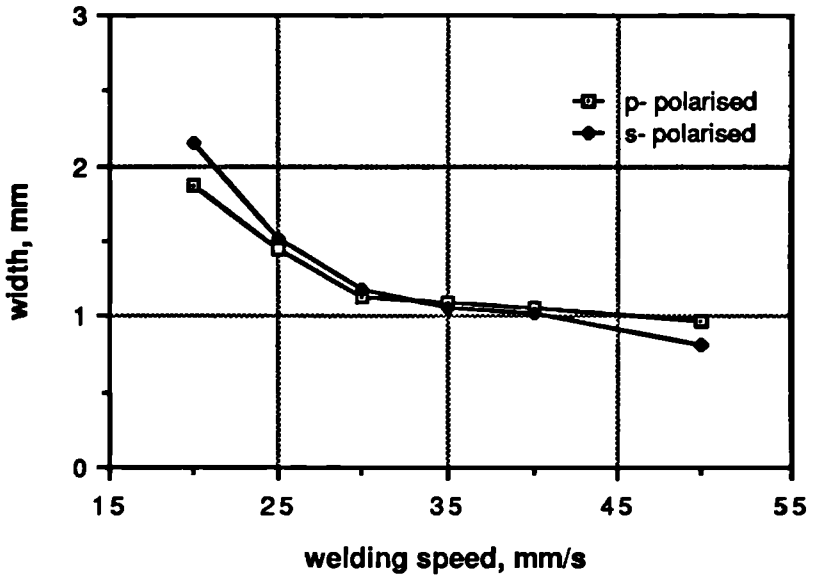


Figure 5.14 Weld width against welding speed for p-polarised and s-polarised beam under same welding conditions.

Figure 5.14 shows the width of the welds performed using p- & s-polarised beam. In the case of p-polarised beam the width of the weld at lower speed (20 mm/s) is less than that of the width of weld made with s-polarised beam. But there after there was hardly any pronounced difference between the width of the two kinds of the welds. However, at higher speed (50 mm/s) the width of the weld obtained with s-polarised beam is less than that of p-polarised. This is probably attributable to the less absorption of s-polarised beam at higher speed as compared to p-polarised beam.

Figures 5.15 (a...f) to 5.16 (a...f) show the weld micrographs obtained using p- and s-polarised beam. It can be seen that the weld is not penetrating to the lower sheet in case of s-polarised beam (for welds at welding speeds of 35, 40 and 45 mm/s) and the presence of a gap also resisted the beam penetration. On the other hand for same welding conditions with p-polarised beam a better penetration is obtained and the presence of a gap does not have much effect on the depth of penetration as compared to s-polarised beam. The p-polarised beam has been found to

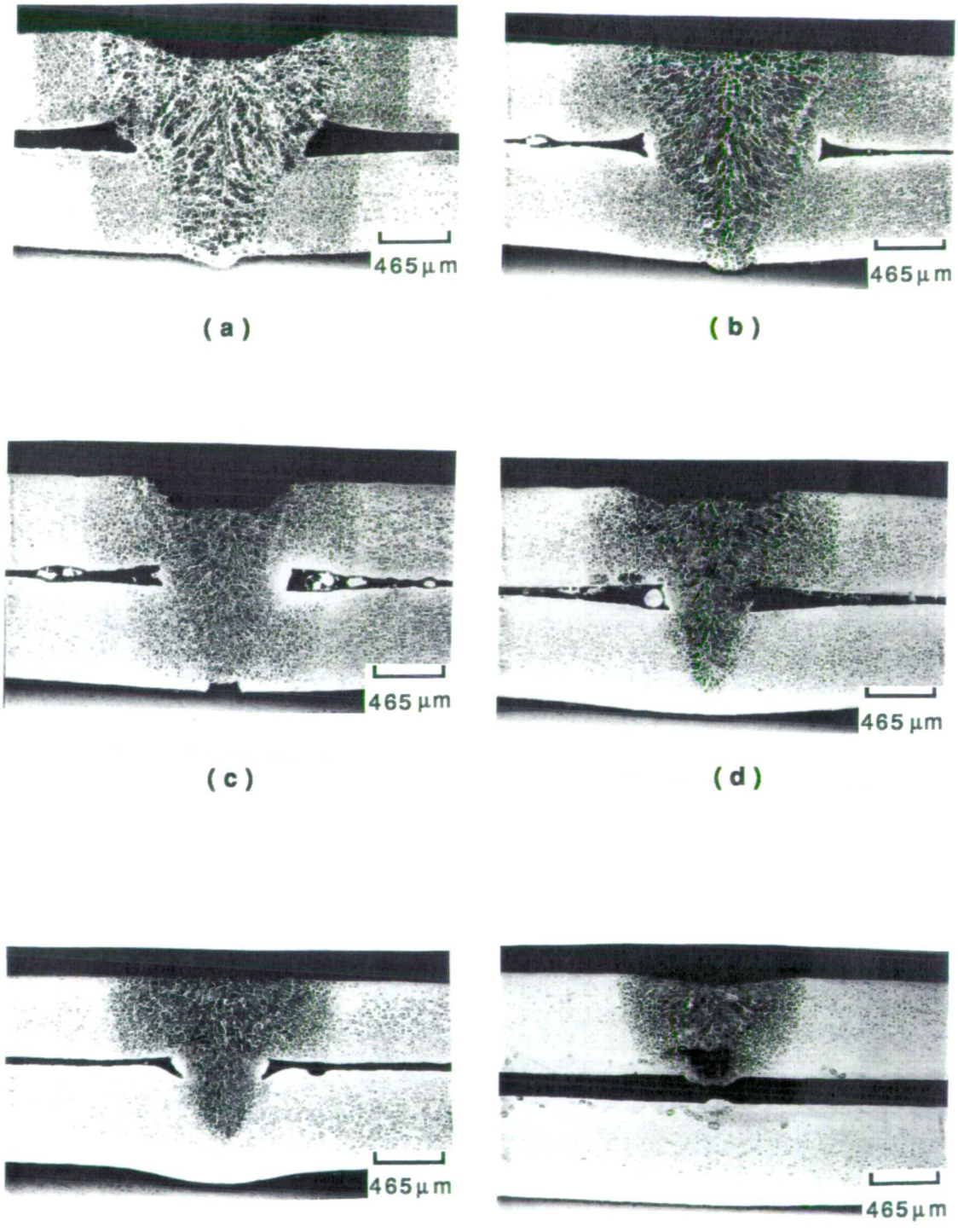


Figure 5.15 The weld microsections at various welding speeds using p-polarised beam. Laser power; 1.77 kW, welding speed; **(a)** 20, **(b)** 25, **(c)** 30, **(d)** 35, **(e)** 40 and **(f)** 50 mm/s.

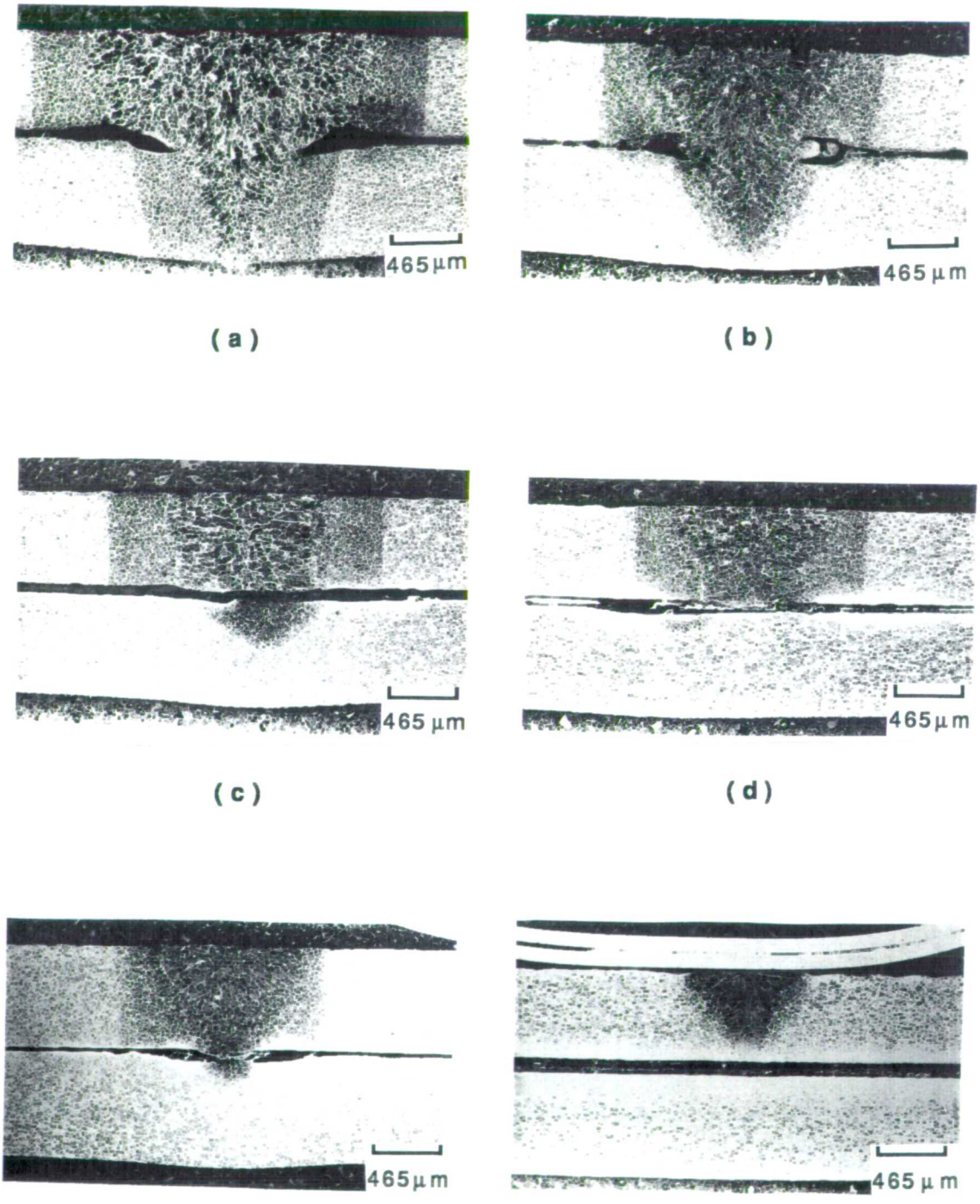


Figure 5.16 The weld microsections at various welding speeds using s-polarised beam. Laser power; 1.77 kW, welding speed; **(a)** 20, **(b)** 25, **(c)** 30, **(d)** 35, **(e)** 40 and **(f)** 50 mm/s.

give a better coupling of the two sheets. While in case of s-polarised beam it was not been able to give a better coupling to the lower sheets and there is no more contact between the two sheets as is evident from Figure 5.16 (d, e, f). Hence to obtain a better contact between the two sheets and to gain a deeper penetration the welding of steel sheet with p- polarised beam is recommended.

5.2.2 Welding Using SF/FAF Oscillator/Amplifier System With Gaussian Beam Mode

Material processing by laser requires a sufficiently high stable power and a correct beam mode. In most laser designs, high power is achieved at the expense of mode structure. The high power lasers use broader cavities, in which many transverse modes are able to oscillate producing high order or multi mode beams. The large plasma volumes used to amplify the beam within the optical cavities of such designs, emphasise plasma irregularities which greatly distort the mode structure of the resulting beam. This is partly due to temperature gradients in the plasma and partly due to the intensity variations of the plasma. Such irregularities could be greatly reduced if the laser beam is passed only once through the plasma, thus using it as an amplifier rather than an oscillator. The main objective was to make a laser oscillator/amplifier system to produce a h'gh power beam without distorting the beam mode structure.

A near Gaussian TEM_{00} beam was generated from an SF/FAF oscillator amplifier mode from a Ferranti MF400 oscillator generating 350 W feeding a Control Laser 2 kW FAF laser operating as an amplifier. Details of the set up are explained in reference [158] and the experimental arrangement is sketched in Figure 5.17. The two laser were situated at a distance of 12 meters apart due to the existing arrangement at the Imperial College. The divergence of the SF laser was measured to be 2 m rad. Hence a collimator was required to ensure the beam size did not exceed the amplifier tube diameter when it enters FAF/amplifier. The combined laser beam

was very close to a pure Gaussian beam and had a maximum power of around 1 kW. Improvement of beam mode structure was found in the amplified beam. This beam was used to carry out some welding trials in lap configuration. The Gaussian beam profile is sketched in Figure 5.18.

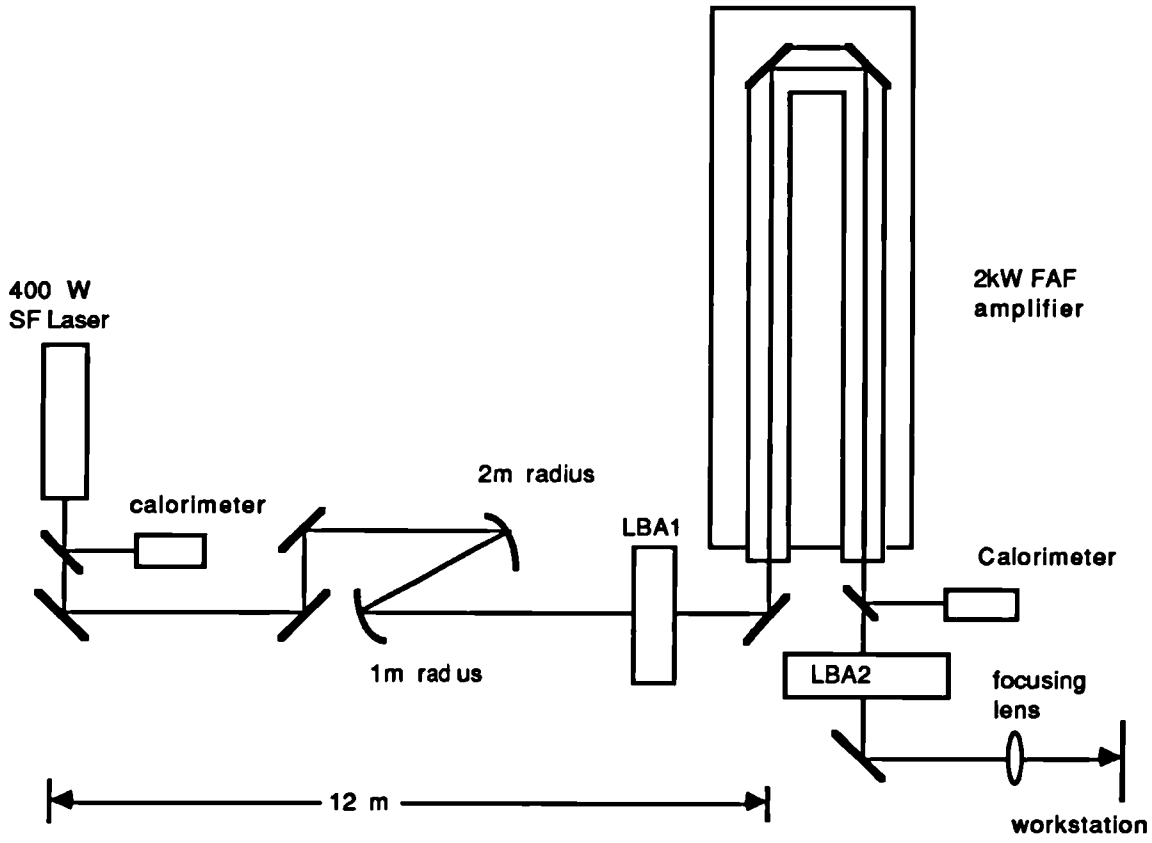


Figure 5.17 Experimental arrangement of SF/FAF oscillator amplifier, producing pure Gaussian beam.

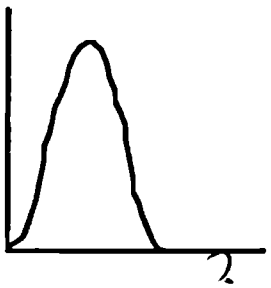


Figure 5.18 The Gaussian beam profile.

The welding experiments were carried out using the oscillator/amplifier system. The experimental welding parameters together with the results obtained are listed in Appendix 9.

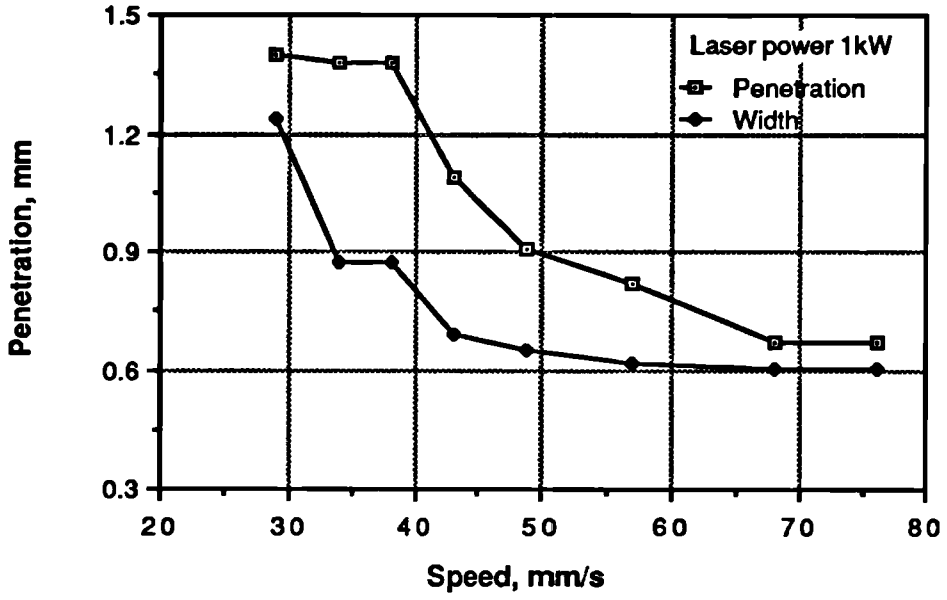


Figure 5.19 Weld penetration and width as function of welding speed.

The variation of welding speed undergoes the expected trend (Figure 5.19), the penetration decreases hyperbolically with increasing speed. It is also evident that the weld width is smaller than the penetration (aspect ratio 1.1-1.5), indicating that much of the energy is utilised for deep penetration into the material, as opposed to multimode beam in which the weld width is greater than the penetration (as discussed later in sections 5.2.3 & 5.2.4.

The beam produced by the oscillator amplifier system gave a pure Gaussian mode structure and was found to be very useful for welding applications. The results obtained were compared to the results of other lasers used. A significantly better penetration was achieved using oscillator amplifier Gaussian beam. It is evident from the Figure 5.53 that the Gaussian beam mode gave the best joining efficiency, indicating that a low power Gaussian beam mode is far better than a high power multi mode beam for welding applications. The cutting results obtained using the same

system have also shown a considerable improvement in the cutting performance with respect to the beam generated by FAF alone [159].

Due to the long beam path and complexity of the system it was difficult to maintain the alignment and stability of the beam for a longer period. Yet the result show clearly that the use of such beams generated by oscillator/amplifier are very useful for welding and cutting processes.

5.2.3 Welding Using AVCO Laser With Multimode Beam

The study was extended to high power lasers. This experimental work was carried out by the author at RTM Laser Centre, Italy. For this study a series of welds were fabricated on zinc coated steel at high powers up to 8 kW. The description of the laser is presented in Chapter 3. The beam profile of AVCO laser is sketched in Figure 5.20 Beam coupling and penetration studies were made with 15 kW AVCO laser (focussed spot size = 0.8 mm) giving a multimode beam. The welds were produced by simply passing the workpiece under the stationary focussed laser beam. These welds were made with laser powers up to 8 kW using a helium side jet. A small optimal gap of 0.2 mm was maintained between the two overlapped sheets to help vent the zinc vapour at the interface. The welding speed was varied until a fully penetrating weld was obtained.

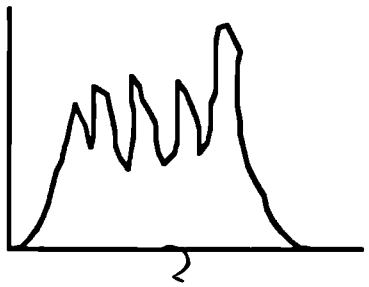


Figure 5.20 The beam profile of AVCO laser.

These experiments were performed to look into the welding parameters at high power and thus an increased welding speed could be achieved in this way. The processing parameters studied were laser power and welding speed. The constant

processing parameters were:

Material	Zinc coated sheet
Thickness	0.7 mm
Zinc coating thickness	7.5 μm
Assist gas	Helium
Focal length of the mirror	952 mm
Focal position	On the surface of the workpiece

All the welding parameters for each set of experiments are listed in Appendix 10, 11, 12. Under each set of experiments, welds were made over a wide range of laser powers and welding speeds. The aims of these welding trials were to find a suitable welding parameters in order to successfully weld the zinc coated sheets at relatively high speed. The results were assessed by means of measuring the depth of penetration of the weld. Since the gap size affected the quality of the weld, the weld quality was also studied as a function of gap size by counting the number of pits/holes per 100 mm of the weld length (discussed in chapter 4).

It has been described in the previous chapter that the lack of a gap between the sheets led to the explosive ejection of zinc vapour which in turn led to laser beam blocking due to zinc plasma thus reducing the weld penetration. Hence it was difficult to know the real penetration when there is pitting or plasma blocking problem, thus for beam penetration measurements the microsections were obtained from that region of weld where it showed no pitting and better weld bead surface. For some of the welds, microsections were also obtained from the region where it showed pits and holes.

The penetration and width of the welds as a function of welding speed for different laser powers are plotted in Figures 5.21 to 5.23. The curves decrease almost hyperbolically with the increase in welding speed. These graphs also show that there is a resistance to penetrating the bottom sheet at certain speeds depending upon the

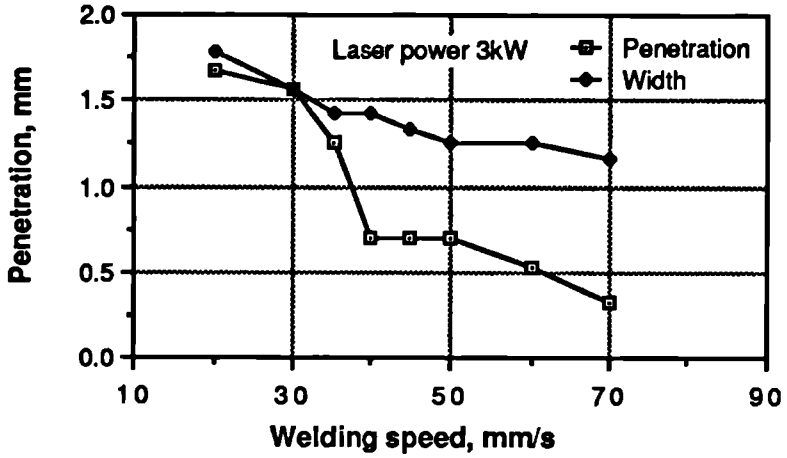


Figure 5.21 Weld penetration and width as a function of welding speed.

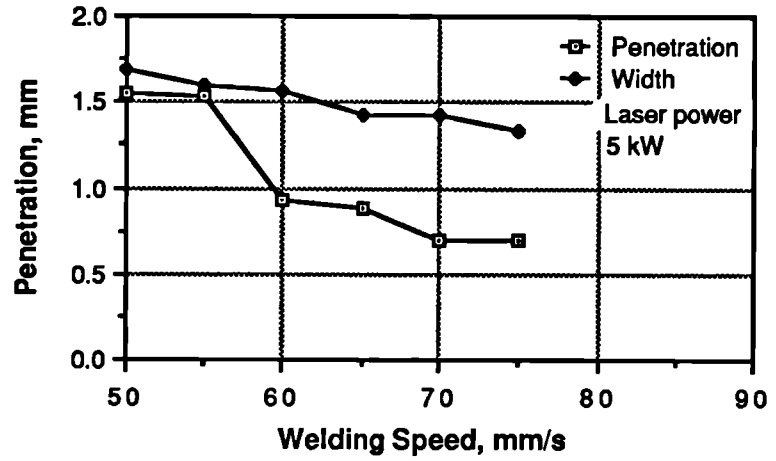


Figure 5.22 Weld penetration and width as a function of welding speed.

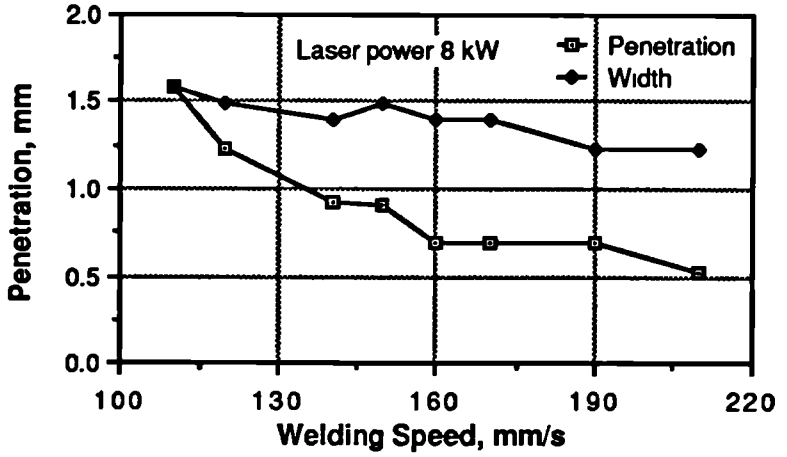


Figure 5.23 Weld penetration and width as a function of welding speed.

laser power. This is due to the presence of a gap between the two sheets (shown by the dwell at 0.7 mm penetration Figures 5.21 to 5.23).

5.2.4 Welding Using MLI Laser With Ring Type Beam Mode

MLI laser had a ring type of beam mode. The beam profile is sketched in Figure 5.24. The experiment was performed on uncoated steel sheet in lap configurations by Quantum Laser Corporation at New Jersey, U.S.A. The welding parameters and the results for this set of experiment are given in Appendix 13. The weld penetration and width are shown in Figure 5.25. It can be seen that the penetration and width decrease hyperbolically with increase in welding speed. The width of the weld was more than the penetration due to a larger spot size of 1 mm.



Figure 5.24 The beam mode of MLI laser.

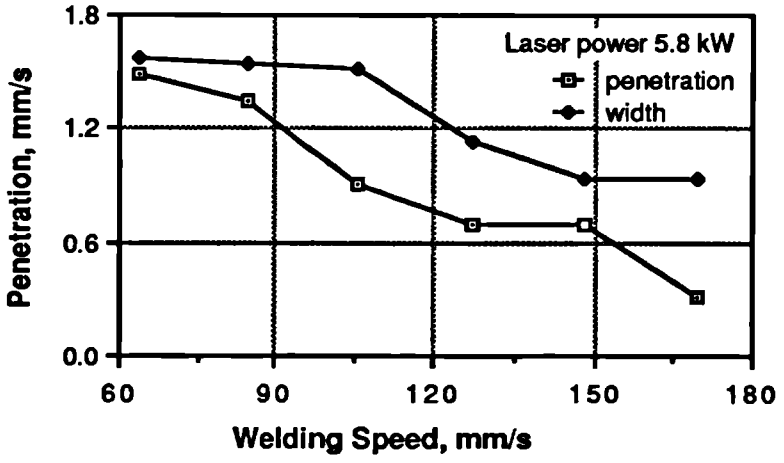


Figure 5.25 Welding speed against penetration and width for MLI laser. Laser power; 5.8 kW, sheet thickness 0.7 mm.

5.2.5 Welding Using UTRC Laser With a Top Hat Beam Mode

A series of welds were produced using a UTRC laser situated at Centre for Industriforksning, Oslo, Norway. The beam profile is roughly sketched in Figure 5.26. The raw beam mode was like top hat and there was little power variations in the beam mode both along x- & y- axis. Uncoated sheets of 0.7 mm thickness were used to weld in lap configuration. The welding parameters and the results are listed in Appendix 14. Beam coupling and penetration studies were made using this laser. The penetration and width of the weld are shown in Figure 5.27. It can be seen that the weld penetration and width decreases hyperbolically with increase in welding speed. Also the width of the weld is lower than the penetration, due to a smaller focal spot size of UTRC laser of 0.7 mm.

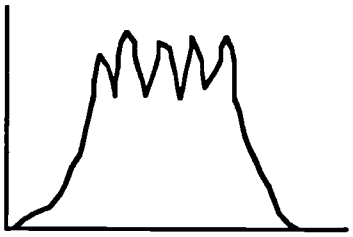


Figure 5.26 The beam mode of UTRC laser.

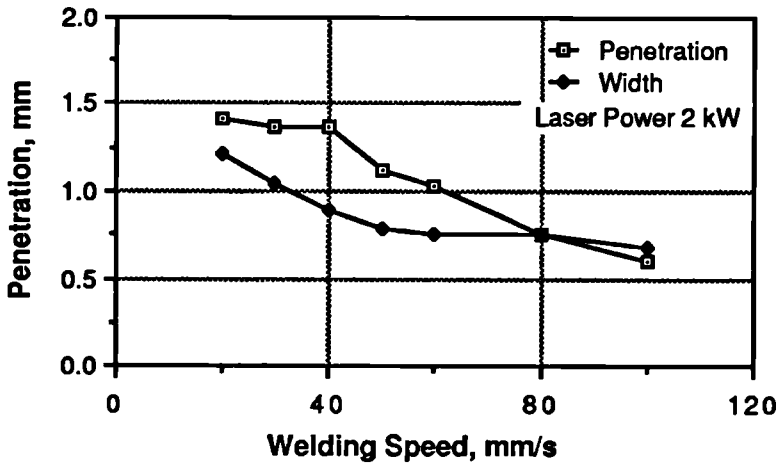


Figure 5.27 Welding speed against penetration and width for UTRC laser. Laser power 2 kW.

5.3 Efficiencies

This part includes the melting and joining efficiency of the welding processes. The joining efficiency gives a comparison between the various lasers used in this study.

5.3.1 Melting Efficiency

It has been observed that only a part of total laser energy available is utilised in the melting of the weldments. A part of the energy which enters the weld is used to melt the weld, the remaining heats up the base metal in forming a heat affected zone. In general, the efficiency is expressed as the ratio of output to input energies.

The melting efficiency can be calculated to find out how much power is being utilised in the substrate for melting. The laser power need to melt a zone can be calculated from the equation (5.4)

$$\eta = \frac{\rho V A (C_p T_m + L_m) 100}{P} \qquad (5.4)$$

= percentage of delivered energy used to melt the substrate.

Where, P = laser power delivered to the workpiece,Watts, η = melting efficiency %, ρ = density of the material,kg/m^3, C_p = specific heat capacity, kJ/kg-°C, T_m = Temperature of melting,°K, L_m = latent heat of melting, kJ/kg, A = cross section area of the fusion zone, m^2.

This equation is derived from a heat balance on an element. It is the heat needed to melt a volume of material V x A per second. The heat balance assumed that no heat is lost by conduction, convection or radiation. Folkes [160] melting titanium using a laser power of 1.5 kW for 0.3 mm deep penetration found that only 20% of the power

had been used for melting and the remaining 80% was reflected. Mazumder [46] also found a melting efficiency of 20% in mild steel sheet of 0.2 mm thickness.

The melting efficiency is calculated for each technique used. The melting efficiency is plotted against welding speed in Figure 5.28 to Figure 5.38. It is evident from the Figures that η_m decreases with welding speed. Mazumder [46] found that the melting efficiency increases with welding speed. This observation, however, does not agree with the present study. This could be due to the fact that he used a different material and a thin sheet of 0.2 mm thickness. At this penetration of 0.2 mm the weld would be expected to be conduction limited and considerable energy lost at low speeds by passing through the substrate. Hence the result would be different from a keyhole welding process.

It is also noted that the melting efficiency increases with the increase in laser power for same beam mode. A higher melting efficiency is achieved in case of a beam mode with a bigger spot size because it increases the width of the weld and thus the melted area. The Gaussian beam also gave a higher melting efficiency because it increases the penetration and hence the melted zone.

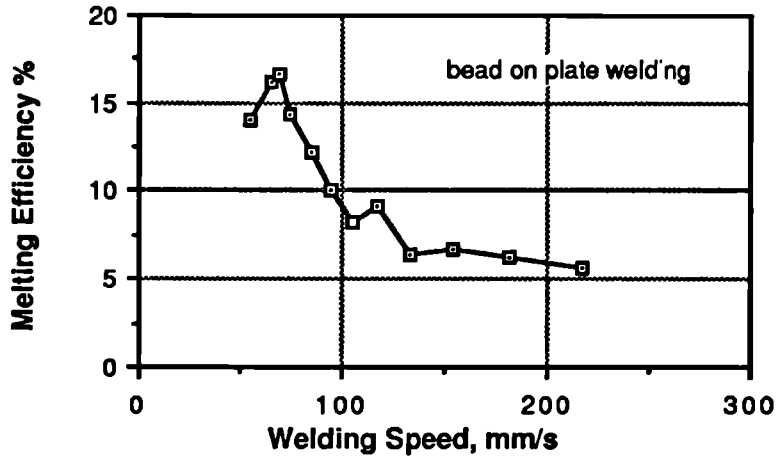


Figure 5.28 Melting efficiency against welding speed using CLL laser. Laser power; 1.62 kW, sheet thickness 1.5 mm.

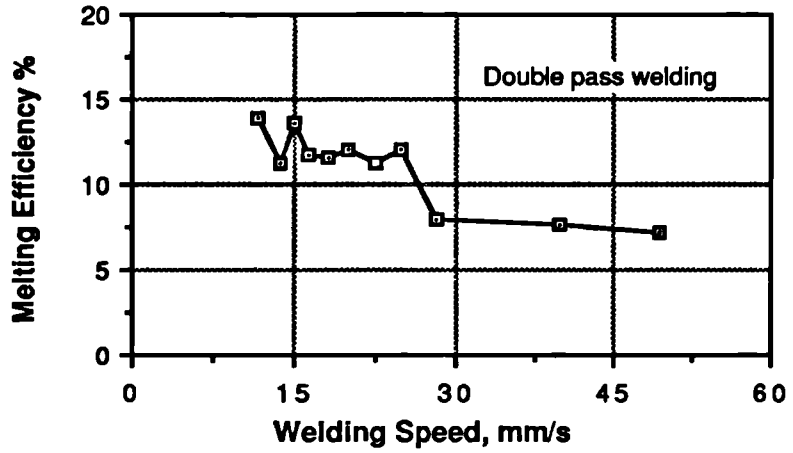


Figure 5.29 Welding speed against melting efficiency using CLL laser. Laser power; 2kW, sheet thickness 0.875 mm.

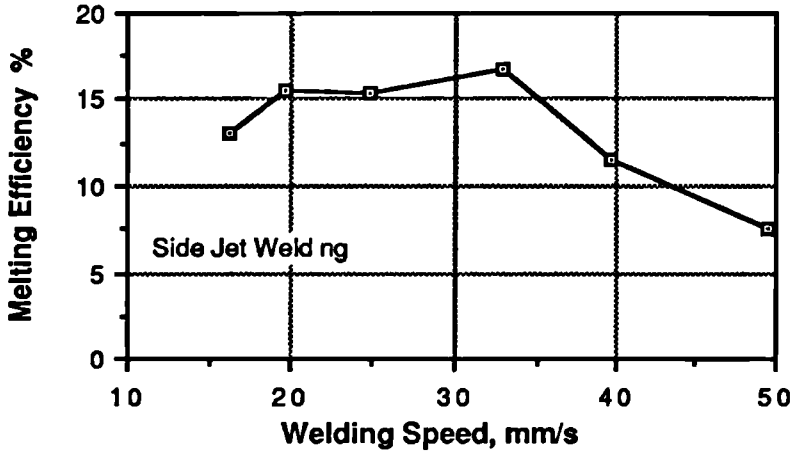


Figure 5.30 Welding speed against melting efficiency using CLL laser. Laser power; 2kW, sheet thickness 0.7 mm.

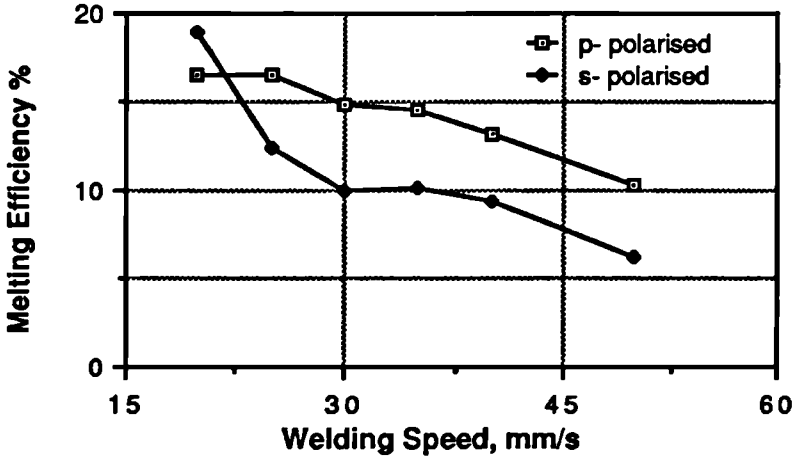


Figure 5.31 Welding speed against melt'ng efficiency using CLL laser. Laser power; 1.77 kW, sheet thickness 0.7 mm.

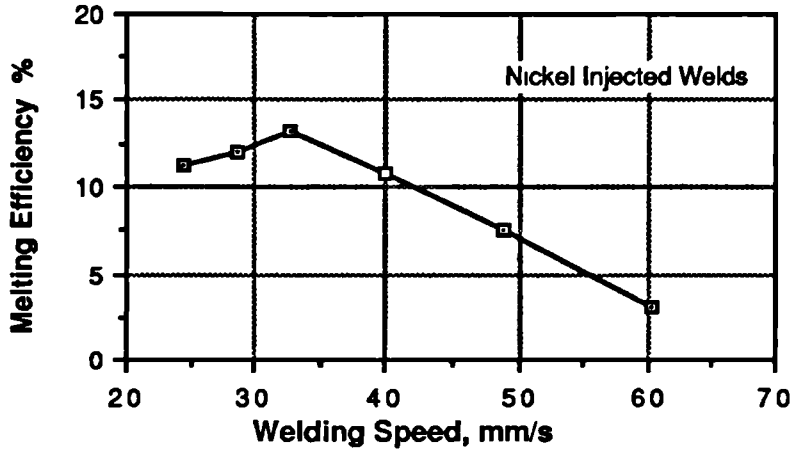


Figure 5.32 Welding speed against melting efficiency using CLL laser. Laser.power; 2 kW, sheet thickness 0.7 mm.

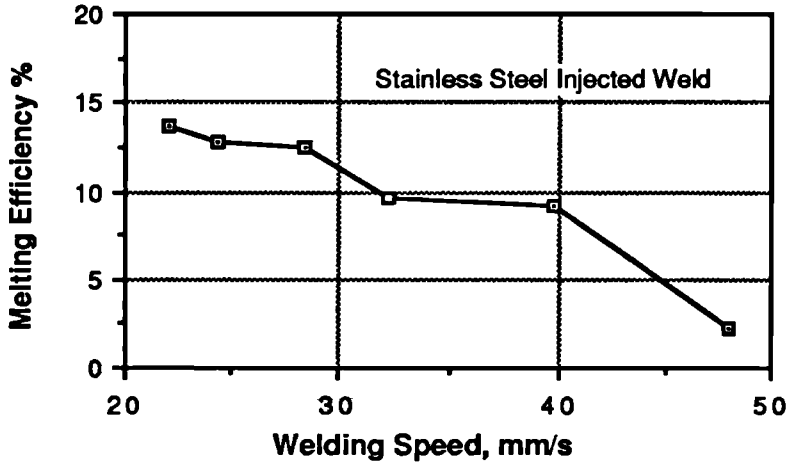


Figure 5.33 Welding speed against melting efficiency using CLL laser. Laser power; 2 kW, sheet thickness 0.7 mm.

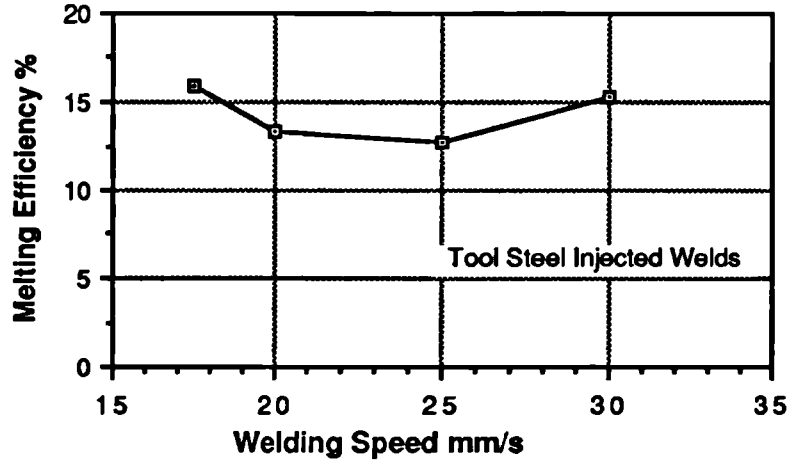


Figure 5.34 Welding speed against melting efficiency using CLL laser. Laser power; 1.54 kW, sheet thickness 0.7 mm.

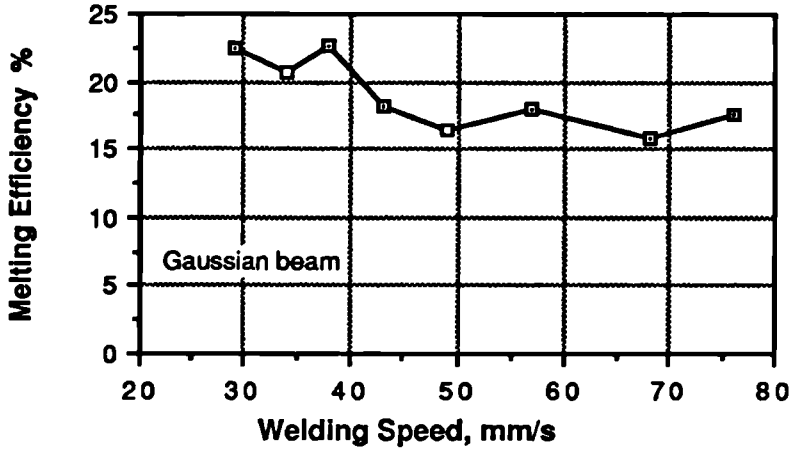


Figure 5.35 Welding speed against melting efficiency using oscillator/amplifier system. Laser power; 1 kW, sheet thickness; 0.7 mm.

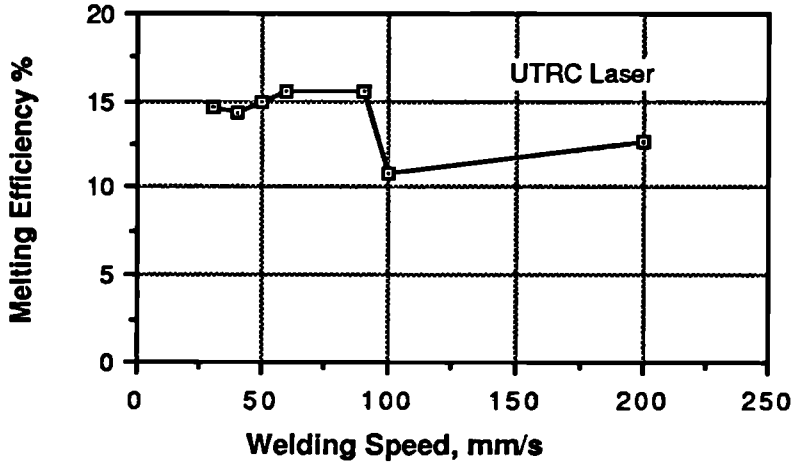


Figure 5.36 Welding speed against melting efficiency. Laser power; 2 kW, sheet thickness 0.7 mm.

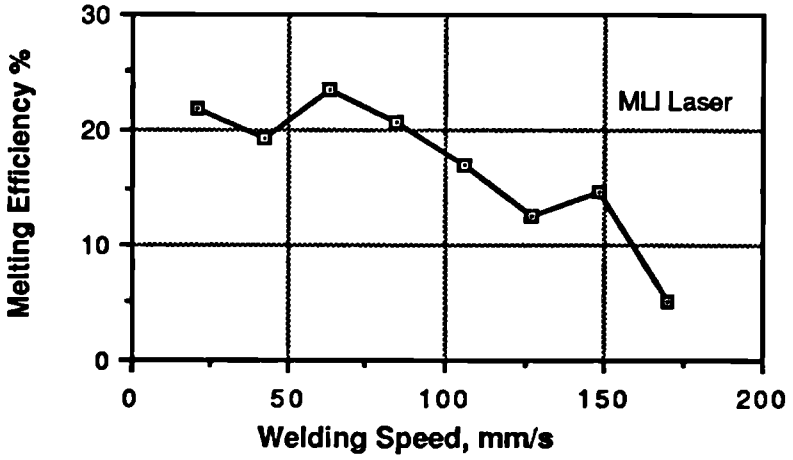


Figure 5.37 Welding speed against melting efficiency. Laser power 5.8 kW, sheet thickness 0.7 mm.

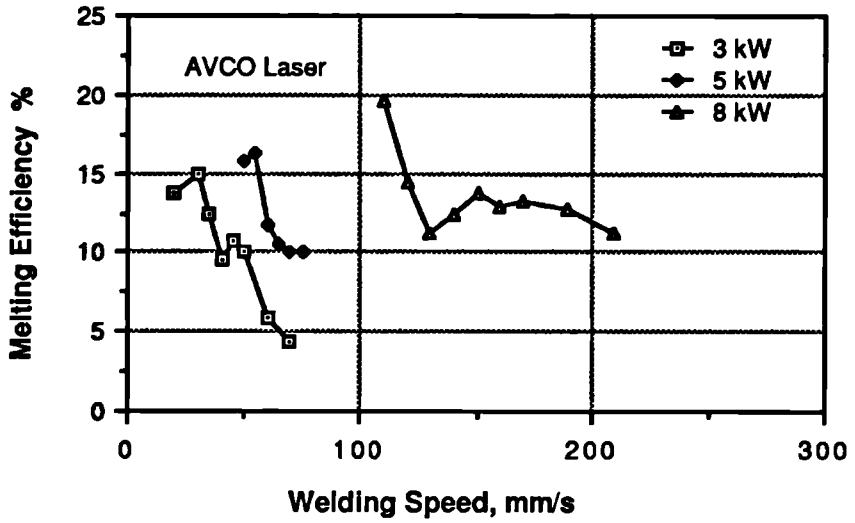


Figure 5.38 Welding speed against melting efficiency for AVCO high power laser. Sheet thickness; 0.7 mm.

5.3.2 Joining Efficiency

The total area of metal joined in unit time per unit of applied energy is considered as useful practical method of comparing processes and their performance. This is termed as the joining efficiency of the process. The experimental values of depth of penetration T, are plotted against 1/V, (V; welding speed). The slope of the curve (VT) when divided by the laser power P, gave the joining efficiency. Thus the parameter (VT/P) is the simplest order of magnitude parameter for calculating the laser performance at other speed and powers. A good correlation was found for penetration T, against 1/V.

Figure 5.39 to 5.50 shows the penetration, T vs (1/V) for all the lasers used in this work. For constant joining efficiency a straight line would be expected. The result follow such a line quite well.

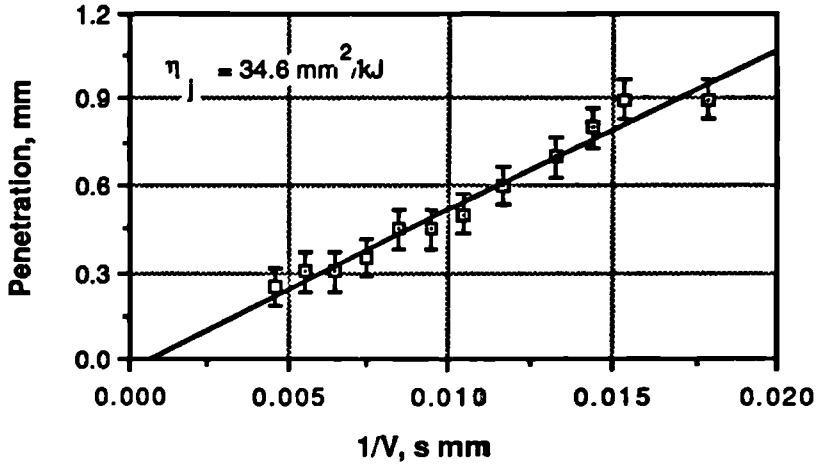


Figure 5.39 Weld penetration against 1/V for bead on plate weld. Laser power 1.60 kW.

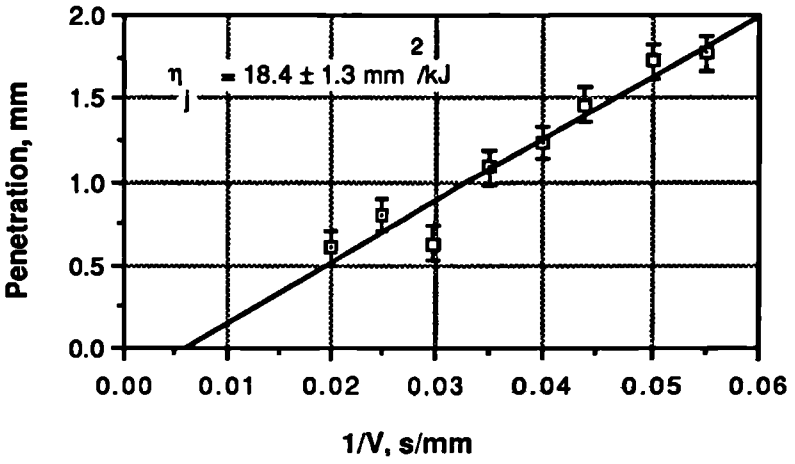


Figure 5.40 Plot of penetration T, against reciprocal of speed, 1/V, for double pass welding.

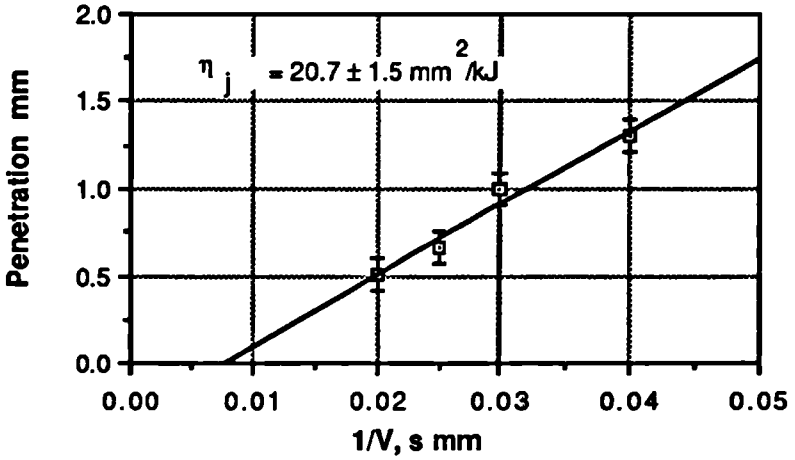


Figure 5.41 Penetration as function of 1/V, side jet welding technique. Laser power 2.00 kW.

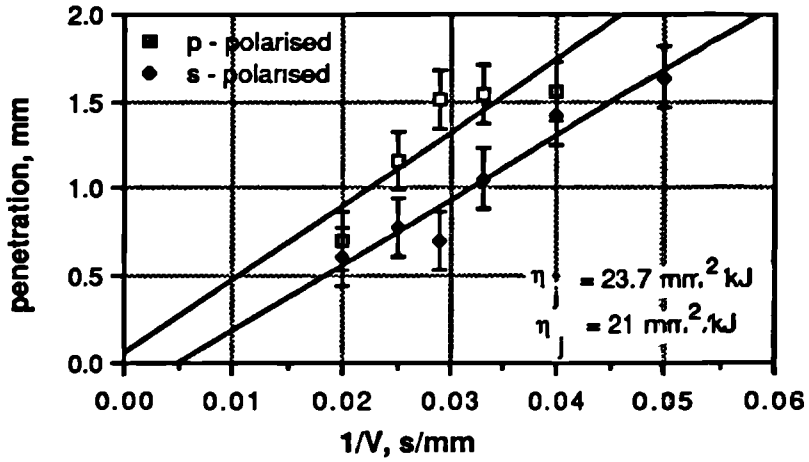


Figure 5.42 Penetration against 1/V for p-polarised and s-polarised beam under same welding conditions, laser power, 1.77 kW.

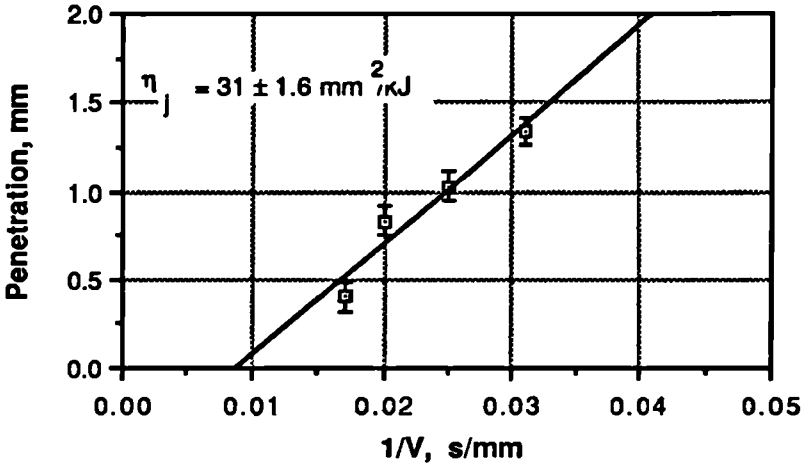


Figure 5.43 Plot of penetration T, against reciprocal of speed, (1/V), for nickel injected weld.

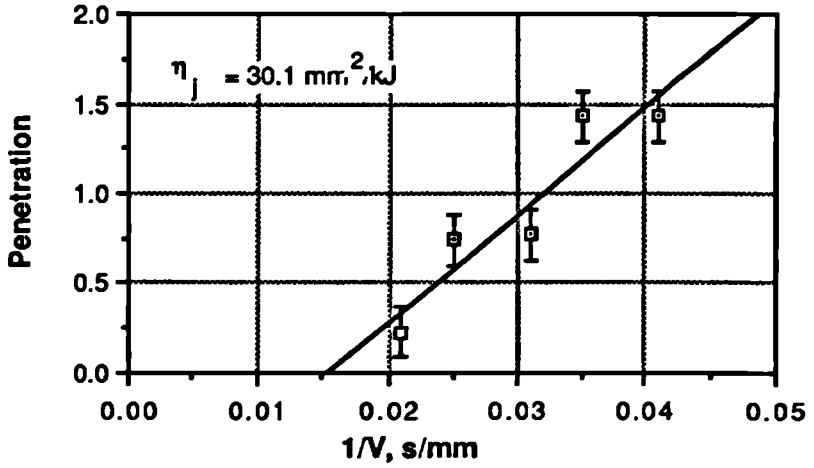


Figure 5.44 Plot of penetration T, against reciprocal of speed, (1/V), for stainless steel injected weld.

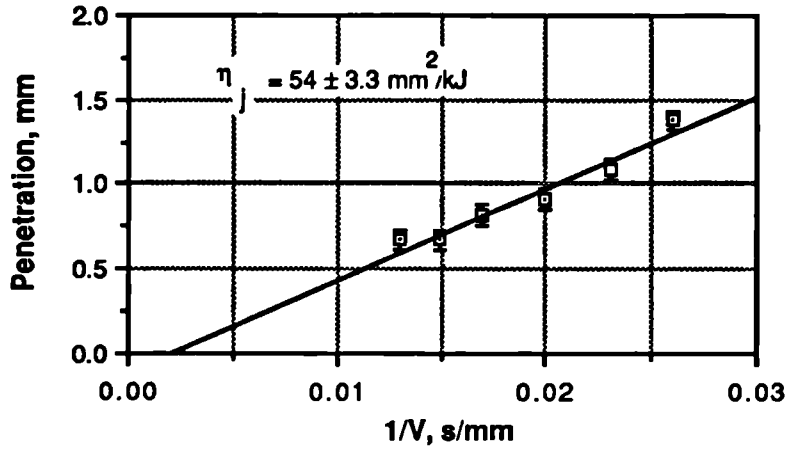


Figure 5.45 Plot of penetration T, against reciprocal of speed, 1/V, for Gaussian beam mode.

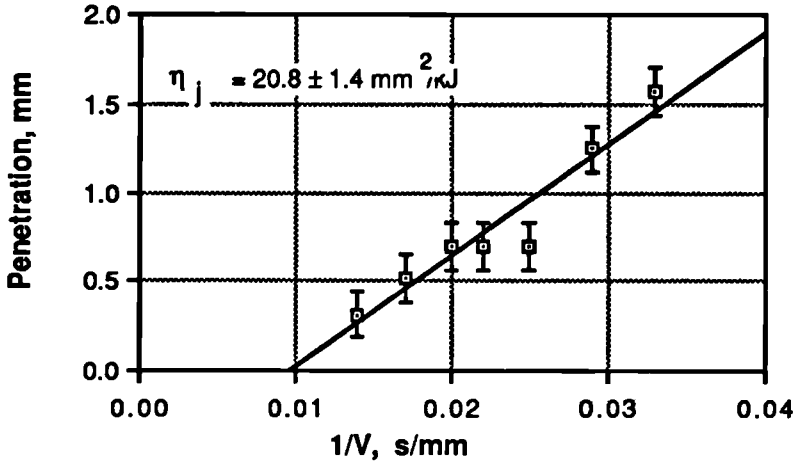


Figure 5.46 Plot of penetration T, against reciprocal of speed, 1/V, for 3kW Multimode beam.

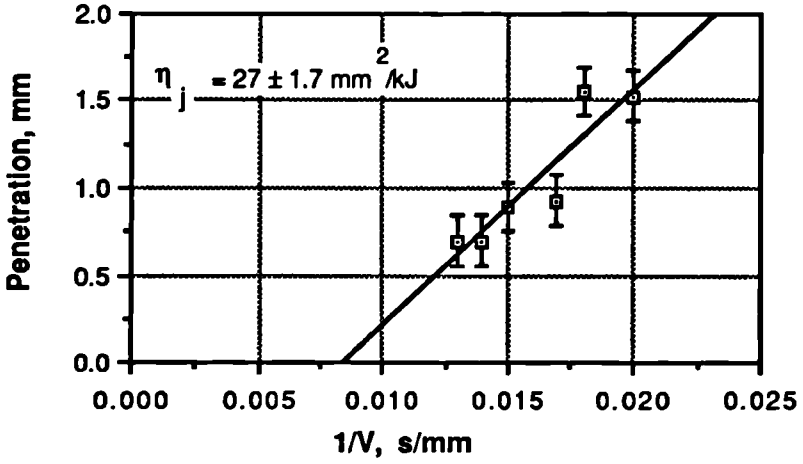


Figure 5.47 Plot of penetration T, against reciprocal of speed, 1/V, for 5 kW Multimode beam.

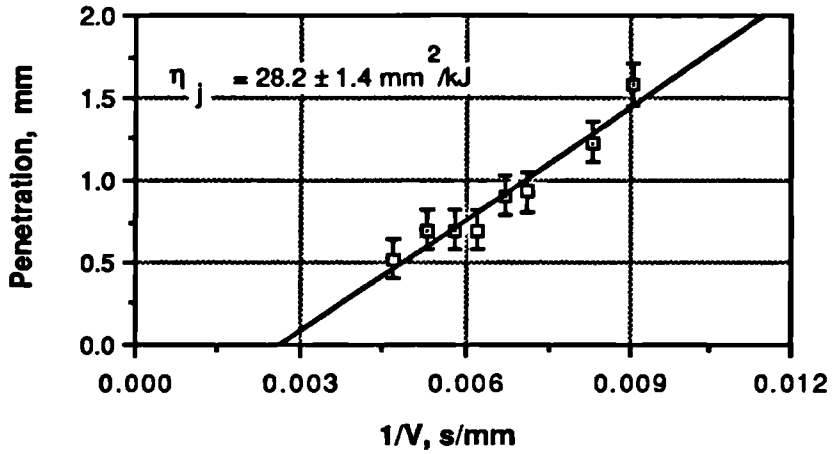


Figure 5.48 Plot of penetration T, against reciprocal of speed, 1/V, for 8 kW Multimode beam.

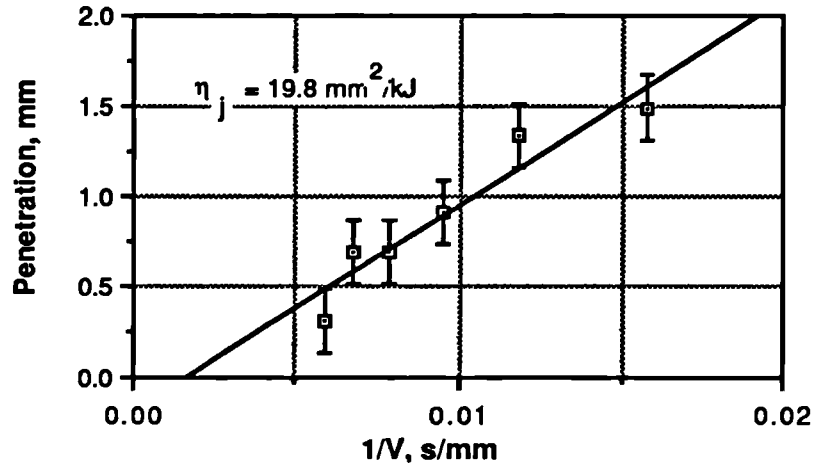


Figure 5.49 Penetration against 1/V. Laser power 5.8 kW.

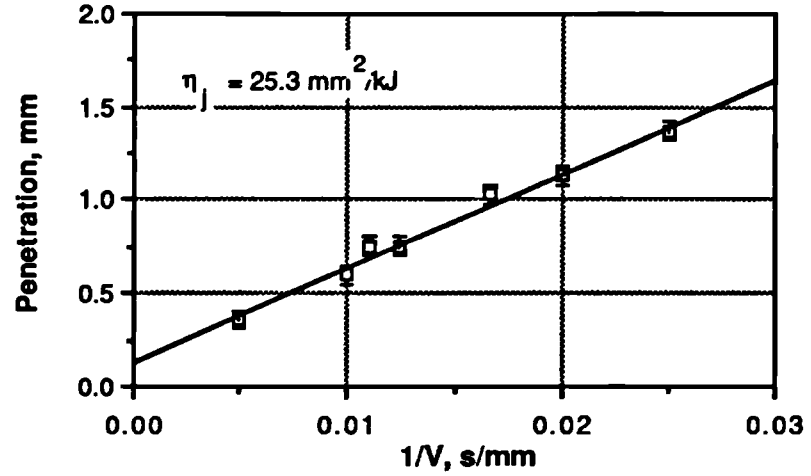


Figure 5.50 Penetration against 1/V for UTRC laser.

The joining efficiency and the average melting efficiency for each process is listed in Table 5.1. The melting efficiency is almost the same as the joining efficiency except it includes the weld width. Thus a mark of merit is a high joining efficiency and low melting efficiency. Joining efficiency is plotted against the melting efficiency in Figure 5.51 for different techniques employed by using CLL laser.

It can be seen that the joining efficiency for bead on plate welds is higher than that for the lap welds. This is due to the poor thermal contact between the two sheets in lap configuration. Also in the presence of a gap between the sheets the penetration is also reduced (as discussed earlier). There is a thermal coupling hiatus when the melt pool arrives at the interface between the sheets. The reason for this problem may be partly that the new surface has a reflectivity higher than the vapour hole penetrating the sheets and partly the sudden appearance of large volume of zinc vapour. Thus the partial penetration could be due to vapour reducing the power density to the lower plate.

In case of nickel and stainless steel injected weld the joining efficiency is higher, which is due to the presence of a powder cloud at the beam metal interaction point trapping the laser radiation between the particles and hence increasing the beam coupling with the substrate. Side jet welding, p- & s-polarised welding (employed the use of a side jet to remove the plasma from the beam metal interaction point) technique had a slightly higher joining efficiency than the double pass welding technique in which no side jet was used. Figure 5.52 shows that the joining and melting efficiency increases with increase in laser power for same laser beam mode.

Figure 5.53 is a plot of joining efficiency against melting efficiency for all the techniques used in this work. The Gaussian beam is seen to be exceptional with nickel and stainless steel injection welding being surprisingly efficient as well. The MLI laser gave a higher melting efficiency due to (i) higher power and (i) wider beam mode (spot size;1 mm), which increases the width of the weld, but the joining efficency is st' l very low. This indicates that the wider beams are not very suitable

for obtaining a deeper penetration. On the other hand the Gaussian beams are most suitable for welding process which can give a very high joining efficiency even at low power (1 kW), and is more efficient than high power multimode lasers.

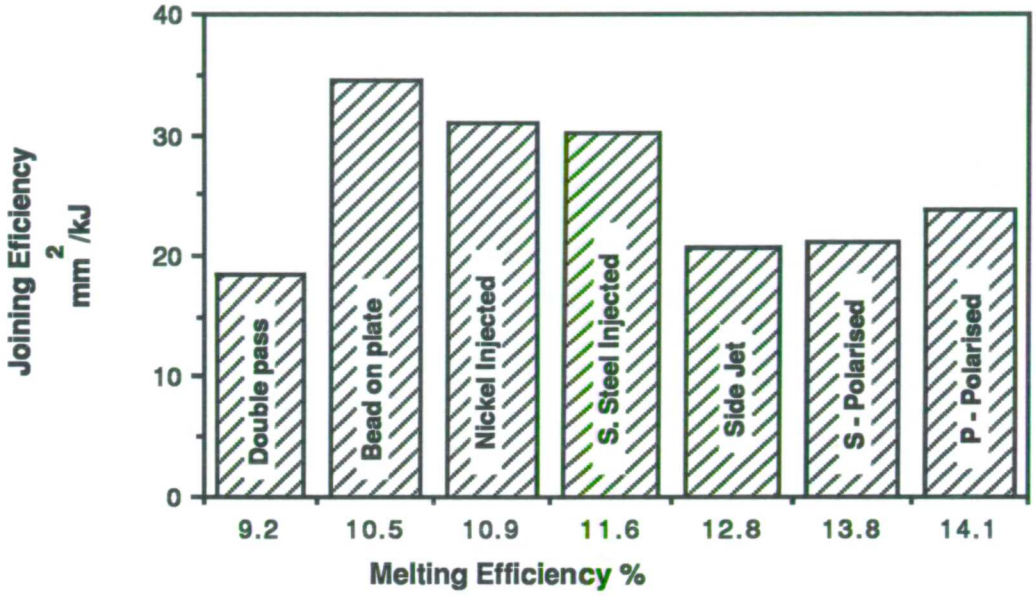


Figure 5.51 Joining efficiency against melting efficiency for different techniques used for welding zinc coated steel by using Control Laser Limited (CLL).

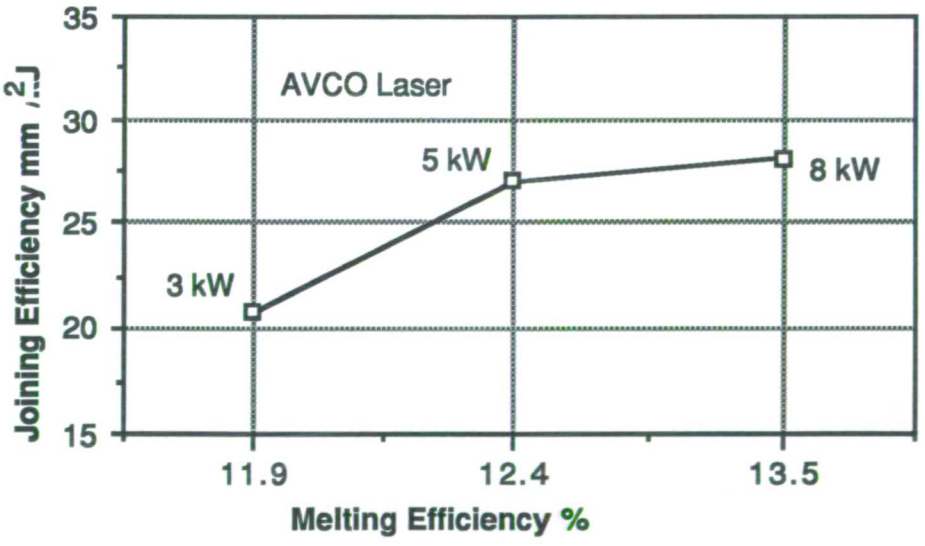


Figure 5.52 Joining efficiency against melting efficiency at higher power for AVCO laser.

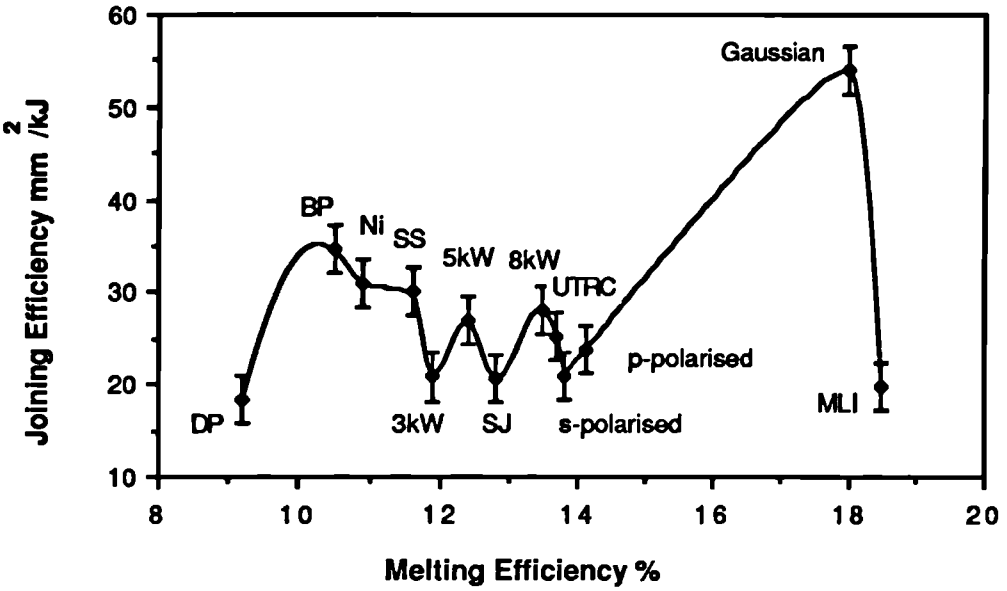


Figure 5.53 Joining efficiency against melting efficiency for various lasers used.

Table 5.1 Joining verses Melting Efficiency

Sr. No	Welding Technique	Laser power (kW)	Joining Efficiency (mm^2/kJ)	Av. Melting Efficiency (%)
1	Bead on plate (BP)	1.62	34.6	10.5
2	Double pass (DP)	2.00	18.4	9.2
3	Side jet (SJ)	2.00	20.7	12.8
4	p-polarised	1.77	23.7	14.1
5	s-polarised	1.77	21.0	13.8
6	Nickel injection (Ni)	2.00	31.0	10.9
7	Stainless steel injection (SS)	2.00	30.1	11.6
8	AVCO Laser 3 kW	3.00	20.8	11.9
9	AVCO Laser 5 kW	5.00	27.0	12.4
10	AVCO Laser 8 kW	8.00	28.2	13.5
11	Gaussian (CLL + FERRANTI)	1.00	54.0	18
12	MLI Laser	5.80	19.8	18.5
13	UTRC Laser	2.00	25.3	13.7

5.3.3 Effect of Gap Size on Joining and Melting Efficiency

Figure 5.54 shows the plot of gap size against the joining and melting efficiency. The joining efficiency depends upon the depth of penetration and welding speed and is independent of the width of the weld. On the other hand the melting efficiency depends upon the area of the fusion zone. As described earlier, the weld penetration decreases with increasing gap, hence for constant welding speed the joining efficiency also decreases with the increase in gap size as shown in Figure 5.54. Also it has been seen in the previous chapter that the increase in gap size resulted in an increase in the weld width of top sheet and a decrease in weld penetration. It is found that the melted area is almost same for all welds. Hence there is not much difference in the melting efficiency of the weld with the variation in the gap size.

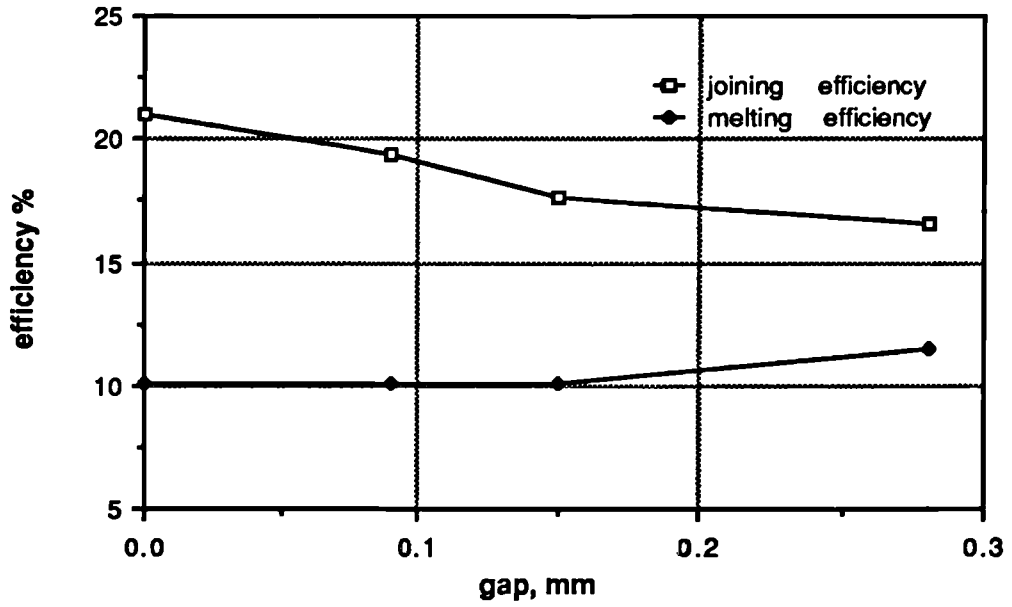


Figure 5.54 Joining and melting efficiency as a function of gap size for a constant welding speed of 15 mm/s. Laser power, 1.00 kW.

5.4 Mechanical Tests

The mechanical tests performed on the welded specimen are presented in this section. These include tensile, hardness, impact and fatigue tests.

5.4.1 Tensile Tests

A "Hounsfield" hand operated tensile testing machine was used. All the specimens were made with a gauge length of 82 mm with weld transverse to the direction of tension as shown in Figure 3.10 (chapter 3). Several additional samples were made to enable the production of tensile tests specimens. Specimen sizes and loading conditions for tensile tests on laser welded sample are listed in Table 5.2 together with calculations of percentage elongation and percentage reduction in area. Macroscopic photographs of the resulting specimens after the tensile test are shown in Figure 5.55.

These results are useful since they show that fracture in plane, butt and lap welded samples occurred away from the weld zone. This shows that the weld yield strength is greater than that of the parent material. Calculations of percentage elongation and reduction in area were obtained for each test and the results are fairly constant implying that these results are an indication of material properties and not of the properties of the welds themselves. The slight reduction in the values of percentage elongation and reduction in area for the lap welds are possibly due to the discontinuity caused by the weld's presence.

It is observed that the weld properties are similar to the unwelded material and in all cases rupture take place at the or'ginal material instead of weld joint. A similar observation was made for all end edge welds (2Z-8, 2Z-13, and 2Z-15), tool steel injected, and nickel injected weld.

Table 5.2 Tensile Testing of Welded Material.

Sr No.	Type of weld	X-section (mm^2)	Max load (kg)	Max Stress (MPa)	Original length (mm)	Final length (mm)	%Elong -ation	%Reduc -tion
1	Butt 1	8.4	250	290	82.5	112	35.7	67.6
2	Butt 2	8.4	244	283	82.5	109.5	32.7	64.7
3	Plain	8.4	247	286	81.5	111	36.2	67.3
4	Plain	8.4	256	297	80.5	114	41.6	69.8
5	Lap g=0.1	8.4	250	290	86.0	107	24.4	75.1
6	Lap g=0.05	8.4	247	286	82.2	111	35.0	69.0
7	Plain	8.4	264	308	82.0	108	31.7	50.6
8	2Z-8	8.4	259	302	82.0	107	30.5	56.5
9	2Z-13	8.4	256	299	82.0	102	24.4	53.0
10	2Z-15	8.4	250	292	82.0	102	24.4	55.9
11	NKL	8.4	241	281	82.0	99	20.7	48.8
12	TST	8.4	256	299	82.0	102	24.4	49.0

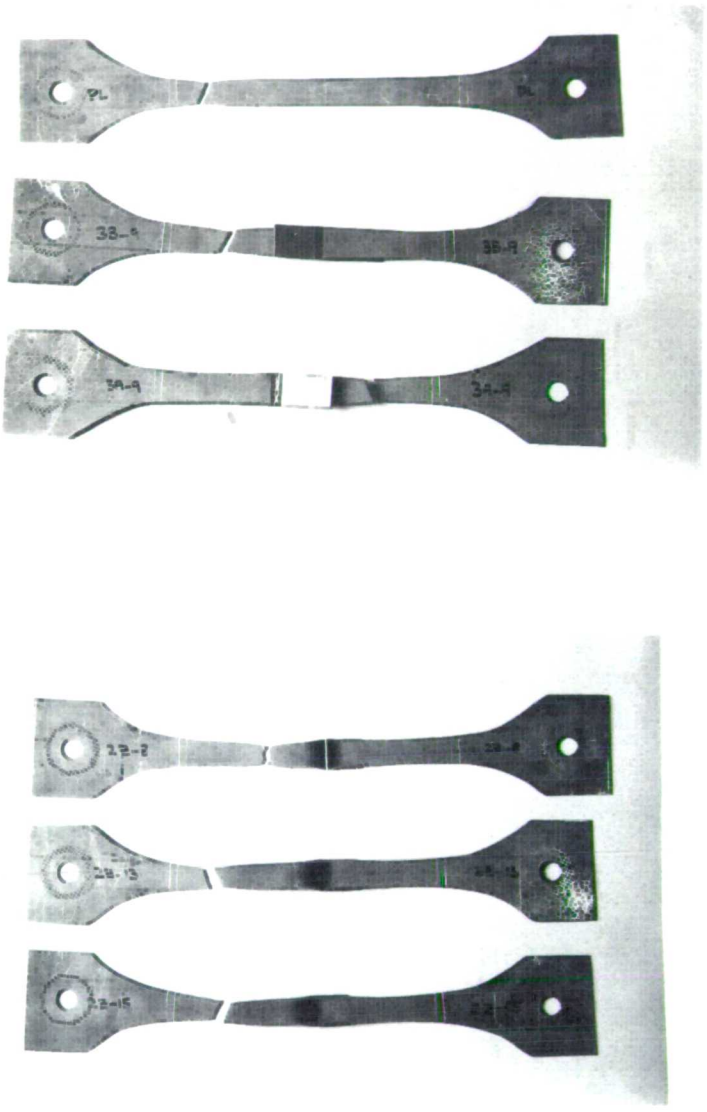


Figure 5.55. Specimens after tensile test.

5.4.2 Hardness Measurement

Microhardness traverse across the weld zone was performed on a few selected samples to investigate the effect of welding speed on hardness within the weld zone and heat affected zone. Hardness values of base material, heat affected zone and fusion zone were measured. Microhardness traverse across the weld revealed that the hardness at the weld fusion zone was higher than that of the parent material and the heat affected zone. The hardness of base material was found to be 132 ± 15 Hv and that of heat affected zone was 232 ± 20 Hv. The hardness of fusion zone was measured at different points, the hardness value ranged from 350 to 370 Hv. Figure 5.56 shows the hardness of the weld fusion zone and the heat affacted zone. It is evident that for same laser power the hardness in the fusion zone and heat affected zone increases with increase in welding speeds. This shows that for higher cooling rates the hardness of the fusion zone and the heat affected zone also increases. These hardness values are in line with those found in welding this form of mild steel.

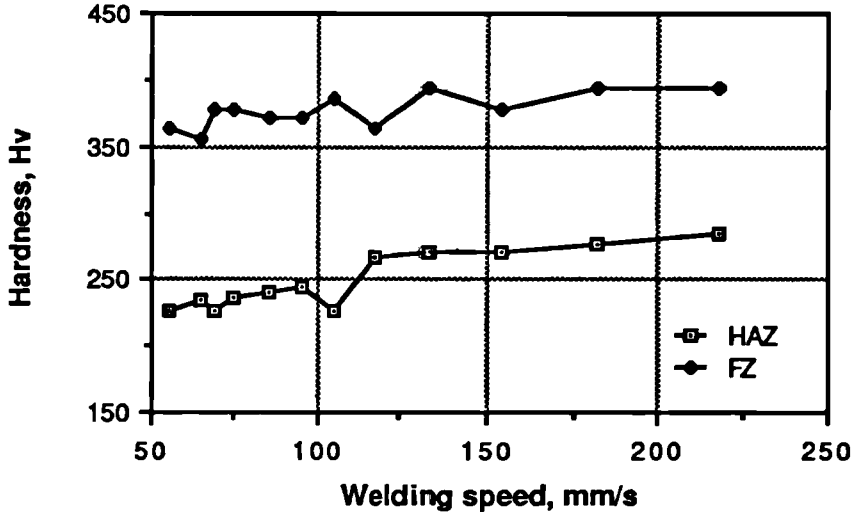


Figure 5.56 The hardness of fusion zone and heat affected zone as a function of welding speed.

5.4.3 Mechanical Testing by Collaborating Partners

5.4.3.1 Impact Testing

The impact testing was performed at Impact Research Centre, Liverpool University by R. S. Birch and Prof. Norman Jones. The test was carried out on thin-walled box section steel structural members supplied by RTM Research Centre, Turin, Italy. The box sections were subjected to static and dynamic axial crushing and its effects were examined. The box sections were manufactured from 0.7 mm steel using either a lap (type A) or flange (type B) joint with a CW CO_2 laser weld as shown in Figure 5.57. A small gap was maintained between the sheets using a shim. The specimen for impact test had a length of 160 mm, approximately.

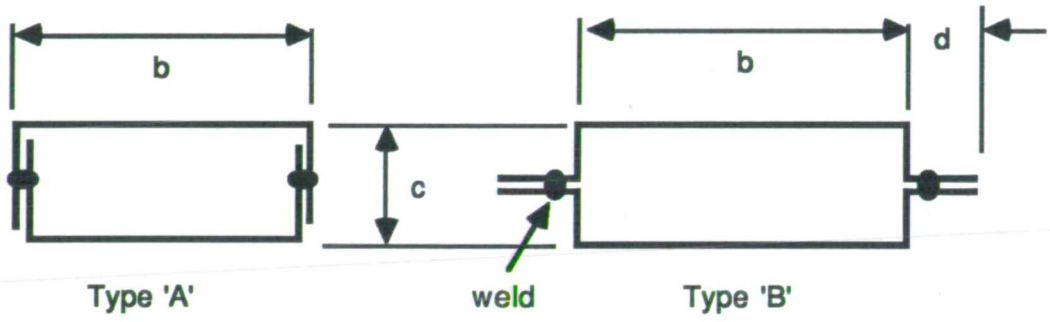


Figure 5.57 Design of box sections. Where b = 50.5, c = 30 mm, and d = 15 mm.

(i) Static compression tests were carried out on a 25 Tonne Dartec tensile/compression testing machine with a cross head speed of 0.05 mm.

(ii) The dynamic tests were performed on the 9 m drop hammer rig at the Impact Centre, Liverpool University. Three tup masses and several drop heights between 2.5 and 8 m, approximately, were used. Velocity and load measurements were made using a Laser Doppler Velocimeter (LDV) together with a DL 1080 20 M Hz transient recorder.

The basic dimensions and data for each specimen are listed in Table 5.3.

TABLE 5.3 The Basic Dimens ions and Data For Each Specimen

Code	+type	L (mm)	M (Kg)	H (m)	Vi (m/s)	Pm (kN)	s (mm)	*Mode of failure
1	A uncoated	165	- -	static	- -	6.4	96.5	2, 3
2	B uncoated	165	- -	static	- -	10.8	77.0	1, 4
3	B coated	165	- -	static	- -	12.6	96.5	1, 3
4	A uncoated	165	11.5	2.47	6.81	9.3	22.5	1
5	A uncoated	165	11.5	3.95	8.8	- -	31	1
6	A uncoated	165	11.5	7.2	11.79	8.8	67.5	1, 3
7	B coated	162	20	2.47	6.81	18.1	18.5	1
8	B coated	163	20	3.77	8.58	2.5	88	1, 4
9	B coated	163	20	5.95	10.8	- -	51.5	1, 3
10	B coated	163	20	5.95	10.64	18.5	51	1
11	B uncoated	162	20	2.48	6.88	18.8	16	1
12	B uncoated	162	20	5.95	10.71	16.9	48.5	1, 3
13	B uncoated	162	20	3.95	8.72	18.5	31	1
14	A uncoated	162	20	2.46	6.95	- -	32	2, 3
15	A uncoated	162	20	2.45	6.77	9.8	33	2, 3
16	A uncoated	162	20	3.96	8.7	8.8	62	2, 3
17	A uncoated	162	20	5.95	10.8	- -	88	2, 4
18	A uncoated	162	20	5.96	10.68	8.9	109.5	2, 3
19	B uncoated	162	20	8.08	12.6	- -	69	1, 3
20	B uncoated	162	20	8.09	12.42	14.6	79	1, 3
21	B coated	162	20	8.1	12.43	13.9	79	1, 3
22	A uncoated	162	20	8.12	12.47	12.1	143.5	2, 4
23	B uncoated	162	28	8.02	12.54	- -	108	2, 4
24	B coated	162	28	8.02	12.23	15.4	138.5	1, 4
25	B coated	162	28	5.95	10.8	- -	120	1, 4
26	B uncoated	162	28	5.95	10.65	16.7	80	1, 3
27	B coated	162	28	5.95	10.62	13.9	86	1, 4

\+ A = lap jointed type A
B = flange jointed type B

* 1 = regular progressive collapse
2 = irregular progressive collapse
3 = some overall buckling
4 = extensive overall buckling.

Where L = initial length of a specimen, M = tup mass, H = drop height, V_i = impact velocity, P_m = mean axial collapse load, overall axial deformation.

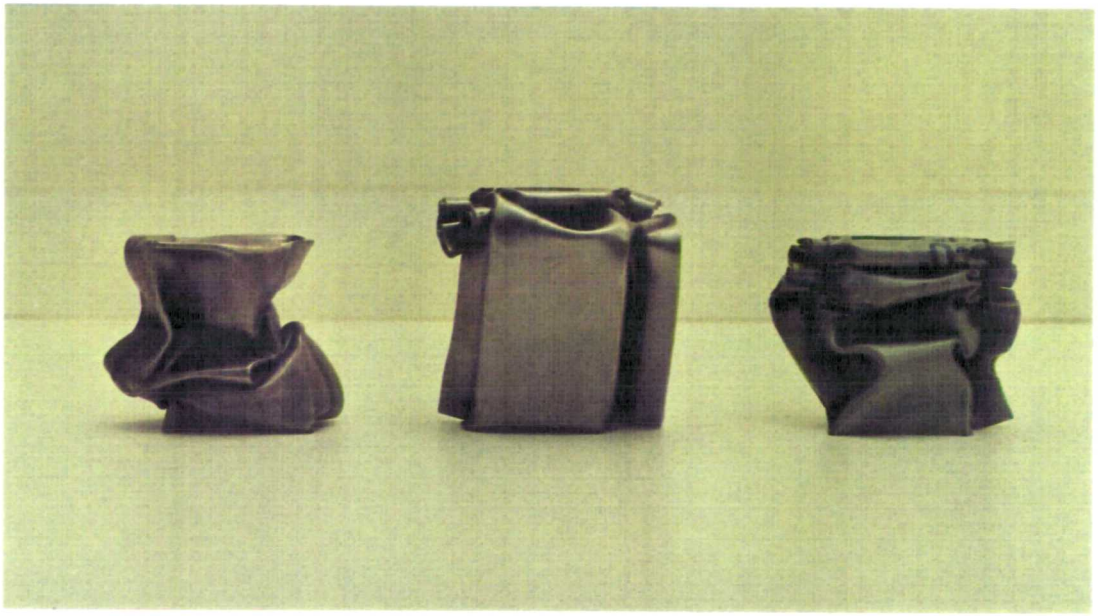
(i) Static Test The static collapse mode of the box was progressive with overall buckling (Figure 5.58). In type A and type B uncoated specimens the overall buckling occurred at an early stage of the collapse process while the coated type B specimen was stable almost throughout the entire deformation history. More over there was no evidence of weld failure in any of the specimens.

(ii) Dynamic Test A photograph of the dynamically crushed specimens is shown in Figure 5.59 with the impacted specimens arranged from left to right with increasing impact energy.

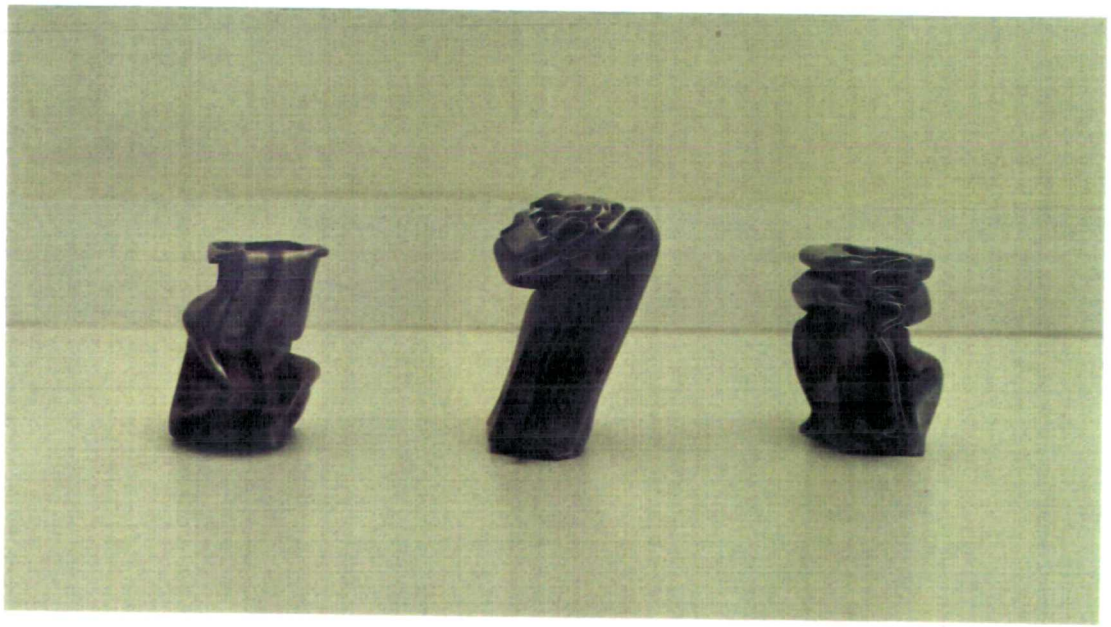
The dynamic collapse modes were similar to those found in the static case. However, the local buckling pattern or mode lengths tended to be shorter, more regular and usually confined to the impacted end of the specimen. Overall buckling was observed in many specimens. Several tests were carried out to examine the repeatability of the impact tests using almost the same impact energy. It was found that changes in the collapse mode would effect the energy absorption capability of the box section. Specimen 17 and 18 shown in Figure 5.60 illustrate this effect.

Figure 5.61 shows the relationship between permanent overall axial deflection and impact energy and it can be seen that type A specimens have an almost linear relationship. Similarly, type B specimens have an approximately linear deflection-energy relationship but there is significant scatter in the coated specimen results. Examination of the coated specimens indicated a higher incidence of unstable overall buckling failure.

The velocity-time history of the tup during crushing was recorded by a laser Doppler velocimeter and a typical curve is shown in Figure 5.62 . This curve may be differentiated with respect to time to give the decceleration of the tup and , therefore, the variation of the axial force when multiplying by the tup mass. The mean loads were found to be approximately 1.5 higher than those recorded during the static tests and was probably due to the reduction in mode length and material strain rate effects.

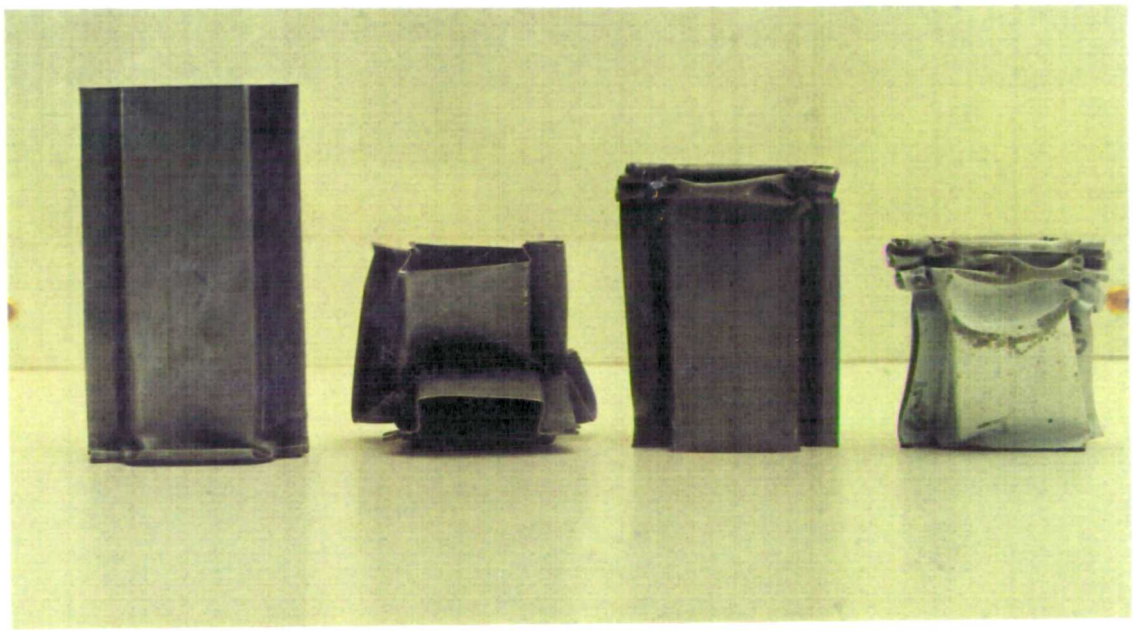


(a) Specimen 1 2 3

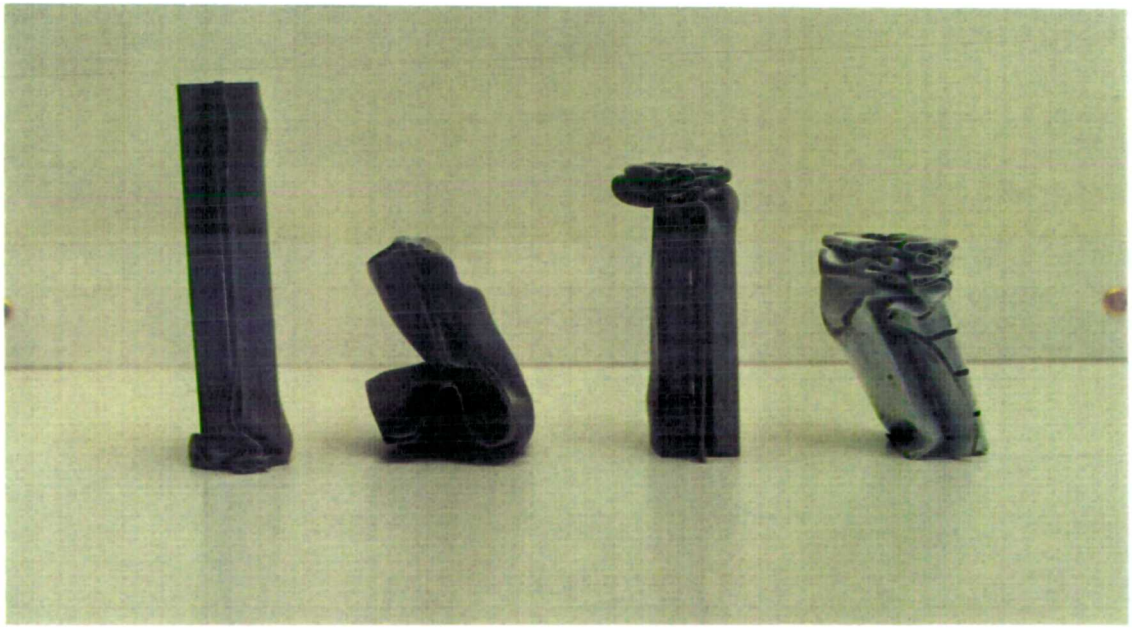


(b)

Figure 5.58 The static collapse mode of the box section, **(a)** front view and **(b)** side view of the same specimen.

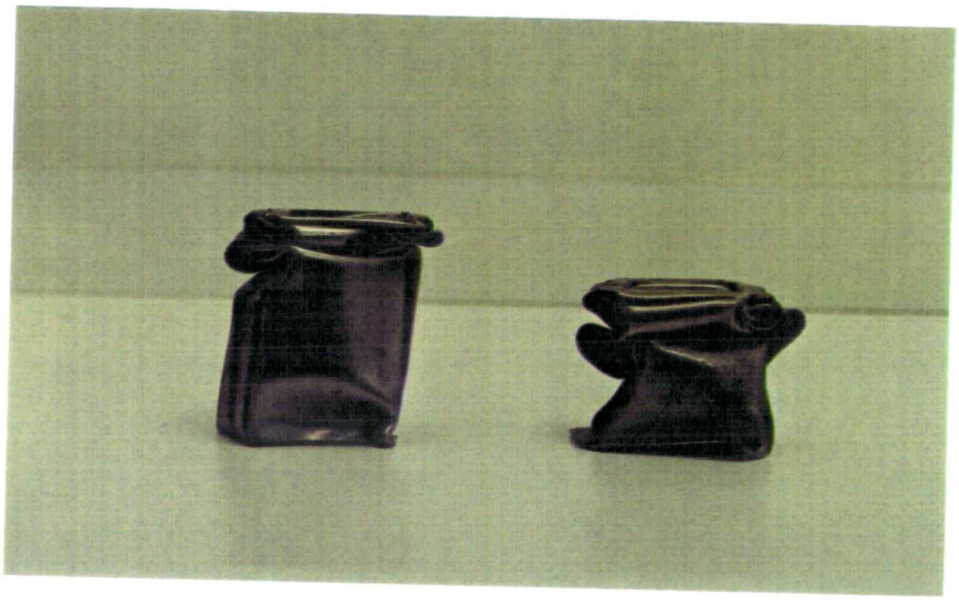


(a) Specimen 7 8 9 21



(b)

Figure 5.59 The dynamically crushed specimen arranged from left to right with increasing impact energy, **(a)** front view and **(b)** side view of the same specimen.



(a) Specimen 17 18



(b)

Figure 5.60 The collapse mode affects the energy absorption capability of the box section, **(a)** front view and **(b)** side view of the same specimen.

Again, there was no evidence of weld failure in any of the specimens.

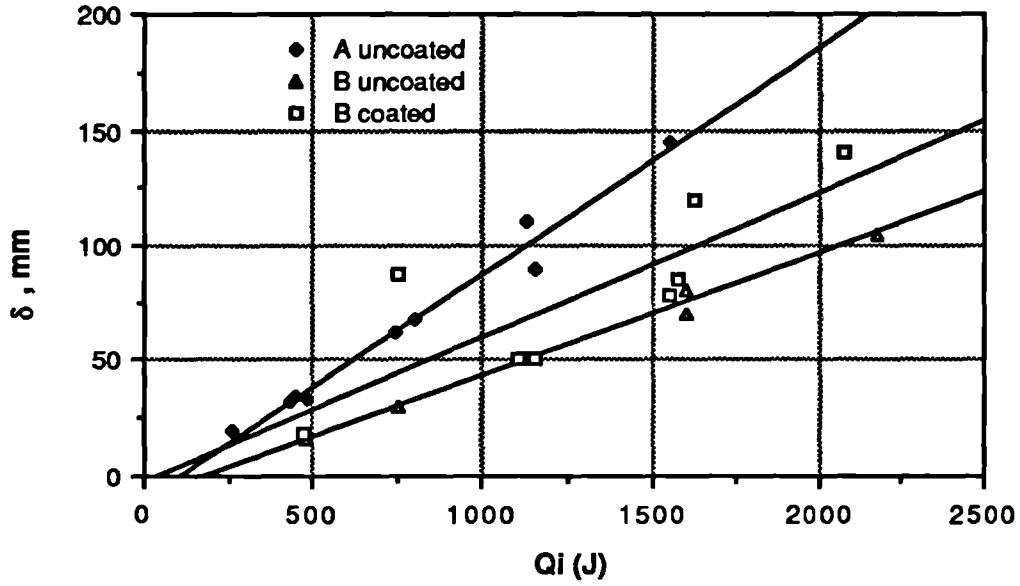


Figure 5.61 Absorbed energy against axial deflection.

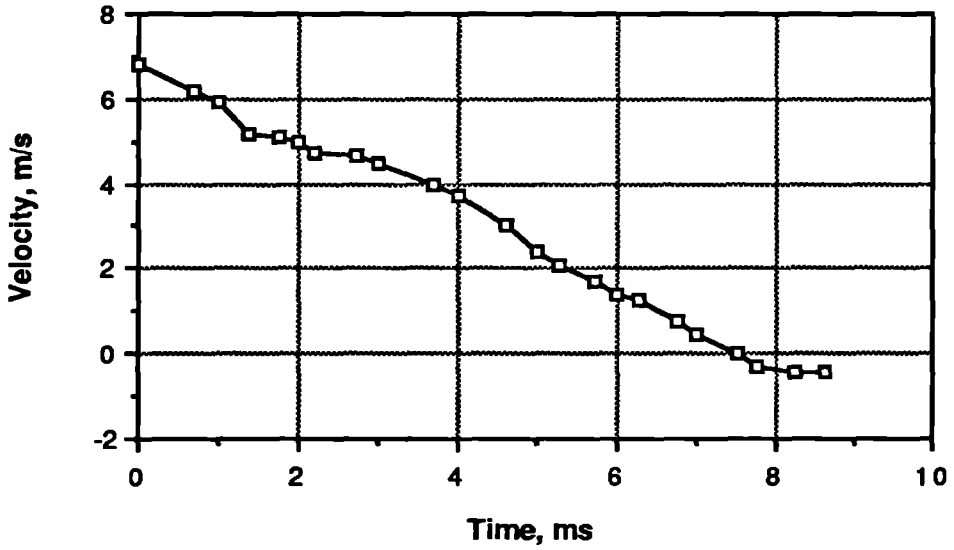


Figure 5.62 Velocity against time.

In conclusion the performance of the laser welded joints appeared to be satisfactory with no evidence of weld failure or tearing in the joint region.

The results indicate that the zinc coated box sections are more likely to fail with an unstable overall buckling form of collapse mode. This de-stabilising effect may be due to the necessity of a gap being maintained at the joint interface during the weld operation. It appears, from a careful study of the photographs, that the failure mode of type A box with lap joints, although mostly irregular, was stable and progressive while the type B flange jointed box tended towards an unstable overall buckling mode. Further experimental work would be necessary to confirm these results specially the possibility of destabilising effect of gap size.

5.4.3.2 Fatigue Test at Renault Motors

These tests was performed by Mr. De Boine of Renault Motors at Senlis (Paris). Fatigue tests were performed on samples of steel sheets of 0.7 mm thickness joined together by lap weld with complete penetration. The welds were performed at Renault (France) and RTM (Italy). The welding conditions are listed in table 5.4.

Table 5.4 Laser Parameters for Fatigue Testing Specimens

Sr. no.	Laser type	Power kW	Speed mm/s	Gap mm	Supplier
1	AVCO	1.5	33	0.068	RTM
2	CILAS	1.25	33	0.016	RENAULT
3	CILAS	1.5	54	0.016	RENAULT

The overall size of the specimen was 250 x 40 mm.

The fatigue test was performed on a JACOTET servohydraulic machine. The test frequency was 24 Hz and a stress ratio R ($R = \partial_{min}/\partial_{max}$) equal to 0.1 was applied. All the tests were carried out till failure or stopped at 10^7 cycles. The S-N curves

corresponding to each welding condition is shown in Figure 5.63.

The results obtained on RTM specimen were compared with Renault specimen. No noticeable difference in results was found between RTM and Renault specimen due to the welding conditions. A fatigue strength of about 85 MPa at 5 x 10^6 cycles was found to be reasonable value regardless of the welding conditions.

No fatigue fracture within the fusion zone was observed in any case. The crack propagation was observed along the interface between the fusion zone and the heat affected zone. Observations of the fractured surface showed that the crack initiated at the interface between the two sheets rather than from the external faces. No effect of width of the gap was found in the initiation site.

Few cavities with a mean diameter of 0.15 mm were observed on the fractured surface. These cavities were probably produced during the welding and do not appear to have any significant effect on the fatigue life. Although the location of the crack initiation is usually difficult to define, none of the cavities appear to be an initiation site.

5.4.3.3 Fatigue Test at CETIM

These tests were performed by Mr. Flavenot of CETIM at Senlis (Paris). Fatigue tests were performed on an electromagnetic fatigue machine (INSTRON Figure 5.64). A stress ratio ($\partial_{min}/\partial_{max}$) of 0.1 was applied. A test frequency of 90-110 Hz was used for various weld geometries shown in the Figure 5.65. The test was considered to be achieved when the frequency decreases by 2 Hz. The use of this criteria was necessary to compare the different weld configurations, whose failure mode much depends upon the weld geometry.

For the continuous linear welds the test is achieved when the crack is about 10 to 50 mm long. The number of cycles necessary to increase the crack length from 10

to 50 mm is very short (10,000 cycles). Hence the fatigue life is approximately equivalent to the number of cycles for which the crack appears on the specimen.

For the continueous non linear welds crack appears on the external face of the specimen at one or several peaks of the sinuous or triangular lines. The crack propagates along the weld 2 to 3 mm and then in the base metal. The number of cycles for propagation to the final number of cycles (for which the machine stops) is greater. For discontinuous welds the crack appears on the external face of the specimen at one or several welding points and then propagates through the base metal.

The graph of fatigue life at 100 MPa against number of cycles for each weld configuration is shown in Figure 5.66. The fatigue life is maximum for the sample without complete penetration. The second maximum fatigue life is in sample in which the weld segments are parallel to the applied stress. Other weld configurations have nearly the same fatigue life. But the spot welded samples have the least fatigue life, of which laser welded samples have more fatigue life than the resistance spot welded samples.

In all the cases the crack initiates on the interface between the welded sheets. For the case to sinusoidal and triangular continuous welds the crack initiate at the peak points of the welds and propagates through the base metal. These peak points acts as a stress raiser hence the crack initiates from the point where the stress is maximum. Similarly spot weded points also acts as stress raiser and crack initiates from the welded spots.

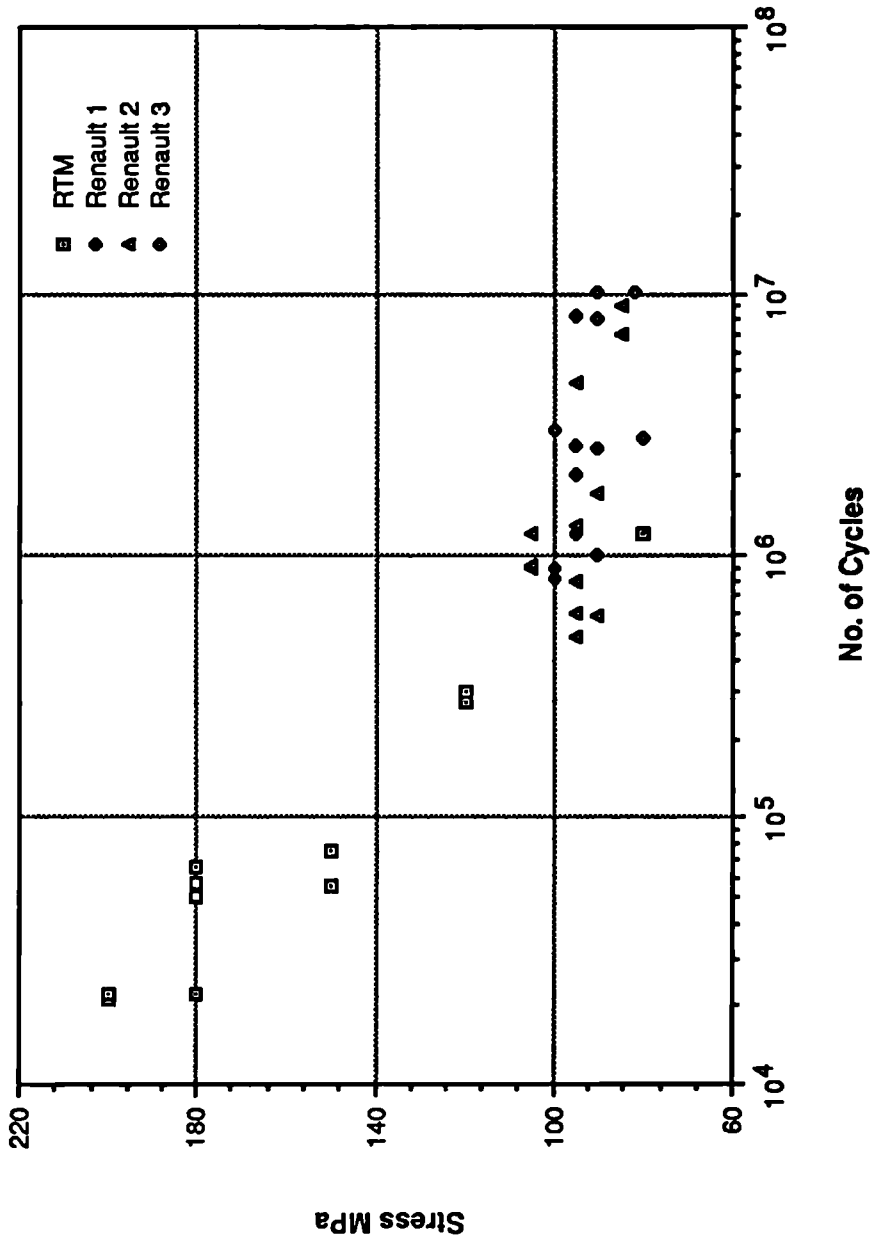


Figure 5.63 S-N diagram corresponding to each welding conditions. Where RTM welding parameters are, power; 1.5 kW, welding speed; 2 m/min, and for Renault 1, power; 1.25 kW, welding speed; 2 m/min, Renault 2, power; 1.5 kW, welding speed; 3.25 m/min, Renault 3, interrupted test of Renault.

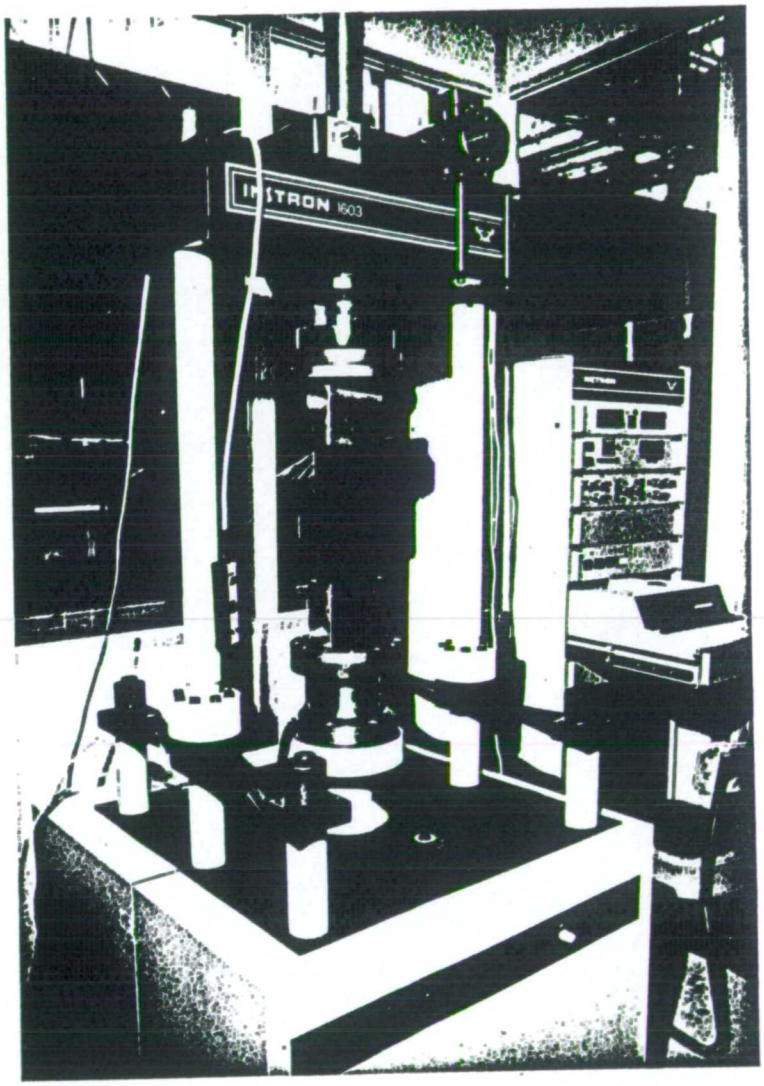


Figure 5.64 View of the fatigue machine at CETIM.

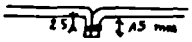
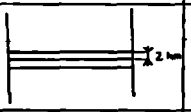
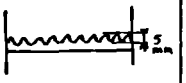
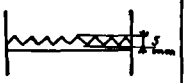
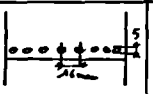
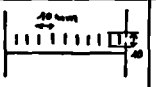
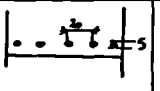
Reference of the specimen	Geometry and weld configuration	Welding laboratory	Conditions Power	Speed
T1	Overlap without complete penetration 	RTM	1,5 kW	30mm/s
T2/1	Overlap with complete penetration 1rst batch 	RTM	1,5 kW	33,3mm/s
T2/2	Overlap with complete penetration sd batch 	RTM	1,5 kW	33,3mm/s
T3		RTM	1,5 kW	33,3mm/s
T4		RTM	1,5 kW	33,3mm/s
L1	Overlap with complete penetration 	LC	8 kW	55 mm/s
L2	Overlap with complete penetration 	LC	5,8 kW	74,1mm/s
TPR	Overlap two parrallel runs 	RTM	1,5 kW	33,3mm/s
SWB	Overlap sinusoidal weld bead 	RTM	1,5 kW	33,3mm/s
TWB	Overlap triangular weld bead 	RTM	1,5 kW	33,3mm/s
CSW	Overlap circular spot weld (laser) 	RTM	1,5 kW	33,3mm/s
O S	Overlap orthogonal segments 	RTM	1,5 kW	33,3mm/s
SWR	Overlap spot wild (resistance) 	RENA LT		

Figure 5.65 Welding configurat'ons for fatigue tests.

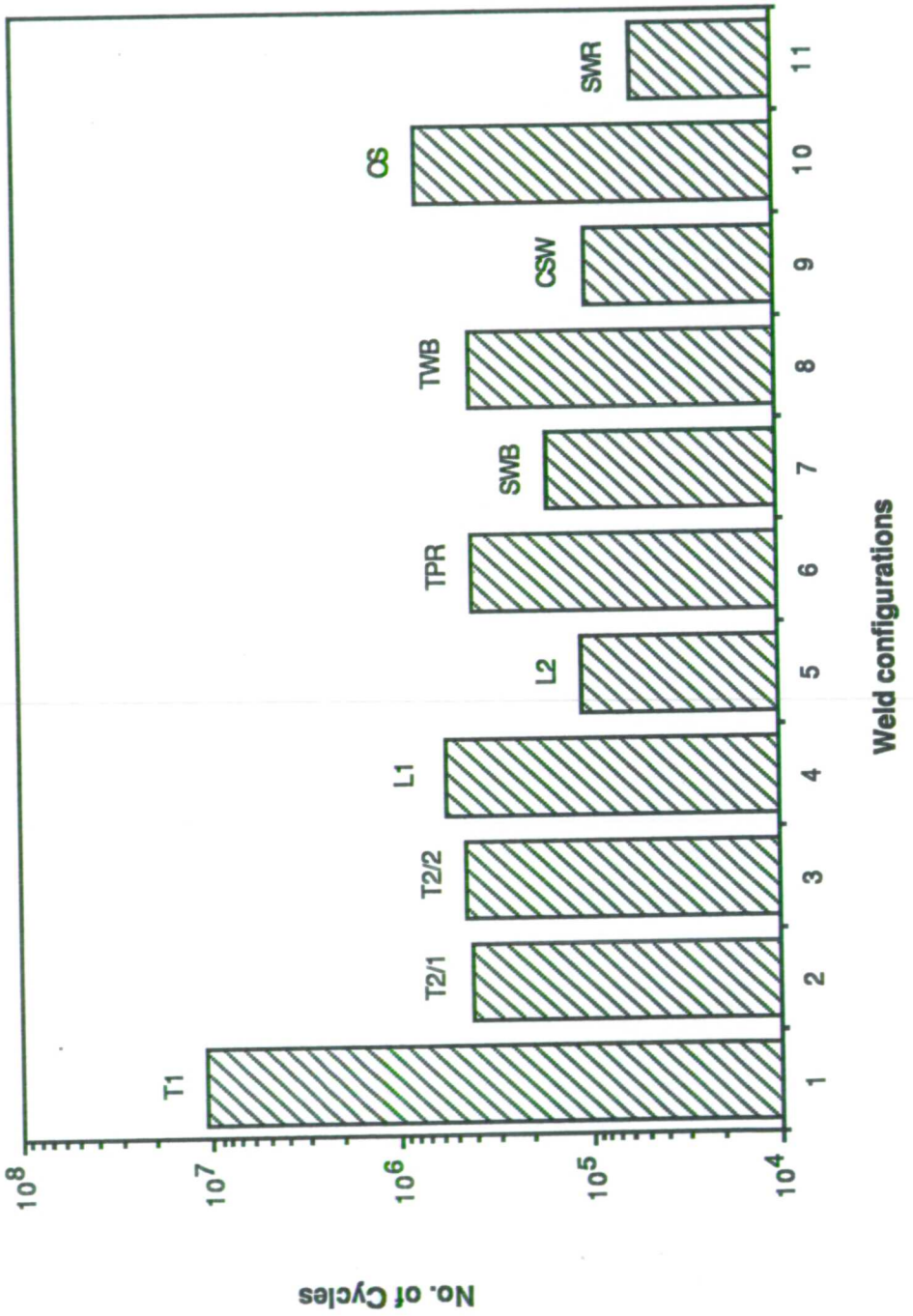


Figure 5.66 Fatigue life for various weld configurations (σ_{max} = 100 M Pa).

Chapter 6

The Gap Model for Welding Zinc Coated Steel

6.1 Introduction

The problem associated with the welding of coated steel sheet is outlined in chapter 1. This problem can be solved by allowing a suitable gap between the sheets during lap welding. Hence full penetration welds without pits or craters can be obtained. There appears to be two basic phenomena which affect the quality of the weld in coated material. Firstly, for large gaps, there is some drop out causing a dip in the upper surface; secondly, at narrow gaps, there is blow out from zinc vapours. It is observed with the blow out type welds that pitting occurs in a remarkably regular manner. It must be remembered that the gap may not be constant along the length of the weld, due to distortion while welding, and so the regularity is not expected to be perfect. The cause of this regularity could be associated with the weld pool size.

6.2 The Gap Model

Considering the welding of coated steel, the zinc coating at the interface is vaporised due to the intense heat produced by the laser Figure 6.1. Since the beam spot is circular, the zinc is removed in the form of a semi circle just ahead of the beam. The problem arises, what happens to zinc just ahead of the beam at point 1, Figure 6.2. This is affected by :

1. The static pressure at point 1 = (Atmospheric + Ferrostatic head),
2. The volume of zinc vapours to be removed per second,

$$= \frac{2t_{zn}V(2b + w)\rho_s}{\rho_v} \qquad (6.1)$$

where

w	= width of weld fusion zone at interface between the plates,	m,
b	= boiling width of zinc,	m,
t_{zn}	= thickness of zinc coating on each plate at interface,	m,
ρ_s	= density of solid zinc,	kg/m^3
ρ_v	= density of vapour zinc,	kg/m^3
V	= welding speed,	m/s.

3. Due to the high vapour pressure developed at the interface the zinc can be exhausted from the molten pool if its vapour pressure is greater than the static pressure at point 1, causing pitting in the weld bead, but if the excess vapour pressure does not exceed the ferrostatic head (say $\rho_l.g_v.t_p$.a mm), then the exhaust of vapour will not be through the "keyhole" or the molten pool but through the gap Figure 6.1. Where 'a' is a wave factor to allow for variations in melt pool depth. It is assumed to be unity here. t_p is the thickness of the sheet. ρ_l is the density of the liquid iron and g_v is the acceleration due to gravity.

4. However in flowing through the gap, the vapour blows over molten zinc which forms waves and condense. This may seal off the gap and the vapour is then exhausted through the weld pool. Also molten zinc may move away from the melt zone due to surface tension effects.

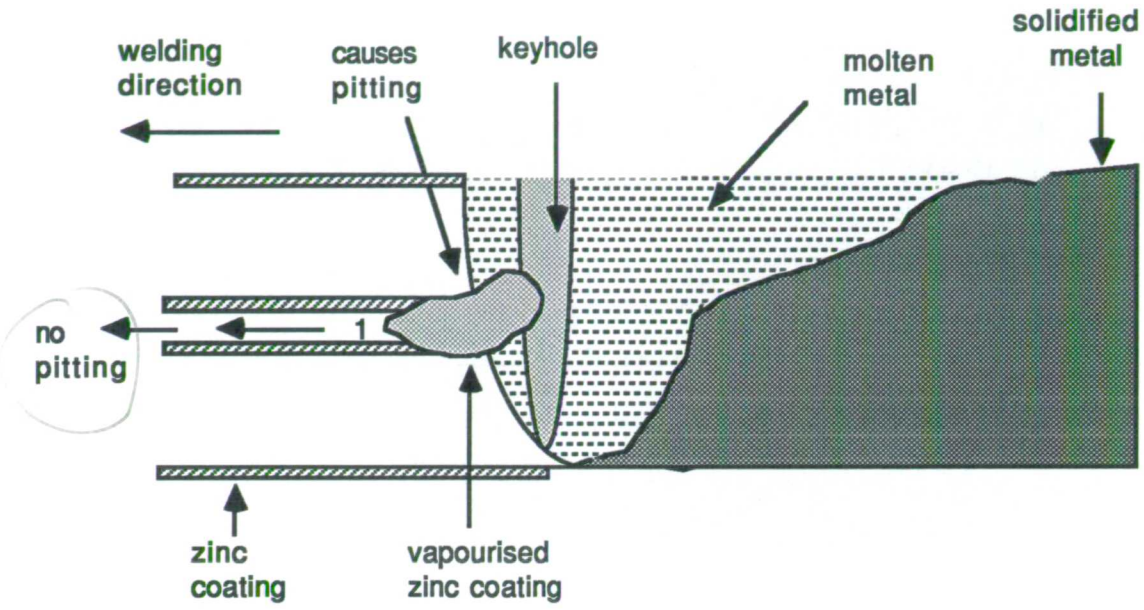


Figure 6.1 The diagram representing the welding of zinc coated steel sheet with a small gap at the interface between the two sheets.

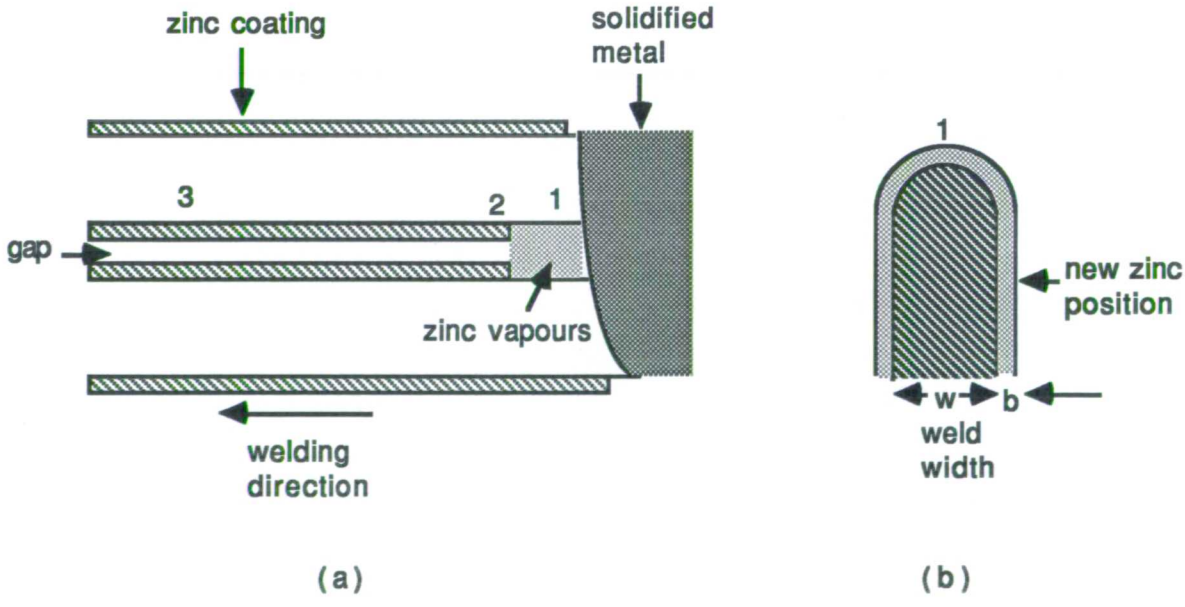


Figure 6.2 The model representing **(a)** the points of pressure variation and **(b)** the new boiling zinc position.

Figure 6.2 shows that the zinc vaporises between points 1 & 2. Now suppose that the zinc vapour condenses at a short distance, r, from the weld pool at point 3. Now applying the equation of Continuity between the two points 2 & 3. Then

$$v_2A_2 = v_3A_3 - \text{condensate}$$

Where v_2 & v_3 are the velocities of vapours at point 2 & 3 and A_2 & A_3 are the areas at points 2 & 3. This condensation may reduce pressure and pull the sheets together. A pulling action of the two sheets, on either side of the weld has been seen in many welds and one such weld is shown in Figure 6.3. This may be due to this phenomenon, the rate of condensation determines flow distance and the pressure drop.

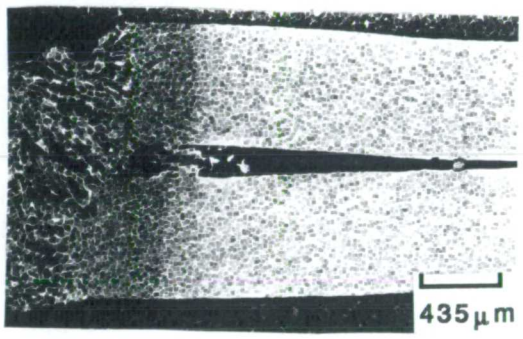


Figure 6.3. Photographs showing that the two sheets are pulled together due to the escape of the zinc vapour at the interface and due to the condensation of the vapours.

To calculate the velocity of the vapours at point 2, we will assume ideal flow and apply the Bernoulli's equation between the points 1 & 2. At point 1 the velocity is zero. Thus

$$\frac{P_1}{\rho_v} = \frac{P_2}{\rho_v} + \frac{v_2^2}{2}$$

Hence

$$v_2 = \sqrt{\frac{2\Delta P_{12}}{\rho_v}} \qquad (6.2)$$

Where P_1 and P_2 are the pressure exerted by vapour at points 1 & 2, and ΔP_{12} is the difference of the two pressures.

Now consider the semi circular area just ahead of the beam spot Figure 6.2 (b), where the zinc vaporises.

The volume per second travelling at velocity, v_2, which can be exhausted through the gap at point 2 is

$$= \frac{v_2 \pi (w + 2b) g}{2} \qquad (6.3)$$

where 'g' is the gap between the two sheets.

Now the volume given in equation (6.3) can be equated with the volume of vapours which must be exhausted to avoid a build up as given is equation (6.1), for a limiting gap size, g. Thus

$$\frac{v_2 \pi (w + 2b) g}{2} = \frac{2 t_{zn} V (w + 2b) \rho_s}{\rho_v}$$

$$v_2 = \frac{4 t_{zn} V \rho_s}{\pi g \rho_v} \qquad (6.4).$$

It is interesting to note here, that the weld width, w, and heat affected zone

(new boiling width of zinc), b, have dropped out of the problem since their action in generating and exhausting vapour are equal.

Now from equations (6.4) & (6.2), we have:

$$\frac{4Vt_{zn}\rho_s}{\pi g \rho_v} = \sqrt{\frac{2\Delta P_{12}}{\rho_v}}$$

Solving for g. We get

$$g_{exit} = \frac{4Vt_{zn}\rho_s}{\pi\sqrt{2\rho_v \Delta P_{12}}} \qquad (6.5)$$

where g_{exit}, is the minimum gap required to exhaust zinc vapour.

Now it has been suggested by correlation with experiments and general reasoning that ΔP_{12} is related to the ferrostatic head in the weld pool:

$$\Delta P_{12} = \rho_l g_v t_p a \qquad (6.6)$$

where ρ_l is the density of liquid iron and a is a wave factor to allow for variations in melt pool depth and is assumed to be unity here.

Thus equation (6.5) becomes

$$g_{exit} = \frac{4 t_{zn} V \rho_s}{\pi\sqrt{2\rho_v \rho_l g_v t_p}}$$

For good quality welds the gap, 'g' should be equal to or greater than g_{exit}. Thus

$$g_{exit} = \frac{AVt_{zn}}{\sqrt{t_p}} \qquad (6.7)$$

where

$$A = \text{Constant} = \frac{4\rho_s}{\pi\sqrt{2\rho_v\rho_l g_v}} \qquad (6.8)$$

To calculate A, the available data are ρ_s = 7135 kg/m^3, ρ_l = 7320 kg/m^3, g_v = 9.8 m/s^2. Here we also need the density of zinc vapour at a temperature of 1800 °K (i.e., at the melting point of steel). Now to calculate the density of zinc vapour, we consider zinc vapour as an ideal gas. Then, we have

$$PV = nRT \qquad (6.9)$$

Now here P is the vapour pressure of zinc. To calculate the vapour pressure P, Clausius Clapeyron equation [161] can be used. The equation can be written as follows:

$$\log p = A.T^{-1} + B.\log T + C.T + D \text{ (mm Hg)} \qquad (6.10)$$

The values of constants available for zinc from ref. [161] are:

A = -6620, B = -1.255, C = 0, D = 12.34

At a temperature of 1800°K, we have

$$\log p = -6620\ (1800)^{-1} + (-1.255).\log 1800 + 12.34$$

Hence p = 37744.63 mm Hg = 49.7 atm = 50.35 x 10^5 N/m^2

Now the data available are

$P = 50.35 \times 10^5$ N/m^2

n = 1

R = 8.314 J/mole-°K

T = 1800 °K

V = ?

Substituting these values in the equation (6.9), we get

$V = 1 \text{ mole} \times 8.314 \text{ J/mole-°K} \times 1800 \text{ °K} / 50.35 \times 10^5 \text{ N/m}^2$

or $V = 0.00297 \text{ m}^3$

Now 1 mole of zinc has a mass = 0.065 kg. Hence the density of zinc vapour is

$\rho_v = 0.065/0.00297 \text{ kg/m}^3$

or $\rho_v = 21.87 \text{ Kg/m}^3$.

Now A can be calculated by putting the appropriate values in equation (6.8). Thus

$A = 16.1 \text{ s/m}^{1/2}$

Hence the equation (6.7) can be written for zinc coated steel as:

$$g_{exit} = \frac{16.1 \, V t_{zn}}{\sqrt{t_p}} \qquad (6.11)$$

It is evident from equation (6.4) that the velocity of the zinc vapour, v_2, is directly proportional to the welding speed, V, and inversly proportional to the gap size. The velocity of the vapour can be calculated for a particular run, in which the data are given as follows:

t_{zn} = 7.5 μm, V = 25 mm/s, g = 0.10 mm

ρ_s = 7135 kg/m^3 ρ_v = 21.87 kg/m^3.

Substituting these values in equation (6.4), we get:

v_2 = 0.78 m/s

Hence the velocity of the vapour at the boiling front for this run is 0.78 m/s.

6.3 Application of the Model

Now applying this theory to the best quality weld obtained, which showed no pitting on the surface of the weld, we have the data for such a good quality weld available from Table 6.5 as:

V = 29 mm/s, g = 0.1 mm, t_p = 0.7 mm, t_{zn} = 10 μm.

The zinc coating in this case is only on one side of the sheet and only one zinc layer is available at the interface. Since our model is based on two layers of zinc at the interface, hence t_{zn} must be divided by 2 in order to evaluate constant (A).

Now from equation (6.7) we have

$$A = \frac{g\sqrt{t_p}}{V\, t_{zn}} \qquad (6.12)$$

Substituting the above values in this equation, we get

$A = 18.25\ s/(m)^{1/2}$

Since the value of A is very near to the theoretical value for a sound weld (i.e., 16.1 $s/(m)^{1/2}$), hence a good quality weld is expected by this theory.

Now applying this theory for a narrow gap g, at which there is pitting in the surface of the weld as given in Table 6.4. The available data are:

$V = 34$ mm/s, $g = 0.04$ mm, $t_p = 0.7$ mm, $t_{zn} = 10\ \mu$m.

Again t_{zn} must be divided by 2, since only one zinc layer was present at the interface. Thus putting these values in equation (6.12), we get:

$A = 6.22\ s/(m)^{1/2}$

The value of A is less than the value for good quality welds, thus at value of g = 0.04 mm, a deteriorated weld is resulted.

Now consider another example this time from a weld made using a variable gap (Table 6.4). The gap was varied from 0.4 mm to zero. The gap was measured at two points, (i) at no pitting and (ii) at the start of pitting. Now first consider the point (i) at which there was no pitting, the data available are

$V = 21.23$ mm/s, $g = 0.345$ mm, $t_p = 0.875$ mm, $t_{zn} = 7.5\ \mu$m.

Putting these values in equation (6.12) we get

$A = 64.1\ s/(m)^{1/2}$

The value of A calculated here is more than the expected value suggesting that the actual gap size is more than the minimum required gap size. The actual gap size can be calculated using equation (6.11), which comes out to be 0.09 mm in this case.

Now consider the case (ii), at which pitting started at a gap of 0.10 mm. The data given are :

$V = 21.23$ mm/s, $g = 0.1$ mm, $t_p = 0.875$ mm, $t_{zn} = 7.5\ \mu m$.

Putting this data in equation (6.12), we get

$A = 18.6\ s/(m)^{1/2}$

The value of A is very close to the value for minimum gap size for sound welds. In fact, a good quality weld should have been obtained at 0.1 mm, but the gap is continuously reducing ahead of the beam, which reduces the available gap required by vapours to exhaust, hence a build up of vapour resulted at 0.1 mm gap and exhausted through the keyhole. Thus pitting started at 0.1 mm gap.

Now applying this model to a pitted weld, made at higher power, 5kW. The data available from (Table 6.4) are

$V = 50$ mm/s, $g = 0.15$ mm $t_p = 0.7$ mm $t_{zn} = 7.5\ \mu m$

Substituting this data in equation (6.12) resulted in $A = 10.6\ s/(m)^{1/2}$. This value of A is less than that of the value for sound quality welds, suggesting that the gap given between the sheets is less than the required gap, hence pitting resulted. Thus it

can be concluded that for a certain value of A equal to or greater than 16.1 $s/(m)^{1/2}$, sound welds without pitting can be obtained and the vapour will exhaust through the gap. Below this value the weld will show pitting because the existing gap size is less than the required gap for sound welds and the vapour is exhausted through the keyhole. The exact gap size required for a sound weld in this case can be predicted using equation (6.11). For this case the predicted gap size is 0.23 mm. Hence a gap of 0.23 mm or greater is required between the sheets for this run. Hence in this way the gap size between the sheet can be predicted for particular laser parameters.

Now the theory is applied using A = 16.1 $s/m^{1/2}$ to a few welds which had an optimum gap size. The data are given in Table 6.1. It can be seen that the plot of gap size, g, against $Vt_{zn}/(t_p)^{1/2}$ is a straight line (Figure 6.4). It is interesting to note that the specimen which had a gap width lower than straight line resulted in pitting on the weld bead (see Table 6.1 for quality of the weld 1J-1). Figure 6.5 shows a plot of experimental and theoretical gap sizes for the same data of Table 6.1. It can be seen that the experimental and theoretical values are very close to each other, and the model we have presented here fits very well with the experimental values.

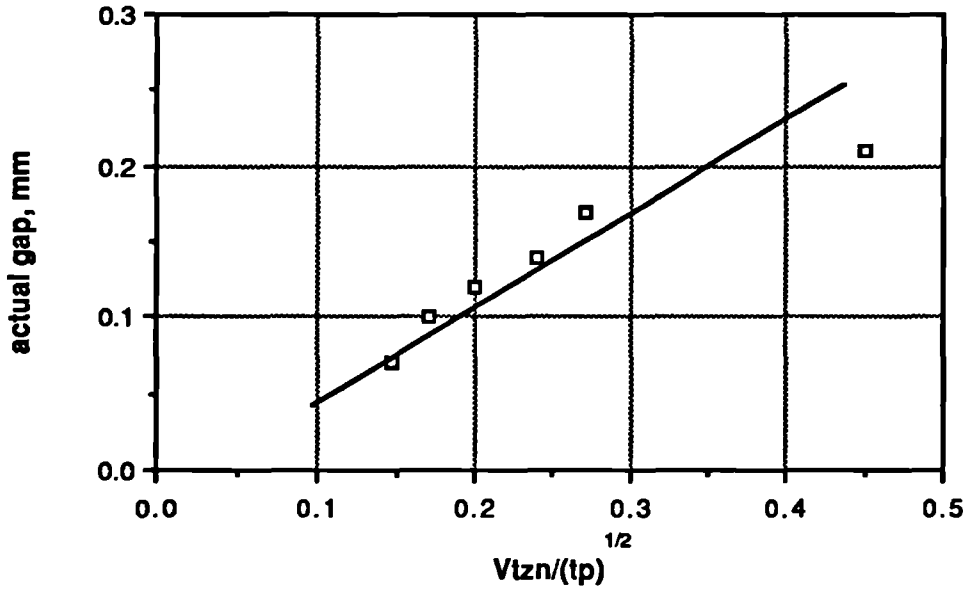


Figure 6.4 Plot of gap, g, against $Vt_{zn}/(t_p)^{1/2}$ shows a straight line.

Table 6.1 Laser Welding Parameters

sample no.	laser power kW	welding speed mm/s	zinc coating μm	zinc at interface μm	sheet thickness mm	theoretical gap mm	measured gap (g) mm	Quality pits/ 100mm	$Vt_{zn}/(t_p)^{1/2}$
M-8	2.00	25	7.5 (2S)	15	0.875	0.10	0.12	S (0)	0.20
Q-1	2.00	24	10 (1S)	10	0.7	0.07	0.07	S (5)	0.15
Q-4	2.00	40	10 (1S)	10	0.7	0.12	0.14	S (0)	0.24
1A-1	1.00	29	10 (1S)	10	0.7	0.09	0.10	S (2)	0.17
1I-2	3.00	30	7.5 (2S)	15	0.7	0.14	0.17	S (3)	0.27
1J-1	5.00	50	7.5 (2S)	15	0.7	0.23	0.15	P (12)	0.45

where, 1S = one sided zinc coated, 2S = two sided zinc coated, S = sound and good quality welds and P = welds with pitting in the weld bead.

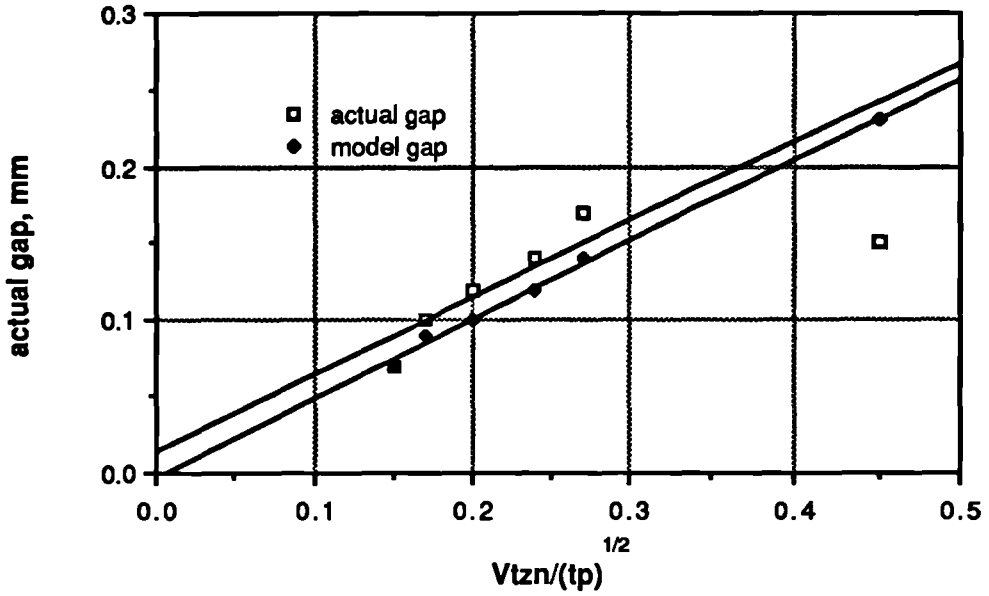


Figure 6.5 Plot of experimental and theoretical results for minimum gap size against $Vt_{zn}/(t_p)^{1/2}$.

Now we apply the theory to a series of welds in order to assess the operating conditions for a good quality weld. It has been found that a smaller gap or zero gap leads to the deterioration of the weld bead because the zinc vapour explodes out of the keyhole weld (Figure 6.6 (a)). An optimum gap size allows the zinc vapour to exhaust through the gap and a good quality weld to be achieved (Figure 6.6 (b)). While a large gap leads to a dip in the weld bead due to a drop out of the molten metal down to the lower sheet making the width of the weld larger at the interface between the two sheets, Figure 6.6 (c) & (d).

Equation (6.7) can be written as follows:

$$\frac{g}{t_p} = \frac{AVt_{zn}}{t_p^{3/2}} \qquad (6.13)$$

Now g/t_p can be plotted against $AVt_{zn}/(t_p)^{3/2}$. Table 6.2 shows the welding parameters for a set of welds in which the gap size was varied keeping all the other parameters constant.

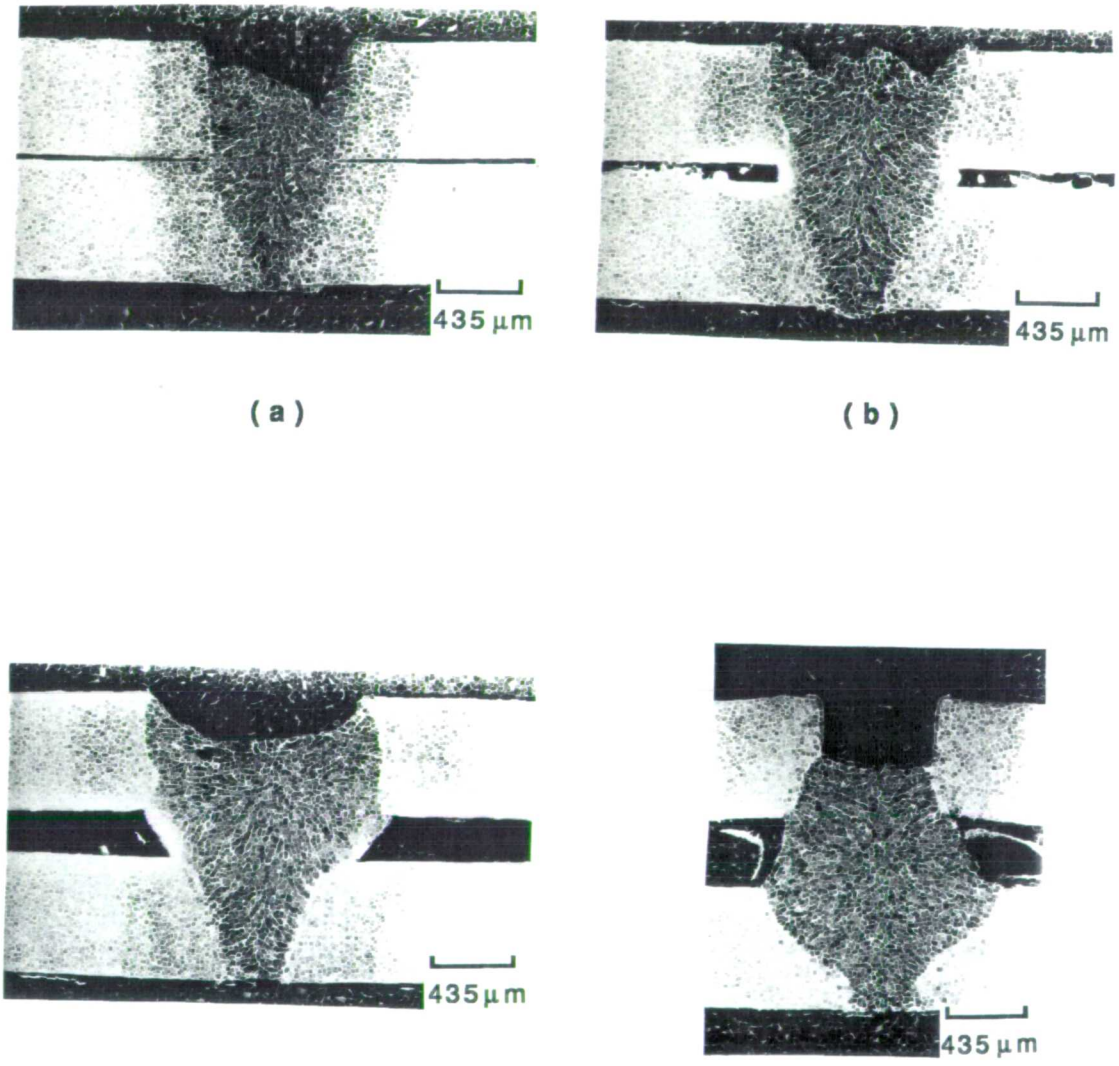


Figure 6.6. Micrographs showing the effect of gap size on weld profile **(a)** zero gap leads to the deterioration of the weld bead, **(b)** an optimum gap leads to a good quality weld, **(c)** large gap size causes extensive heating of the top sheet and make a dip in the weld bead, and **(d)** too large a gap size causes a drop of molten metal down to the bottom sheet leaving a cut in the weld bead.

Table 6.2 Laser Welding Parameters

Laser power, P	1.54 kW
Welding speed, V	20 mm/s
Thickness of zinc coating,	10 μm (1 side)
Zinc thickness at the interface, t_{zn}	10 μm
Sheet thickness, t_p	0.55 mm

sample no.	theoretical minimum gap mm	measured gap, g mm	Quality (pit/100mm)	g/t_p	$AVtzn/(t_p)^{3/2}$
2E-10	0.07	0.11	S (2)	0.200	0.125
2E-11	0.07	0.33	D (20)	0.600	0.125
2E-12	0.07	0.10	S (2)	0.182	0.125
2E-13	0.07	0.04	P (14)	0.073	0.125
2E-14	0.07	0.00	P (26)	0.000	0.125

where S = sound weld; D = drop out; and P = pitting.

Plotting g/t_p against $AVt_{zn}/(t_p)^{3\,2}$ yields a graph as shown in Figure 6.7.

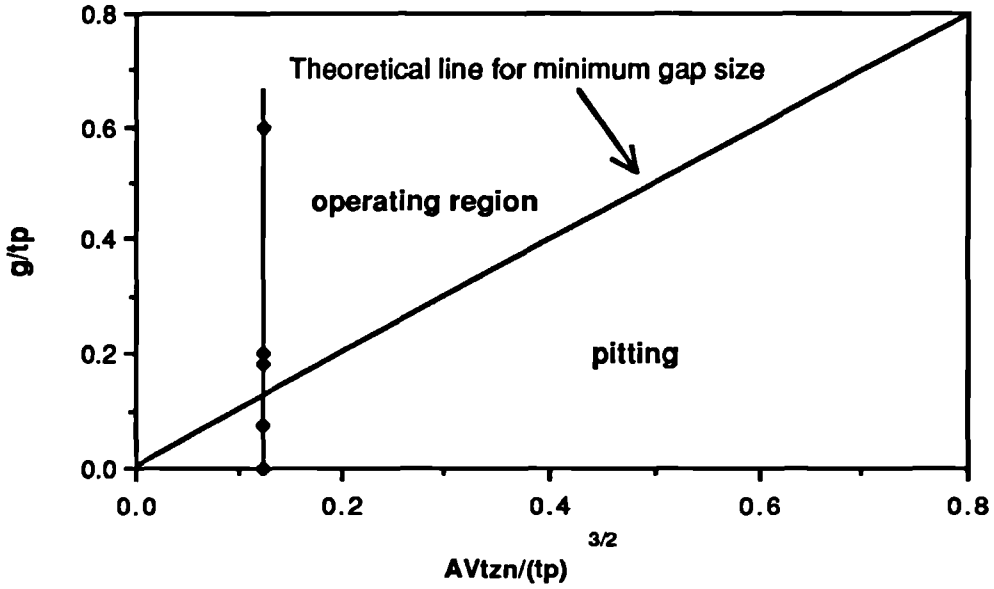


Figure 6.7 Data points plotted for g/t_p against $AVt_{zn}/(t_p)^{3/2}$.

Here the diagonal is the theoretical line taken from the model for minimum gap size required for a sound weld. It is evident that the two points which had a smaller gap than the required gap size and showed pitting are in the pitting region (lower half) of the graph, and other points which gave good quality welds are in the operating region (upper half). Now the theory is applied to a series of weld in which the sheet thickness, the thickness of the zinc coating and the gap size were varied. Figure 6.8 shows a graph of g/tp against $AVt_{zn}/(t_p)^{2/3}$ for such welds. The data is available from Table 6.3.

Table 6.3 Laser Welding Parameters

sample no.	laser power kW	welding speed mm/s	zinc coating µm	zinc at interface µm	sheet thickness mm	theoretical gap mm	measured gap mm	Quality (pits/ 100mm)	g/tp	AVtzn/(tp)$^{3/2}$
2G-2.1	1.54	25	7.5 (2S)	15	0.7	0.11	0.00	P (75)	0.000	0.163
2G-2.2	1.54	25	7.5 (2S)	15	0.7	0.11	0.10	S (0)	0.143	0.163
2G-2.3	1.54	25	7.5 (2S)	15	0.7	0.11	0.24	D (-)	0.343	0.163
2G-2.4	1.54	25	7.5 (2S)	15	0.7	0.11	0.37	D (30)	0.529	0.163
2J-1	1.54	20	10 (1S)	20	0.55	0.14	0.00	P (28)	0.000	0.250
2J-2	1.54	20	10 (1S)	20	0.55	0.14	0.07	P (10)	0.127	0.250
2J-3	1.54	20	10 (1S)	20	0.55	0.14	0.09	Pores	0.164	0.250
2J-4	1.54	20	10 (1S)	20	0.55	0.14	0.18	D (30)	0.327	0.250
2J-5	1.54	20	10 (1S)	20	0.55	0.14	0.37	D (17)	0.673	0.250
2J-6	1.54	20	10 (1S)	20	0.55	0.14	0.37	D (25)	0.673	0.250

Continued.....

sample no.	laser power kW	welding speed mm/s	zinc coating μm	zinc at interface μm	sheet thickness mm	theoretical gap mm	measured gap mm	Quality (pits/ 100mm)	g/tp	$AVtzn/(tp)^{3/2}$
2K-6	1.00	20	10 (1S)	20	0.7	0.12	0.15	S (2)	0.214	0.174
2K-7	1.00	20	10 (1S)	20	0.7	0.12	0.16	S (2)	0.271	0.174
2T-5.1	1.00	15	7.5 (2S)	15	0.7	0.07	0.00	P (40)	0.00	0.098
2T-5.2	1.00	15	7.5 (2S)	15	0.7	0.07	0.09	S (0)	0.129	0.098
2T-5.3	1.00	15	7.5 (2S)	15	0.7	0.07	0.15	S (0)	0.214	0.098
2T-5.4	1.00	15	7.5 (2S)	15	0.7	0.07	0.28	S (0)	0.400	0.098

where S = sound weld; P = welds welds with pitting; D = drop out welds; and Pores = weld which showed good quality weld bead but the cross section revealed a centre porosity in the weld.

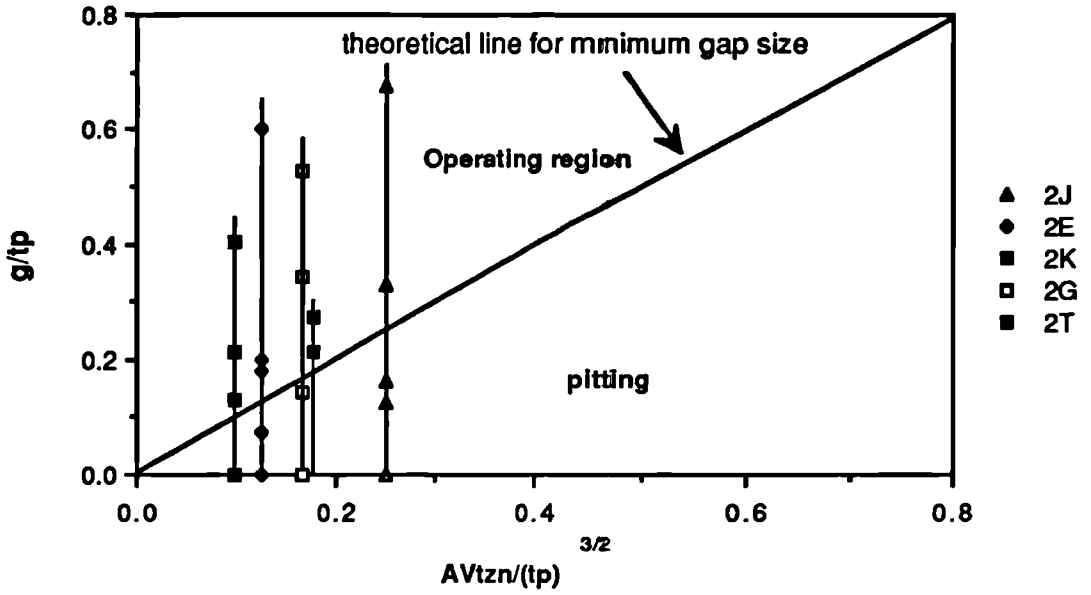


Figure 6.8 Data points plotted for g/t_p against $AVt_{zn}/(t_p)^{3/2}$ for welds with different sheet thickness, and different zinc coating thickness.

It can seen from the Figure 6.8 that there are two distinct regions. First there is a region in which the g/tp is smallar than the required gap size, and where pitting in the weld bead dominated, and secondly there is a region in which g/tp is larger then the required gap size, and where good quality welds are obtained (see table 6.3 for quality of the weld). However, too large a gap size produces a dip in the weld bead by the molten metal flowing down to the bottom sheet.

Now to find the condition under which the drop out occurs, we analyse as under:

During welding the weldment undergoes shrinkage and deformation. The weld pool under consideration is schematically shown in Figure 6.9. The force pulling sheets together comes from the shrinking weld pool.

The amount of metal pulled into the pool/ unit length of the pool $\propto \beta \Delta T\, w\, t_p$. Where β is the coefficent of thermal expansion; ΔT is the temperature; w is the width of the weld pool and t_p is the sheet thickness.

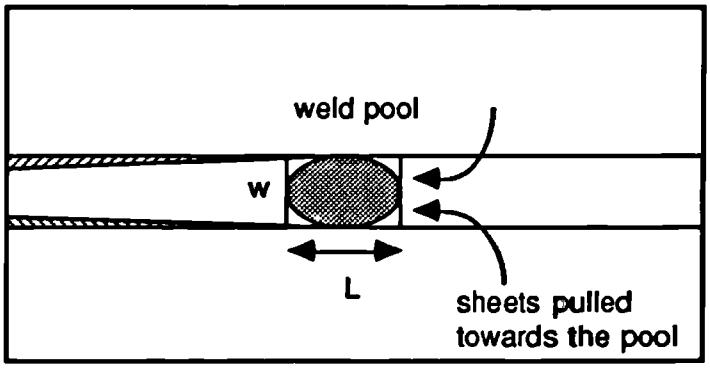


Figure 6.9 The weld pool schematic during shrinkage.

Amount of the molten metal that drops out/unit length of the melt pool $\propto w g$.

Thus when

$$w g \geq A \beta \Delta T w t_p,$$

we have drop out. where A is the constant of proportionality. Therefore,
g/tp = A β ΔT = constant, is the drop out limit.

It has been found from the available data that the drop out occurs for values of g/t_p greater than 0.35 (using Figure 6.6 (c)). Hence, to avoid drop out, g/t_p must be less than 0.35.

Now the theory is applied to a number of welds which showed (i) pitting (ii) no pitting i.e., sound welds and (iii) drop out welds. Table 6.4 shows a number of selected welds which showed pitting on the weld bead, Table 6.5 refered to sound and good quality welds, and Table 6.6 lists those welds which showed drop out on the weld bead. The values of g/t_p and $AVt_{zn} (t_p)^{3\,2}$ were calculated for each weld and are plotted in Figure 6.10.

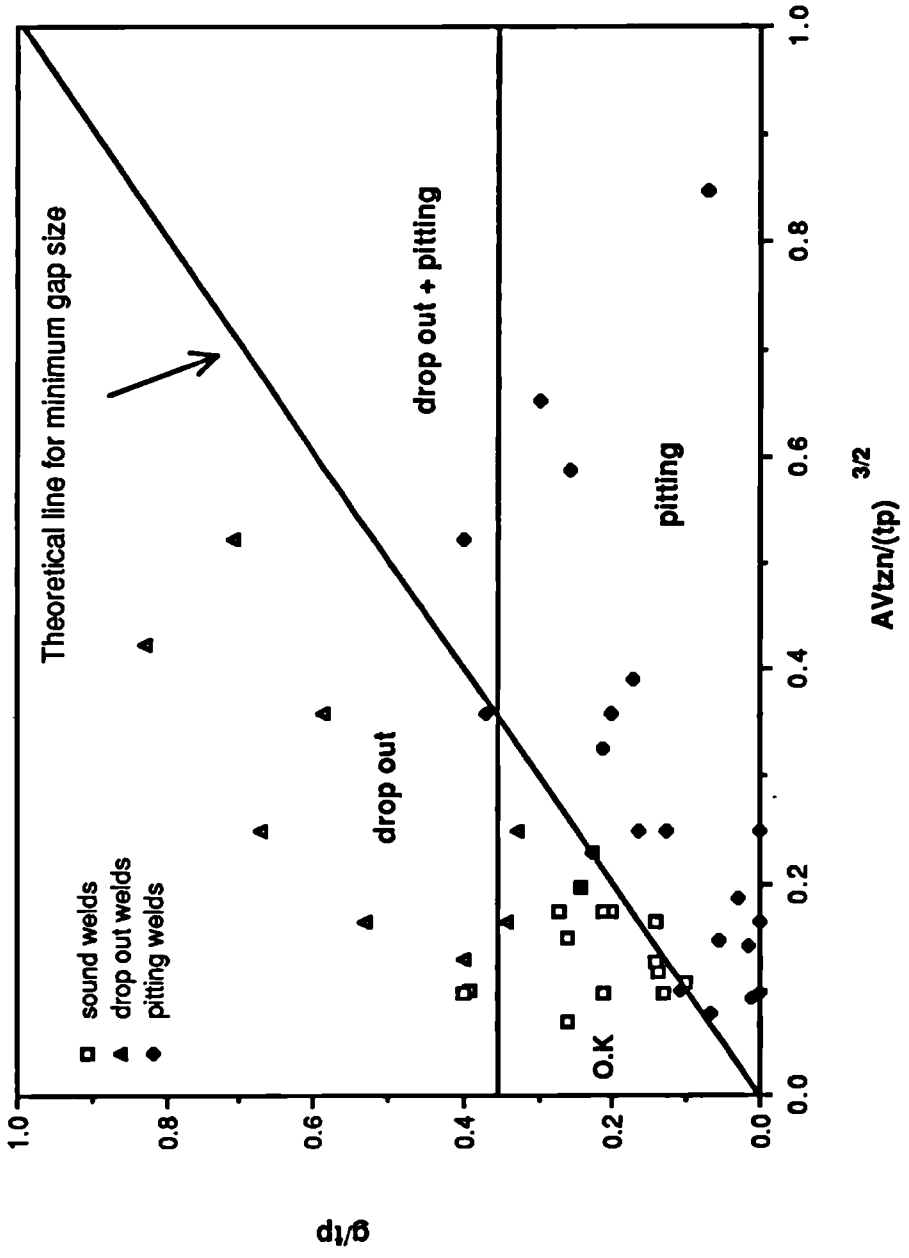


Figure 6.10 Plot of g/t_p against $AVt_{zn}/(t_p)^{3/2}$ for three kinds of welds (i) sound welds (ii) welds showing pitting and (iii) drop out welds. The welding parameters are listed in Tables 6.4 to 6.6.

Table 6.4 Welds With Porosities and Pit on the Surface

sample no.	laser power kW	welding speed mm/s	zinc coating µm	zinc at interface µm	sheet thickness mm	theoretical gap mm	measured gap mm	Quality pits/ 100mm	g/tp	$AVtzn/(tp)^{3/2}$
L-2	1.77	21	7.5 (2S)	15	0.875	0.09	0.1	P (23)	0.11	0.099
M-4	2.00	16	7.5 (2S)	15	0.875	0.07	0.06	P (10)	0.069	0.076
M-6	2.00	20	7.5 (2S)	15	0.875	0.08	0.01	P (13)	0.011	0.093
Q-3	2.00	33	10 (1S)	10	0.7	0.10	0.01	P (14)	0.014	0.142
1A-2	1.00	34	10 (1S)	10	0.7	0.1	0.04	P (11)	0.057	0.148
1A 4	1.00	43	10 (1S)	10	0.7	0.13	0.02	P (43)	0.029	0.187
1I-2	3.00	30	7.5 (2S)	15	0.7	0.14	0.17	P (7)	0.243	0.196
1J-1	5.00	50	7.5 (2S)	15	0.7	0.23	0.15	P (12)	0.214	0.326
1J-2	5.00	55	7.5 (2S)	15	0.7	0.25	0.14	P (22)	0.200	0.359
1J-3	5.00	60	7.5 (2S)	15	0.7	0.27	0.12	P (19)	0.17	0.391

Continued .....

sample no.	laser power kW	welding speed mm/s	zinc coating µm	zinc at interface µm	sheet thickness mm	theoretical gap mm	measured gap mm	Quality pits/ 100mm	g/tp	AVtzn/(tp)$^{3/2}$
1K-2	8.00	90	7.5 (2S)	15	0.7	0.41	0.18	P (9)	0.257	0.587
1K-3	8.00	100	7.5 (2S)	15	0.7	0.46	0.21	P (7)	0.30	0.652
1K-6	8.00	130	7.5 (2S)	15	0.7	0.59	0.05	P (22)	0.071	0.848
2G-2.1	1.54	25	7.5 (2S)	15	0.7	0.11	0.00	P (75)	0.000	0.163
2J-1	1.54	20	10 (1S)	20	0.55	0.14	0.00	P (28)	0.000	0.250
2J-2	1.54	20	10 (1S)	20	0.55	0.14	0.07	P (10)	0.127	0.250
2J-3	1.54	20	10 (1S)	20	0.55	0.14	0.09	Pores	0.164	0.250
2T-5.1	1.00	15	7.5 (2S)	15	0.7	0.07	0.00	P (40)	0.00	0.098
1R-7	5.00	55	7.5 (2S)	15	0.7	0.25	0.23	P (10)	0.371	0.357
1S-9	8.00	80	7.5 (2S)	15	0.7	0.36	0.24	P (21)	0.400	0.522

Table 6.5 Sound and good quality welds

sample no.	laser power kW	welding speed mm/s	zinc coating μm	zinc at interface μm	sheet thickness mm	theoretical gap mm	measured gap mm	Quality pits/ 100mm	g/t_p	$AVt_{zn}/(t_p)^{3/2}$
L-1	1.77	32	7.5 (2S)	15	0.875	0.13	0.23	S (0)	0.260	0.149
L-2	1.77	21	7.5 (2S)	15	0.875	0.09	0.345	S (0)	0.39	0.099
M-3	2.00	15	7.5 (2S)	15	0.875	0.06	0.23	S (3)	0.26	0.07
M-8	2.00	25	7.5 (2S)	15	0.875	0.1	0.12	S (0)	0.137	0.117
Q-1	2.00	24	10 (1S)	10	0.7	0.07	0.07	S (5)	0.1	0.106
Q-4	2.00	40	10 (1S)	10	0.7	0.12	0.14	S (0)	0.200	0.174
1A-1	1.00	29	10 (1S)	10	0.7	0.09	0.10	S (2)	0.14	0.126
1I-2	3.00	30	7.5 (2S)	15	0.7	0.14	0.17	S (3)	0.243	0.196
2G-2.2	1.54	25	7.5 (2S)	15	0.7	0.11	0.10	S (0)	0.143	0.163

Continued .....

sample no.	laser power kW	welding speed mm/s	zinc coating µm	zinc at interface µm	sheet thickness mm	theoretical gap mm	measured gap mm	Quality pits/ 100mm	g/t_p	$AVt_{zn}/(t_p)^{3/2}$
2K-6	1.00	20	10 (1S)	20	0.7	0.12	0.15	S (2)	0.214	0.174
2K-7	1.00	20	10 (1S)	20	0.7	0.12	0.16	S (2)	0.271	0.174
2T-5.2	1.00	15	7.5 (2S)	15	0.7	0.07	0.09	S (0)	0.129	0.098
2T-5.3	1.00	15	7.5 (2S)	15	0.7	0.07	0.15	S (0)	0.214	0.098
2T-5.4	1.00	15	7.5 (2S)	15	0.7	0.07	0.28	S (0)	0.400	0.098

Table 6.6 Welds With Drop out on the Surface

sample no.	laser power kW	welding speed mm/s	zinc coating µm	zinc at interface µm	sheet thickness mm	theoretical gap mm	measured gap mm	Quality pits/ 100mm	g/t_p	$AVt_{zn}/(t_p)^{3/2}$
1I-1	3.00	20	7.5 (2S)	15	0.7	0.09	0.28	D (15)	0.400	0.130
1I-3	3.00	35	7.5 (2S)	15	0.7	0.16	0.42	D (21)	0.229	0.228
1K-1	8.00	80	7.5 (2S)	15	0.7	0.36	0.50	D (10)	0.71	0.522
2G-2.3	1.54	25	7.5 (2S)	15	0.7	0.11	0.24	D (-)	0.343	0.163
2G-2.4	1.54	25	7.5 (2S)	15	0.7	0.11	0.37	D (30)	0.529	0.163
2J-4	1.54	20	10 (1S)	20	0.55	0.14	0.18	D (30)	0.327	0.250
2J-5	1.54	20	10 (1S)	20	0.55	0.14	0.37	D (17)	0.673	0.250
2J-6	1.54	20	10 (1S)	20	0.55	0.14	0.37	D (25)	0.673	0.250

It is evident from the Figure 6.10 that almost all the welds which have shown deterioration and pitting in the weld bead fall into the pitting region defined by a smaller gap size. Those welds which showed no pitting fell into the operating region (O.K.) of optimum gap size. Welds with drop out in the weld bead fell into the region of higher gap. Hence this model predicts the accurate gap size required for welding zinc coated steel. Sound welds can be obtained if the welding parameters are matched in the operating region according to Figure 6.10. Hence this model is a useful tool for welding zinc coated steel in lap configuration.

A few welding runs were performed by FIAT Motors, Italy, according to this model using cw CO_2 laser at Liverpool University. A small gap was maintained between the overlapped sheets. Their results confirmed that if the gap given was more than the theoretically calculated gap a sound weld bead was achieved, but if the gap given was less than the theoretically calculated gap, the weld bead showed pits in the surface. The experimental data and the results are shown in Table 6.7.

Table 6.7 Laser Welding Parameters and Results Using the Model

Sr. no.	laser power (kW)	welding speed (mm/s)	zinc coating (μm)	zinc at interface (μm)	sheet thickness (mm)	theoretical gap (mm)	nominal gap (mm)	Quality pits/ 100mm
1	1.9	22	10	20	0.8	0.13	0.15	0
2	2.0	30	10	20	1.2	0.14	0.15	0
3	2.0	35	10	20	1.2	0.16	0.15	4

6.4 How to Use the Model

It should be remembered that for a constant power and sheet thickness, there is a range of welding speed beyond which welding is not possible. Higher welding speeds

lead to improper penetration, while lower welding speeds lead to extensive heating of the workpiece and drop out of molten metal leaving holes in the weld bead. Our model is based on that range of welding speed where welding is possible. Hence to use the model one needs to first find the range of welding speed for full penetration to the sheet. This can be done on an uncoated sheet. After selecting a certain welding speed, a minimum gap size required to weld zinc coated steel sheet can be predicted by equation (6.11). Alternatively a certain welding speed can be predicted for a particular gap size. The laser power can be varied until full penetration to the bottom sheet is achieved.

The increase in laser power serves to increase the range of welding speed. Hence the increase in power affects the model only by increasing the welding speed. Such an increase in welding speed requires the gap size to be increased according to equation (6.11). But the gap size is limited for a good quality weld, smaller gap size leads to the pitting of the weld bead and higher gap size leads to a drop out in the weld bead. Thus at a higher gap and higher welding speed it is almost impossible to obtain a good quality weld free of pits and drop out.

Chapter 7

Corrosion Studies

7.1 Introduction

Sheet steel is the main material used for the construction of the body of a motor vehicle. Steel is relatively cheap, with good mechanical properties, and can be formed economically to make parts with complicated shapes. Car manufacturers are aiming to guarantee cars for 5 years against cosmetic corrosion (on the outer surface of the car body) and for 10 years against perforation corrosion (propagating from the inner surface of car body) [115]. This challenge is particularly difficult to meet in regions where salt damage may occur as a result of snow-melting agents that are deposited on roads to ensure safe traffic in the winter. To meet this challenge the automotive industry has dramatically increased the usage of zinc coated steels.

This chapter considers aspects of the corrosion resistance of laser welded electrogalvanised steel sheet. In particular, this work considers the provision of sacrificial protection of the weld by the zinc coating at a lower self corrosion rate (and hence with a longer life) as a result of compositional modifications made to the weld metal by the techniques of metal powder injection or redeposition of volatilised zinc during welding.

Corrosion tests are made for a variety of reasons, for example, (i) to assess the quality of a protective coating, metallic or non-metallic, (ii) to determine how long a material will survive in a specified environment, (iii) to determine the corrosion resistance of a new metal or alloy, while alloys of known corrosion resistance are included for comparison, (iv) to study the corrosion mechanism.

The corrosion testing parameters are temperature, aeration of electrolyte, duration of the test and type of solution (i.e., the aggressive ions e.g., Cl^-). Temperature is an important factor and should be controlled. An increase in temperature exponentially increases the reaction rate. However, raising the temperature can reduce the solubility of a dissolved gas, or it can form a protective film of corrosion products tending to lower the corrosion rate.

Test duration is another significant factor. If the test is too short, the protective film of corrosion product may not have time to develop and passivity may not be achieved. Then the long-term corrosion rate is not obtained. If the test is too long the specimen may be destroyed by corrosion or the data may no longer be needed.

Aeration is of importance since in many cases corrosion is theoretically impossible without oxygen. Many corrosion mechanisms are controlled by the rate of diffusion of dissolved oxygen to the metal surface.

In most of the applications the car body is normally phosphatised and painted for better appearance and to improve its corrosion resistance. But a scratch or scribe mark in the coating leads to the corrosion of the substrate which increases underneath the paint coating. Standish [162] studied the atmospheric corrosion behaviour of painted steel in two cases. In the first case aluminum killed cold rolled steel was given a paint coating and in the second case the steel was given a phosphate treatment before painting. In both cases a scribe was applied through the coating to reveal the steel surface. The steel panels were then subjected to atmospheric corrosion and the corrosion was monitored approximately each month for five months. Standish found that the corrosion initiated beneath the paint film in a crevice formed by scribing. The build up of corrosion products beneath the paint film drove a crack along the paint/substrate interface thus spreading the corrosion. The build up of corrosion products caused defects to form in the paint film. He found that phosphating reduced the corrosion rate by increasing the polymer/substrate adhesion and slowing down the crack growth at the interface.

The application of a zinc coating to steel reduces the corrosion of the steel substrate. Most of the car manufacturers are changing over to zinc coated steel due to its better corrosion properties. There are two main reasons [5,163] why zinc is chosen as a protective coating for iron and steel. The first is the natural resistance of zinc itself against corrosion in most atmospheric conditions, and the second is the fact that zinc is electronegative to iron and steel and can protect it sacrificially (see section 7.2). Zinc is protected against further attack by a film of corrosion product. It is remarkably resistant to atmospheric corrosion except perhaps in the most heavily contaminated industrial areas, and even there its use as a protective coating is still a sound practical and economic proposition. The natural resistance of zinc is therefore its most important property in relation to zinc coating.

The electrochemical property becomes important when the zinc coating is damaged in any way to expose the steel, when sacrificial corrosion of zinc occurs and the steel is thereby protected [164-174]. Moreover, the corrosion product of the zinc normally fills the break in the coating and prevents further corrosion of the exposed steel.

7.1.1 The Mechanism of Sacrificial Protection

The mechanism of the sacrificial protection of steel by zinc has been widely investigated [5,171,172] and can be summarised as follows (Figure 7.1). For a metal M immersed in an aerated aqueous electrolyte, a steady state free corrosion potential, E_{corr}, is established when the rate of the anodic (metal wastage) reaction which generates electrons is balanced exactly by suitable cathodic reactions which consume electrons.

For steel the anodic reaction is:

$$Fe \rightarrow Fe^{++} + 2e^{-} \qquad (7.1)$$

and the cathodic reactions are:

$$1/2\ O_2 + H_2O + 2e^- \rightarrow \quad 2OH^- \qquad (7.2)$$

and/or

$$H_2O + e^- \rightarrow \quad 1/2\ H_2 + OH^- \qquad (7.3).$$

Then the corrosion rate w'll be given by i_{corr} (Figure 7.1). General corrosion of steel would occur by the rapid periodic shifting of small anodic and cathodic sites, or by the simultaneous operation of the above anodic and cathodic reactions over the whole exposed surface.

If a potential is applied that polarises the corroding metal cathodically, electrons are supplied. This serves to increase the rate of the cathodic reaction (equation 7.2 and/or 7.3) while decreasing the rate of the metal wastage reaction (equation 7.1). As a result the cathodic reaction rate is increased to i'_c while the rate of the metal wastage reaction is reduced to i'_a by the application of cathodic polarisation potential ε_c. However, in the case of sacrificial protection of steel by zinc this polarising potential must be supplied as a result of the self corrosion of zinc which generates electrons by:

$$Zn \rightarrow \quad Zn^{++} + 2e^- \qquad (7.4).$$

Figure 7.2 shows for a system controlled by oxygen reduction that polarisation of steel to a potential, $E_{coup\ e}$, close to the open circuit potent al of zinc as a result of galvanic coupling results in a reduction of the corrosion rate of steel to i_{Fe}. However, zinc must self corrode at a rate i_{Zn} and hence this form of protection, while it is highly effective, is accurately referred to as 'sacrificial' since the life of zinc under these conditions will be limited.

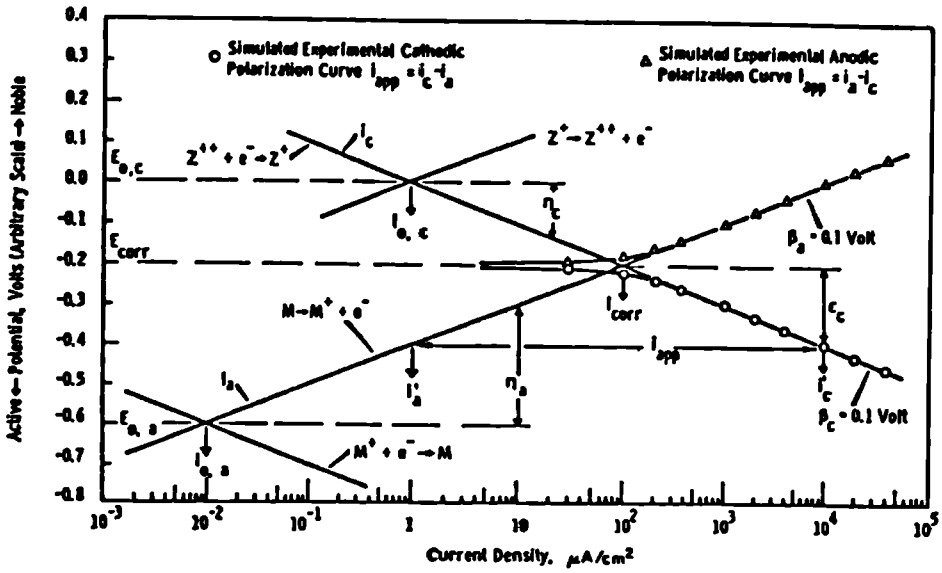


Figure 7.1 Anodic and cathodic Tafel curves for corrosion of metal M showing the principle of cathodic protection [171].

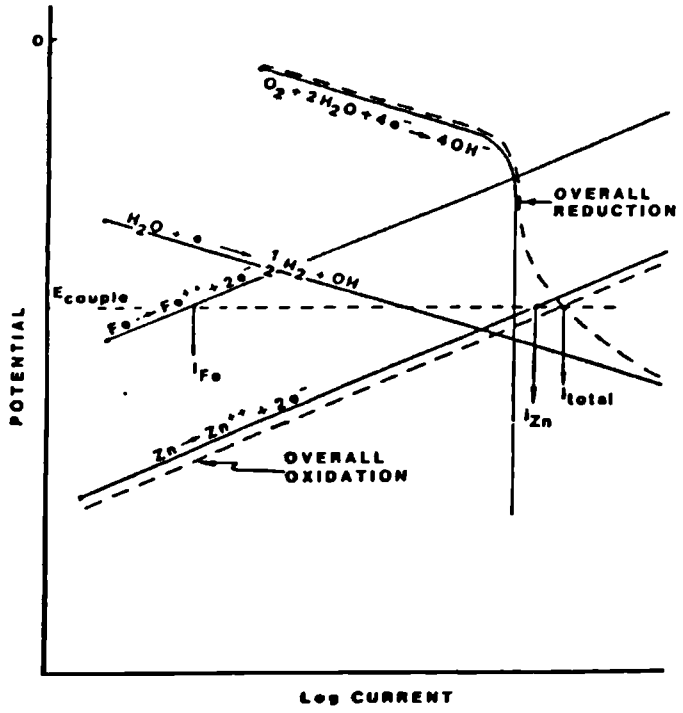


Figure 7.2 Schematic mixed potential diagram for a zinc-steel couple in aerated salt water solution [172].

Haynie [175] studied the environmental factors which affect the corrosion of galvanised steel. He found that in polluted environments, sulphur dioxide reacts with zinc of galvanised steel to form soluble zinc sulphate. Zinc corrosion damage has been shown to vary directly with the atmospheric concentration of SO_2 [176-178]. In clean environments a protective film of zinc carbonate is formed on galvanised steel. In the absence of acidic deposition and marine influences, the atmospheric corrosion of zinc involves first the formation of zinc oxide, or hydroxide [179]. Equilibration with atmospheric CO_2 then leads to the formation of basic zinc carbonates [180]. This film also provides some degree of protection to the underlying zinc [181]. Rain contributes significantly to the corrosion of zinc by dissolving the protective corrosion product film [182]. The film structure and solubility may vary with the season in which exposure started. The solubility of zinc carbonate is proportional to the concentration of carbon dioxide (CO_2) in solution [183], which in turn is proportional to atmospheric level of CO_2. The solubility of CO_2 in water decreases with increasing temperature [184].

Berke and Friel [185] conducted electrochemical tests on galvanised and several aluminum-zinc coatings whose long term atmospheric corrosion resistance was known. They used different electrolytic solutions (1N NaCl, 0.5 Na_2SO_4, 1N HCl, 1N H_2SO_4) to rank each coating and then compared the ranking with the available data of long-term marine and industrial exposures. They found that the relative corrosion rates determined by polarisation resistance and mass loss of the coatings in aerated pH 4 chloride and sulphate solutions were in agreement with those observed in long-term marine and industrial exposure, while the corrosion rates in 1N HCl and 1N H_2SO_4 acid were exaggerated for the zinc coatings. Thus the linear polarisation testing in pH 4 solution showed promise as a screening tool for predicting the relative long-term atmospheric corrosion performance of metallic coated steels.

Jones and Nair [164] studied the corrosion behaviour of pure Zn, Al-Zn and Zn-Ni coatings on sheet steel. They found that (in both aerated and deaerated chloride

solution of pH 7) steel was protected cathodically when exposed by machining a scribe through a zinc or zinc-alloy coatings in the steel. In aerated solutions, the corrosion rates of the coatings were high and thus the coating life time was low during continuous immersion. In deaerated solution corrosion rates were considerably lower, and hence the coating life time could be expected to be improved. For all coatings, the corrosion rate in deaerated solutions with a scribe was higher than the corrosion rate of the unscribe coating. This increase was a measure of the galvanic current between the exposed steel in the scribe and the surrounding coating materials (Figure 7.3).

Jones and Nair [164] found that there was no significant difference between the corrosion potential (E_{corr}) of scribed and unscribed specimens, which indicated that the steel surface exposed by the scribe was cathodically polarised to a potential very near the coating corrosion potential, resulting in cathodic protection of the steel surface. They found that the corrosion is controlled by the combined reduction of dissolved oxygen and hydrogen evolution.

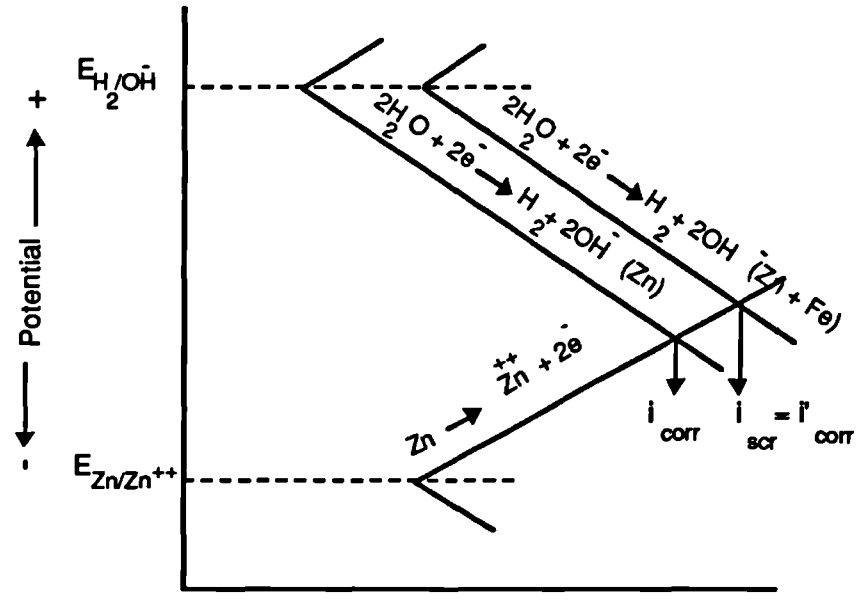


Figure 7.3 Mechanism of corrosion rate increase from i_{corr} to $i'_{corr} = i_{scr}$ on scribed specimen in deaerated solution [164].

For the case of a Zn-Ni (13 % Ni, Bal. Zn) coating Jones & Nair [164] found that the coating did not maintain an active potential with time, presumably because the surface became enriched in nickel, which has a rather noble corrosion potential. Hence the Zn-Ni coating appeared to protect steel by a barrier layer mechanism rather than by galvanic dissolution after a certain period of exposure. Al-Zn (55% Al, 43.4% Zn, 1.6% Si) coatings exhibited an active corrosion potential and lower corrosion rate in both aerated and deaerated solutions. They reported that the Al-Zn coating showed a considerably lower corrosion rate than pure zinc in both aerated and deaerated solutions.

Watkins *et al.* [169] studied a number of metallic coatings on steel strip including Zn, Zn-Fe, Zn-Ni, and Al for their sacrificial action. They reported that there is a relation between the free corrosion potential of the coating with respect to bare steel and the corrosion rate. The increasingly negative free corrosion potential exhibited an increase in corrosion rate of the coatings. They found that the coating types displayed the following order of increasing corrosion rate: Al, Zn-Ni, Zn-Fe, Zn. This had the same order as that obtained by considering increasing negative difference in potential with steel. The Zn and Zn-Fe coatings showed a relatively large difference in potential with steel suggesting that the coating would be expected to sacrificially protect bare steel. In the case of the Zn-Ni coating the preferential depletion of zinc led to a more noble potential, hence prolonged exposure would not be expected to provide a sacrificial action to the steel. The Al coating initially showed a more noble potential than the bare steel for a short period of time and hence, it was not expected to provide a sacrificial action to the bare steel.

The corrosion tests on 55 Al-Zn coating were also studied by Watkins *et al.* [170]. The tests on this type of coating showed a free corrosion potential close to that of zinc, which indicates that the free corrosion potential was sufficiently negative with respect to bare steel and hence this coating is expected to provide sacrificial protection to the underlying steel. However, selected dissolution of the Zn rich phase resulted in a progressively more noble potential and subsequent loss of sacrificially

protective effect.

Lambert *et al.* [186] studied the mechanism of Zn-Ni alloy electrodeposited coatings containing 13% Ni. They reported that during the early stages of corrosion the Zn-Ni alloy coating behaved sacrificially to the steel substrate, but the coating was not as active as an unalloyed zinc coating. As the corrosion proceeded the zinc dissolved preferentially (dezincification) from the alloy coating, leaving a nickel rich coating which was more noble. Thus the coating was transformed into a less galvanically protective composite comprising deposits of zinc corrosion product and the nickel rich metallic phase. However the Zn-Ni coating showed superior salt-spray corrosion resistance than the unalloyed zinc. This is probably attributable to the slower anodic dissolution kinetics leading to a lower corrosion rate and secondly to the barrier protection provided by the composite remaining subsequent to dezincification.

Hadden [187] reported the results of atmospheric exposure tests at Euston, London, on heat treated galvanised sheets and wires. He showed that with up to 12% iron in the coating (due to interdiffusion of iron during heat treatment), the life of zinc coating was almost the same as that of unannealed coatings, but with a coating containing 22% iron, the life of the coating increased to more than three times the life of an unannealed coating. He suggested that the longer life of zinc coating is a characteristic of the corrosion product. The rate of corrosion may be reduced because of a thin black layer of an insoluble compound on the surface of the corrosion products.

Campbell [188] confirmed that heat treatment of zinc coated steel to introduce more than about 15% iron in the coating gives longer lives for specimens exposed to a moderately severe industrial atmosphere. But the coating containing around 10% iron gave shorter lives than the corresponding un-heat treated coatings.

7.1.2 Corrosion Resistance of Welded Joints

Shatov *et al.* [189] compared the corrosion resistance of welded joints in zinc coated and uncoated pipes used in water supply systems. A nozzle of diameter 21.3mm was welded with the main pipe of 26.8 mm diameter in T configuration. The weld with respect to zinc coating showed three distinct regions: (i) in the region of heat affected zone (HAZ) adjacent to the fusion boundary, where temperature exceeds 906° C, the zinc burns out completely, (ii) in the region in which the temperature is near the melting point of zinc 419° C, the zinc melts and partially oxidises; (iii) the region with a temperature of less than 419° C is characterised by the partial melting and recrystallisation of zinc.

To ascertain the corrosion resistance of the welded joints, the pipe with the nozzles welded to them were installed in a circuit for internal hot water (of hydrocarbonate grade at 30-40° C) supply. The main corrosion rate was determined by the weight loss method. They reported that the corrosion rate of uncoated pipes was 20-25 times greater than that of zinc coated pipes. Wirth [103] using a laser for welding zinc coated steel found that the the weld seam was very narrow and hence the weld was still protected due to the presence of zinc around the weld.

Fedrizzi *et al.* [190] studied the corrosion behaviour of laser welded AISI'304 and 316 stainless steel plates (5mm thick). They correlated the corrosion behaviour to the microstructure of the weld. They found that during the first minutes of immersion the weld bead acted as a cathode as a result of its better tendency to passivity. Yet, after a few minutes the polarity changed, but there was no evidence of galvanic corrosion. The microstructure mainly consisted of austenite. Also delta ferrite presence was noted in various amounts and shape due to the different cooling rates originating in the weld bead. They reported that the laser welded structure showed better corrosion resistance than the base metal. However a shallow intergranular corrosion attack was found at the interface between bulk material and weld bead.

7.2 Experimental

Welds fabricated under normal welding conditions and those in which weld composition was modified as described in chapter 4, were used for corrosion testing.

7.2.1 Corrosion Testing

The zinc coated steel with weld at the centre, for all types of welds, were subjected to two types of corrosion tests (i) linear polarisation technique and (ii) galvanic coupling test.

Corrosion rate is found to be increased in the presence of an aggressive electrolyte containing, for example, chloride ions. Similar conditions normally exist when a car body gets wet during rain. The rain water picks up sodium chloride from the road which is deposited on the roads for melting of snow. The salt water stays on the car body for some time. But when it starts drying off, the sodium chloride concentration is increased in the thin layer of electrolyte that remains. At this point the corrosion of the metal sheet is found to be at its maximum. For laboratory corrosion testing an electrolyte which contains chloride ions in the solution will approximate the conditions the car body faced during corrosion. To simulate these conditions, an aggressive electrolyte consisting of 1N NaCl (pH 4) was used in these tests to accelerate the test [185].

7.2.1.1 Linear Polarisation Technique

The linear polarisation technique offers the advantage over other techniques in that the test can be completed in a short time and because the polarisation applied is small, the applied potential does not disturb the system, thereby permitting the periodic monitoring of instantaneous corrosion rates. In addition very low corrosion rates can be measured with the same precision and degree of accuracy obtained in

measuring high corrosion rates [191].

When a metal is not in equilibrium with a solution of its ions, the electrode potential differs from the free corrosion potential by an amount known as the polarisation (also called overvoltage or overpotential). Polarisation is an important corrosion parameter which enables useful statements to be made about the rates of corrosion processes.

Disc specimens of diameter 2 cm^2 were cut from the welded sample with the weld at the centre of the disc. Some unwelded specimens were also prepared in order to compare the corrosion rates of welded and unwelded samples. A specimen holder was used to expose an area of 1.77 cm^2 of the disc and provide an electrical contact for the application of a polarising potential.

The polarisation cell (Figure 7.4) consisted of a flask containing an electrode, the specimen holder and a probe filled with 1N NaCl solution which provided a salt bridge to an external saturated calomel electrode (S.C.E). The working electrode is the name given to the electrode being investigated. The auxiliary electrode is the second electrode which is present specifically to carry the current in the circuit created by the investigation. It is not required for measurement of potential. Usually, it is made of any material which will not introduce contaminating ions into the electrolyte. In this investigation a platinised titanium electrode was used. The reference electrode is present to provide a very stable datum point against which the potential of the working electrode can be measured. The cell was filled with 1N NaCl solution of pH 4. This solution was employed to provide a short term test to simulate the effect of aggressive electrolytes encountered in exposure to road salt environments. The procedure followed was to allow the specimen to freely corrode in the test solution whilst monitoring the corrosion rate established at intervals during a 50 h period by means of the linear polarisation technique.

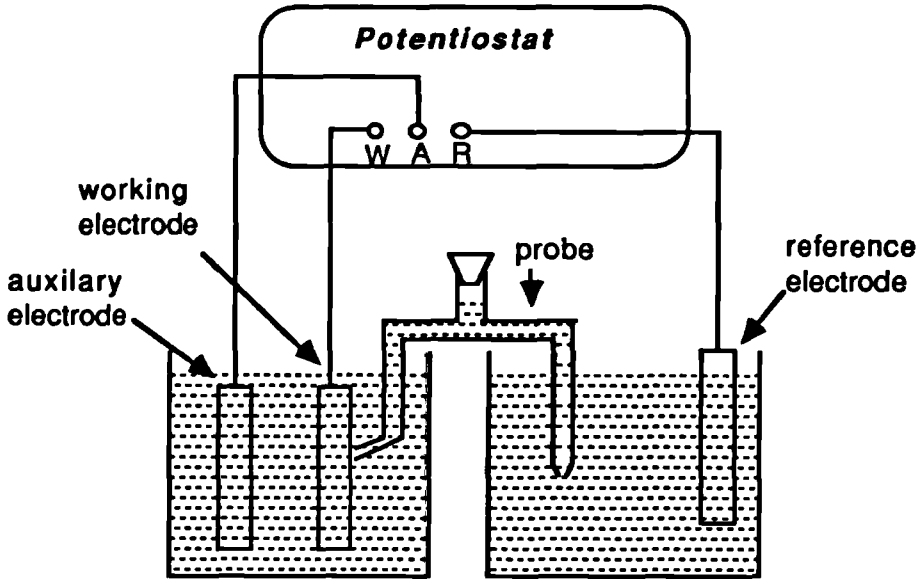


Figure 7.4 Schematic diagram of cell for measuring polarisation.

The cell was partially immersed in a water bath maintained at 30°C. The potentiostat employed was a Thompson Electrochem Autostat Auto 25 which was software controlled by means of a BBC Master microcomputer.

Stern and Geary [192] derived the following relationship for the determination of corrosion rate, i_{corr}, from polarisation data at potentials close to the free corrosion potential:

$$i_{corr} = \frac{b_a . b_c}{2.3\ (b_a + b_c).R_p} \qquad (7.5)$$

Where, R_p is the slope of the potential vs current curve at the free corrosion potential, i.e, the polarisation resistance.

The principle limitation of this techn'que is that the values of the anodic Tafel constant (b_a) and the cathodic Tafel constant (b_c) are required for the determination of the corrosion rate. Hence b_a and b_c, determ ned from the gradient of the potential versus logarithmic current curve in the activation polarisation region, must be

derived from a separate experiment on a duplicate specimen involving polarisation at large applied potentials to E_{corr} (typically 200 or 300mV). In determining the variation with time of i_{corr} by means of equation (7.5), it is assumed that b_a and b_c do not change with time. The theoretical basis of the technique and its application has been reviewed by Mansfeld [193].

The values of b_a and b_c were determined in prior experiments in which two samples were polarised one anodically and the other cathodically from 0 to 300 mV and 0 to -300 mV with respect to the stabilized free corrosion potential at a scan rate of 50 mV/min. The potential was then plotted against the logarithm of the current required for polarisation and the b_a and b_c values were determined as the gradient of the activation polarisation region. The values of b_c obtained from the slope had a very high value, (i.e $b_c \rightarrow \infty$) since the cathodic process was largely controlled by limitation in the diffusion of dissolved oxygen (see Figure 7.2). Thus the above equation (7.5) was modified [194] as follows for the calculation of corrosion rate:

$$i_{corr} = \frac{b_a}{2.3 R_p} \qquad (7.6).$$

R_p was then determined in subsequent tests in which samples were anodica ly polarised from -20 to +20 mV with respect to the free corrosion potential. The potential was plotted against the current required for polarisation and R_p values were determined as the grad'ent at the free corrosion potential (Figure 7.5). For each weld type, R_p was determined at regular intervals over a 50 h period of exposure and i_{corr} as a function of time determined from equation (7.6).

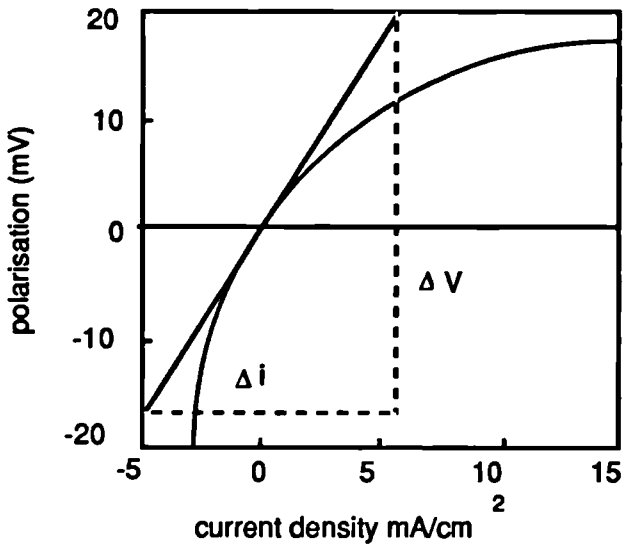


Figure 7.5 Typical plot for polarisation at potential close to E_{corr}.
Where, $R_p = \Delta V/\Delta i$, $\Omega\text{-cm}^2$.

7.2.1.2 Galvanic Coupling Test

Galvanic corrosion results from the reaction which occurs when two (or more) dissimilar metals are in contact or are otherwise electrically connected in a conductive solution. Because of the difference in the electrical potentials of the dissimilar metals of the couple, a galvanic current is generated. The anode, the more active metal of the couple, corrodes more rapidly than it would if it were uncoupled in the same medium. The less active metal, the cathode, generally corrodes less than would be the case if it were uncoupled in the same medium or it could be made resistant to corrosion.

In this test the apparatus shown schematically in Figure 7.6 was used to investigate the galvanic current established between the weld and the surrounding zinc and to construct an Evans diagram [195] of potential versus current for the system.

Two identical specimens of size 2.5 x 2.0 cm were coated with lacquer so that for one specimen only the welded area was exposed while for the other specimen only the

zinc coating was exposed. The area of the zinc was 5 cm^2 and the area of the weld was 0.4 cm^2 resulting in a zinc to weld area ratio of 13:1.

The specimens were galvanically coupled in 1N NaCl solution of pH 4 at 30° C. Variation in the galvanic current with respect to time was monitored by means of Sycopel zero resistance ammeter when the value of resistance set on the resistance box was zero and switches S1 and S2 were open (Figure 7.6). This test was periodically interrupted to allow the determination of the Evans diagram. Here the value of the resistance in the external circuit was increased in a step wise manner by means of the resistance box. The galvanic current at each setting of the resistance was recorded from the zero resistance ammeter while simultaneously the potential of both elements of the couple was recorded with respect to the saturated calomel reference electrode by selection of switches S1 or S2.

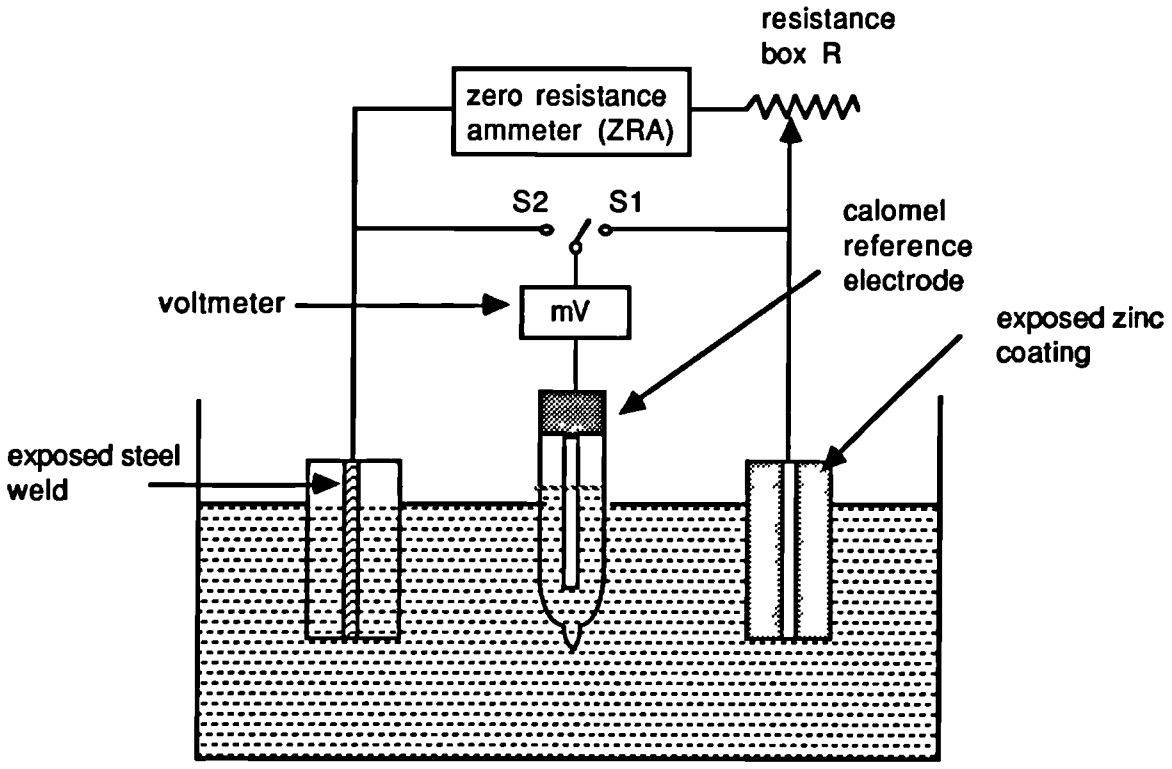


Figure 7.6 Schematic diagram for measuring the flow of current from zinc coating to the steel weld and to determine the Evans diagram [195].

A series of tests were performed on each type of weld i.e., normal weld (NRM), nickel injected weld (NKL), stainless steel injected weld (SST), tool steel injected weld (TST), zinc vapour incorporated weld (ZIC) and weld made by zinc powder incorporation (ZPI).

7.3 Results and discussion

7.3.1 Linear Polarisation Technique

The value of the anodic Tafel constant, b_a, for the zinc coating was determined in a separate experiment, and was found to be 36 mV/decade. This was the case for both as received and normal welded samples with values being determined in duplicate in each case. Figure 7.7 shows the construction of the tangent to the activation polarisation region of the anodic branch of the curve. Figure 7.8 shows that the cathodic branch of the curve is typical of current limitation by diffusion of dissolved oxygen, hence justifying the use of equation (7.6). The anodic and cathodic curves obtained for the zinc coating in the presence of modified weld composition (Table 7.1) were essentially similar to that shown in Figures 7.7 & 7.8.

Typical data for polarisation from -20 mV to +20 mV to the free corrosion potential is shown in Figure 7.9. The pronounced curvature that is displayed was characteristic of all such tests carried out on these materials. This emphasises the importance of determining R_p as the gradient of the tangent at E_{corr}.

The variation of the polarisation resistance, R_p, with time for normal welded zinc coated steel sheet and the unwelded material is shown in Figure 7.10. These values of R_p were used to determined the variation of corrosion rate with time (Figure 7.11) by use of equation 7.6. The corrosion rate can be expressed in terms of corrosion current since corrosion current is directly proportional to the corrosion rate. The variation of free corrosion potential with time for the same samples is

shown in Figure 7.12.

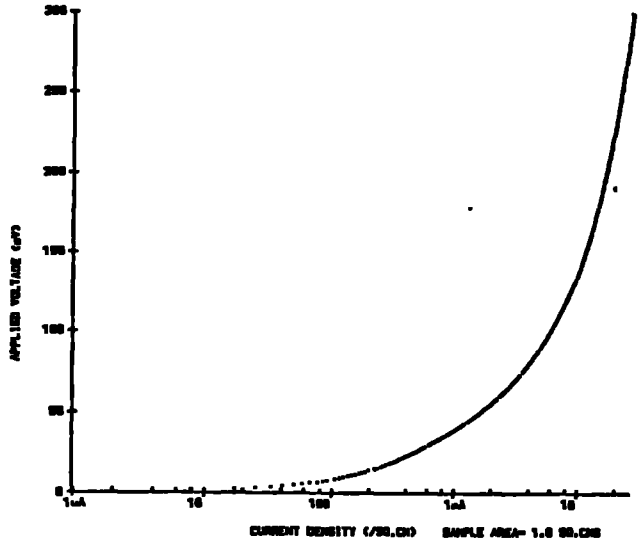


Figure 7.7 Anodic polarisation curve for zinc coated steel sheet in 1N NaCl solution pH 4.

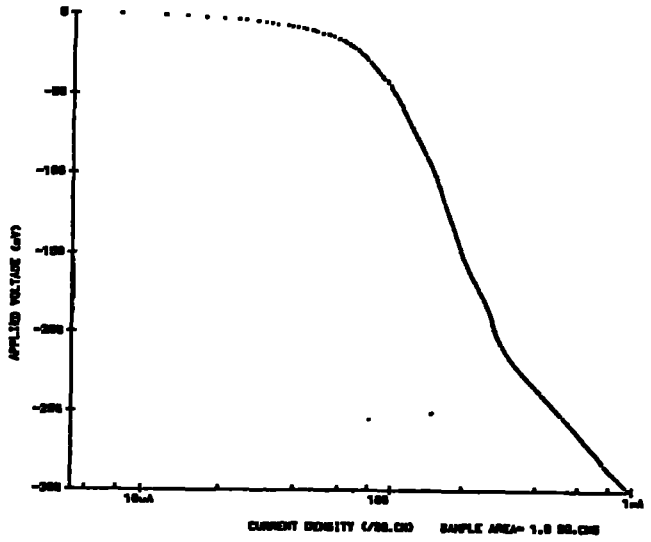


Figure 7.8 Cathodic polarisation curve for zinc coated steel sheet in 1N NaCl solution pH 4.

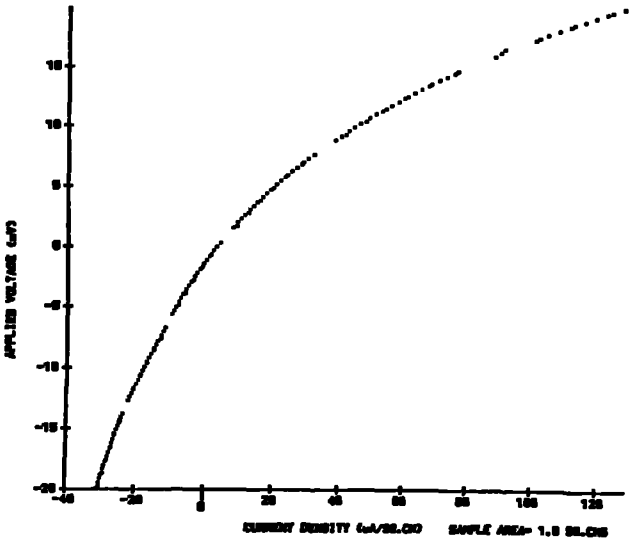


Figure 7.9 Typical data for polarisation of zinc coated steel sheet at potential close to E_{corr} in 1N NaCl solution pH 4.

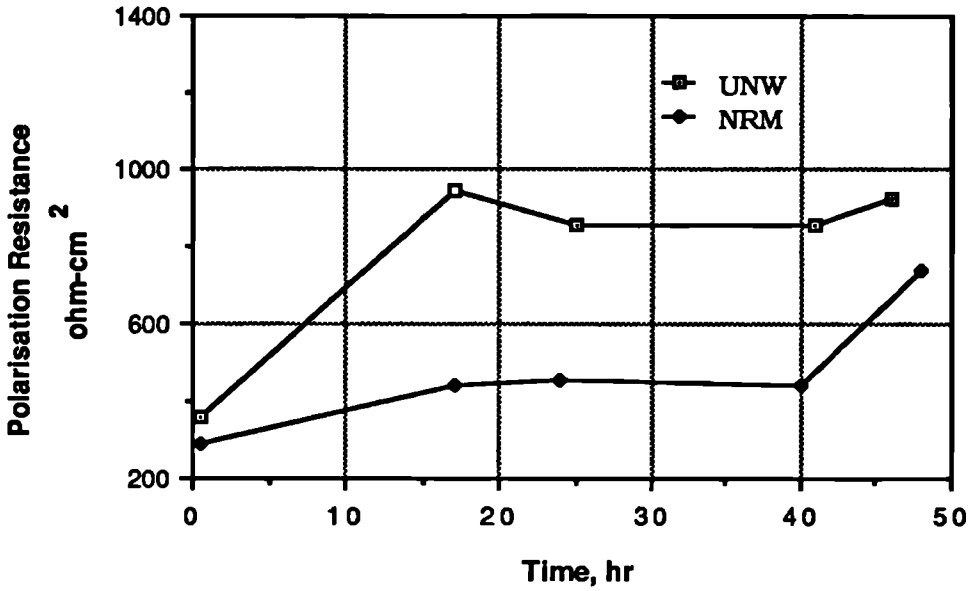


Figure 7.10. Polarisation resistance vs time for unwelded (UNW) and normal welded (NRM) specimens in 1N NaCl solution, pH 4.

Comparison of the corrosion rates of the unwelded and normal welded samples (Figure 7.11) revealed that the zinc self corrosion rate was higher in the case of the welded sample. This was expected since in the welded sample sacrificial protection of the exposed steel weldment was taking place and hence the rate of zinc self corrosion (equation 7.4) was higher. The potential/time data (Figure 7.12) showed that the welded sample displayed a potential close to the open circuit potential of zinc, indicating that the weld metal had been cathodically polarised to this potential. On exposure beyond 40 h the corrosion rate (Figure 7.11) declined markedly. At this point visual observations confirmed that while the weld metal had been completely protected and showed no sign of corrosion, the zinc coating had become exhausted with bare steel revealed beneath the coating location. The corrosion rate observed was then approaching the corrosion rate of Zn-Fe alloy (discussed later) in the solution. These results showed that while the e ectrogalvanised coating was effective in offering sacrificial protection to the weld metal, the life of the coating was limited, particularly in this aggressive testing solution and with the small coating/weldment area ratio employed.

The data for the variation with time of the corrosion current for material with a weld containing injected nickel powder is shown in Figure 7.13, where the previous data for the corrosion rate of the unwelded and normal welded specimen is also included. The potential/time data (Figure 7.14) revealed that the weld metal was polarised to potential close to the open circuit potential of zinc throughout the test. It can be observed that the polarisation of the nickel injected weld to a potential close to that of free corrosion potential of zinc has resulted in a significant increase in the self corrosion rate of zinc compared with that required for the normal welded sample. One explanation for this behaviour is that, since the potential of the nickel containing weld metal will be more noble than that of the normal weld metal, a greater polarisation potential is required to achieve a potential close to the open circuit potential of zinc and hence zinc self corrosion rate is higher. The weld was observed to have been completely protected during the exposure period. The lack of decline in corrosion rate beyond 40 h can be attributed to the use of a thicker zinc coating in this case (see Table 7.1).

Data for welded material containing injected stainless steel powder is shown in Figures 7.15 and 7.16. Here, as in the case of the nickel powder injected weld, the self corrosion rate of zinc required for polarisation of the weld metal to a potential close to the open circuit potential of zinc was generally greater than that required for the normal welded sample. This is probably attributable to the establishment of a potential for the weld metal that was more noble than that of the normal weld metal.

Similar data for welded material containing injected tool steel powder is shown in Figure 7.17 and Figure 7.18. Here the result of polarisation to a potential close to the open circuit potential of zinc was to produce a self corrosion rate of the zinc coating which was initially similar to that of the normal welded sample. After 18 h, and for the remainder of the test, the corrosion rate of the tool steel weld showed a somewhat lower rate of corrosion then the normal welded specimen. This lower rate of corrosion can be explained in terms of the influence of chromium additions in promoting a potential such that the polarisation required to achieve a potential close

to the open circuit potential of zinc was smaller and hence, the zinc self corrosion rate was smaller.

Data for the weld in which tool steel powder was incorporated just after the welding process are shown in Figure 7.19 and 7.20, where the previous data of unwelded and normal welded specimen is also plotted. It is evident that the corrosion rate of the tool steel incorporated weld is similar to that of the unwelded specimen for an initial period of time (Figure 7.19). The corrosion rate then decreases with time as is expected. The corrosion rate is lower than the normal welded specimen suggesting an improvement in the corrosion resistance of the zinc coating in the presence of a tool steel incorporated weld. The curve of corrosion rate versus time is very similar to that of the curve for the weld in which the tool steel powder was injected into the weld pool (Figure 7.17) except for the initial period, where the injected tool steel weld showed a higher corrosion rate. The potential/time data for the tool steel incorporated weld is shown in Figure (7.20). It can be seen from the graph that the potential of the tool steel incorporated weld is close to the open circuit potential of zinc. This approaches a more positive potential toward the potential of Fe-Zn alloy (see later) at the end of the test.

The data for the variation with time of the corrosion current for the weld with zinc vapour incorporation is shown in Figure 7.21. The potential/time data (Figure 7.22) revealed that the weld metal was polarised to a potential close to the open circuit potential of zinc except towards the end of the test. The self corrosion rate of zinc in this case was substantially lower than in the normal welded case for an initial period. However this low corrosion rate was not sustained and after a few hours time of exposure the corrosion rate of the zinc incorporated material was essentially similar to that of the normal welded material. This shows that the incorporation of zinc into the weld metal is advantageous from the point of view of the corrosion resistance of the surrounding zinc coating. However the volatilised zinc retained as a result of argon entrainment during laser welding was present as a relatively thin layer deposited on the weld. On the exhaustion of this zinc layer, as a result of general

corrosion in the electrolyte, the weld displayed corrosion properties similar to those of normal welded material with a corresponding increase in the self corrosion rate of the surrounding zinc. These results point to the advantage of zinc incorporation during laser welding.

It was observed that while the zinc coating had been consumed as a result of sacrificial action during the test, a dark layer remained in a zone of width of 2 mm on either side of the weld. EDAX analysis identified this as Zn-Fe intermetallic alloy. This layer, which initially had been covered with a layer of unreacted zinc which had been consumed during the test, had been formed as a result of interaction between the steel substrate and the zinc coating in the heat affected zone during welding.

In order the asses the corrosion behaviour of the heat affected zone Zn-Fe alloy, the test ZIC was prolonged beyond 48 h. At the end of test the ZIC specimen was taken out after the completion of 48 h, and was cleaned with acetone to remove the corrosion products. The base metal steel and the heat affected zone (HAZ) Zn-Fe alloy was revealed in this way. The specimen was then inserted again in the electrolyte and the corrosion rate and the rest potential of the HAZ Zn-Fe alloy was monitored for the next 48 h.

Figure 7.23 shows the corrosion rate of heat affected zone Fe-Zn intermetallic layer (exposed area, Zn-Fe alloy; 0.6 cm^2, bare steel + weld; 1.2 cm^2) measured using the linear polarisation technique. It is evident that the corrosion rate of the Zn-Fe alloy is lower than that of the unwelded and normal welded specimen. Figure 7.24 shows the free corrosion potential of Zn-Fe intermetallic layer against time. It is evident that the free corrosion potential of the specimen gradually shifted from an initial potential typical of Zn-Fe alloy in this solution to a potential typical of steel. This is attributable to the gradual dep etion of zinc from the intermetallic layer by selective dissolution. Visual observations during the 48 h test confirmed that the Zn-Fe alloy protected the base metal steel surface and the weld. There was no sign of the

corrosion of exposed bare steel or the weld for at least 24 h, while the Zn-Fe alloy was corroding and provided protection to the steel. Hence this intermetallic layer was responsible for an additional period of protection of the weld and the bare steel.

The data for the variation with time of the corrosion current for the weld with zinc powder incorporation (ZPI) are shown in Figure 7.25. The potential/time data (Figure 7.26) revealed that the free corrosion potential of zinc powder incorporated weld was similar to that of the unwelded specimen throughout the 48 h exposure. The self corrosion rate (Figure 7.25) of the zinc incorporated weld was lower than that of normal welded (NRM) specimen and very close to that of the unwelded (UNW) specimen. But this lower corrosion rate was not sustained and after around 16 h exposure the corrosion rate was very close to that of the normal welded specimen. This behaviour persisted until 40 h exposure. After 48 h exposure the test was continued for another 48 h. The corrosion rate increased at 50 h exposure but decreased again thereafter until a period of 90 h exposure. The potential/time data revealed that the free corrosion potential of the specimen gradually shifted to became close to the potential of the Zn-Fe intermetallic layer after an exposure of 90 h. This means that the zinc has lasted for quite a substantial period of time as compared to that of the normal welded specimen. Hence this test suggested that the addition of zinc powder has prolonged the sacrificial protection of the steel to at least twice the duration as compared with the normal welded specimen.

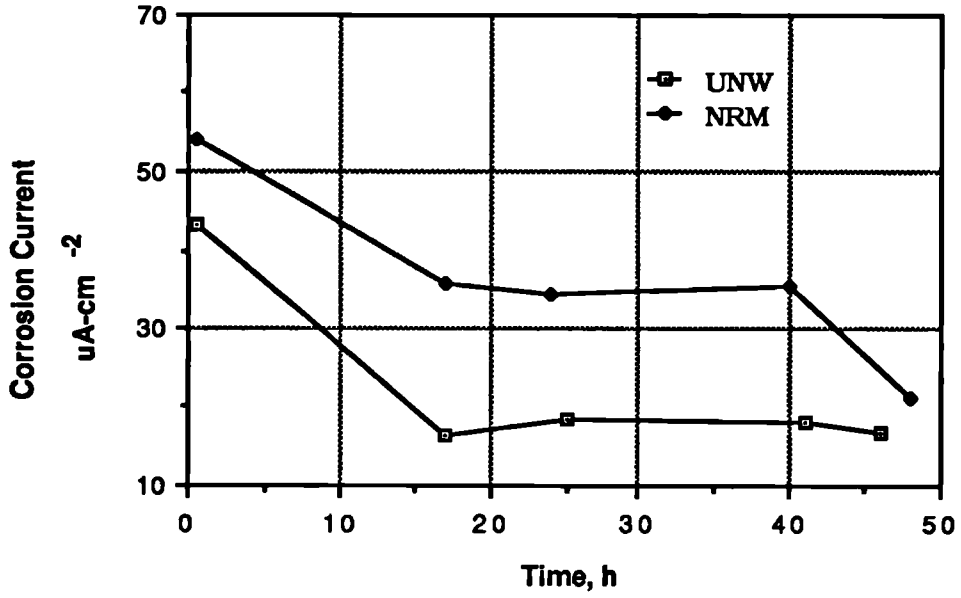


Figure 7.11 Corrosion current vs time for unwelded (UNW) and normal welded (NRM) specimens in 1N NaCl solution, pH 4.

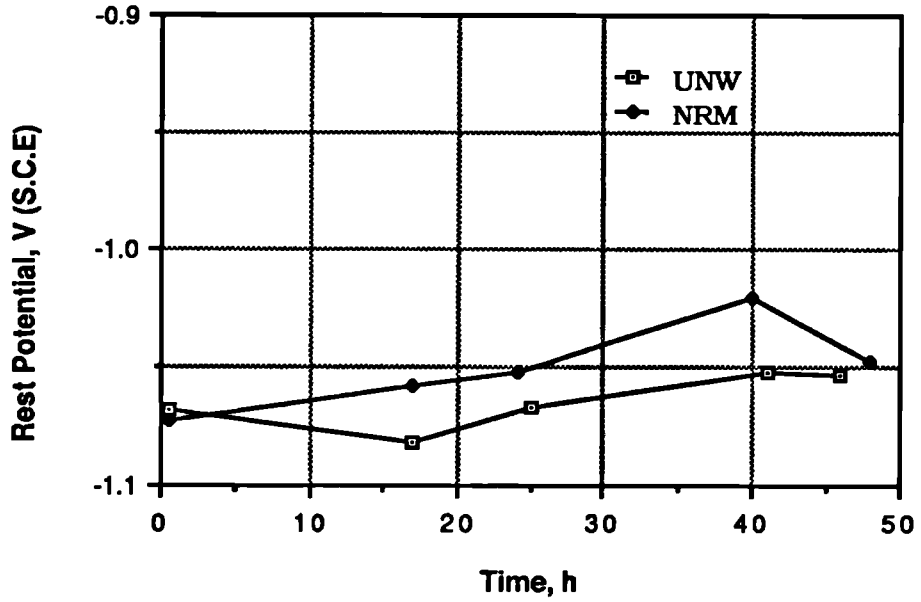


Figure 7.12. Rest potential vs time for unwelded (UNW) and normal welded (NRM) specimens in 1N NaCl solution, pH 4.

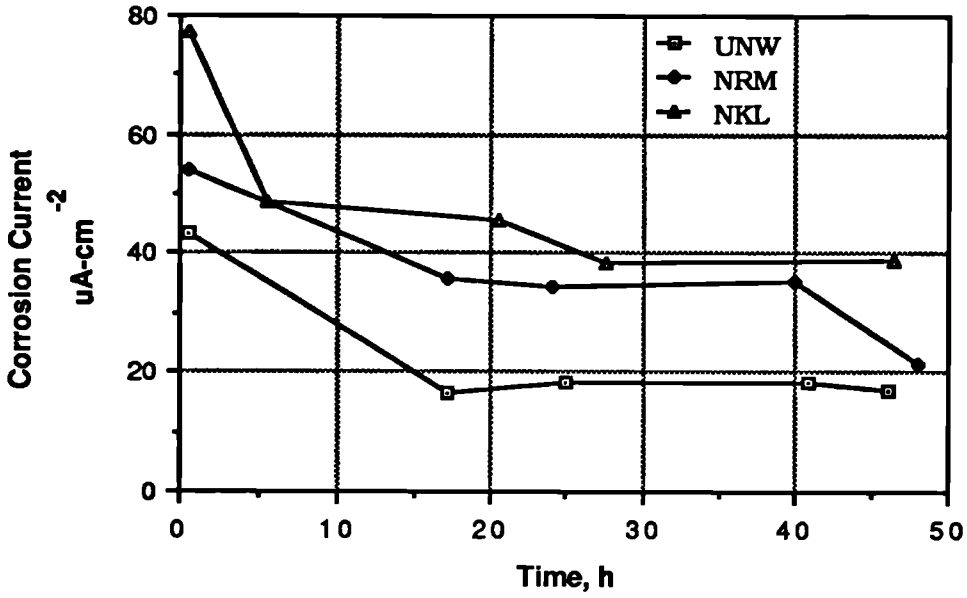


Figure 7.13. Corrosion current vs time for unwelded (UNW), normal welded (NRM) and nickel injected weld (NKL) specimens in 1N NaCl solution, pH 4.

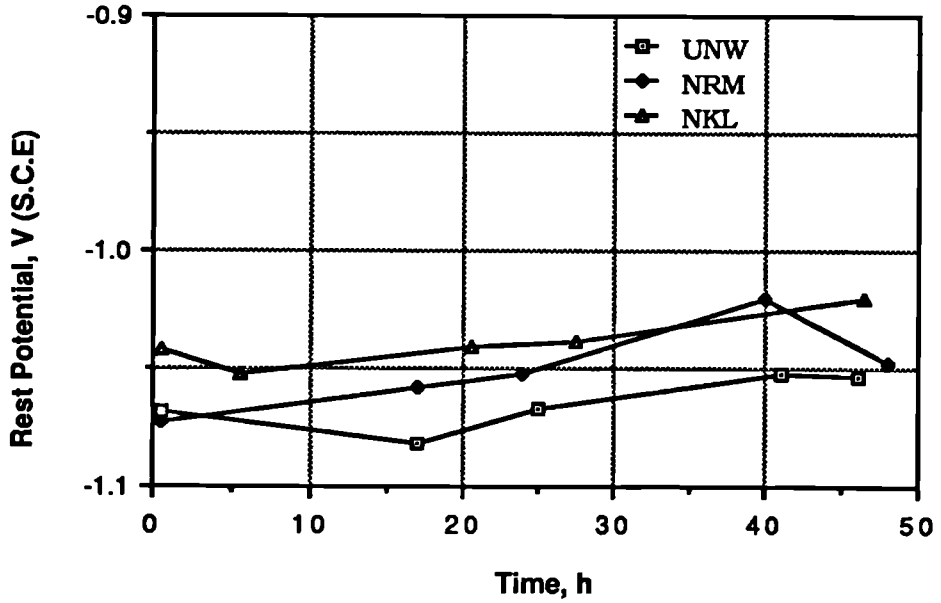


Figure 7.14 Rest potential vs time for unwelded (UNW), normal welded (NRM) and nickel injected weld (NKL) specimens in 1N NaCl solution, pH 4.

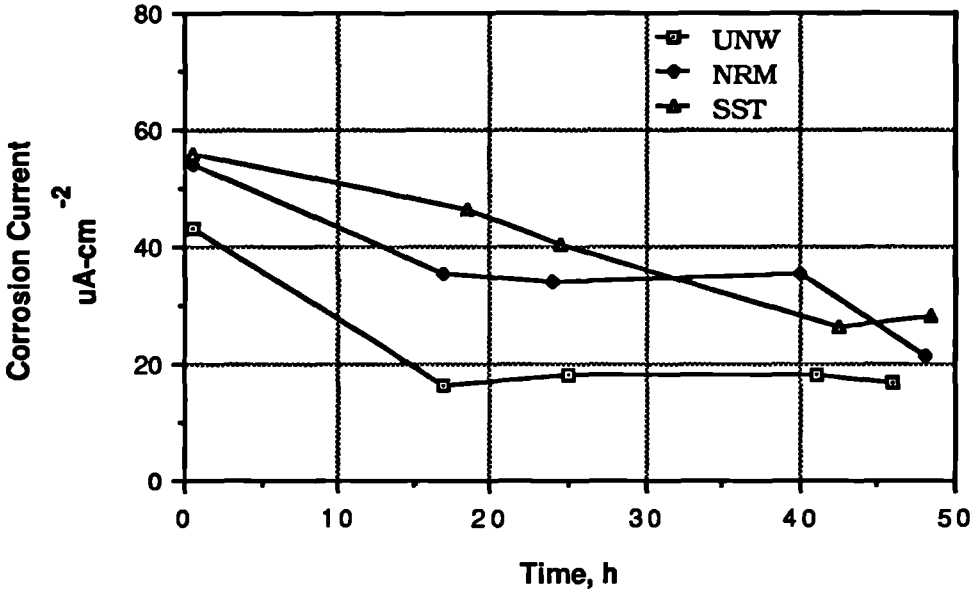


Figure 7.15 Corrosion current vs time for unwelded (UNW), normal welded (NRM) and stainless steel injected weld (SST) specimens in 1N NaCl solution, pH 4.

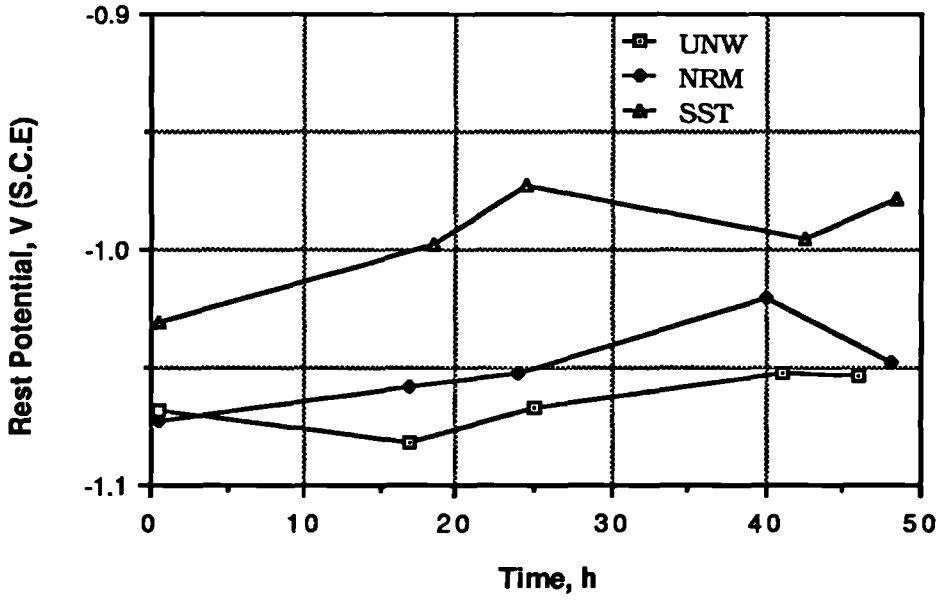


Figure 7.16 Rest potential vs time for unwelded (UNW), normal welded (NRM) and stainless steel injected weld (SST) specimens in 1N NaCl solution, pH 4.

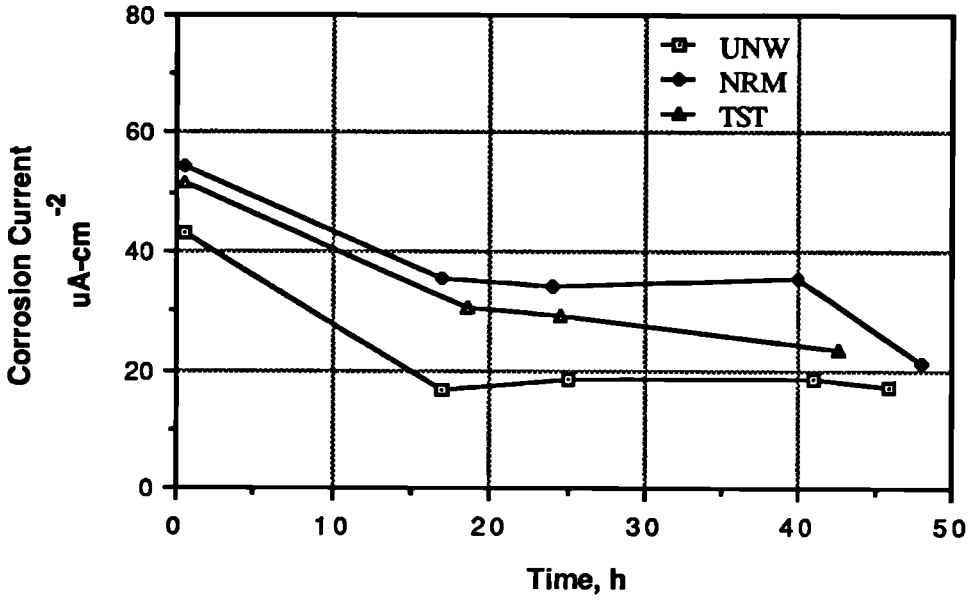


Figure 7.17 Corrosion current vs time for unwelded (UNW), normal welded (NRM) and tool steel injected weld (TST) specimens in 1N NaCl solution, pH 4.

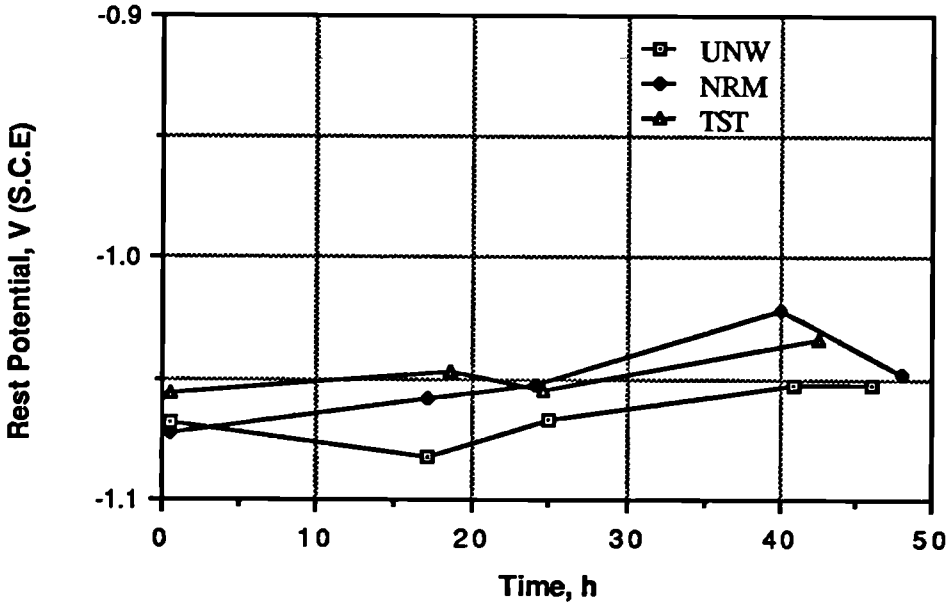


Figure 7.18 Rest potential vs time for unwelded (UNW), normal welded (NRM) and tool steel injected weld (TST) specimens in 1N NaCl solution, pH 4.

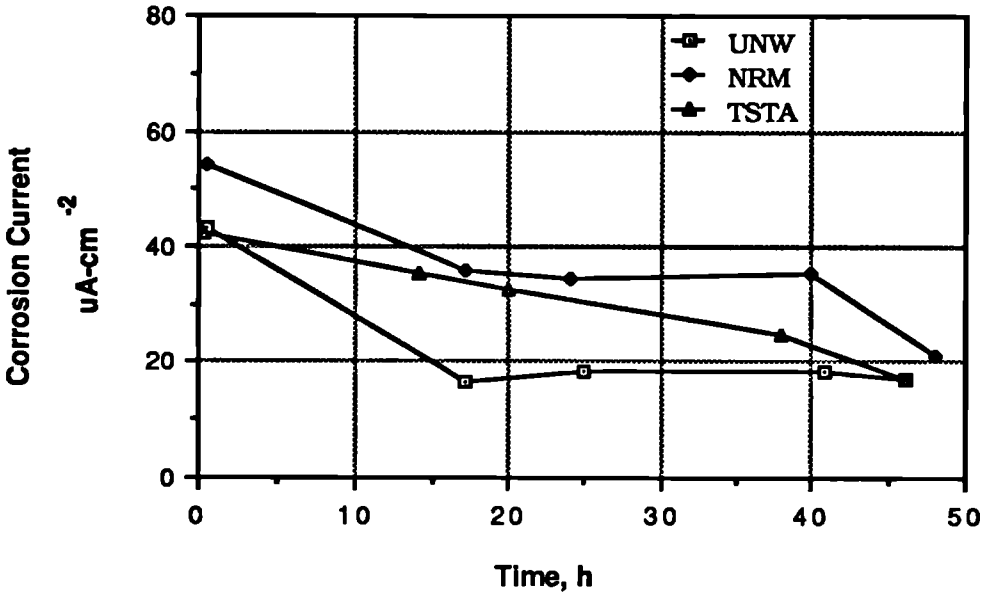


Figure 7.19 Corrosion current vs time for unwelded (UNW), normal welded (NRM) and tool steel coated weld (TSTA) specimens in 1N NaCl solution, pH 4.

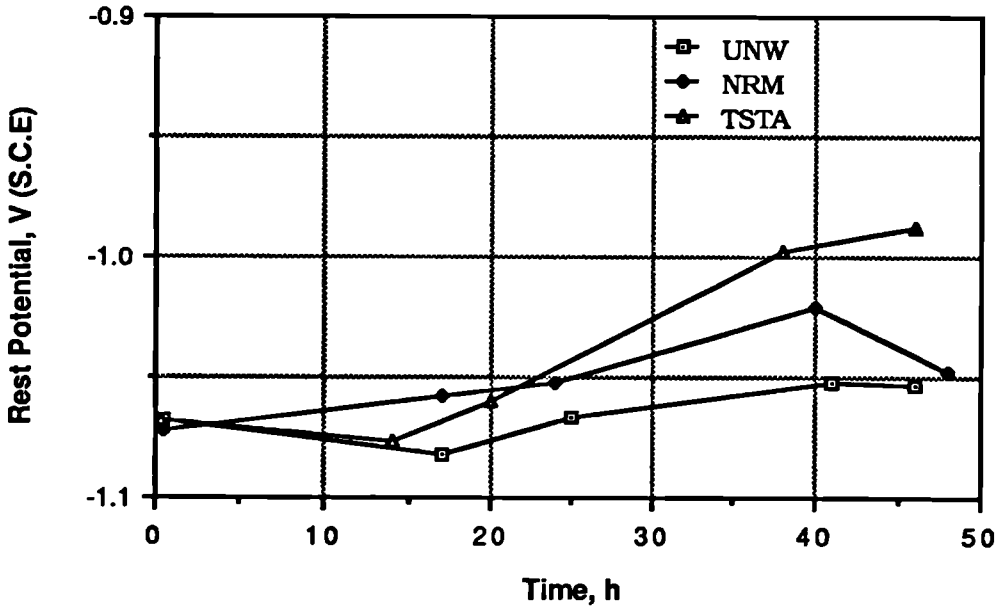


Figure 7.20 Rest potential vs time for unwelded (UNW), normal welded (NRM) and tool steel coated weld (TSTA) specimens in 1N NaCl solution, pH 4.

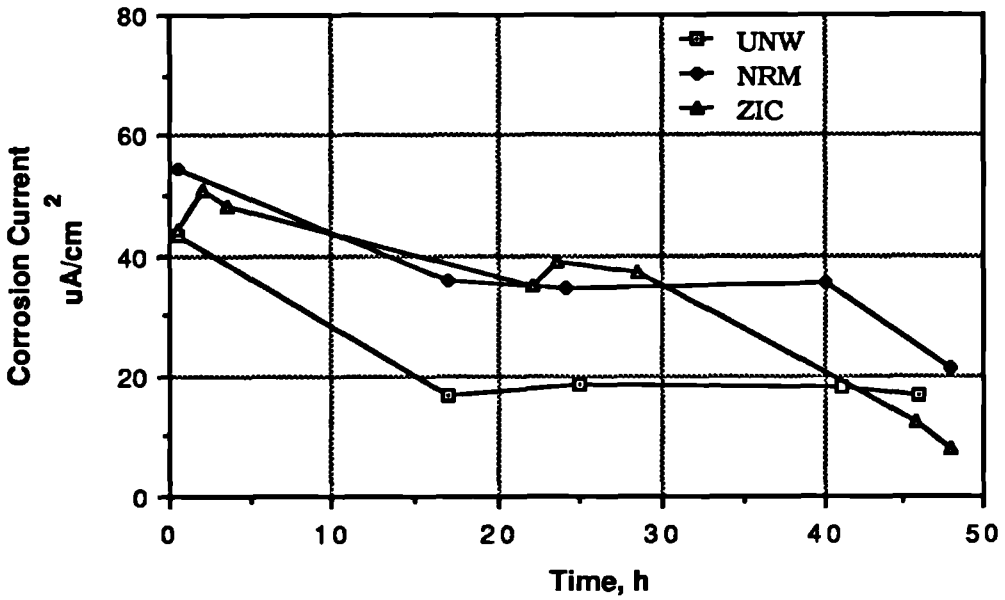


Figure 7.21 Corrosion current vs time for unwelded (UNW), normal welded (NRM) and zinc incorporated weld (ZIC) in 1N NaCl solution, pH 4.

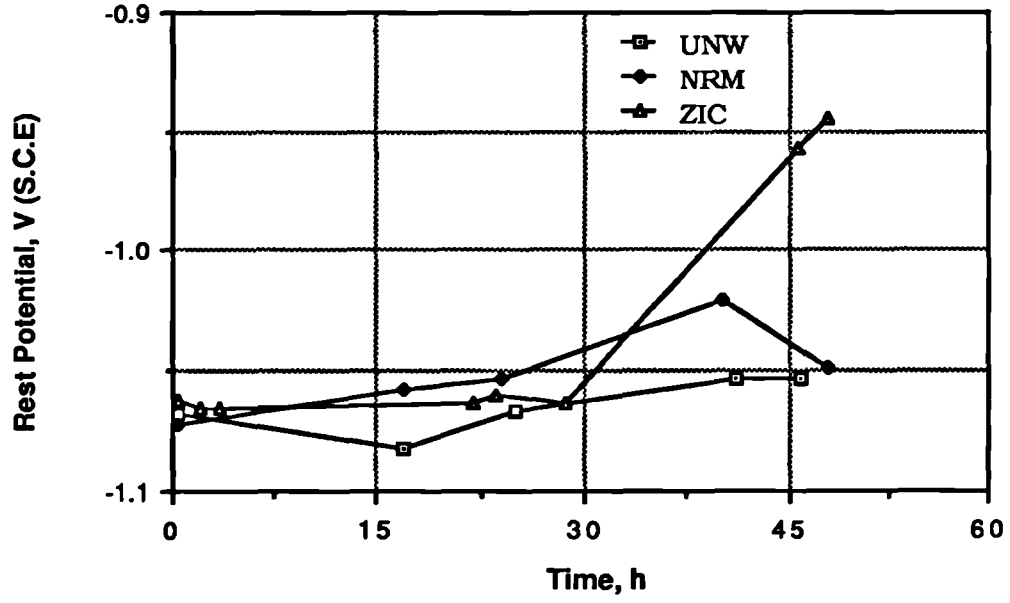


Figure 7.22 Rest potential vs time for unwelded(UNW), normal welded (NRM) and zinc incorporated weld (ZIC) in 1N NaCl solution, pH 4.

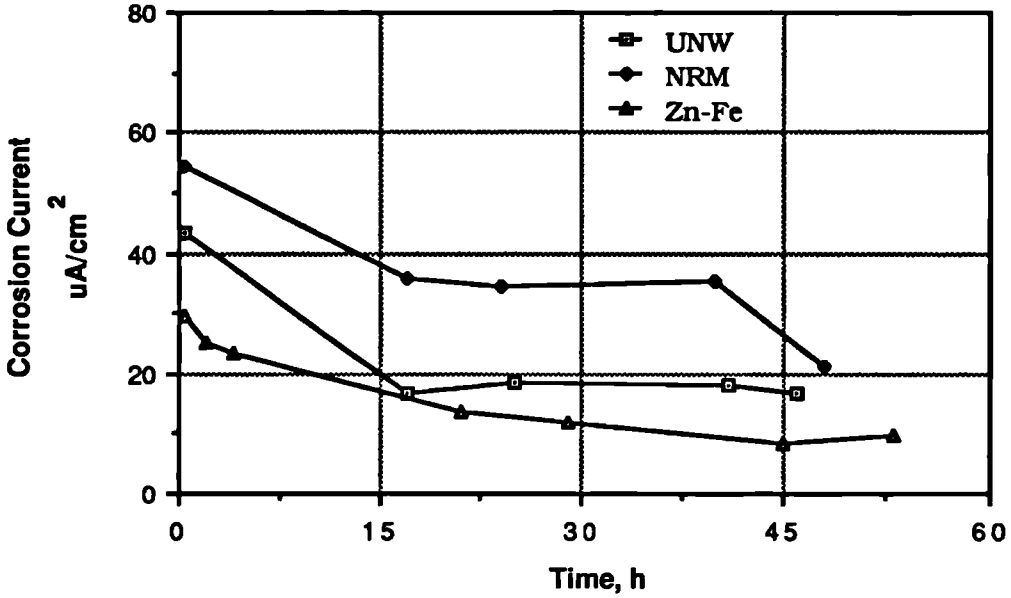


Figure 7.23 Corrosion current against time of heat affected zone Zn-Fe alloy, compared with unwelded (UNW) and normal welded (NRM) specimen. Exposed HAZ area 0.6 cm^2 in 1N NaCl solution, pH 4.

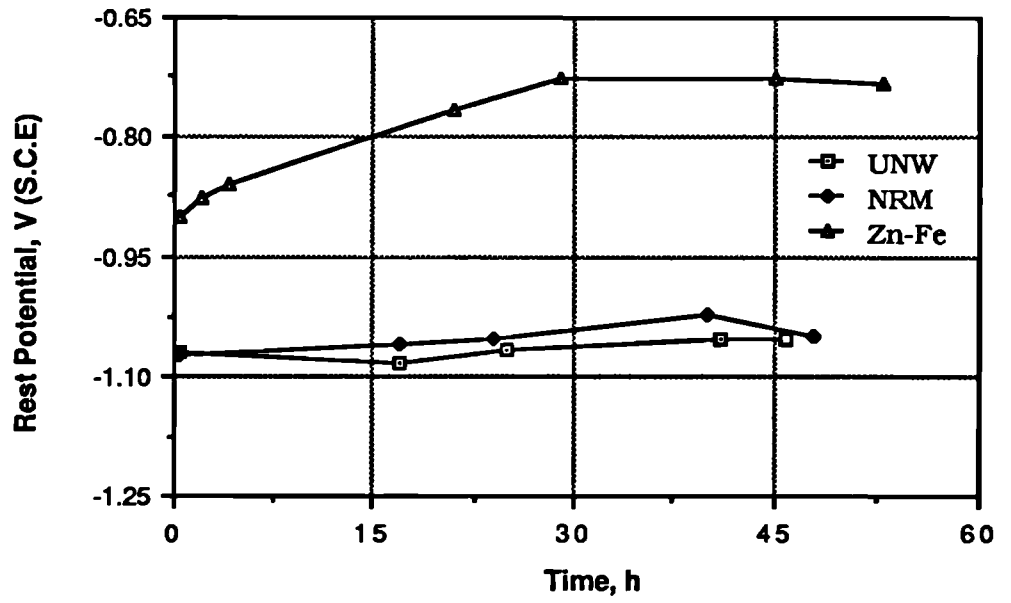


Figure 7.24 Rest potential against time of heat affected zone Zn-Fe alloy, compared to unwelded (UNW) and normal welded(NRM) specimen. Exposed HAZ area 0.6 cm^2 in 1N NaCl solution, pH 4.

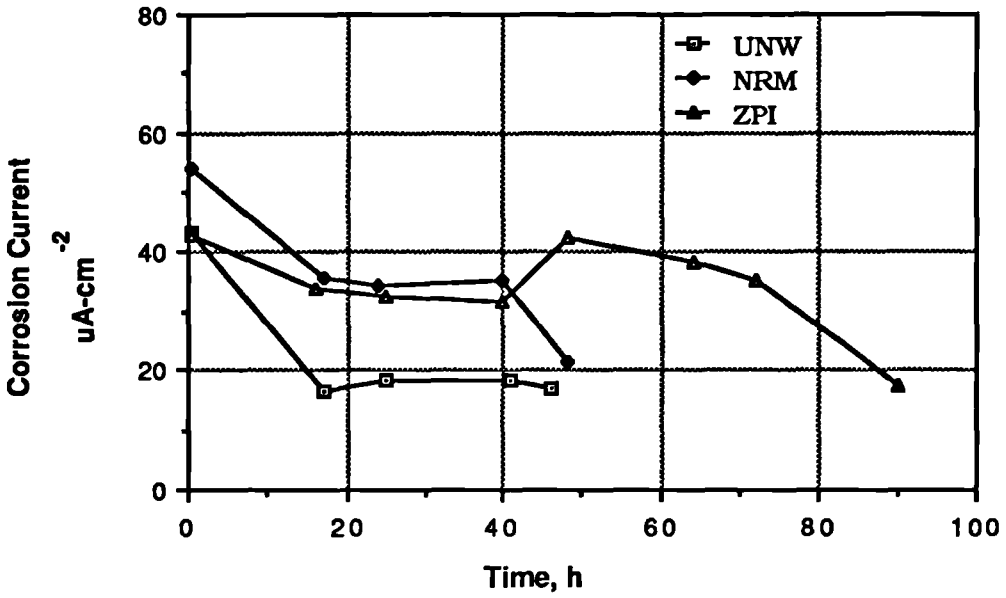


Figure 7.25 Corrosion current vs time for unwelded (UNW), normal welded (NRM) and zinc powder incorporated weld (ZPI) in 1N NaCl solution, pH 4.

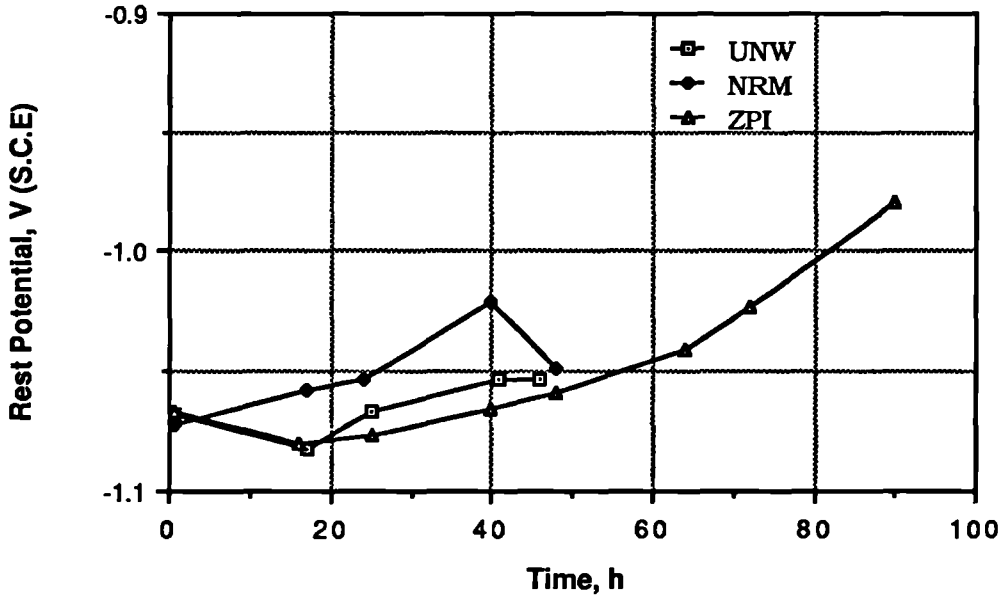


Figure 7.26 Rest potential vs time for unwelded(UNW), normal welded (NRM) and zinc powder incorporated weld (ZPI) in 1N NaCl solution, pH 4.

7.3.2 Galvanic Coupling Test

The variation of current with time (Figure 7.27) and the Evans diagram (Figure 7.28) for coupled specimens of the normal welded material in which the weld and surrounding zinc coating were separately exposed to the electrolyte provided additional information on the mechanism of cathodic protection in this case.

The galvanic current (Figure 7.27) declined from an initial value of approximately 70 μA to take up after 10 minutes a value of 18 μA. This value increased gradually with time and reached 36 μA at the end of the test after 60 h exposure. These latter values represent the current required to polarise the weld to the open circuit potential of zinc and hence provide cathodic protection of the weld.

As shown in the Evans diagram (Figure 7.28) the potential of the couple was determined by the polarisation characteristics of the cathode (the weld) and hence the system is under cathodic control. The form of the cathodic branch of the curve agrees well with that put forwarded by Budinski and Wilde [172] on theoretical grounds (Figure 7.2) and hence confirms the assumption that the cathodic reaction is maintained by mixed oxygen reduction and hydrogen evolution at the free corrosion potential. The assumption that the cathodic Tafel constant, b_c, at the free corrosion potential is large and hence equation 7.6, can be used is also seen to be justified by the large gradient of the cathodic branch of the curve. There was little fundamental variation in the Evans diagram with time of exposure except that the galvanic current at the free corrosion potential of the couple varied as shown in Figure 7.27.

Since the system is under cathodic control the magnitude of the galvanic current will be determined by the area of the cathode - that is, the corrosion rate of the zinc coating required to protect the weld will be dependent on the area of the weld. In the case of the couple the area ratio of zinc to weld was 13:1 while in the case of the linear polarisation tests (Figure 7.11) the area ratio was 7:1. Allowing for this difference in area ratio, the corrosion rate of zinc in the galvanic couple is essentially

similar to the difference in corrosion rates between the unwelded and normal welded samples in the linear polarisation test (Figure 7.11). The galvanic couple test has revealed that after an initial period this current is gradually increasing. It can therefore be inferred that the variation with time of the corrosion rate of the welded sample determined in the linear polarisation tests includes two components - a component arising from the sacrificial corrosion of zinc to protect the weld and a component representing the the self corrosion rate of zinc in this electrolyte (as shown in Figure 7.11) that declines with time.

The Evans diagrams constructed for the coupled zinc coating and welds with modified compositions (NKL, SST, TST, TSTA, ZIC and ZPI) are shown in Figures 7.29 to 7.34. It can be seen that in each type of weld the potential of the couple is determined by the polarisation characteristics of the cathode (the weld) and hence the system for each weld type is under cathodic control. The weld with zinc powder incorporation (ZPI) (Figure 7.34) had a potential very close to that of the zinc coating, still it tends to provide the information that the system is under cathodic control.

The data for the variation of current with time for welds with modified composition (NRM, NKL, SST, TST, TSTA, ZIC, and ZPI) is shown in Figure 7.35. These results show that the galvanic current for sacrificial protection of the weld with nickel injection (NKL), stainless steel injection (SST) and zinc vapour incorporation (ZIC) showed relatively higher galvanic currents than that for the normal welded specimen (NRM), while the welds with tool steel injection (TST), tool steel incorporation just after welding (TSTA), and zinc powder incorporation (ZPI) exibited lower galvanic currents tham that for the normal welded specimen (NRM).

The weld with tool steel powder incorporation (TSTA) showed that a very small amount of galvanic current is drawn by the weld for sacrificial action. This means that the corrosion rate of the zinc coating is lower in the presence of tool steel

incorporated weld, as is also seen in the linear polarisation technique (Figure 7.19). The free corrosion potential of (TSTA) weld was found to be -0.92 V, (Figure 7.32), which is noble to the free corrosion potential of zinc. The difference in free corrosion potentials between the zinc coating and the weld is reduced due to the presence of tool steel as compared to that of the normal weld (NRM). The use of tool steel has lowered the potential of the weld near to the free corrosion potential of the zinc coating, and hence, a lower corrosion rate has been observed in the case of tool steel weld. Hence this justified the idea put forward by Watkins et al. [169] that increasingly negative free corrosion potential with respect to the bare steel exhibits an increase in corrosion rate of the coatings. In other words a decrease in the difference of the free corrosion potentials between anode and cathode leads to a decrease in the corrosion rate of the coating. By this theory a more negative free corrosion potential of the weld to a potential close to the coating's free corrosion potential will result in a lower corrosion rate. Thus the use of tool steel in the weld led to a decreased corrosion rate of the coating.

The most interesting result is that of the weld with zinc powder incorporation just after the weld formation (Figure 7.35). The variation of galvanic current with time data showed that the zinc on the weld bead was acting as an anode and corroded for the first 30 h, while it protected the base metal zinc coating. The galvanic current increased for the first 5 h and then it decreased for the next 25 h. However, after 30 h exposure the polarity was reversed and the zinc on the weld bead acted as cathode and the corrosion started on the base metal zinc which acted as anode. Testing beyond 30 h showed that the corrosion rate of the zinc coating was the least (Figure 7.35) for the case of zinc powder incorporated (ZPI) weld as compared to all the other modified composition welds.

The reason for the change in polarity could be attributed to the different condition of the application of zinc on the material. The base metal zinc is electrogalvanised at room temperature while the zinc applied at the weld had undergone a heating and cooling process. In this technique the zinc powder had been

melted by the hot reacting weld and then was cooled down to room temperature. This means a variation in temperature was experienced by the coating thus obtained as a result of incorporation of the zinc powder on the weld bead, thus changing the properties of the coating at different depths.

When the top zinc coating on the weld bead is exhausted (as a result of corrosion of the coating and sacrificial protection provided to the base metal zinc coating) the new coating revealed consists of an iron zinc alloy with the amount of iron increasing towards the base steel surface. The iron-zinc alloy had a more noble potential than zinc (discussed earlier). This acted as cathode and was protected by the base metal zinc coating. When the zinc coating at the base metal around the weld was exhausted the Zn-Fe alloy provided an additional protection to the base metal and the steel weld (described earlier).

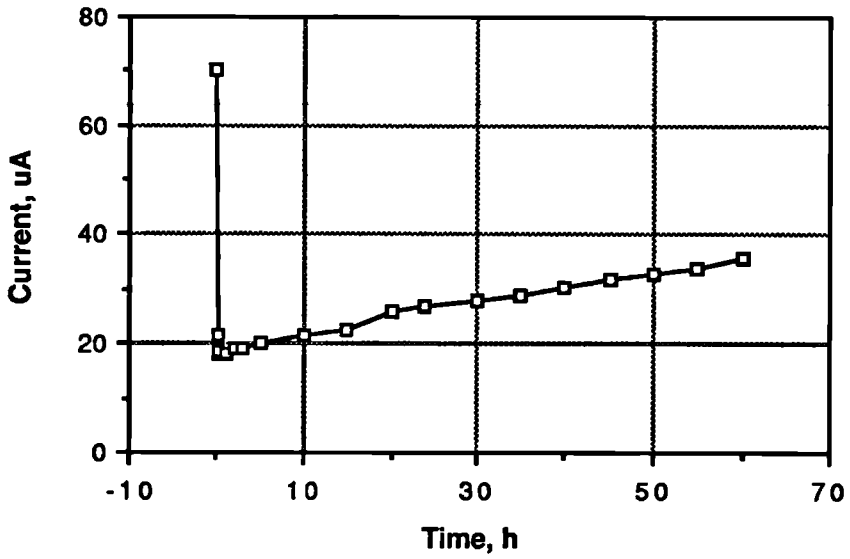


Figure 7.27. Current variation with time for coupled zinc coating and normal steel weld (NRM) in 1N NaCl solution, pH 4.

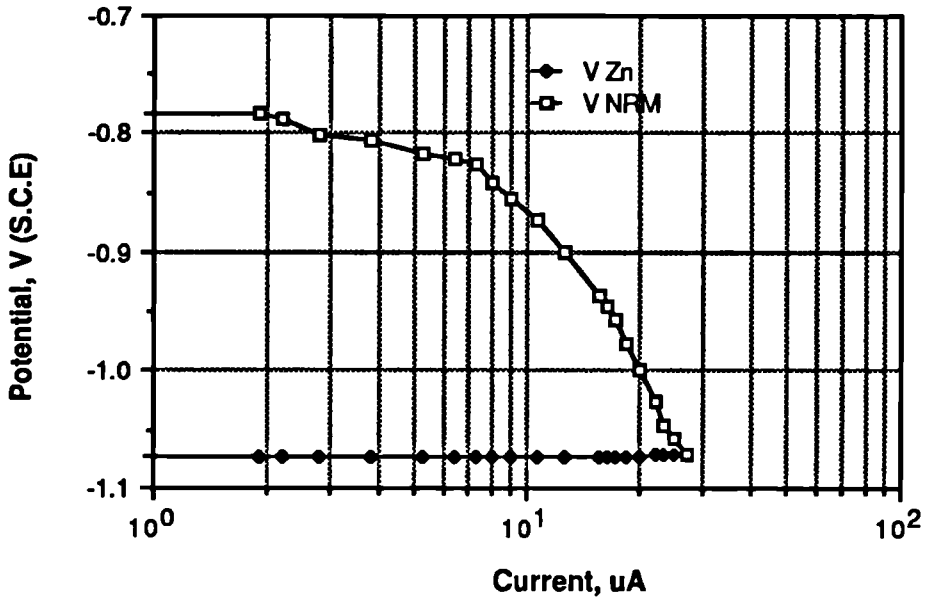


Figure 7.28 Evans diagram for coupled zinc coating and normal steel weld (NRM) after 24 hr exposure in 1N NaCl solution, pH 4.

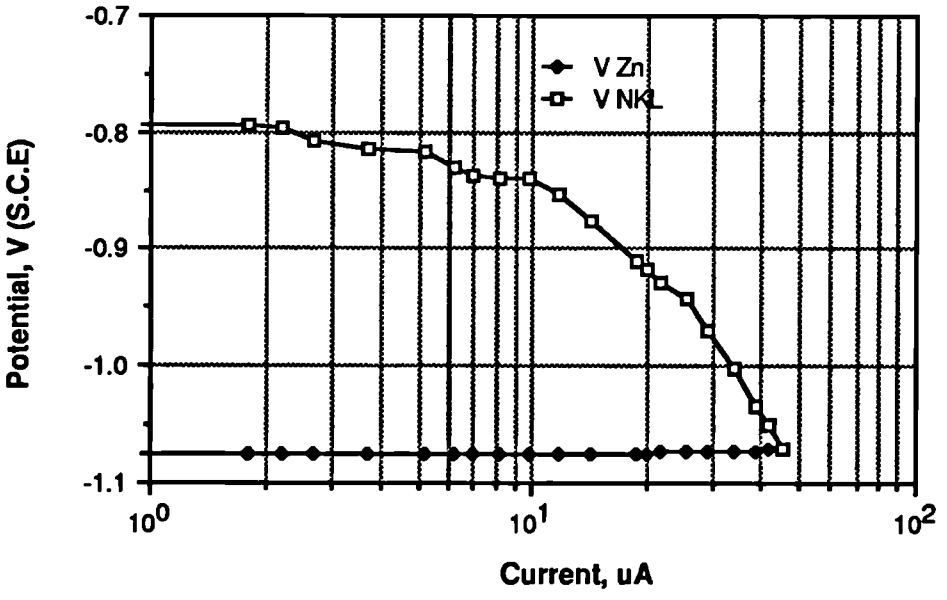


Figure 7.29 Evans diagram for coupled zinc coating and weld with injection of nickel powder (NKL) in 1N NaCl solution, pH 4, after 24 hr exposure.

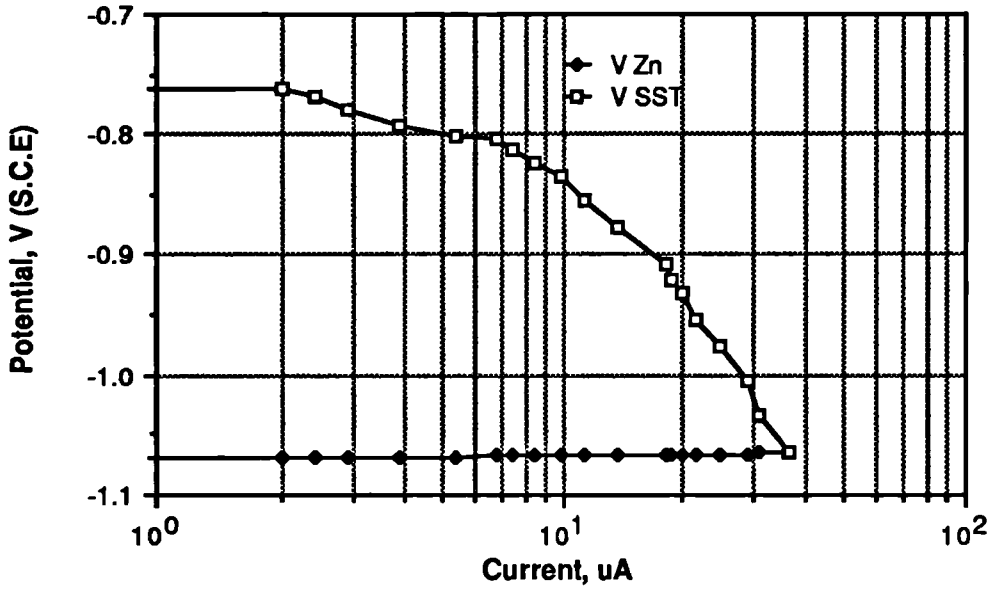


Figure 7.30 Evans diagram for coupled zinc coating and weld with injection of stainless steel powder (SST) in 1N NaCl solution, pH 4, after 24 hr exposure.

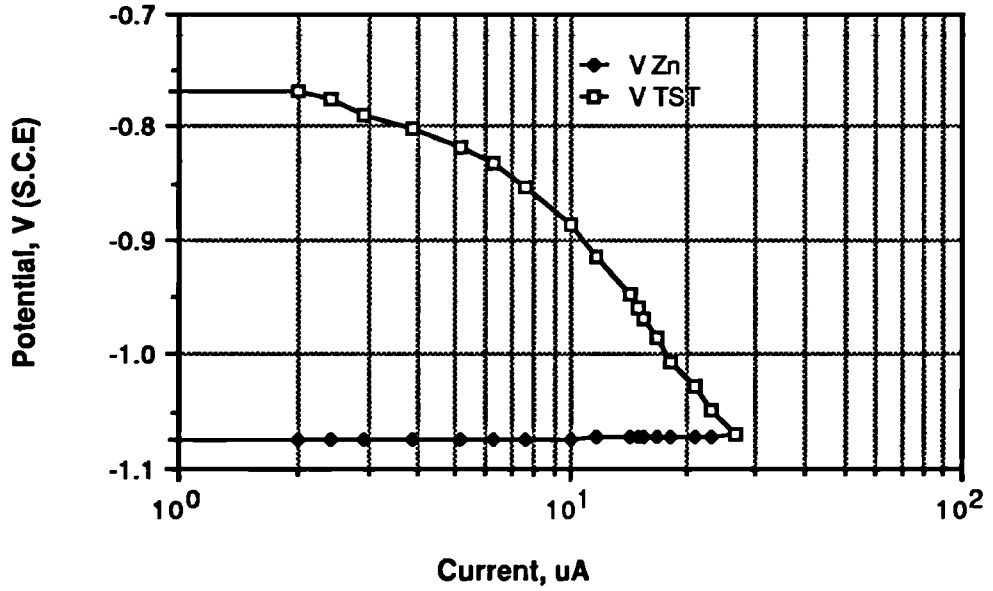


Figure 7.31 Evans diagram for coupled zinc coating and weld with injection of tool steel powder (TST) in 1N NaCl solution, pH 4, after 24 hr exposure.

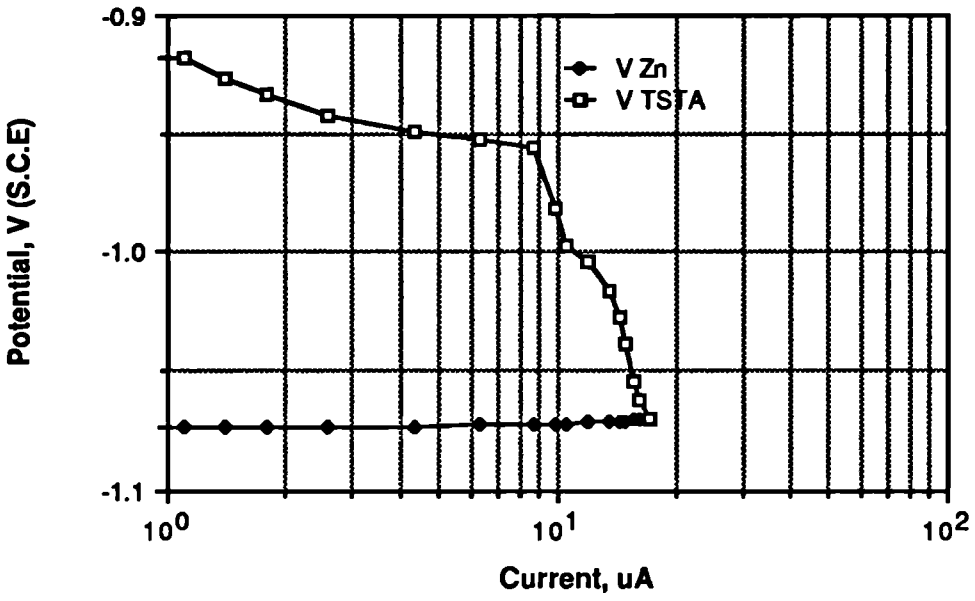


Figure 7.32 Evans diagram for coupled zinc coating and weld with tool steel powder incorporation (TSTA) in 1N NaCl solution, pH 4, after 24 hr exposure.

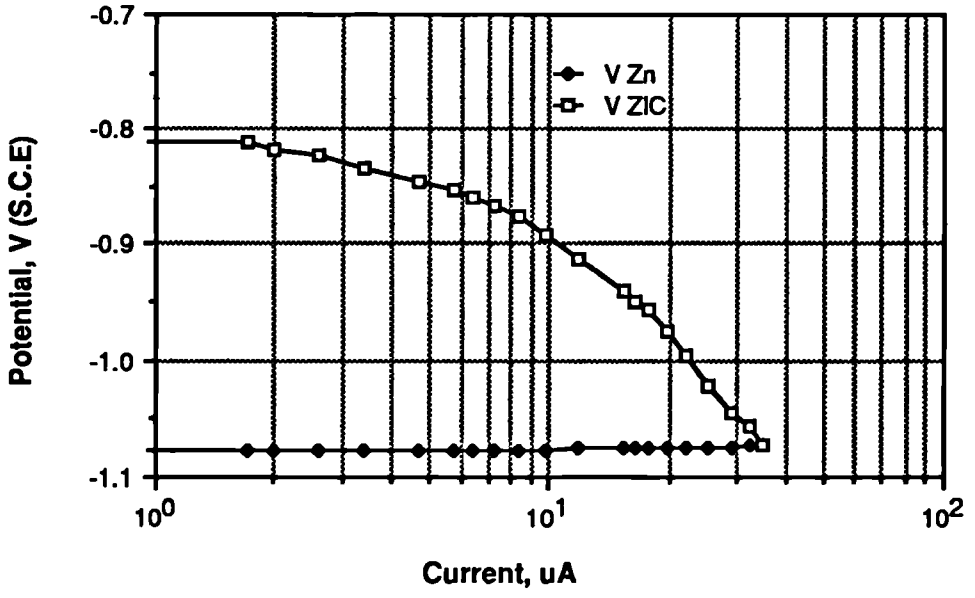


Figure 7.33 Evans diagram for coupled zinc coating and weld with zinc vapour incorporation (ZIC) in 1N NaCl solution, pH 4, after 24 hr exposure.

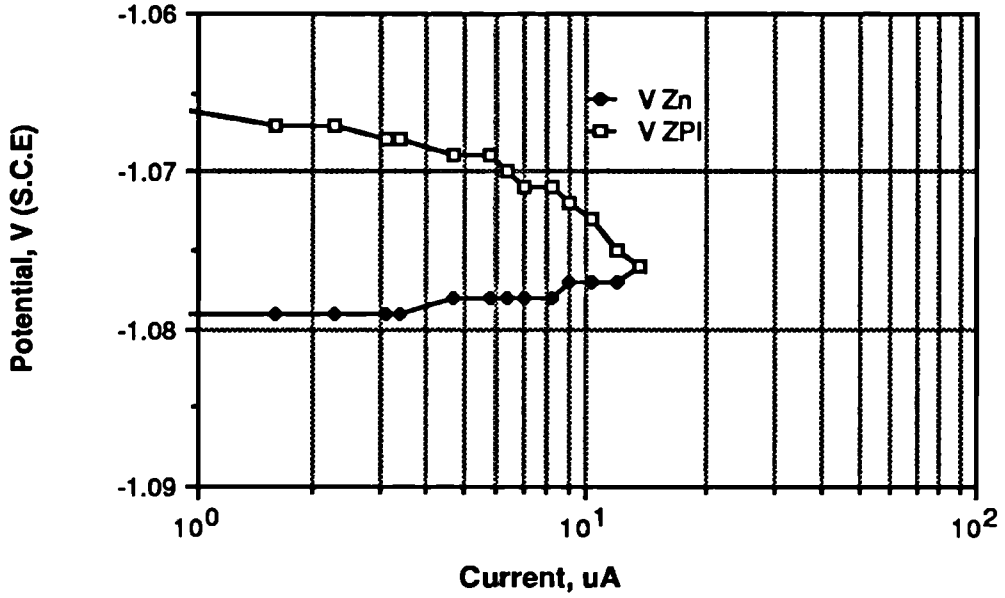


Figure 7.34 Evans diagram for coupled zinc coating and weld with zinc powder incorporation (ZPI) in 1N NaCl solution, pH 4, after 24 hr exposure.

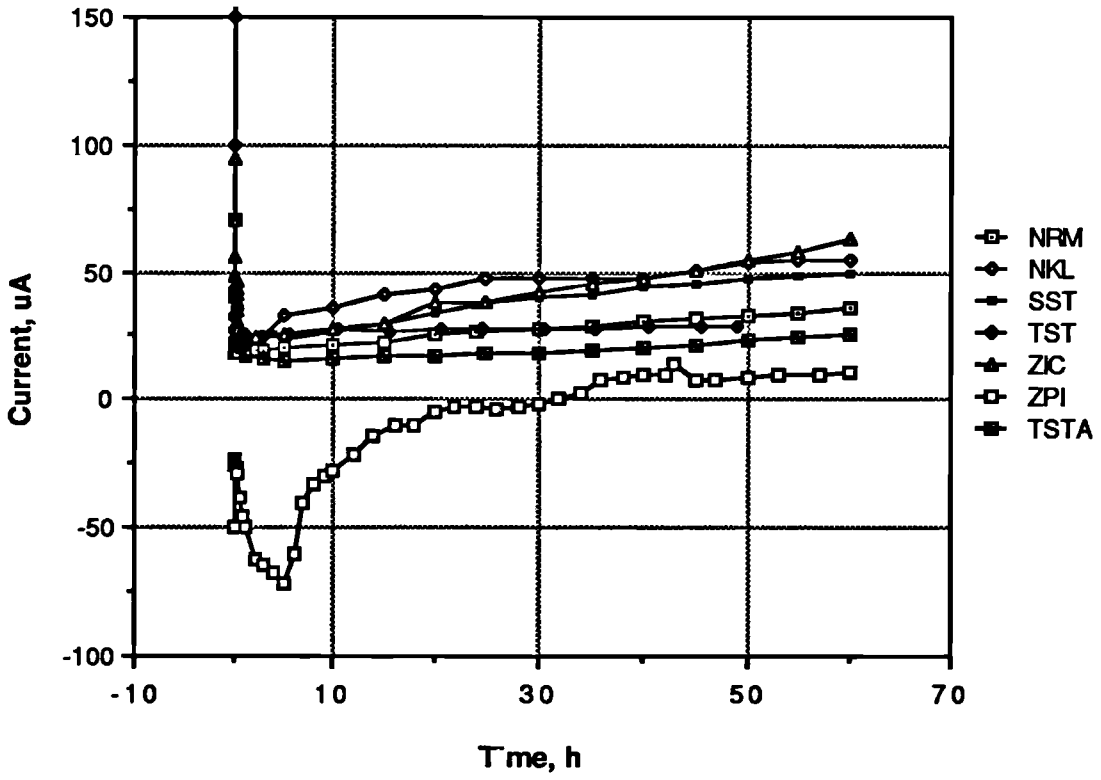


Figure 7.35 Current variation with time for coupled zinc coating and different modified composition welds in 1N NaCl solution, pH 4.

7.4 The Corrosion Morphology of Laser Welded Zinc Coated Steel

The material used in this study is electrogalvanised zinc coated steel. In this material, the zinc coating is adhered to the steel but it does not form an alloy between iron and zinc due to the process being carried out at low temperature (50-75°C). The use of a laser to weld two sheets together causes the volatilisation of the zinc coating at the welded area. The laser provides intense heat at the welded area. This heat is utilised for the melting of steel but some of the heat is also conducted into the base metal. Figure 7.36 shows a laser welded sample before corrosion starts. There is a large difference between the melting and boiling points of steel and zinc (For steel M.P = 1530° C, and B.P = 3000° C, for zinc M.P = 419.4° C, and B.P = 907° C [196]).

The heat conducted into the material on either side of the weld causes a reaction between steel and the zinc coating at the heat affected zone. This forms an intermetallic alloy adjacent to the weld beneath the actual zinc coating at the steel-zinc coating contact point. The cross section revealed that an Zn-Fe alloy existed at the interface of the steel and the zinc coating (Figure 7.37). The thickness of the intermetallic alloy decreases in the direction away from the weld (i.e., in the direction perpendicular to both the laser beam and the direction of the welding), until it has diminished completely at a certain distance. This is due to the decrease in the temperature away from the welded area so that at a given distance the temperature of the base material is not high enough to react with the zinc coating and to form an intermetallic alloy (Figure 7.38). The weld and intermetallic layer is schematically represented in Figure 7.40.

When the welded sample is subjected to a vigorous corrosion environment the zinc coating is first to be corroded. The weld was found to be protected by the adjacent zinc coating. The intermetallic layer can be revealed as a black layer on either side of the weld once the overlying zinc coating has been removed by self corrosion (Figure 7.39, which shows a top view of weld bead and HAZ). EDAX analysis (Figure 7.41)

on the black layer shows that it consisted of Zn-Fe alloy. The remaining zinc away from the heat affected zone area will protect the HAZ area in addition to the weld. When all the zinc is exhausted the Zn-Fe alloy, due to its more electronegative potential, as compared to iron weld, will act as an anode. Thus the corrosion, then starts on the Zn-Fe alloy while the weld will remain protected. The intermetallic layer corrodes at a lower rate than zinc, and can be compared to a Zn-Fe electrodeposited coating [132].

The corrosion of the Zn-Fe alloy is shown in Figure 7.39. The Zn-Fe alloy started corroding in the form of patches and the base steel was revealed beneath the alloy. EDAX analysis (Figure 7.42) made of the patches showed only iron is present in the patches and no zinc is there, i.e., the intermetallic alloy has corroded from that part revealing the iron of the base metal. It can be seen from the Figure 7.39 that the weld is still protected and there is no sign of the corrosion of weld. For a specimen exposed for a longer time the visual observations revealed that when all the zinc from the base metal and Zn-Fe from the HAZ was exhausted then the corrosion of the bare steel and weld was started.

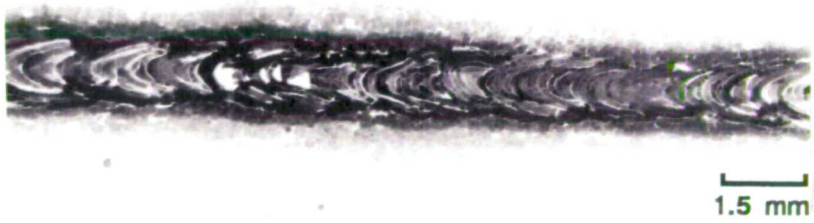


Figure 7.36 Laser welded zinc coated steel specimen before corrosion.

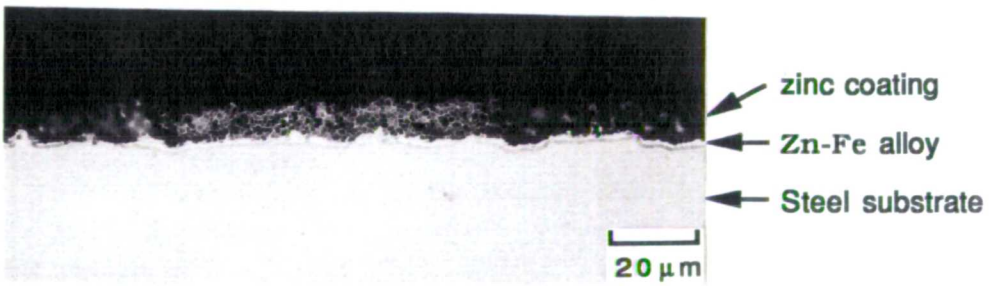


Figure 7.37 Intermetallic zinc-iron alloy formed at HAZ at steel-zinc coating contact point.

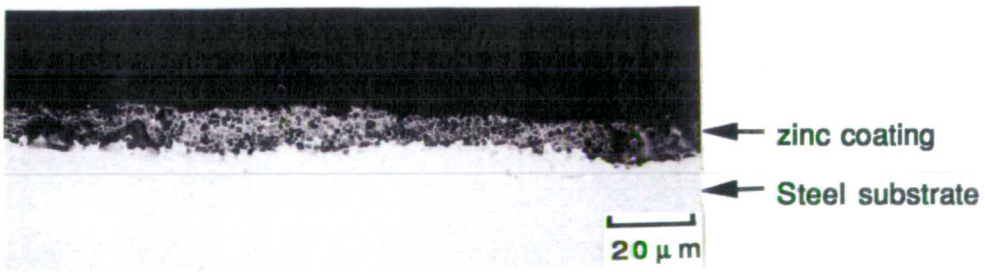


Figure 7.38 Zinc coating on steel far from the weld, no evidence of intermetallic compound.

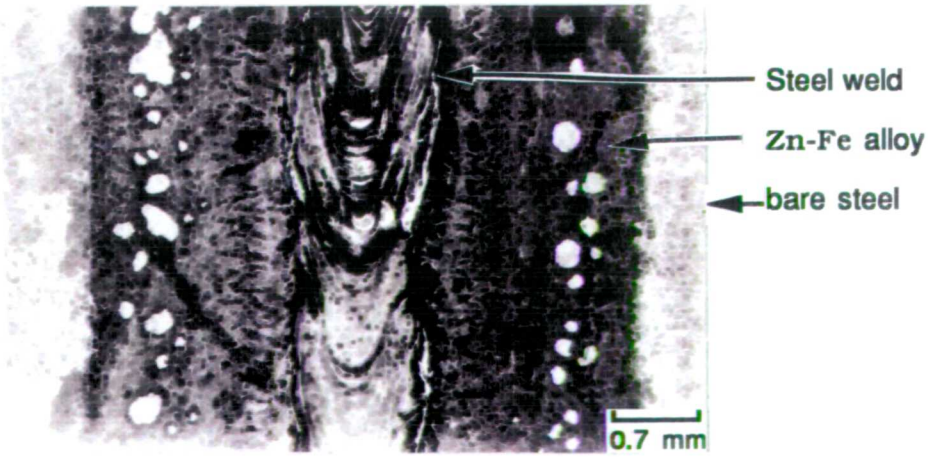


Figure 7.39 Laser welded zinc coated steel specimen after the corrosion of zinc coating revealed intermetallic Zn-Fe alloy (black layer).

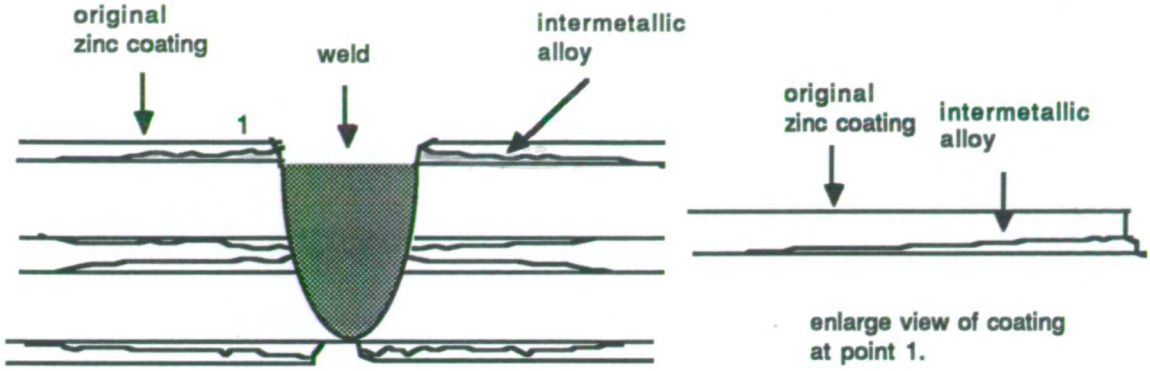


Figure 7.40 The schematic diagram representing the formation of intermetallic as a result of welding of the zinc coated steel sheet.

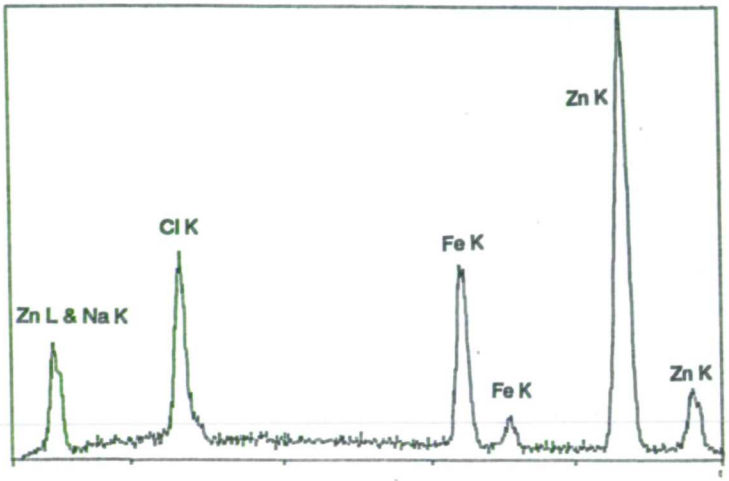


Figure 7.41 SEM analysis on intermetallic (black) layer showing the presence of zinc-iron alloy.

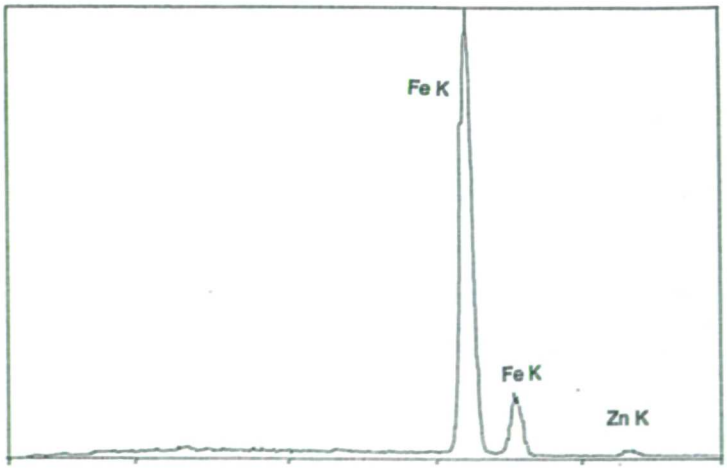


Figure 7.42 The SEM analysis in Figure 7.39 on a patch which showed the corrosion of intermetallic alloy.

Table 7.1 Laser Welding Parameters for Modified Composition Welds

Serial no.	Weld type	Laser power (kW)	Welding speed mm/s	Zn coating thickness (μm)	Weld width (mm)	Weld area (cm^2)	Area of coating exposed (cm^2)
1	UNW	---	---	7.5	---	---	1.770
2	NRM	1.54	20.0	7.5	1.5	0.225	1.545
3	NKL	2.00	32.7	10.0	1.3	0.195	1.575
4	SST	2.00	22.1	10.0	1.7	0.255	1.515
5	TST	1.54	20.0	7.5	1.5	0.225	1.545
6	TSTA	1.78	20.0	7.5	1.3	0.195	1.575
6	ZIC	1.54	20.0	7.5	1.5	0.225	1.545
7	ZPI	1.80	25.0	7.5	1.2	0.180	1.590

Where UNW = unwelded specimen, NRM = normal weld, NKL = nickel injected weld, SST = stainless steel injected weld, TST = tool steel injected weld, TSTA = tool steel incorporated weld, ZIC = zinc vapour incorporated weld, and ZPI = zinc powder incorporated weld.

Chapter 8

Conclusions and Future Work

8.1 Conclusions

The following conclusions has been drawn from the welding of zinc coated steel.

8.1.1 Welding Zinc Coated Steel

Three phenomena identified during the laser welding of zinc coated steel with similar laser parameters were:

(i) no welding but a slight melting of the workpiece,
(ii) deteriorated welds, and
(iii) sound welds.

The laser welding of zinc coated steel is a highly complex process. In the first case it has been found that the zinc plasma formed as a result of welding operation blocked the incoming laser beam and hence only slight melting resulted. This also depends upon the thickness of the zinc coating. A higher thickness of the zinc coating will produce more zinc vapour and hence thicker zinc plasma thus making the welding of this material more difficult.

In the second case the welds were deteriorated when the two overlapping sheets were tightly clamped and no gap was left between the sheets. The welds

showed a lot of pits and holes due to the explosive ejection of zinc vapour from the keyhole.

In the third case the sound welds were produced due to the presence of a small gap between the two sheets which helped vent the zinc vapour through the gap and hence a weld free of pits and holes was obtained. Thus good quality welds can be obtained in lap configuration using a small gap between the sheets.

8.1.2 The Formula for Welding Zinc Coated Steel

The following formula has been derived for welding zinc coated steel in lap configuration.

$$g_{exit} = \frac{AVt_{zn}}{\sqrt{t_p}} \qquad (8.1)$$

where g_{exit}; the minimum gap size required between the overlapped sheets, A; the constant equal to 16.1 $s/(m)^{1/2}$, V; welding speed, t_{zn}; zinc coating thickness, and t_p is thickness of the sheet.

The formula has predicted a gap size for welding zinc coated steel in lap configuration, the gap size is directly proportional to the welding speed and zinc coating thickness and inversely proportional to the square root of the thickness of steel sheet. Alternatively, the model predicted a welding speed for a particular gap size. The welding of zinc coated steel at higher welding speeds (and hence, at higher laser powers) was found to be very difficult depending upon the zinc coating thickness and the thickness of the steel sheet.

Four regions dependent on the gap setting were identified in the welding of zinc coated steel:

(i) Pitting region, in which the actual gap is less than that required for the venting of the zinc vapour. Thus the zinc vapour generated explodes out of the keyhole causing pitting in the weld bead (Figure 6.10).

(ii) Drop out region, in which the actual gap is very large and the molten metal drops into the gap leaving a dip in the upper sheet which can seriously affect the tensile strength of the weld (Figure 6.10).

(iii) Dropout and pitting region, in which the actual gap is large enough to produce a dip in the upper sheet but too small to exhaust the zinc vapour (Figure 6.10).

(iv) Operating region, in which the sound weld can be produced by matching the welding parameters according to the formula (Figure 6.10).

8.1.3 Effect of Welding Parameters

(i) *Effect of Gap Size on Penetration:*

Since a gap is necessary for welding zinc coated steel, this leads to a thermal barrier between the two sheets. Hence to overcome this barrier the welding speed has to be lowered for a full penetration of the bottom sheet. The reduction in speed is a function of gap size. The beam penetration in the lower sheet decreases with increasing gap size, possibly due to the thermal barrier aspect as well as the loss of focus of the beam energy. It has been found in these experiments that for a gap of 0.1 mm between the sheets the weld showed only 8 % decrease in penetration, a higher gap of 0.3 mm showed a 21 % decrease in weld penetration. Hence the welding speed can be adjusted accordingly with a gap size.

(ii) *Effect of Gap Size on Width:*

The width of the weld at the upper sheet increases with increase in gap size and the width at the interface decreases with increase in the gap

size. It has been found that for a gap of 0.1 mm, the width of the weld at the interface is almost the same as that without any gap. Also, if the width of the weld on the top sheet is more than the thickness of the sheet then surface tension pulls the liquid towards its edges and an undercut results.

(iii) ***Effect of Speed on Penetration:***

The weld penetration decreases hyperbolically with increase in welding speed for normal welds. The weld penetration decreases more sharply with welding speed in the case of metal powder injected welds.

(iv) ***Effect of Side Jet on Penetration:***

The use of a side jet effectively removed the zinc plasma at the beam metal interaction point. An optimum gas flow rate from the side jet gives a relatively deeper penetration.

(v) ***Effect of beam polarisation on penetration:***

Beam polarisation also effect the weld penetration. For electric vector parallel to welding direction (p-polarised beam) the penetration is 1.4 times higher than for the s- polarised radiation. Welding zinc coated steel with p-polarised beam penetrates the lower sheet better than the s-polarised beam.

(vi) ***Effect of beam mode on joining efficiency:***

The comparison of the welding performance of different laser systems available (with different beam mode structures or beam quality) in terms of joining efficiency has been described which showed that the beam mode is also an important parameter in the welding process. It has been found that the Gaussian beam mode gave the best joining efficiency as compared to doughnut, multimode and ring type beams.

(vii) ***Effect of Beam Mode on Penetration:***

The Gaussian beam mode due to a smaller spot size gave best penetration as compared to multimode, doughnut or top hat beams.

(viii) ***Effect of beam mode on width:***

Due to a bigger spot size of the multimode beam the width of the weld is higher for higher order mode.

(ix) ***Effect of metal powder addition on joining efficiency:***

Joining efficiency (beam coupling) increases with the addition of metal powder at optimum flow rate.

(x) ***Effect of gap size on joining and melting efficiency:***

Joining efficiency decreases with increase in gap size while the melting efficiency remains almost the same.

(xi) ***Effect of speed on melting efficiency:***

Melting efficiency decreases by increasing the welding speed.

(xii) ***Effect of laser power on melting and joining efficiency:***

Both melting and joining efficiency for same beam mode increase with increase in laser power.

(xiii) ***Using dimples as a method of setting the gap size:***

Use of dimples to establish gap size for sheet material in lap configuration is a more accurate alternative to the use of shims. Welds can be made successfully through the position of dimples thus eliminating surface marks near the weld. An optimum gap size of approximately 0.07-0.10 mm was determined to minimise defects during the laser welding of zinc coated sheet in lap configuration using dimples, on 0.7 mm sheet with a 7.5 μm coating of zinc on both sides.

(xiv) ***Mechanical Tests:***

Tensile, fatigue and impact tests on welded material have shown that fracture is not initiated at the weld, but in the base material,

8.1.4 Modification of Weld Composition

Three methods have been developed to modify the composition of the weld bead. They were:

(i) the injection of metal powder into the melt pool,

(ii) using an off axis gas assist jet to redeposit volatilised zinc on to the weld as it forms,

(iii) incorporation of metal powder on hot weld just after the welding which produced a coating of the required composition on the weld.

8.1.5 Corrosion Testing

(i) The short term electrochemical test employed discriminates between the coating self corrosion rate required for sacrificial protection of unwelded and welded samples and also between different weld material types.

(ii) The zinc coating was found to be successful in offering sacrificial protection to weld metal of all types during the life of the coating .

(iii) A corrosion resistant Zn-Fe intermetallic alloy is formed (as a result of laser welding) on either side of the weld to a distance of approximately 2 mm. This material prolonged the sacrificial action of the coating.

(iv) The following effects on the coating self corrosion rate for the sacrificial protection of welds of modified composition were observed:

(a) injection of nickel powder or stainless steel powder resulted in a higher coating corrosion rate compared with the normal weld.

(b) injection of tool steel powder resulted in a corrosion rate that was slightly lower than that of the normal weld.

(c) incorporation of volatilised zinc resulted in a corrosion rate that was initially substantially lower than that of normal weld, but on prolonged exposure corrosion rates became similar, indicating that insufficient zinc had been incorporated into the weld metal.

(d) The incorporation of tool steel powder after the weld, which produces a tool steel coating on the weld, showed a very low corrosion rate of the zinc coating.

(e) The incorporation of zinc powder just after the weld formation gave a lower rate of corrosion. The coating life time was prolonged to almost double due to the presence of a higher thickness of zinc coating (50-75 μm) at the weld bead.

The weld bead obtained with zinc powder incorporation (ZPI) just after the weld formation was found to be more corrosion resistant than the other modified composition welds and this may prove to produce welds of higher corrosion resistance. Hence the use of zinc powder to coat the weld just after the weld formation is beneficial from the corrosion point of view.

8.2 Suggestion for Future Work

(a) The present work has established a potential for laser welding of zinc coated steel as a method of high speed welding compared with conventional welding processes. Further work on the welding of zinc coated steel is suggested using a pulse laser and to obtain a correlation between the pulsed frequency and the plasma fluctuation for welding zinc coated steel.

(b) Some further work could be done in getting the gap welding into the production process.

Reference

[1] Porter, F. C. "Slowing down the rate of corrosion" *Eng. Mater. Design*, Vol. 19, pp. 25. (1975).

[2] Porter, F. C., Stoneman, A. M. and Thilthrope, R. G. "The range of zinc coatings" Trans. Instt. Met. Finish (ZDA), Vol. 66, Part. 1, pp. 28-33, ISSN-0020-2967 (1988).

[3] Mackowiak, J. and Short, N. R. "Metallurgy of galvanised coatings" *International Metals Reviews* Vol. 24, pp. 1-19, (1979).

[4] Belleau, C. Kelley, D. K and Marttila, W. A. "Some considerations in the welding of automotive galvanised steels". Proc. Conf. *Sheet metal welding*, Detroit, Michigan. American welding society 2501 N. W. 7th st. Miami 33125 U.S.A. paper no. 17 (Oct.Nov, 1984).

[5] Shreir, L. L. Corrosion. Vol. 2, Newnes-butterworths London, Boston, (1976).

[6] Williams, N. T., and Waddell, W. "High speed resistance seam welding of uncoated and coated steels" Technical steel research. Commission of the European Communities. Report no EUR 11550 EN. (1988).

[7] Anderau, E. A. and Opprecht, J. "Resistance seam welding of coated steel sheets" Proc. Conf. Sheet metal welding, Detroit, Michigan USA. American Welding Society 2501 N.W. 7th st. Miami, Florida 33125 USA. Paper no. 18, pp. 1-20 (Oct.Nov. 1984).

[8] Gregory, E. N. " Arc welding of galvanised steel". *Sheet Metal Industries*, Vol. 45, No. 495, pp. 501-507 July (1968).

[9] "Welding galvanised steel" *Canadian Welder and Fabricator.* Vol. 79, No. 7, pp. 16-17 (July 1988).

[10] Lundquist, B. "Sandvik welding handbook" pp. 70, (1977).

[11] Andrews, J. G. and Atthey, D. R., "Hydrodynamic limit to penetration of a material by a high-power beam", *J. Phys (D): Appl. Phys.*, No. 15, Vol. 9, (1976).

[12] Banas, C. M., Breinan, E. M.,"Evaluation of basic laser welding capabilities" United Technologies Report. R75-911989-4.

[13] Meleka, "Electron beam welding", London, Published for the Welding Institute by McGraw-Hill, (1971).

[14] Tomsic, J. "Energy distribution in keyhole model in plasma arc welds" *Weld. Res. Supp.* (March 1984).

[15] Crafer, R. "Welding with a 2kW laser" Weld. Instt. Res. Bull.17(2), pp. 29-33, (1976).

[16] Merchant, V. E. "New developments in high power laser welding" UPDATE'85, The welding institute of Canada. Laser Applications Science and Engineering Research, Canada. (1985).

[17] Duley, W. W. "CO_2 Lasers: Effect and Applications" Academic Press (1976).

[18] Swift-Hook, D. T. and Gick, A. E. F. "Penetration welding with Lasers" *Weld. Res. Supp.* pp. 492-S, (Nov. 1973).

[19] Klemens, P. G. "Heat balance and flow conditions for electron beam and laser welding" *J. Appl. Phys.* Vol. 47, No. 5, (May 1976).

[20] British Standard, steel plate, sheet and strip, BS 1449: Part 1: pp. 11, (1983).

[21] O'shea, D. C., Callen, W. R., and Rhodes, W. T. An introduction to lasers and their applications. Addision-Wesley Publishing Company, (1978).

[22] Ready , J. F., Industrial application of lasers. Academic Press, (1978).

[23] Beesley, M. J., Lasers and their applications. Taylor and Francis Ltd. (1972).

[24] Rockstroh, T. J., and Mazumder, J., "Characterisation of laser induced plasma and temperature measurement during lasre surface treatment" Laser Surface Treatment of Metals, eds. C. W. Draper, P. Mazzoldi, Martinus Nijhoff Publisher Dordrecht (Netherland) ISBN 90-247-3405-3, pp. 23-29 (1986).

[25] Baardsen, E. L., Schmatz, D. J., and Bisaro, R. E., "High speed welding of sheet steel steel with a CO_2 laser" *Welding, J.*, pp. 227-229 (April 1973).

[26] Lock, E. V., Hoag, E., and Hella, R., "Deep penetration welding with high

power CO_2 laser" *Welding , J.*, Vol. 51,pp. 245S, (1972).

[27] Wilgoss, R. A., Megaw, J. H. P. C., and Clark, J. N., "Assessing the laser for power plant welding", *Weld. Metal Fabr.* pp. 117 (March, 1979).

[28] Carslaw, H. S., and Jaeger, J. C., Heat conduction in solids, 2nd ed. Oxford University Press, (1959).

[29] Harry, J. E., Industrial lasers and their applications, McGraw Hill Book Company (1974).

[30] Sharp, M., and Steen, W. M., Surface Engineering Conf., Brighton, July (1985).

[31] Sharp, M., Henry, P., Steen, W. M., and Lim, G. C., "An analysis of the effect of mode structure on laser materials processing" Optoelectronik, Munich, (June,1983).

[32] Roessler, D. M., "An introduction to the laser processing of materials" The Industrial Laser Annual Handbook, eds. David Belforte & Morris Levitt, pp. 16-30 (1986).

[33] Ready, J. F., Effects of high power laser radiation, Academic Press, (1971).

[34] Seamen, F. D. "The role of focus in heavy plate laser welding" SME Technical Paper No. MR78-345, Michigan, (1977).

[35] Engel, S. L., "Kilowatt welding with a laser", *Laser Focus*, pp. 44-53, February, (1976).

[36] Alexender, J., Ph. D Thesis, University of London, (1982).

[37] Petesch, B., Robin, M., Chabenat, A., Binard, J., " Laser welding of nickel sheets" Proc. 3rd Int. Conf. on Lasers in Manufacturing (LIM-3), pp. 145, 3-5 June, (1986).

[38] Banas, C. M. "High power laser welding" ASM/NASA/GWU Symposium on Welding, Bonding and Fastening, Williamsburg, Virginia, U.S.A. May 30-June 1, (1972).

[39] Russell, J. D., Dinsdale, W. O., Bishop, D. I. "Laser welding of aero-engine materials" Welding Institute Research Bulletin, January (1978).

[40] Eboo, G. M., Ph.D. Thesis London University (1979).

[41] Herziger, G., Kreutz, E. W., and Wissenbach, K., "Fundamentals of laser

processing of materials", Laser Processing, Fundamentals, Applications, and System Engineering, *SPIE*, Vol. 668, (1986).

[42] Herziger, G. "The influence of laser induced plasma on laser material processing" The Industrial Laser Annual Hand Book, eds. D. Belforte, and M. Levitt, PennWell Books (Laser Focus), (1987).

[43] Herziger, G., "Physics of laser materials processing" Proc. Conf. High Power Lasers and Their Industrial Applications, *SPIE*- Vol. 650, pp. 188-194 (1986).

[44] Beyer, E., Bakowsky, L., Loosen, P., Poprame, R., and Herziger, G., "Development and optical absorption properties of a laser-induced plasma during CO_2 laser processing" *SPIE*- Vol. 455, pp. 75-80, (1983).

[45] Arata, Y., and Miyamoto, I., "Laser welding" *Technocrate*, Vol. 11, No. 5, pp. 33 (May, 1978).

[46] Mazumder, J., Ph. D Thesis, University of London, (1978).

[47] Belforte, D., and M. Levitt, M. The Industrial Laser Annual Hand Book, PennWell Books (Laser Focus), (1987).

[48] Metzbower, E. A., Hella, R. A., and Theodorski, G., "Laser beam welding at NIROP, a navy manufacturing technology programme" Proc. Conf. Lasers in Materials Processing, Ed. Metzbower, E. A., American Society for Metal, (1983).

[49] Mazumder, J., and Steen, W. M., " Welding of Ti-6Al-4V by a continuous wave CO_2 laser" *Met. Constr.* Vol. 12, No. 9, pp. 423 (1980).

[50] Adams, H. J., Met. Constr. Br. Weld. J., Vol. 2, No.1 (1970).

[51] Seamen, F. D. " The role of shield gas in high power CO_2 (CW) laser welding" SME, MR77-982 (1977).

[52] Bousseau, M., and Signamarcheix, J. M. "Example of possibilities offered by high power lasers in welding applications" Proc. 3rd Int. Conf. on Lasers in Manufacturing (LIM-3) Paris,France, 3-5 June (1986).

[53] Herziger, G., Kreutz, E. W., and Wissenbach, K., "Fundamentals of laser processing of materials" Laser Processing, Fundamentals, Applications and System Engineering, *SPIE* Vol. 668, (1986).

[54] Arata, Y., Zhu, Z., Oda, T., and Abe, N., "Some problems on laser plasma control with argon assits gas" Trans. JWRI, Vol. 15, No. 1, pp. 155-156 (1986).

[55] Engel, S. L., "How to make better laser welds" *Weld. Des. Fabr.* pp. 62, January (1978).

[56] Bass, M., Laser Materials Processing, North Holland Publishing Company (1983).

[57] Shewell, J. R., "Design for laser beam welding", *Weld. Des. Fabr.* pp. 106 (June 1977).

[58] Baranov, M. S., Vershok, B. A., Geinrikhs, I. N., and Privezenster, V. I. "The influence of gap size on the formation and strength of a spot lap joint in laser welding" *Weld. Prod.* Vol. 23, No. 5, pp. 19 (1976).

[59] Velichko, O. A., Garashchuk, U. P., and Maranski, V. E., "Special features of the pulsed laser beam welding of lap joints with a gap" *Auto. Weld*, Vol. 25, Pt. 4, pp. 75 (1972).

[60] Anthony, T. R., and Cline, H. E. " Surfase rippling induced by surface tension gradients during laser surface melting and alloying" J. Appl. Phys. Vol. 48, No. 9, pp. 3888-3894, (1977).

[61] Hawkes, I. C., Lamb, M., Steen, W. M. " Surface topography and fluid flow in laser surface melting" Proc. Conf. 3rd Int. Collq. on welding and melting by Electrons and Laser Beams. pp. 125-131 (5-9 Sept, 1983).

[62] Ishizaki, K, "A new approach to the mechanism of penetration" Proc. Conf. Arc Physics and Weld Pool Behaviour, Welding Institute England (1980).

[63] Copley, S. M., Beck, D. G., Esquivel, O., and Bass. M. "Solidification of continuous laser melted trails" Proc. Conf. Lasers in Metallurgy (eds). K. Mukherjee and J. Mazumder, AIME Chicago, pp. 11-19, (1981).

[64] Moore, P. G., and Weinman, L. S., "Surface alloying using high power continuous lasers" *Laser Applications in Materials Processing SPIE*- Vol. 198, pp. 120-125 (1979).

[65] Kotecki, D. J., Cheever, D. L., and Howden, D. G., "Mechanism of ripple formation during weld solidification" Weld. Res. Suppl. pp. 386s-391s,

August (1972).

[66] Beyer, E., Gasser, A., Gatzweiler, W., and Sokolowski, W., "Plasma fluctuations in laser welding with cw-CO_2 lasers" Proc. Conf. *ICALEO' 87*, pp. 17-23, (1987).

[67] Albright, C. E., and Chiang, S., "High speed laser welding discontinuities" Journal of Laser Application, Vol. 1, No. 1, pp. 18-24, October (1988).

[68] Bradstreet, B. J., "Effect of surface tension and metal flow on weld bead formation" *Weld. Res. Suppl.* Vol. 47, No. 7, pp. 314s-322s, July (1968).

[69] Wealleans, J. W., and Adams, B. " Undercutting and weld bead turbulence in TIG welding" *Welding and Metal Fabrication*, pp. 255-257, June (1969).

[70] Bass, M. Laser Materials Processing, North Holland Publishing Company, Amsterdam, (1983).

[71] Pirri, A. N., Root, R. G., and Wu, P. K. S., "Plasma energy transfer to metal surfaces irradiated by pulsed lasers" *AIAA Journal*, Vol. 16, No. 12, pp. 1296-1304 (1978).

[72] Dixon, R. D., Lewis, G. K., " The influence of a plasma during laser welding" Proc. Conf. *ICALEO'83*, Laser Institute of America,Los Angeles, Materials Processing, Vol. 38, pp. (14-17 Nov. 1983).

[73] Poprawe, R., Beyer, E., Bakowsky, L., Brumme, G., and Herziger, G., *Optoelectronic in engineering* Springer-Verlag, Berlin, pp. 361 (1983).

[74] Beyer, E., et al. "Influence of shielding gas in laser beam welding" Proc. Conf. *Laser' 85*, Munchen, ed. W. Waidelich, Springer Verlag, (1986).

[75] Matsunawa, A., Yoshida, H., and Katayama, S., "Beam plume interaction in pulsed YAG laser processing" Proc. Conf. *ICALEO'84* Boston, pp. (1984).

[76] Krokhin, O. N., *Laser Handbook 2,* eds. F. T. Arecci and E. O. Schulz-Deboise, North Holland Publishing Co, Amsterdam, (1972).

[77] Afanas'ev, Y. V., and Krokhin, O. N. "Vaporisation of matter exposed to laser emission" *Sov. Phys. JETP,* Vol. 24 No. 4, pp 639 -645 (1967).

[78] Beyer, E., Heziger, G., Gasser, A., and Sokolowski, W. "Plasma fluctuation during laser machining with cw CO_2 laser" SPIE-Vol. 101-29 Den Haag, (1987).

[79] Kreutz, E. W., "Physical requirements for lasers in processing" Proc. 4th Int. Conf. on *Lasers in Manufacturing* (LIM-4), ISBN-0-948507-53-5. pp. 263-278 (May 1987).

[80] Gatzweiler, W., Maischnur, D., Faber, F. J., Derichs, C., and Beyer, E., "Model of dynamic behaviour in lasr beam welding" Proc. Conf. High Power Lasers and Laser Machining Technology, Paris, eds. M. L. Gaillard and A. Quenzer. SPIE-Vol. 1132, pp. 157-165, (25-28 April 1989).

[81] Welding Handbook, Vol. 2, 7th Ed. American Welding Society, Miami, FL. (1978).

[82] Nielbock, F. "MAG welding of galvanised steel sheets" Bander Bleche Rohre, Vol. 28, Part. 6, pp. 121-124 (1987).

[83] Gillette, G. H., and Breymeier, R. T. Welding Journal. Vol. 30, pp. 151s, (1951).

[84] Lavery, R. C., and Williams, N. T. Sheet Metal Industries, Vol. 43, pp. 201-210, (1970).

[85] Gedeon, S. A., and Eagar, T. W., "Resistance spot welding of galvanised steel: Part 1. Materials variations and process modification" Met. Trans. B, Vol. 17B, Part. 4, pp. 879-885, Dec. (1986).

[86] Lavery, R. C., and Williams, N. T. " Resistance spot welding of galvanised steel" Met. Constr. Br. Weld. J. Vol. 1, No. 1, January (1969).

[87] Williams, N. T. "Problems in resistance welding of coated steels" Sheet Metal Industries, Vol. 49, No. 7, pp. 625-633, October (1972).

[88] Krause, H. J., and Simon, G.,"Electrode life of spot welding electrodes depending on varies parameters" Proc. Conf. Resistance Welding, Essen. pp. 85-100, Sept. (1981).

[89] Connel, L. D., Met. Constr. Vol. 2, pp. 68-72 (1970).

[90] Nadkarni, A. V. and Weber, E. P. "A new dimension in resistance welding electrode materials" Weld. J. Vol. 56, pp. 331s-338s, (1977).

[91] Campbell, D. H., and Evarts, G. L. "Improved resistance welding of galvanised steel" U.K. Patent Application No. 8812351, 21- December, (1988).

[92] Lane, C. T., Sorensen, C. D., Hunter, G. B., Gedeon, S. A., and Eagar, T. W.

"Cinematography of resistance spot welding of galvanised steel sheet" Weld. Res. Suppl. pp. 260s-265s, Sept. (1987).

[93] Opprecht, P., "Continuous welding of coated steel sheet by means of wire electrodes" Bander Bleche Rohre, Vol. 19, Part. 2, pp. 68-71 (1978).

[94] Brown, B. "A comparison of AC and DC resistance welding of automotive steel" Weld. J., Vol. 66, Part. 1, pp. 18-23 (1987).

[95] Bennington, R. J. "Speed doubled on robotic arc welding of complicated automotive assembly" Weld. J., Vol. 65, Part. 11, pp. 27-30 (1986).

[96] Ganowski, F. J., and Williams, N. T. "Advances in resistance spot and seam welding of zinc coated steel strip" Sheet Metal Industries, November (1972).

[97] Gregory, E. N., Porter, F. C., Roswell, S. L., Snee, R. K., Toseland, P. W., Williams, N. T. Welding Coated Steels, The Weld. Instt. Abington Hall Abington, Cambridge, ISBN- 0 85300115 4 (1978).

[98] Sievert, W. C., and Franks, L. L. "A two side hot dip galvanised steel product for exposed automotive body panels" SAE Technical Paper Series, Paper No. 800146 (1980).

[99] Belleau, C., and Kelley, D. K., "Galvanised coating effects in outer body panels" SAE Technical Paper Series, Paper No. 830516, (1983).

[100] Thorne, J. P., and Geiermann, T. J., " A new approach for projection welding coated sheet metal" Sheet Metal Welding Conf. Detroit, Michigen, Am. Weld. Soc. Paper no. 19, October (1984).

[101] Jessop, T. J., and Roswell, S. L. "Projection weld ng of coated steels" Weld. Instt. Conf. Advances in welding processes, Harrogate, paper no. 19, pp. 185-193 (1974).

[102] Newman, R. A. A. "Laser welding in mass production at Moulinex" *Welding and Metal Fabrication*, Vol. 44, part. 8, pp. 563-569, October (1976).

[103] Wirth, P. "Laser welding in the German automotive industry" Proc. Conf. The laser vs the electron beam in welding, cutting and surface treatment: State of art. Reno Nevada U.S.A. Vol. 1, pp. 164-170, 6-8 November (1985).

[104] Prange, W., Schneider, C., and Jack, K. "Zinc sheet for deep drawing is laser welded at Thyssen" *Steel Times*, Vol. 216, Part. 1, pp. 25-28, January

(1988).

[105] Kellock, B. "Lasers cut a dash in the motor industry" *Mach. Prod. Eng.* Vol. 146, pp. 26-30, March (1988).

[106] "Laser beam welding without additional material" Ind-Auz, Vol. 108, Part. 76, pp. 32-33 (1986).

[107] Haniche, L. "Laser technology within the Volvo car corporation" Proc. 4th Int. Conf. on *Lasers in Manufacturing*,Ed. Dr. W. M. Steen, pp. 49-68, Birmingham, U. K. (12-14 May 1987)

[108] Imhoff, R., Behler, K., Gatzweiler, W., and Beyer, E. "Laser beam welding in car body making" Proc. 5th Int. Conf. *Lasers in Manufacturing.* Stuttgart, West Germany. Edited by Prof. Hugel, pp. 247-258 (September 1988).

[109] Akhter, R., Steen, W. M., Cruciani, D. "Laser Welding of Zinc Coated Steel" Proc. 5th Int. Conf. *Lasers in Manufacturing.*Stuttgart, West Germany, Edited by Prof. Hugel, pp. 195-206. (September1988).

[110] Imhoff, R., Beyer, E., and Behler, K. "Car body welding with laser radiation". Proc. Conf. 20th-ISATA Vol. III, pp. 2251-2261, Florence, Italy, (29th May-2nd June 1989).

[111] Belforte, D. A. "Laser applications in the auto industry". Proc. 5th Int. Conf. *Lasers in Manufacturing.*Stuttgart, West Germany, Edited by Prof. Hugel, pp. 195-206. (September1988).

[112] Hanicke, L. "Laser technology within the Volvo car corporation". Proc. 5th Int. Conf. *Lasers in Manufacturing.*Stuttgart, West Germany, Edited by Prof. Hugel, pp. 97-115. (September1988).

[113] Heyden, J., Nilsson, K., and Magnusson, C. "Laser welding of zinc coated steel" Proc. 6th Int. Conf. on *Lasers in Manufacturing*, Birmingham, U.K. Ed. Prof. W. M. Steen, pp. 93-104 (May 1989).

[114] Decker, I., Matzeit, A., Ruge, J., and Schielke, A. " Influence of surface layers on the metallurgical properties of laser beam welds" 2nd European Conf. on *Laser Treatment of Materials*, ECLAT'88, DVS 113, pp. 42-45 (1988).

[115] Winand, R. "Continuous strip coating: New znc alloy tailored coatings" *Surface and Coatings Technology.* Vol. 37, pp. 65-87, (1989).

[116] Jones, D., Brinn, D. "Zinc coated steels in buildings" British Steel Corporation Report No. WL/RSC/202/83/D(R), (August 1983).

[117] Sedzimir, T. "Process and apparatus for coating metallic objects with layers of other metals" U.K. Patent No. 453 803, September, (1936).

[118] "Hot dip galvanising and rust prevention" Hot dip galvanisers association. A member of the zinc development association, Alden Press, Oxford (1949).

[119] "Hot dip galvanised coatings" Metals Handbook, American Society for Metals, Metals Park, Ohio. Vol. 5, 9th ed. pp. 323-332, (1982).

[120] Dinda, S., Traficante, R. J., "Worldwide supply of zinc coated sheet steel for automotive applications. SAE Technical Paper Series Paper No. 840283. International Congress and Exposition Detroit, Michigan (February 27-March 2, 1984).

[121] "New galvanising line at Ebbw Vale" *Sheet Metal Industries.* Vol. 46, pp. 387-394 (1969).

[122] Gailer, J. W. and Vaughan, E. J. Protective Coatings for Metals, Charles Griffin & Company Ltd. London (1950).

[123] Lowenheim, F. A., (ed.) Modern Electroplating, John Wiley New York (1974).

[124] Fleischmann, M., and Thirsk, H. R., " Advances in Electrochemistry and Electrochemical Engineering. Ed. Delahay, P and Tobias, C. W. Vol. 3 Chapt. 3, Interscience New York (1963).

[125] Silman, H., Chemical and Electroplated finishes, Chapman & Hall Ltd. (1952).

[126] Froman, G. W. "Zinc-rich precoated steel" Coatings for Corrosion Prevention. Symp. ASM Materials & Processing Congress, Pennsylvania, pp. 9-18, November 9, (1978).

[127] Be eau, C., and Kelley, D. K., "Characterisation of one-and-a-half side galvanised steels for automotive applications. SAE Technical paper series, Paper No. 840284, International Congress & Exposition Detroit, Michigan. February 27-March 2, (1984).

[128] Satoh, N. "Effect of heavy metal additions and crystal modification on the zinc

phosphating of electrogalvanised steel sheet". Surface and Coatings Technology, Vol. 30, pp. 171-181 (1987).

[129] Basu, S. R., Pal, P. K., and Mukhopadhyay, B. N. "Corrosion resistant precoated autobody steel sheets". Key Eng. Mater. Vol. 20-28, Part. 2, pp. 1355-1369 (1988).

[130] Dasarathy, C., and Goodwin, T. J. "Recent developments in automotive steels" Metals and Materials, Vol. 6, No. 1, pp. 21-28 January (1990).

[131] Belleau, C., and Kelley, D. K. " Effect of galvanised steel defects on painted appearance of exposed panels. SAE Technical Paper Series. Paper No. 830491 (1983).

[132] Watanabe, T., Ohmura, M., Honma, T., and Adaniya, T. "Iron-zinc alloy electroplated steel for automotive body panels" SAE Technical paper Series, Paper No. 820424 (1982).

[133] Noumi, R., Nagasaki, H., Foboh, Y., and Shibuya, A., "Newly developed Ni-Zn alloy plated steel sheet and its application to automotive usages" SAE Technical Paper Series, Paper No. 820332 (1982).

[134] Saito, T., Oka, J., Wake, R., and Kitayama, M., "Development and properties of Zn-Ni alloy electroplated steel" Durzinklite Nippon Steel Tech. Rep. pp. 1-10, (25 April 1985).

[135] Herrschaft, D. C., Radtke, S. F., Coutsouradis, D., and Pelerin, J. " Galfan- A new zinc alloy coated steel for automotive body use" SAE Technical Paper Series, Paper No. 830517, International Congress and Exposition Detroit, Michigan, pp. 67-74 (1983).

[136] Kokubo, I., Nomura, S., Sakai, H., Sakaguchi, M., and Iwai, M., "Newly developed Zn-Fe/ Zn-Ni double-layer electroplated steel sheet" SAE Technical Paper Series, Paper No. 830518 pp. 75-82 (1983).

[137] Catanzano, A., Arrigoni, G., Palladino, M., and Sarracino, M. " Multilayer eletrogalvanised (Zn-Cr-CrO_X) steel sheet for optimum corrosion protection of car bodies" SAE Technical Paper Series, Paper No. 830583 pp. 107-124 (1983).

[138] British Steel increases coated steel production" News, *Metals and Materials*

Vol. 5, No. 10, pp. 578 (1989).

[139] Pierre, M. "Utilization of zinc coated sheet metal in the automotive industry" Galvano-Organo-Traitments De Surface, MAI/88/586, Vol. 57, pp. 383-386 (1988).

[140] Mathews, A., "How the auto industry sits in the electrogalvanising driving seat" Steel Times Int. (BSC Strip Mill Product), VOL. 11, Part. 3, ISSN-0-0143-7798 (September, 1987).

[141] Handbook for the BOC model 901 CO2 gas laser. BOC Industrial power beam division, Daventry, England.

[142] HPL Industrial Laser Operators Manual by AVCO Everett Research Laboratory Inc., Everett, Massachusetts, (August 1976).

[143] Davis, J. W. "United Technologies Industrial Laser Systems In Production". Seminar on the Industrial Applications of Lasers, Philips' Congress Centre, Eindhoven, The Netherlands, March 6-7, (1984).

[144] Ferranti MF400, CO_2 Industrial Laser, Operating Manual. Ferranti Industrial Electronics Limited, Dunsinane Avenue, Dundee DD2 3PN, Scotland.

[145] Lin, Li. Ph. D Thesis, University of London, (1989).

[146] Weerasinghe, V. M. Ph. D. Thesis, University of London, (1985).

[147] Seferain, D. "The metallurgy of welding". Wiley, New York, (1962).

[148] Evans, U. R. "The corrosion and oxidation of metals" Edward Arnold (Publishers) Ltd. London (1976).

[149] Quigley, M. B. C. "High power density welding". The Physics of Welding, Edited by J. F. Lancaster, Pergamon Press, pp. 268-290 (1986).

[150] Berns, H. Private Communications, Ruhr-Universitat Bochum (1988).

[151] Olsen, F. O. "Cutting with polarised laser beams" Berichte Stabltechnik, D. V. S 63, pp. 197-200 (1980).

[152] Olsen, F. O. "Laser cutting". Laser Technologies in Industry, SPIE- Vol. 952, pp. 572-582 (1988).

[153] Charschan, S. S. (ed.), Lasers in Industry, Van Nostrand-Reinhold, (1972).

[154] Dausinger, F., Beck, M., Rudlaff, T., and Wahl, T. " On coupling mechanisms in laser processes". Proc. 5th Int. Conf.*Lasers in Manufacturing*.Stuttgart, West Germany, Edited by Prof. Hugel, pp. 177-185. (September 1988).

[155] Beyer, E., Behler, K., and Herziger, G. "Influence of laser beam polarisation in welding" Proc. 5th Int. Conf.*Lasers in Manufacturing*.Stuttgart, West Germany, Edited by Prof. Hugel, pp. 233-240. (September 1988).

[156] Behler, K., Beyer, E., Schulz, W., Wolf, N., and Welsing, O. "Accommodation of polarisation and shaping in laser beam welding" Proc. 5th Int. Conf. *Lasers in Manufacturing*.Stuttgart, West Germany, Edited by Prof. Hugel, pp. 187-194. (September1988).

[157] Garashchuk, V. P., and Kirsey, V. I. " Effct of polarisation of continuous CO_2 laser radiation on the weld formation" Proc. Conf. Power Beam Processing, Electron, Laser, Plasma Arc. San Diego Cal., U.S.A. pp. 185-189, 2-6 May (1988).

[158] Shah, S. T. and Steen, W. M. "SF/FAF laser oscillator" 4th International Symposium on Optical and Optoelectronics Optical Science and Engineering. The Hague, Netherlands, SPIE- Vol. 101, pp. 3 (March 1987).

[159] Gabzdyl, J. T. Ph. D Thesis. University of London. (1989).

[160] Folkes, J. A. Ph. D. Thesis London University, (1986).

[161] Kubaschewski, O., and Alcock, C. B. Metallurgical Thermochemistry. 5th ed. Vol. 24, Int. series on Materials Science and Technology, Pergamon Press (1979).

[162] Standish, J. V. "Atmospheric corrosion mechanisms of painted steel" Society of Automotive Engineers, Metals Park Ohio, SAE paper no. 830489, (1983).

[163] Barnett, W. "The corrosion resistance of galvanised coatings in various environments" *Corrosion and coatings South Africa*- pp. 23-24 October (1988).

[164] Jones, D. A., Nair, N. R. "Electrochemical corrosion studies on zinc coated steel" *Corrosion*, Vol. 41, No. 6, pp. 357-362 (1985).

[165] Einspanier, J. A. "How zinc-rich primers combat corrosion".*Industrial Finishing*. Vol. 63, No. 3, pp. 22-24 (1987).

[166] Uhlig, H. H. Corrosion and Corrosion Control, John Wiley and Sons Inc. (1971), ISBN 0-471-89563-6.

[167] Fontana, M. G., Greene, N. D. Corrosion Engineering, McGraw Hill Book Company (1978) ISBN 0-07-021461-1

[168] Bakhvalov, G. T., Turkovskaya, A. V. Corrosion and protection of metals, Pergamon Press, (1965).

[169] Watkins, K. G., Jones, R.D., and Lo, K.M. "Electrochemical investigation of the corrosion rate of sacrificial coatings on steel" *Materials Letters* Vol. 8, No. 1,2, pp. 21-25. April (1989).

[170] Watkins, K. G., Jones, R.D., and Beahan, P.G. "Electrochemical investigation of the corrosion rate of 55 aluminum-zinc alloy coated steel" *Materials Letters*, Vol. 8, No. 1,2, pp. 26-30, April (1989).

[171] Jones, D. A. "The application of electrode kinetics to the theory and practice of cathodic protection". *Corrosion Science*. Vol. 11, pp. 439-451 (1971).

[172] Budinski, M. K., Wilde, B. E. "An electrochemical criterion for the development of galvanic coating alloy for steel". *Corrosion*. Vol. 43, No. 1, pp. 60-62 (January 1987).

[173] Dexter, S. C., Moettus, L. M., and Lucas, K. E. "On the mechanism of cathodic protection" *Corrosion*, Vol. 41, No. 10, pp. 598-607 October (1985).

[174] Jones, R. D., Watkins, K. G., Spittle, J. A., and Lo, K. M. "Short term electrochemical evaluation of coated steel strip". Proc. 2nd Int. zinc steel sheet Conf. Rome; 5A5 /1-8 June (1988).

[175] Haynie, F. H. "Environmental factor affecting the corrosion of galvanised steel". *The Degradation of Metals in the Atmosphere, ASTM STP 965.* Eds. S. W. Dean and T. S. Lee, pp. 282-289 (1988).

[176] Guttman, H. *Metal Corrosion in the Atmosphere*, ASTM STP 435. pp. 223-239 (1967).

[177] Haynie, F. H., Spence, J. W. and Upham, J. B. "Atmospheric factors affecting the corrosion of engineering materials". ASTM STP 646, pp. 30-47 (1978).

[178] Schikorr, G. "Behaviour of zinc in the atmosphere" *Metall-Verlog GmbH*, Berlin Grunewals, Vol. 1, pp. 72 (1964) (English ed. published by American

Zinc Institute and the Zinc Development Association (1965).

[179] Flinn, D. R., Cramer, S. D., Carter, J. P., Hurwitz, D. M. and Linstrom, P. J. *Degradation of Meterials due to acid rain.* Edited by R. Baboian. American Chemical Society (1986).

[180] Barton, K. Protection Against Atmospheric Corrosion, John Wiley, New York, pp. 49 (1973).

[181] Cramer, S., Carter, J. P., Linstrom, P. J., Flinn, D. R. "Environmental effects in the atmosphric corrosion of zinc". Degradation of Metals in the Atmosphere, ASTM STP 965, Edited by S. W. Dean and T. S. Lee, pp. 229-247 (1988).

[182] Spence, J. W., Haynie, F. H., Edney, E. O. and Stiles, D. C. "A field experiment to partition the effects of dry and wet deposition on metallic materials". *Materials Degradation caused by acid rain.* Edited by R. Baboian. American Chemical Society, pp. 194-199 (1986).

[183] Linke, W. F. "Solubilities" *Inorganic and Metal-Organic Compounds, K-Z,* Vol. 2, American Chemical Society, pp. 658 (1965).

[184] Spence, J. W., Haynie, F. H., Stiles, D. C. and Edney, E. O. *The Degradation of Metals in the Atmosphere, ASTM STP 965.* Eds. S. W. Dean and T. S. Lee, pp. 282-289 (1988).

[185] Berke, N. S., and Friel, J. J. "Applications of electrochemical techniques in screening metallic-coated steels for atmospheric use" Laboratory Corrosion Tests and Standards, ASTM STP 866, Eds. G. S. Haynes and R. Baboian, pp. 143-158 (1985).

[186] Lambert, M. R., Hart, R. G., and Townsend, H. E. "Corrosion mechanism on Zn-Ni alloy electrodeposited coatings" SAE Technical Paper No. 831817 pp. 81-87 (1984).

[187] Hadden, S. E. "Effect of annealing on the resistance of galvanised steel to atmosphere corrosion" *J. of Iron and Steel Instt.* Vol. 171, pp. 121-127 June (1952).

[188] Campbell, H. S., Stanners, J. F., and Watkins, K. O. " Effect of heat treatment on the protection properties of zinc coatings on steel" J. *of Iron and Steel*

Instt. Vol. 203, pp. 248-251 March (1965).

[189] Shatov, A. P., Smirnov, B. A., and Steklov, O. I. "A comparison of the corrosion resistance of welded joints in zinc coated and uncoated pipes welded by manual arc and semi-automatic CO_2 welding" *Svar.Proiz.* No. 12, pp. 34-36 (1978).

[190] Fedrizzi, L., Molinari, A., and Tiziani, A. " Microstructural characterisation and corrosion behaviour of laser welded austenitic stainless steel. Proc. Conf. 4th Int. Colloq. on welding and melting by electrons and laser beam. pp. 417-424, Cannes, France, 26-30 September (1988).

[191] Jones, D. A., and Greene, N. D. "Electrochemical measurements of low corrosion rates" Corrosion, Vol. 22, pp. 198 (1966).

[192] Stern, M., and Geary, A. L. "Electrochemical polarisation: A theoretical analysis of the shape of polarisation curves"J. of the Electrochem. Soc. Vol. 104, pp. 56-63 (1957).

[193] Mansfeld, F. "Tafel slopes and corrosion rates from polarisation resistance measurements" *Corrosion*, Vol. 29, No. 10, pp. 397-402 October (1973).

[194] Stern, M. "A method for determining corrosion rates from linear polarisation data" *Corrosion*, Vol. 14, pp. 440t-444t (1958).

[195] Evans, U. R. "The corrosion and oxidation of metals" Edward Arnold (Publishers) Ltd. London (1976).

[196] Perry's Chemical Engineers' Handbook. 6th Edition, McGraw-Hill Book Company, pp. 3-14, 24 (1984) ISBN-6-07-049479-7.

[197] Cruciani, D., Ghiringhello, G., and Perotti, G. Laser sheet metal welding, BRITE Technical Report (March 1987).

List of Publications

1. R. Akhter, W. M. Steen, and D. Cruiciani. "Laser welding of zinc coated steel". Proc. 5th Int. Conf. on Lasers in Manufacturing (LIM-5), Ed. Prof. H. Hugel, pp. 195-206, IFS-Publications, ISBN 1-85423-021-2, Stuttgart, West Germany,13-14 September (1988).
2. R. Akhter, M. Davis, J. Dowden, P. Kapadia, M. Ley and W. M. Steen. "A method for calculating the fused zone profile of laser keyhole welds". J. Phys; D: Appl. Phys. Vol. 21, pp. 23-28, (1989).
3. R. Akhter, K. G. Watkins and W.M. Steen. "The effect of weld metal composition on the corrosion rate of laser welded zinc coated steel sheet" Proc. 6th Int. Conf on Lasers in Manufacturing (LIM-6), Ed. Prof. W. M. Steen, pp. 121-134, Birmingham (U.K.) IFS - Publications, 10-11th May (1989).
4. R. Akhter, K. G. Watkins and W. M. Steen. "Corrosion studies on laser welded zinc coated steel sheets" Proc. Conf. 20th International Symposium on Automotive Technology and Automation (ISATA), Vol. III, pp. 2191-2207, , Florence, (Italy). 29th May-2nd June (1989). ISBN 0 947719 26 1
5. K. G. Watkins, R. Akhter, and W. M. Steen. "Determination of the corrosion rate of laser welded zinc coated steel sheet by the linear polarisation technique". Proc. Conf. Electrochemical and Optical Techniques for the Study and Monitoring of Metallic Corrosion. NATO Advanced Study Institute. Viana do Castelo, (Purtugal). July 9-21, (1989).
6. R. Akhter, K. G. Watkins, and W. M. Steen, "Modification of the composition of Laser welds in electrogalvanized steel and the effect on corrosion properties". Journal of Materials and Manufactur ng Processes,Vol. 5, No.4 (1990). In press.
7. R. Akhter, K. G. Watkins, and W. M. Steen. "Electrochemical characterisation of the laser welded zinc coated steel". Materials Letters, August (1990). In press.
8. R. Akhter and W. M. Steen " The gap model for welding zinc coated steel sheet". To be published in Proc. Int. Conf. Laser Systems Application in Industry Turin, (Italy),7-9 November (1990).

Appendix 1. Laser Parameters for Bead on Plate Welding

Laser power	1.62 kW	Laser type	CLL	Beam dia	0.2 mm	Beam mode	Doughnut
Zn at top sheet	7.5 μm	Zn at bottom sheet	7.5 μm	Zn at interface	0 μm		

Run	Welding speed	Penetration	Width	Melted area	Specific energy	Melting efficiency	Gap	Quality
	mm/s	mm	mm	mm^2	J/mm^2	%	mm	Pits/100 mm
1	55.9	0.9	0.9	0.58	145	14.0	- - -	- - -
2	65.4	0.9	0.9	0.57	124	16.2	- - -	- - -
3	69.4	0.8	0.85	0.55	117	16.6	- - -	- - -
4	75.2	0.7	0.85	0.44	108	14.4	- - -	- - -
5	85.5	0.6	0.79	0.33	95	12.2	- - -	- - -
6	95.2	0.5	0.73	0.24	85	10.0	- - -	- - -
7	105.3	0.45	0.65	0.18	77	8.2	- - -	- - -
8	117.7	0.45	0.73	0.18	69	9.2	- - -	- - -
9	133.3	0.35	0.55	0.11	61	6.4	- - -	- - -
10	153.9	0.30	0.49	0.10	53	6.7	- - -	- - -
11	181.8	0.30	0.49	0.08	45	6.3	- - -	- - -
12	217.4	0.25	0.43	0.06	37	5.7	- - -	- - -

Appendix 2. Laser Welding Parameters for Double Pass Welding Technique

Laser power	2.00 kW	Laser type	CLL	Beam dia	0.2 mm	Beam mode	Doughnut
Zn at top sheet	7.5 μm	Zn at bottom sheet	7.5 μm	Zn at interface	15 μm		

Run	Welding speed mm/s	Penetration mm	Width mm	Melted area mm^2	Specific energy J/mm^2	Melting efficiency %	Gap mm	Quality Pits/100 mm
1	11.7	1.91	2.86	3.19	427	13.9	0.22	22
2	13.6	1.86	1.86	2.23	368	11.3	0.08	15
3	15.0	1.91	3.00	2.43	333	13.6	0.23	3
4	16.3	1.83	1.71	1.93	307	11.7	0.06	10
5	18.2	1.77	1.86	1.72	275	11.6	0.01	12
6	20.0	1.72	1.71	1.61	250	12.0	0.01	13
7	22.5	1.46	1.68	1.35	222	11.3	0.08	16
8	24.8	1.23	1.51	1.31	202	12.1	0.12	13
9	28.2	1.08	1.2	0.76	177	7.9	0.08	20
10	39.7	0.80	1.06	0.51	126	7.6	- - -	- -
11	49.3	0.6	0.97	0.39	101	7.2	- - -	- -

Appendix 3. Laser Welding Parameters for Side Jet Welding Technique

Laser power	2.00 kW	Laser type	CLL	Beam dia	0.2 mm	Beam mode	Doughnut
Zn at top sheet	10 μm	Zn at bottom sheet	10 μm	Zn at interface	0 μm		
Side Jet Position	At right angle to both laser beam and welding direction.						

Run	Welding speed mm/s	Penetration mm	Width mm	Melted area mm^2	Specific energy J/mm^2	Melting efficiency %	Gap mm	Quality Pits/100 mm
1	16.3	1.31	1.31	2.16	306.7	13.1	0.09	0
2	19.7	1.31	1.31	2.13	253.8	15.6	0.00	0
3	24.7	1.31	1.11	1.68	202.4	15.4	0.02	0
4	32.9	1.00	1.20	1.37	152.0	16.8	0.02	0
5	39.7	0.66	1.08	0.79	126.0	11.6	- -	0
6	49.5	0.51	0.77	0.41	101.0	7.6	- -	0

Appendix 4. Laser Welding Parameters for Nickel Powder Injection Technique

Laser power	2.00 kW	Laser type	CLL	Beam dia	0.2 mm	Beam mode	Doughnut
Zn at top sheet	10 μm	Zn at bottom sheet	0 μm	Zn at interface	10 μm		
Side Jet Position	At right angle to both laser beam and welding direction.						

Run	Welding speed mm/s	Penetration mm	Width mm	Melted area mm^2	Specific energy J/mm^2	Melting efficiency %	Gap mm	Quality Pits/100 mm
1	24.4	1.46	1.37	1.23	205	11.2	0.07	5
2	28.6	1.34	1.34	1.12	175	11.9	0.01	12
3	32.7	1.34	1.29	1.08	153	13.2	0.01	14
4	40.0	1.03	0.97	0.73	125	10.8	0.14	0
5	48.8	0.83	0.86	0.42	102	7.6	0.08	2
6	60.2	0.40	0.60	0.14	83	3.0	- - -	0

Appendix 5. Laser Welding Parameters for Stainless Steel Injection Technique

Laser power	2.00 kW	Laser type	CLL	Beam dia	0.2 mm	Beam mode	Doughnut
Zn at top sheet	10 μm	Zn at bottom sheet	0 μm	Zn at interface	10 μm		

Run	Welding speed mm/s	Penetration mm	Width mm	Melted area mm^2	Specific energy J/mm^2	Melting efficiency %	Gap mm	Quality Pits/100 mm
1	22.1	1.43	1.71	1.76	452	13.7	0.01	0
2	24.4	1.43	1.60	1.49	410	12.8	0.04	0
3	28.4	1.43	1.43	1.25	352	12.5	0.01	7
4	32.2	0.77	1.20	0.85	310	9.6	0.05	24
5	39.8	0.74	1.03	0.66	251	9.2	0.04	0
6	48.0	0.23	0.60	0.13	208	2.2		

Appendix 6. Laser Welding Parameters for Tool Steel Injection Technique

Laser power	1.54 kW	Laser type	CLL	Beam dia	0.2 mm	Beam mode	Doughnut
Zn at top sheet	7.5 μm	Zn at bottom sheet	7.5 μm	Zn at interface	15 μm		

Run	Welding speed mm/s	Penetration mm	Width mm	Melted area mm^2	Specific energy J/mm^2	Melting efficiency %	Gap mm	Quality Pits/100 mm
1	17.5	1.57	1.81	2.00	440	15.9	0.17	2
2	20.0	1.45	1.40	1.47	385	13.4	0.12	3
3	25.0	1.22	1.20	1.12	308	12.8	0.15	0
4	30.0	1.25	1.14	1.12	257	15.3	0.09	2

Appendix 7. Laser Welding Parameters for P - Polarised Beam

Laser power	1.77 kW	Laser type	CLL	Beam dia	0.2 mm	Beam mode	Doughnut
Zn at top sheet	7.5 μm	Zn at bottom sheet	7.5 μm	Zn at interface	15 μm		

Run	Welding speed mm/s	Penetration mm	Width mm	Melted area mm^2	Specific energy J/mm^2	Melting efficiency %	Gap mm	Quality Pits/100 mm
1	20	1.64	1.87	2.08	442	16.5	0.24	0
2	25	1.56	1.45	1.66	354	16.5	0.16	0
3	30	1.54	1.13	1.25	295	14.9	0.14	0
4	35	1.51	1.09	1.04	253	14.5	0.16	0
5	40	1.16	1.06	0.83	221	13.2	0.09	0
6	50	0.70	0.97	0.52	177	10.3	- - -	0

Appendix 8. Laser Welding Parameters for S - Polarised Beam

Laser power	1.77 kW	Laser type	CLL	Beam dia	0.2 mm	Beam mode	Doughnut
Zn at top sheet	7.5 μm	Zn at bottom sheet	7.5 μm	Zn at interface	15 μm		

Run	Welding speed mm/s	Penetration mm	Width mm	Melted area mm^2	Specific energy J/mm^2	Melting efficiency %	Gap mm	Quality Pits/100 mm
1	20	1.64	2.16	2.39	442	19.0	0.16	0
2	25	1.42	1.52	1.25	354	12.4	0.09	0
3	30	1.06	1.19	0.83	295	10.0	0.06	0
4	35	0.70	1.06	0.73	253	10.1	0.09	0
5	40	0.80	1.00	0.59	221	9.4	0.06	0
6	50	0.61	0.81	0.31	177	6.2	- - -	0

Appendix 9. Laser Welding Parameters for Gaussian Beam Mode

Laser power	1.54 kW	Laser type	CLL + FERRANTI	Beam dia	0.1 mm	Beam mode	Gaussian
Zn at top sheet	10 μm	Zn at bottom sheet	0 μm	Zn at interface	10 μm		

Run	Welding speed mm/s	Penetration mm	Width mm	Melted area mm^2	Specific energy J/mm^2	Melting efficiency %	Gap mm	Quality Pits/100 mm
1	29	1.40	1.24	1.1	345	22.4	0.10	2
2	34	1.38	0.87	0.87	294	20.8	0.04	11
3	38	1.38	0.87	0.85	263	22.7	0.04	10
4	43	1.09	0.69	0.60	233	18.1	0.02	47
5	49	0.91	0.65	0.48	204	16.5	0.02	43
6	57	0.82	0.62	0.45	175	18.0	0.02	42
7	68	0.67	0.60	0.33	147	15.8	0.00	55
8	76	0.67	0.60	0.33	132	17.6	0.00	53

Appendix 10. Laser Welding Parameters for AVCO Laser

Laser power	3.00 kW	Laser type	AVCO	Beam dia	0.8 mm	Beam mode	Multimode
Zn at top sheet	7.5 μm	Zn at bottom sheet	7.5 μm	Zn at interface	15 μm		

Run	Welding speed mm/s	Penetration mm	Width mm	Melted area mm^2	Specific energy J/mm^2	Melting efficiency %	Gap mm	Quality Pits/100 mm
1	20	1.68	1.78	2.93	187	13.7	0.28	15
2	30	1.57	1.57	2.14	125	15.0	0.17	7
3	35	1.25	1.43	1.53	107	12.5	0.42	21
4	40	0.70	1.43	1.02	94	9.6	- - -	22
5	45	0.70	1.34	1.02	83	10.7	- - -	26
6	50	0.70	1.25	0.86	75	10.1	- - -	20
7	60	0.52	1.25	0.41	62	5.8	- - -	0
8	70	0.32	1.16	0.26	54	4.3	- - -	0

Appendix 11. Laser Welding Parameters for AVCO Laser

Laser power	5.00 kW	Laser type	AVCO	Beam dia	0.8 mm	Beam mode	Multimode
Zn at top sheet	7.5 μm	Zn at bottom sheet	7.5 μm	Zn at interface	15 μm		

Run	Welding speed mm/s	Penetration mm	Width mm	Melted area mm^2	Specific energy J/mm^2	Melting efficiency %	Gap mm	Quality Pits/100 mm
1	50	1.55	1.69	2.23	125	15.7	0.15	12
2	55	1.53	1.60	2.10	114	16.2	0.14	22
3	60	0.93	1.57	1.40	104	11.8	0.12	19
4	65	0.89	1.43	1.15	96	10.5	- - -	23
5	70	0.70	1.43	1.02	89	10.0	- - -	22
6	75	0.70	1.34	0.96	83	10.1	- - -	21

Appendix 12. Laser Welding Parameters for AVCO Laser

Laser power	8.00 kW	Laser type	AVCO	Beam dia	0.8 mm	Beam mode	Multimode
Zn at top sheet	7.5 μm	Zn at bottom sheet	7.5 μm	Zn at interface	15 μm		

Run	Welding speed mm/s	Penetration mm	Width mm	Melted area mm^2	Specific energy J/mm^2	Melting efficiency %	Gap mm	Quality Pits/100 mm
1	110	1.58	1.58	2.03	91	19.6	0.17	10
2	120	1.23	1.49	1.38	83	14.5	0.03	19
3	130	0.70	1.58	0.98	77	11.2	0.05	22
4	140	0.93	1.40	1.01	71	12.4	0.05	19
5	150	0.91	1.49	1.05	67	13.8	0.12	22
6	160	0.70	1.40	0.92	62	12.9	- - -	18
7	170	0.70	1.40	0.89	59	13.3	- - -	15
8	190	0.70	1.23	0.77	53	12.8	- - -	5
9	210	0.52	1.23	0.61	48	11.2	- - -	4

Appendix 13. Laser Welding Parameters for MLI Laser

Laser power 5.80 kW Laser type MLI Beam dia 1.0 mm Beam mode Ring Type

Uncoated sheet

Run	Welding speed mm/s	Penetration mm	Width mm	Melted area mm^2	Specific energy J/mm^2	Melting efficiency %	Gap mm	Quality Pits/100 mm
1	21.2	1.46	2.28	7.71	273.6	21.8	0.11	7
2	42.3	1.43	1.54	3.40	137.1	19.2	0.06	5
3	63.5	1.49	1.57	2.76	91.3	23.4	0.19	33
4	84.7	1.34	1.54	1.84	69.0	20.8	0.11	4
5	105.8	0.91	1.51	1.19	55.2	16.9	0.07	1
6	127	0.69	1.14	0.74	45.0	12.5	- - -	4
7	148.2	0.69	0.94	0.74	39.1	14.6	- - -	0
8	169.3	0.31	0.94	0.23	34.3	5.2	- - -	1

Appendix 14. Laser Welding Parameters for UTRC Laser

Laser power 2.00 kW Laser type UTRC Beam dia 0.75 mm Beam mode Multimode

Uncoated sheet

Run	Welding speed mm/s	Penetration mm	Width mm	Melted area mm^2	Specific energy J/mm^2	Melting efficiency %	Gap mm	Quality Pits/100 mm
1	20	1.42	1.22	1.67	133	11.7	0.05	0
2	30	1.37	1.04	1.38	89	14.6	0.00	0
3	40	1.37	0.89	1.02	67	14.3	0.00	0
4	50	1.13	0.78	0.85	53	14.9	0.00	0
5	60	1.03	0.75	0.74	44	15.6	0.00	0
6	80	0.75	0.75	0.47	33	13.2	0.00	0
7	100	0.60	0.67	0.31	27	10.9	- - -	0